

# Global-local progressive failure analysis of composite panels including skin-stringer debonding and intralaminar damage

Von der Fakultät für Bauingenieurwesen und Geodäsie  
der Gottfried Wilhelm Leibniz Universität Hannover  
zur Erlangung des Grades

DOKTOR-INGENIEUR

- Dr.-Ing. -

genehmigte Dissertation  
von

**Margarita Akterskaia M. Sc.**

**2019**

Hauptreferent: Prof. Dr.-Ing. habil. Raimund Rolfes  
Leibniz Universität Hannover  
Korreferent: Prof. Dr. Pedro P. Camanho  
Universidade do Porto  
Tag der Promotion: 19. Juli 2019



# Acknowledgements

The work presented in this thesis was carried out during the years 2016 and 2019 at the Institute of Structural Analysis (ISD) at the Leibniz Universität Hannover. This research and its outcomes could not have been possible without the support and advice of many people.

First of all, I would like to express my endless gratitude to Professor Dr.-Ing. habil. Raimund Rolfes, main advisor of this thesis and a head of the ISD, for giving me the opportunity to develop this work, as well as for his scientific and personal support. I felt his confidence in me throughout this time.

A special mention to Dr. Eelco Jansen, co-advisor of this thesis, my sincere acknowledgement for his infinite help and patience. I also want to thank Dr. Benedikt Daum for our productive talks. Moreover, I want to thank all my colleagues at the ISD for creating such a friendly atmosphere and always-cheerful mood, especially Christian Hente, Gerrit Gottlieb, Andreas Ehrmann and Ayan Haldar for our exploratory lunches together, and my office mate Ricarda Berger for a tireless support in my settling down in Germany. I also greatly appreciate the assistance of my colleagues in organizing a workshop in Hannover, in particular, Jasmin Hörmeyer, Marlene Bruns and Cornelia Kluge among others for the kind support and always ready-to-help attitude.

I want to thank Professor Paul Weaver for the invitation to stay at the Bristol Composites Institute (former ACCIS) at the University of Bristol (UK). I highly appreciate the opportunity to collaborate with this Research Group. Special thanks to my colleagues there, Sergio Minera and Mayank Patni, and their wives Andrea and Sakshi, who made my stay in Bristol a memorable one letting me feel at home. I want to thank Luiz Kawashita, who welcomed my questions and offered his time for the productive discussions. Especially I want to thank Professor Stephen Hallett who guided me through the hardest part of my PhD generously sharing his expertise and inspiration.

Next, I want to thank Professor Pedro Camanho for the rewarding opportunity to visit him in the University of Porto, Faculdade do Engenharia (Portugal). I appreciate a lot the immense knowledge that Professor Pedro Camanho shared with me, that has been invaluable to the development of this work and myself as a researcher leading to a personal enrichment. Especially I want to thank Dr. Albertino Arteiro for our prolific discussions and his constant support.

I would also like to thank Tom Sill for a wonderful and welcoming stay at Tecosim Hamburg (Germany) and for providing me an insight and guidance on industrial applications of research projects.

I must also mention that my PhD studies were supported by European Union's Horizon 2020

research and innovation program (FULLCOMP/2015-2019) under Marie Skłodowska-Curie actions grant agreement number 642121 for which I am very grateful. This project introduced fellow colleagues in my life. It was always a great pleasure to meet them during various conferences, workshops and project meetings, and to share motivation and dedication. They became very fast a source of inspiration for me, providing a high level of technical discussion and advice. Enjoying the life together and becoming friends made these moments very precious to me. I hope to keep these friendships over years.

Last but most importantly, I want to thank my family and friends, who believed in me and always supported my enthusiasm and curiosity. Without them, this work would never have come true. Especially I want to mention my two school-friends Elena and Ekaterina for our long-distance friendship and for always being there for me, as well as my friends Sergei and Galina for the wonderful trips we shared. I want to thank my grandmother for her encouragement and support. I would like to thank my mother for her love and incredible belief in me.

Finally, I want to express my endless gratitude to a love of my life - my husband Andrei for the tremendous moral support from my first days in Germany and overall in my life, for the optimism and patience, for always showing how proud he is of me. This thesis is dedicated to him.

# Abstract

An increasing application of fibre-reinforced composites in aircraft and aerospace engineering contributed to the rise of development of highly effective numerical tools. On the one hand, computational simulations help to overcome the problems related to expensive experimental testings by partially substituting them. This in turn could result in decrease of design and certification costs. On the other hand, the need of effective numerical methods emerged from the desire to increase the limit loads and thus, to further exploit possible reserves of composite components. However, the complexity of problems commonly associated with the modelling of composites requires thorough understanding of the material and structural behaviour. For this reason, an efficient and reliable progressive failure analysis capability is required. Moreover, it is indispensable to be able to combine different levels of precision in one model to effectively examine large structures.

Extensive usage of composite stiffened panels is justified by their slenderness, which results in desired light weight jointly with high stiffness in designated direction due to accordingly aligned reinforcing parts called stringers or stiffeners. These stiffeners not only prevent the skin of the panel from premature buckling under compressive loading, but they also increase the overall structural strength leading to final failure detected far beyond initial buckling. Successfully employed in modelling fuselages and wing boxes as primary components, composite stiffened panels have gained recognition. However, substantial enhancements are to be envisaged in terms of computational methods, as various effects, such as damage initiation and propagation, plasticity or impact damage, for example, require investigation at different levels of accuracy. That leads to development of various multiscale and global-local methods. A literature review has been conducted with a special attention to damage mechanisms and their importance as well as a following discussion dedicated to the existing multiscale algorithms with their strong and weak points.

To address a need in computationally efficient strategies, during this work a novel global-local coupling approach has been developed that is able to model progressive separation of the skin and the stringer together with intralaminar damage in stiffened CFRP panels under compression. The main goal of this methodology is to examine the damage at two levels of accuracy, taking advantage of the fast calculations at the global level and assessing in detail the damage propagation at the local level. An appropriate information exchange between the global and local levels in both directions is particularly challenging and it has been achieved in the demonstrated global-local approach.

According to the proposed method, at the global level a linear elastic coarse model with shell elements is employed to detect the probable areas of damage. Afterwards, local models are generated using a fine mesh with solid elements. Kinematic constraints are used as boundary conditions to prescribe corresponding displacements from the global to the local model. The damage evolution is simulated by means of a material degradation model and cohesive

elements are applied at the local level. To ensure a full information exchange between the two levels, a transfer of the reduced material properties from the local to the global level is carried out. As the relative element sizes of the global and local models are different, a special homogenization procedure is implemented that preserves energies dissipated between the local and global levels. The global-local steps are executed until the final failure takes place.

The new developed approach is illustrated on the basis of one-stringer and multi-stringer laminate panels considering intact and predamaged cases with initial debonding with an aim to demonstrate advantages of the proposed method for modelling progressive failure in the stiffened composite panels with localized damage.

**Keywords:** Composite structures; Global-local method; Progressive failure analysis; Multi-scale analysis; Skin-stringer debonding; Delamination; Matrix cracking; Fibre damage

# Kurzfassung

Der zunehmende Einsatz von faserverstärkten Verbundwerkstoffen in der Luft- und Raumfahrttechnik beschleunigt die Entwicklung hochwirksamer numerischer Werkzeuge. Einerseits helfen Computersimulationen, schwierige und kostspielige experimentelle Tests zu vermeiden um Design- und Zertifizierungskosten zu senken. Andererseits ergibt sich die Notwendigkeit effektiver numerischer Methoden aus dem Wunsch, Lasten in die Nahe der Belastungsgrenze zu erhöhen und damit mögliche Reserven von Verbundbauteilen besser zu nutzen. Die Komplexität der Probleme, die häufig mit der Simulation von Verbundbauteilen verbunden ist, erfordert allerdings ein umfassendes Verständnis des Werkstoff- und Strukturverhaltens. Aus diesem Grund ist eine effiziente und zuverlässige progressive Fehleranalysefähigkeit erforderlich. Darüber hinaus ist es unerlässlich, verschiedene Detailgrade in einem Modell kombinieren zu können, um große Strukturen effektiv zu untersuchen.

Der umfangreiche Einsatz von Faserverbundpaneelen kann auf ihre Schlankheit zurückgeführt werden, die aufgrund der entsprechend ausgerichteten Versteifungskomponenten, die als Stringer bezeichnet werden, das gewünschte niedrige Gewicht gemeinsam mit einer hohen Steifigkeit in der erforderlichen Ausrichtung erzielen. Diese Versteifungen verhindern nicht nur, dass die Paneele unter Druckbelastung vorzeitig beult, sondern sie erhöhen auch die Gesamttragfähigkeit, was wiederum zu einem endgültigen Strukturversagen weit jenseits des initialen Beulens führt. Bei der Modellierung von Rumpf- und Flügelkästen erfolgreich als Hauptkomponenten eingesetzt, haben Faserverbundpaneele Bedeutung erlangt. Bezüglich der Berechnungsmethoden sind jedoch erhebliche Verbesserungen erforderlich, da unterschiedliche Effekte, wie beispielsweise die Schadenseinleitung und -ausbreitung, Schäden durch Plastizität oder Aufprall, auf verschiedenen Genauigkeitsniveaus untersucht werden müssen. Dies führt zur Entwicklung unterschiedlicher Multiskalen- und Global-lokal-Ansätzen. Es wurde eine Literaturrecherche mit besonderem Augenmerk auf Schadensmechanismen und deren Bedeutung sowie eine anschließende Diskussion über die bestehenden Multiskalenalgorithmen mit ihren Stärken und Schwächen durchgeführt.

Um einem Bedarf an rechentechnisch effizienten Strategien gerecht zu werden, wurde im Rahmen dieser Arbeit ein neuartiger global-lokaler Kopplungsansatz entwickelt, der in der Lage ist, die progressive Trennung von Außenhaut und Stringer zusammen mit intralaminaren Schäden in versteiften CFK- Paneele unter Druckbeanspruchung zu modellieren. Das Hauptziel dieser Methodik ist es, den Schaden auf zwei Skalen-Ebenen zu untersuchen. Zum Einem wird eine globale Struktur mit relativ grober Vernetzung erstellt, die den Vorteil von zügigen Berechnungen aufweist. Zum Anderem wird die Schadensausbreitung auf lokaler Ebene im Detail bewertet. Ein angemessener Informationsaustausch zwischen der globalen und der lokalen Ebene ist besonders herausfordernd und wurde im Rahmen des dargestellten global-lokalen Ansatzes erreicht.

Nach dem in dieser Arbeit vorgeschlagenen Verfahren wird auf globaler Ebene ein linear-

elastisches Modell mit Schalenelementen eingesetzt. Die Vernetzung wird so gewählt, damit die alle möglichen Schadensbereiche erfasst werden. Anschließend werden lokale Modelle mit einem feinen Netz aus Volumenelementen erzeugt. Kinematische Kopplungen werden als Randbedingungen verwendet, um entsprechende Verschiebungen vom globalen zum lokalen Modell vorzugeben. Die Schädigungsentwicklung wird mit Hilfe eines entsprechenden Materialmodells simuliert und Kohesivzonenelemente auf lokaler Ebene angewendet. Um einen umfassenden Informationsaustausch zwischen den beiden Ebenen zu gewährleisten, wird eine Übertragung der reduzierten Materialeigenschaften von der lokalen auf die globale Ebene durchgeführt. Da die relativen Elementgrößen der globalen und lokalen Modelle unterschiedlich sind, wird ein spezielles Homogenisierungsverfahren implementiert, welches sicherstellt, dass auf der lokalen und globalen Ebene die gleiche dissipierte Energie vorliegt. Die global-lokalen Schritte werden ausgeführt, bis das endgültige Strukturversagen eintritt.

Der neu entwickelte Ansatz wird auf Basis von Einstringer- und Multistring-Laminatpaneelen unter Berücksichtigung intakter und vorgeschädigter Fallbeispiele mit initialem Ablösungen veranschaulicht, um die Vorteile des vorgeschlagenen Verfahrens zur Modellierung des fortschreitenden Versagens in den versteiften Faserverbundpaneel mit lokaler Schääufzuzeigen.

**Schlagworte:** Faserverbundstrukturen; Global-lokale Methode; Progressive Versagensanalyse; Multiskalen-Analyse; Haut-Stringes-Ablösung; Delamination; Matrixversagen; Faserver-sagen



# Contents

<b>List of Figures</b>	<b>III</b>
<b>List of Tables</b>	<b>V</b>
<b>List of Papers</b>	<b>VII</b>
<b>Notation</b>	<b>IX</b>
<b>1 Introduction</b>	<b>1</b>
1.1 Motivation . . . . .	1
1.2 State of the art . . . . .	3
1.2.1 Failure mechanisms . . . . .	3
1.2.2 Multi-scale and global-local modelling . . . . .	18
1.2.3 Summary . . . . .	28
1.3 Research objectives . . . . .	28
1.4 Outline and connection of publications . . . . .	29
<b>2 Paper A: Efficient progressive failure analysis of multi-stringer stiffened composite panels through a two-way loose coupling global-local approach</b>	<b>31</b>
<b>3 Paper B: Analysis of skin-stringer debonding in composite panels through a two-way global-local method</b>	<b>41</b>
<b>4 Paper C: Progressive failure analysis using global-local coupling including intralaminar failure and debonding</b>	<b>57</b>
<b>5 Paper D: Progressive delamination analysis through two-way global-local coupling approach preserving energy dissipation for single-mode and mixed-mode loading</b>	<b>71</b>
<b>6 Validation of the global-local method on a five-stringer composite panel</b>	<b>87</b>
6.1 Model description . . . . .	87
6.2 Reference model for the pre-damaged D1 panel . . . . .	88
6.3 Coupling results . . . . .	92
<b>7 Summary and outlook</b>	<b>101</b>
7.1 Summary . . . . .	101
7.2 Outlook . . . . .	102



# List of Figures

1-1	Current and future design scenarios for typical stringer stiffened composite panels from [33]. . . . .	3
1-2	Sections of the master fracture body for $\psi = 90^\circ$ and $\psi = 0^\circ$ [113]. . . . .	6
1-3	Fracture surface for the Puck failure criterion from [114] for plane stress state. . . . .	7
1-4	Determination of the fracture plane from [113]. . . . .	8
1-5	Fracture plane for a 3D stress state [109] similar to Puck et al. [114]. . . . .	8
1-6	Physical model for kink-band formation [111]. . . . .	9
1-7	Yield and failure surface of the transversely-isotropic material model in $\sqrt{I_1}$ - $I_3$ -invariant-plane of IQC criterion (from [139]) . . . . .	10
1-8	VCCT for 2D solid element with four nodes from [81]. . . . .	14
1-9	Bilinear traction-separation law. . . . .	15
1-10	Overview of two-way loose coupling procedure with stiffened panel [68]. . . . .	25
1-11	Local part tests (Left: Test 1, Middle: Test 2, Right: Test 3) [68]. . . . .	26
6-1	Thermography scan after 3700 cycles from the skin side for the pre-damaged D1 panel [103]. Both dark areas in the second and the central stringers correspond to pre-damaged regions. . . . .	88
6-2	Experimental load-displacement curve with radial displacement contours (mm) (stiffener side) for the pre-damaged D1 panel [103]. . . . .	90
6-3	Curved five-stringer composite panel from the skin side. . . . .	91
6-4	Thermographic image and approximated geometry of the debonded areas [103]. . . . .	92
6-5	Experimental results of the buckling shapes from the stringers side [140]. . . . .	93
6-6	Reference shell results of the buckling shapes from the stringers side. . . . .	93
6-7	Load-displacement curves of the experimental panel [103] and reference shell numerical solution. . . . .	94
6-8	Degraded cohesive elements of the reference shell model. View from the stringers side. . . . .	95
6-9	Reference model. Left: matrix damage at applied displacement of 1.40 mm. Middle: matrix damage at applied displacement of 2.52 mm (final failure). Right: fibre damage at applied displacement of 2.52 mm (final failure). View from the stringers side. . . . .	96
6-10	New areas of the fibre damage in the global model detected at each step of the global-local coupling procedure in the stringer. View from the stringers side. . . . .	97
6-11	New areas of the matrix damage in the global model detected at each step of the global-local coupling procedure in the skin. View from the stringers side. . . . .	97
6-12	Global model and six local models created in the regions of the initial debonding. Cohesive elements in red in local models to account for the initial debonding. . . . .	98

---

6-13 Load-displacement curves of the experimental panel [103], reference shell numerical solution and global-local coupling results. . . . .	99
--	----

# List of Tables

6-1	Geometry of a pre-damaged D1 five-stringer composite panel. . . . .	89
6-2	Material data of the unidirectional CFRP material IM7/8552 UD. . . . .	89
6-3	Computational characteristics of models. . . . .	96



# List of Papers

A AKTERSKAIA, M., JANSEN, E., HÜHNE, S., AND ROLFES, R. Efficient progressive failure analysis of multi-stringer stiffened composite panels through a two-way loose coupling global-local approach. *Composite Structures* 183 (2018), 137-145. . . . . 32

B AKTERSKAIA, M., JANSEN, E., HALLETT, R.S., WEAVER, P., AND ROLFES, R. Analysis of skin-stringer debonding in composite panels through a two-way global-local method. *Composite Structures* 202 (2018), 1280-1294. . . . . 42

C AKTERSKAIA, M., JANSEN, E., HALLETT, R.S., WEAVER, P., AND ROLFES, R. Progressive failure analysis using global-local coupling including intralaminar failure and debonding. *AIAA Journal* 57 7 (2019), 3078-3089. . . . . 58

D AKTERSKAIA, M., CAMANHO P.P., JANSEN, E., ARTEIRO A., AND ROLFES, R. Progressive delamination analysis through two-way global-local coupling approach preserving energy dissipation for single-mode and mixed-mode loading. *Composite Structures* 223 (2019), 110892. . . . . 72





# Notation

## Latin symbols

Symbol	Name
$A$	Area
$\mathbf{C}$	Material stiffness matrix
$d$	Damage variable for cohesive element
$d_f$	Damage variable for the fibre degradation by Linde
$d_m$	Damage variable for the matrix degradation by Linde
$E$	Young's modulus
$F$	Force
$f_f$	Fibre failure condition for Linde criterion
$f_m$	Matrix failure condition for Linde criterion
$G$	Shear stiffness
$G_f$	Fracture energy of fibre
$G_m$	Fracture energy of matrix
$G_{Ic}$	Total critical energy release rate in mode I
$G_{IIc}$	Total critical energy release rate in mode II
$G_I, G_{II}, G_{III}$	Energy release rates in mode I, II and III
$\mathbf{K}$	Interface stiffness matrix
$K_0$	Initial interface stiffness
$L$	Length
$L_C$	Characteristic element length
$l_e$	Cohesive element mesh size
$l_{czl}$	Cohesive zone length
$N_e$	Number of elements
$p$	Slope parameter of Puck criterion
$S_A$	Axial shear strength
$S_T$	Transverse shear strength
$t$	Thickness
$w$	Width
$X_C$	Longitudinal compressive strength
$X_T$	Longitudinal tensile strength
$Y_C$	Transverse in-plane compressive strength
$Y_T$	Transverse in-plane tensile strength

## Greek symbols

Symbol	Name
$\delta$	Maximum relative displacement
$\epsilon$	Strain

$\eta$	Empirical parameter in Benzeggagh and Kenane criterion
$\eta_L$	Slope or frictional coefficient in LaRC05 criteria
$\eta_T$	Slope or frictional coefficient in LaRC05 criteria
$\theta_{fp}$	Fracture plane angle for Puck criterion
$\nu$	Poisson's ratio
$\sigma$	Stress
$\tau$	Shear stress

## Abbreviation

Latin letters	Name
COCOMAT	EU project "Improved Material Exploitation of Composite Airframe Structures by Accurate Simulation of Postbuckling and Collapse"
CFRP	Carbon fiber-reinforced plastic
C3D8	Solid linear elements with eight nodes and full integration scheme (Abaqus library)
DOF	Degree of freedom
FE	Finite element
FEM	Finite element method
HIMSA	Homogenisation-based iterative two-way multiscale approach
ISD	Institute for Structural Analysis, Institut für Statik und Dynamik
LUH	Leibniz Universität Hannover
MPC	Multipoint constraints
PDM	Progressive damage modelling
RVE	Representative volume element
S4R	Shell elements with four nodes and reduced integration scheme (Abaqus library)
UMAT	User-defined subroutine to define material behaviour for implicit simulations (Abaqus)
VCCT	Virtual crack closure technique
WWFE	World-wide failure exercise
XFEM	Extended finite element method
2D	Two-dimensional
3D	Three-dimensional

# 1 Introduction

The incentive for the present thesis is an existing need of partial substitution of expensive experimental tests of composite structures by efficient virtual mechanical testing tools. In order to carry out numerical calculations reliable and effective computational methods are necessary to simulate the complex structural and material behaviour of composite materials. A reasonable desire to increase an ultimate load and to exploit possible reserves of composite structures also requires an accurate numerical prediction of the failure behaviour, as the first failure does not necessarily lead to a final collapse and the structure may further carry substantial loads. Contemporary restrictions on the computational capacities inspired a development of various multi-scale strategies to alleviate the costs of numerical analyses. Therefore, to address these demands, a two-way global-local coupling approach has been developed in this work to capture progressive failure in application to composite stiffened panels.

The first chapter consists of description of a motivation that drove the current research. Afterwards a state of the art is presented with a following discussion on the research objectives of this thesis aimed at reducing a gap between existing methodologies and desired modelling of advanced composite materials. Finally, an outline of the thesis is presented.

## 1.1 Motivation

An increasing application of the composite structures over the past decades occurred due to the possibility to tailor their mechanical properties allowing to achieve desired parameters and to overcome the limitations commonly associated with homogeneous materials. Primarily designed for an application in the aircraft and aerospace industries, the composite materials step by step are gaining a fair place in the automotive industry, civil engineering and marine engineering, medicine and even in creation of sport equipment.

Light-weight laminated stiffened panels made of carbon-fibre reinforced plastic (CFRP) with high-to-strength and high-to-stiffness ratio are actively used for modelling fuselages and wing boxes in today's aircrafts. These panels are commonly reinforced with so-called stiffeners or stringers to increase load-carrying capabilities especially under compressive loads that are typical during their lifetime. The stringers that are usually aligned with main load directions also enhance the post-buckling response of these panels. While weight saving results in a reduction of emission which is beneficial for the environment, resistance to corrosion and fatigue leads to decrease in maintenance costs. Another aspect, that is important in many industrial applications, is a possibility of complex designs that offer composite materials, which in turn may lead to decrease in the number of assembled components and, thus, reduce manufacturing costs. Nevertheless, application of composite materials is also associated with several disadvantages. One of the most important drawbacks of composites is high raw material costs. Another important aspect might be associated with high fabrication and

assembly costs. Also difficulties related to the detection of the damage and repairing it are often mentioned. Hence, it is essential to develop reliable numerical modelling tools that would be able to predict the damage onset and propagation through the structure.

There exist several challenges that should be addressed to ensure a successful implementation of composite components in general and stiffened panels as a particular case. First of all, substitution of the initially used metal parts by advanced composites and further enhancement of the design characteristics inevitably leads to increase in design and certification costs. Therefore, it is desirable not only to improve the mechanical performance of the overall structure, but also to decrease required experimental testings by partially replacing them through reliable virtual testing tools [26, 27, 126]. Hence, the development of robust structural design tools is a substantial step towards reduction of the expensive physical tests. This strategy requires the thorough understanding of the damage mechanisms and the ability to incorporate the detailed modelling of the critical regions into the global structural simulation.

This approach is also inspired by the possibility of further exploitation of the composite parts after first occurrence of the damage as composite structures could potentially maintain load-carrying capacities beyond the load of the initial damage. However, the current design of composite structures is relatively conservative and the onset of the damage is not allowed to happen before the limit load due to high safety factors. In order to exploit the potential reserve of the load-carrying capability and consequently to further reduce structural weight, a confidence in simulation of the response of composite structures is targeted. Following the future design scenario suggested in the scope of the COCOMAT project [33] and illustrated in Fig. 1-1, the onset of the damage of stiffened panels that are prone to buckling could be allowed to take place between the limit and ultimate loads. This aim of increasing the current limit load of stiffened panels longer into the postbuckling regime was motivated by the damage tolerance that stiffened panels typically exhibit before final collapse. The current design scenario is restricted to non damaged behaviour during the service time due to the risk of unstable crack propagation that could significantly reduce the load bearing capacity and might lead to a premature failure. In order to include the effects of damage and consequent material degradation in the analysis, efficient and reliable numerical techniques are required. Only when these tools will be developed and carefully validated against the experimental data, the limit load could be firstly shifted deeper into the postbuckling regime, which corresponds to "Future design scenario", see Fig. 1-1. And finally, the limit load could be moved even to tolerate the damage initiation in stiffened panels during the flight operational time. This is even more challenging future step forward than that was envisaged by the COCOMAT project.

Although during the last decades significant knowledge has been accumulated regarding structural and damage behaviour of stiffened composite panels, no agreement has been attained on the universal failure criterion or no computational capabilities have been developed that would allow to numerically simulate a complex postbuckling behaviour of the stiffened panel with various damage mechanisms in one model. Therefore, various multi-scale techniques that couple different levels of accuracy have been proposed in the literature. However, there is still a gap in the research of the progressive failure analysis as it requires to increase an applied load gradually and to ensure information transition in both directions as well as to consider the most relevant damage mechanisms. That motivated the current work to

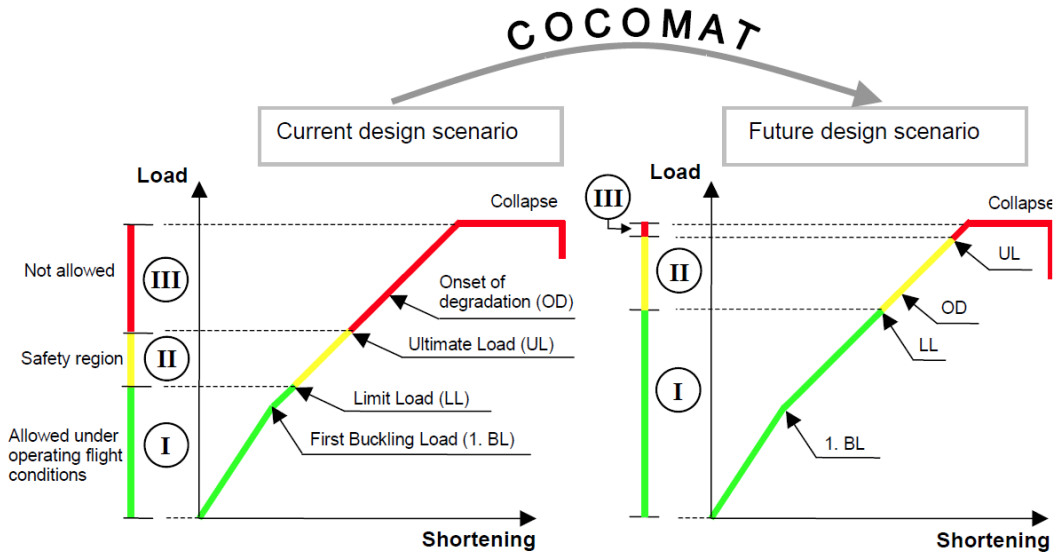


Figure 1-1: Current and future design scenarios for typical stringer stiffened composite panels from [33].

contribute into the research and development of the reliable and efficient method that would allow to examine different failure scenarios including prediction of the damage initiation and propagation on the one hand, and to model large composite structures on the other hand.

## 1.2 State of the art

An overview of the state of the art regarding damage mechanisms and multi-scale approaches is given in this section with particular attention on stiffened panels and global-local methods. The aim is to discuss the most relevant techniques of predicting the damage onset and then modelling the damage propagation. It is also important to gain an understanding of the advantages and disadvantages of existing multi-scale and global-local algorithms and establish a further potential of development of a new fast and accurate method for coupling global and local scales while taking into account the typical material damage behaviour. This section is divided into two parts. First part deals with the available failure mechanisms for fibre-reinforced composites. The second part describes existing multi-scale and global-local modelling approaches with a later focusing on stiffened panels.

### 1.2.1 Failure mechanisms

Fibre-reinforced composite laminates consist of stacked laminae of different orientations, where each lamina represents a single layer of polymer matrix with embedded uni-directional or woven fibres. In the current studies only uni-directional fibres are considered. Composite laminates may experience various failure mechanisms as a result of applied loads, boundary conditions or material properties of constituents. These failure modes could be classified into two categories: intralaminar and interlaminar failure. Intralaminar failure includes

matrix cracking, fibre breakage and matrix-fibre decohesion. Interlaminar damage describes separation of adjacent layers, called delamination. Failure criteria have been extensively developed in order to determine the critical regions where the damage occurs, to identify failure types and final loads that the composite structure could sustain. Material degradation models have been derived by many authors to account for a gradual or instant decrease of the load carrying capacity simulating real failure mechanisms [49].

### 1.2.1.1 Intralaminar failure

Three main types of intralaminar failure are to be distinguished: matrix cracking, fibre breakage and debonding of the interface between matrix and fibre. Matrix cracking is typically not a catastrophic failure mode which means that it does not actually lead alone to a final collapse and the structure with matrix cracks can still bear applied loads due to fibre reinforcement. However, matrix cracks tend to grow and especially crack coalescence can provoke delamination of a composite laminate which was investigated by Hallett et al. [58], van der Meer and Sluys [137], Maimi et al. [90, 91], Zubillaga et al. [151] and Zubillaga et al. [152]. Fibres are the main constituents of the composite designed to withstand loads. Hence, fibre failure is a crucial damage mechanism that can lead to a spontaneous structural collapse. Fibre-matrix interface decohesion is commonly a result of a fibre pull-out from the matrix. Fibre kinking occurs due to initial misalignment of the fibres and fibre rotation under compressive loadings and leads to fibre failure.

Failure analysis of composite structures requires determination of failure criteria in order to account for the damage initiation. Strength-based criteria comprising different stress-based and strain-based criteria are generally used. These criteria can be formulated as global failure criteria defined by one equation or they can distinguish between failure modes as well as between tension or compressive load applied. An extensive overview and comparison of different failure criteria that have been actively developed and extended since 1950s is given in World Wide Failure Exercises (WWFE), see Hinton et al. [64], Kaddour and Hinton [72], Kaddour et al. [74] and Kaddour et al. [73], but was also conducted by Talreja [131]. In the following several important criteria are discussed in more detail.

### Hashin criterion

The Hashin criterion [61] is a mode-based failure criterion that distinguishes between fibre and matrix failure as well as between tension and compression. The criterion is based on quadratic stress invariants and assumes transversely isotropic laminate. Not only the fracture plane could not be defined, but also the fibre compression criterion does not account for the effects of in-plane shear, which decreases the effective compressive strength of a ply [109].

Fibre failure under tension ( $\sigma_1 > 0$ ) is expressed as following:

$$\left(\frac{\sigma_1}{X_T}\right)^2 + \frac{1}{S_A^2}(\tau_{12}^2 + \tau_{13}^2) = 1 \quad (1.1)$$

where  $X_T$  and  $S_A$  represent the tensile strength in fibre direction and the axial shear strength, respectively. For fibre failure under compression ( $\sigma_1 < 0$ ) the simple maximum stress criterion is used:

$$\left(\frac{\sigma_1}{X_C}\right)^2 = 1 \quad (1.2)$$

where  $X_C$  is the compressive strength in fibre direction. Matrix failure under tension ( $\sigma_2 + \sigma_3 > 0$ ) is expressed in the following form:

$$\frac{1}{Y_T^2}(\sigma_2 + \sigma_3)^2 + \frac{1}{S_T^2}(\tau_{23}^2 - \sigma_2\sigma_3) + \frac{1}{S_A^2}(\tau_{12}^2 + \tau_{13}^2) = 1 \quad (1.3)$$

where  $Y_T$  and  $S_T$  are the tensile strength in transverse direction and the transverse shear strength, respectively. Matrix failure in compression ( $\sigma_2 + \sigma_3 < 0$ ) is defined as:

$$\frac{1}{Y_C} \left[ \left(\frac{Y_C}{2S_T}\right)^2 - 1 \right] (\sigma_2 + \sigma_3) + \frac{1}{4S_T^2}(\sigma_2 + \sigma_3)^2 + \frac{1}{S_T^2}(\tau_{23}^2 - \sigma_2\sigma_3) + \frac{1}{S_A^2}(\tau_{12}^2 + \tau_{13}^2) = 1 \quad (1.4)$$

The Hashin criterion does not account for the increase in the shear strength of the ply during transverse compression. Moreover, compressive stress provokes reduction of the effective compressive strength of a ply due to the in-plane shear, which is not considered by this criterion.

### Puck criterion

Among several modifications and extensions to the Hashin criterion proposed in the literature, the Puck criterion [112] attracted attention to the definition of the fracture plane. It is based on the following assumption that inter-fibre fracture plane is parallel to the fibres and is determined only by normal and two shear stresses acting on this plane. The Puck criterion differentiates between three failure modes (A, B and C) of matrix cracking depending on fracture surface, that in its turn is based on the Mohr failure theory. The guidance on determination of the action plane parameters are discussed in detail by Puck et al. [113]. The Puck criterion includes the effect of increasing of the matrix shear strength during transverse compression. For the plane stress state of stress the angle of the fracture plane for the mode C, see Fig. 1-3, is calculated with the following equation:

$$\theta_{fp} = \arccos \sqrt{\frac{R_{\perp\perp}^A}{-\sigma_2}} \quad (1.5)$$

where  $R_{\perp\perp}^A$  is the fracture resistance of the action plane against its fracture due to transverse shear stress. Mode A defines matrix failure under transverse tension ( $\sigma_2 \geq 0$ ):

$$\sqrt{\left(\frac{\tau_{21}}{R_{\perp\parallel}}\right)^2 + \left(1 - p_{\perp\parallel}^{(+)} \frac{R_{\perp\perp}^{(+)}}{R_{\perp\parallel}}\right)^2 \left(\frac{\sigma_2}{R_{\perp\perp}^{(+)}}\right)^2} + p_{\perp\parallel}^{(+)} \frac{\sigma_2}{R_{\perp\parallel}} = 1 \quad (1.6)$$

where  $R_{\perp\perp}^{(+)}$ ,  $R_{\perp\parallel}$ , and applied later  $R_{\perp\perp}^{(-)}$  are basic strengths obtained from the experiments.

$p_{\perp\parallel}^{(+)}$ , and used later  $p_{\perp\parallel}^{(-)}$  and  $p_{\perp\perp}^{(-)}$  are inclination parameters of the fracture envelope, see Fig. 1-3. They should be defined as gradients at the zero normal stress acting at the fracture plane.  $p_{\perp\parallel}^{(-)}$  and  $p_{\perp\parallel}^{(+)}$  are defined from  $(\sigma_2, \tau_{21})$  fracture curves as gradients at  $\sigma_2 = 0$ , see Fig. 1-2. As the fracture angle  $\theta_{fp}$  is zero for both modes A and B, the stresses at the fracture plane are  $\sigma_n = \sigma_2$  and  $\tau_{n1} = \tau_{21}$ . However, due to unavailable fracture curves for  $p_{\perp\perp}^{(-)}$  and  $p_{\perp\perp}^{(+)}$ , they could be defined only indirectly and based on the assumption that all inclination parameters should be of the same magnitude [113]. Thus, first  $p_{\perp\perp}^{(-)}$  is defined from the transverse compression fracture tests based on the fracture angle  $\theta_{fp}$ :

$$p_{\perp\perp}^{(-)} = \frac{1}{2\cos^2\theta_{fp}} - 1 \quad (1.7)$$

and then it is assumed that  $p_{\perp\perp}^{(+)} = p_{\perp\perp}^{(-)}$ .

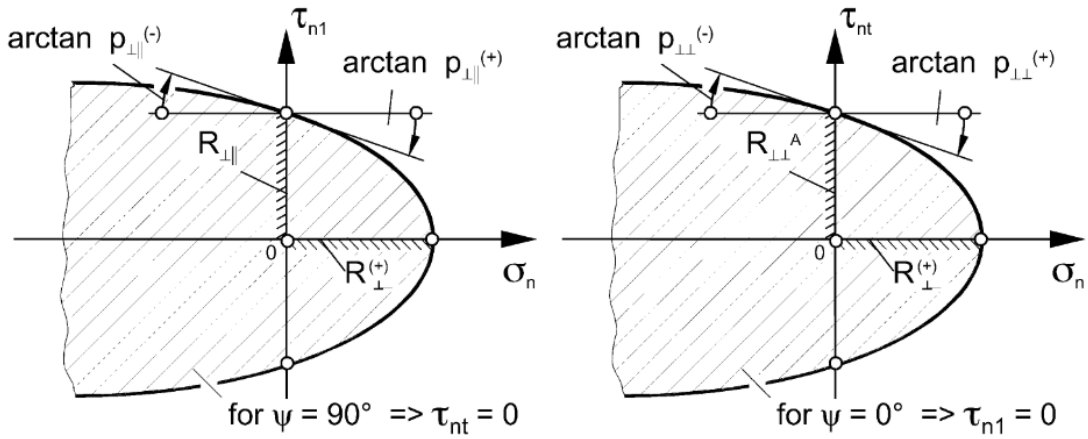


Figure 1-2: Sections of the master fracture body for  $\psi = 90^\circ$  and  $\psi = 0^\circ$  [113].

Mode B stands for the matrix failure under transverse compression:

$$\frac{1}{R_{\perp\parallel}} \left( \sqrt{\tau_{21}^2 + (p_{\perp\parallel}^{(-)}\sigma_2)^2} + p_{\perp\parallel}^{(-)}\sigma_2 \right) = 1 \quad (1.8)$$

The fracture plane for the Modes A and B is normal to the ply and parallel to the fibre direction ( $\theta_{fp}=0$ ). Mode C is a matrix failure under large transverse compression ( $\sigma_2 < 0$ ) with a fracture angle defined from Eq. 1.5:

$$\left[ \left( \frac{\tau_{21}}{2(1 + p_{\perp\perp}^{(-)})R_{\perp\parallel}} \right)^2 + \left( \frac{\sigma_2}{R_{\perp}^{(-)}} \right)^2 \right] \frac{R_{\perp}^{(-)}}{-\sigma_2} = 1 \quad (1.9)$$

It should be emphasized that in a general 3D stress state case the fracture angle  $\theta_{fp}$  should be determined numerically. That means that normal and both shear stresses acting on a plane parallel to the fibres should be identified as  $\sigma_n(\theta)$ ,  $\tau_{nt}(\theta)$  and  $\tau_{n1}(\theta)$  and by repeating this for sufficiently large number of angles  $\theta$ , the stresses satisfying failure criteria are detected together with the corresponding fracture angle  $\theta_{fp}$ , which is illustrated in Fig. 1-4.



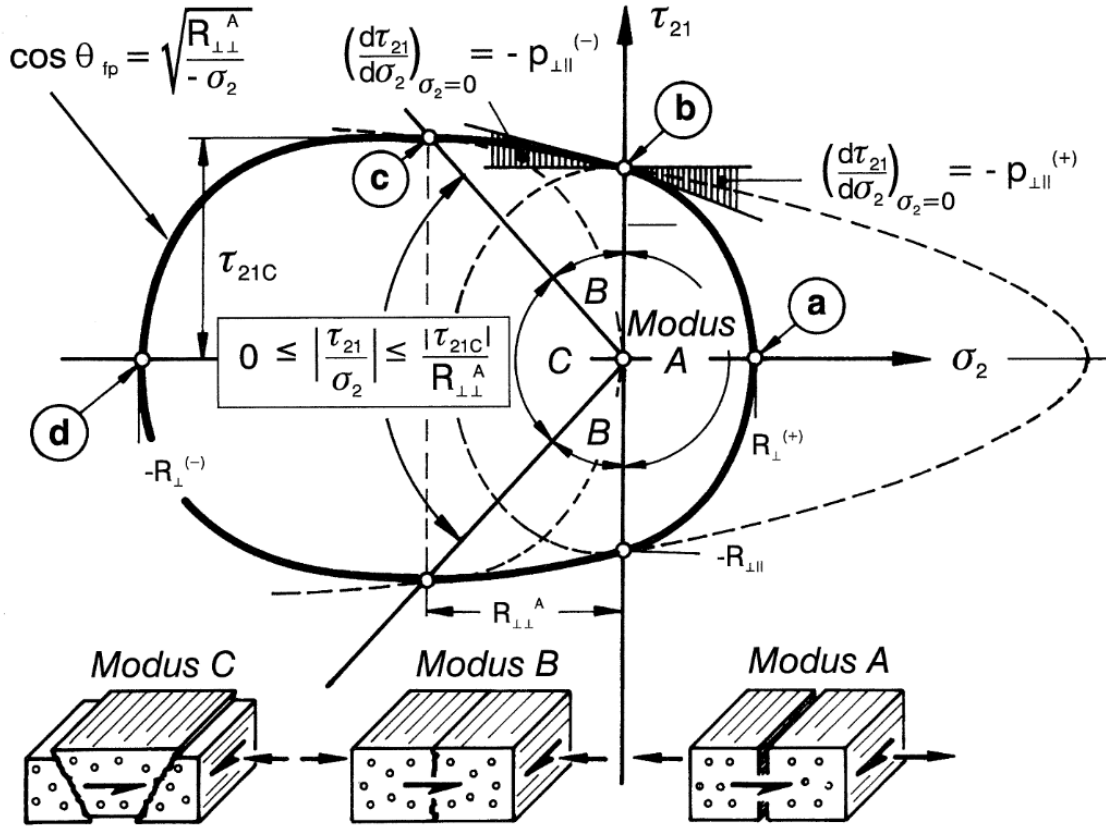


Figure 1-3: Fracture surface for the Puck failure criterion from [114] for plane stress state.

### LaRC05 failure criteria

Following the idea of a fracture plane, Dávila et al. [30] suggested six phenomenological failure criteria in terms of plane stress assumptions denoted as LaRC03 failure criteria, starting from LaRC02 failure criteria [31]. Later on the criteria were extended to a 3D stress state by Pinho et al. [109] considering in-plane shear non-linearity in matrix behaviour and then by Pinho et al. [110] with attention to the fibre kinking. The latest LaRC05 failure criteria presented by Pinho et al. [111] define the matrix failure by following:

$$\left( \frac{\tau_T}{S_T^{is} - \eta_T \sigma_N} \right)^2 + \left( \frac{\tau_L}{S_L^{is} - \eta_L \sigma_N} \right)^2 + \left( \frac{\langle \sigma_N \rangle_+}{Y_T^{is}} \right)^2 = 1 \quad (1.10)$$

As the last term in Eq. 1.10 is responsible only for the traction of the matrix crack, the criterion distinguishes between tensile and compressive failure mechanisms. The McCauley brackets are defined as  $\langle x \rangle_+ = \max\{0, x\}$ .  $\tau_T$ ,  $\tau_L$  and  $\sigma_N$  are the transverse shear, longitudinal shear and normal stresses acting on the fracture plane depicted in Fig. 1-5, similar as defined by Puck et al. [114].

The slope or friction coefficients  $\eta_T$  and  $\eta_L$  allow to change the respective shear strengths depending on the traction. In the case of the compressive normal traction they allow to

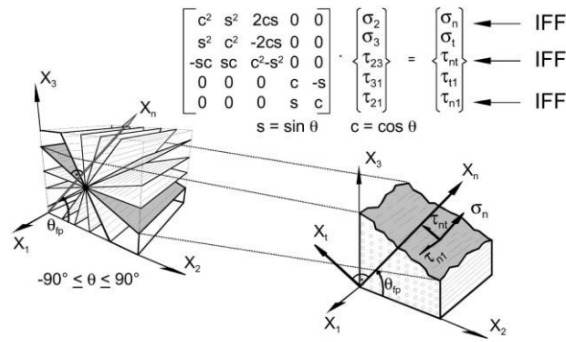


Figure 1-4: Determination of the fracture plane from [113].

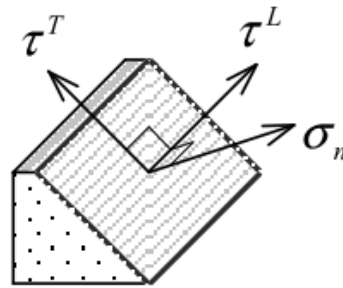


Figure 1-5: Fracture plane for a 3D stress state [109] similar to Puck et al. [114].

increase the respective shear stresses, whereas when the normal traction is tensile, the respective shear strengths are reduced. Both slope or frictional coefficients  $\eta_T$  and  $\eta_L$  are material properties that are required to be defined experimentally.  $\eta_T$  is determined from the pure transverse compression test, while  $\eta_L$  is found from the condition similar to one proposed by Puck et al. [113], see [109]:

$$\frac{\eta_L}{S_L} = \frac{\eta_T}{S_T} \quad (1.11)$$

where  $S_T$  and  $S_L$  are transverse and longitudinal shear strengths respectively.

Pinho et al. [111] argued that the strengths for the matrix-dominated failure should not be considered as material properties as they depend on the ply thickness and the stacking sequence of the neighbouring plies. That is why the in-situ strengths  $S_T^{is}$ ,  $S_L^{is}$  and  $Y_T^{is}$  as transverse shear strength, longitudinal shear strength and transverse tensile strengths are introduced.

Fibre compressive failure is associated with fibre kinking and matrix splitting in between

fibres and is described by the following criterion:

$$\left( \frac{\tau_{23}^m}{S_T^{is} - \eta_T \sigma_2^m} \right)^2 + \left( \frac{\tau_{12}^m}{S_L^{is} - \eta_L \sigma_2^m} \right)^2 + \left( \frac{\langle \sigma_2^m \rangle_+}{Y_T^{is}} \right)^2 = 1 \quad (1.12)$$

If the magnitude of the longitudinal compression  $\sigma_1 \leq -X_C/2$ , then there is a fibre kinking, if not and  $\sigma_1 \geq -X_C/2$  then there is a fibre splitting. Here Pinho et al. [111] assumed that under lower longitudinal compression the shear-dominated matrix failure results in fibre splitting, while fibre kinking starts at higher compressive stresses. The superscript  $m$  denotes the rotation to the misalignment frame after the rotation to the kink-band plane  $\psi$ , refer to Fig. 1-6 and [111]. As has been mentioned above, fibre kinking is highly sensitive to fibre misalignments as well as to matrix defects, which require consideration of uncertainties at microscopic length scale such as statistical distributions of fibre waviness [18]. But in the proposed above criterion the probability aspect of the fibre misalignment distribution is not considered.

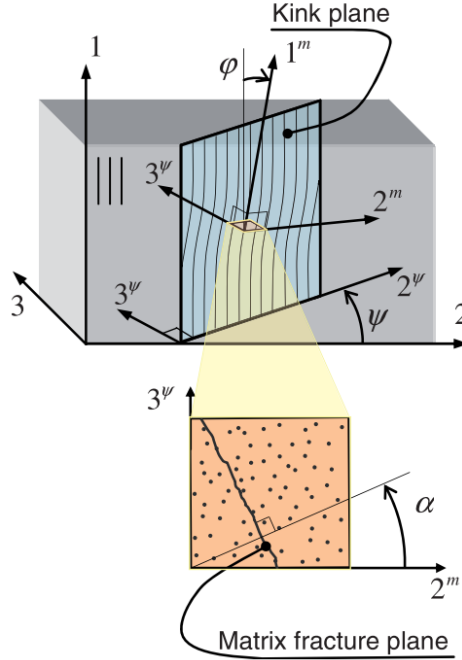


Figure 1-6: Physical model for kink-band formation [111].

Fibre tensile failure is detected by the maximum stress failure criterion:

$$\frac{\langle \sigma_1 \rangle_+}{X_T} = 1 \quad (1.13)$$

### IQC criterion

Vogler et al. [139] formulated the invariant-based quadratic failure criterion (IQC) that does not require definition of the fracture surface. However, the criterion distinguishes between matrix and fibre failure as well as between tension and compression. While fibre

failure is determined similarly to the Puck criterion, matrix failure is identified through the invariant-based criterion. This criterion may be regarded as computationally more efficient as compared to Puck and LaRC05 criteria, as it does not require iterative procedure to identify fracture surface.

Fibre failure is determined similarly under compression and tension:

$$\frac{a\sigma a}{R_{\parallel}} = 1 \quad (1.14)$$

where  $R_{\parallel}$  represents either tensile strength  $R_{\parallel}^t$ , or compressive strength  $R_{\parallel}^c$  depending on the loading condition,  $\mathbf{a}$  is a preferred direction characterizing transversely-isotropic material. The material response is invariant with respect to arbitrary rotations around this preferred direction  $\mathbf{a}$ . The term  $\mathbf{a}\sigma\mathbf{a}$  is the projection of the stress tensor onto the preferred direction.

Matrix failure surface is defined:

$$r = \beta_1 I_1 + \beta_2 I_2 + \beta_3 I_3 + \beta_{32} I_3^2 - 1 \quad (1.15)$$

where the failure occurs when  $r = 0$ . Parameters  $\beta_1$ ,  $\beta_2$ ,  $\beta_3$  and  $\beta_{32}$  are obtained from material strengths.

Fig. 1.15 illustrates shapes of yield and failure surface of the transversely-isotropic material model.

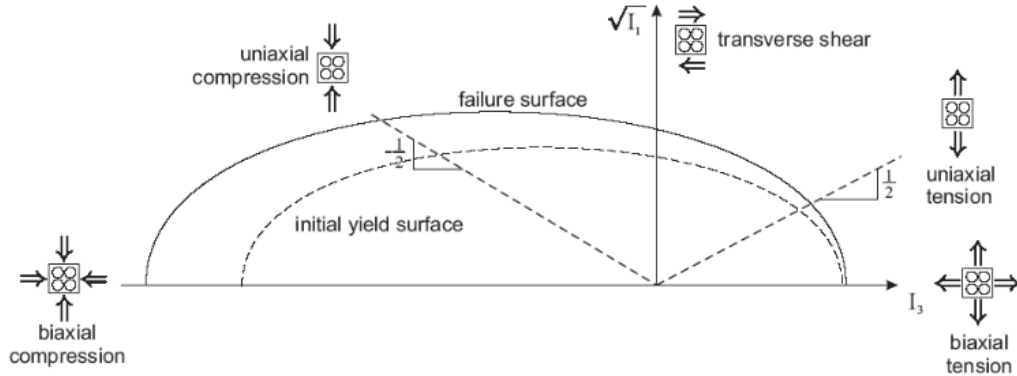


Figure 1-7: Yield and failure surface of the transversely-isotropic material model in  $\sqrt{I_1}$ - $I_3$ -invariant-plane of IQC criterion (from [139])

### Linde criterion and degradation model

The Linde criterion [86] distinguishes between fibre and matrix damage without differentiating between compressive and tensile stresses. This criterion is based on strains and does not introduce a fracture surface definition. The material damage model performs a gradual degradation of material properties based on the fracture energies of fibre and matrix. In the following,  $X_T$  and  $X_C$  are the longitudinal tensile and compressive strength, correspondingly,

and  $Y_T$  and  $Y_C$  denote the transverse in-plane tensile and compressive strength, respectively, whereas  $S_A$  is the axial shear strength and  $C_{ij}$  are the components of the stiffness matrix. The appearance of the matrix and fibre damage is detected by the following two equations:

$$f_m = \sqrt{\frac{Y_T}{Y_C}(\epsilon_{22})^2 + \left(Y_T - \frac{Y_T^2}{Y_C}\right) \frac{\epsilon_{22}}{C_{22}} + \left(\frac{Y_T}{S_A}\right)^2 \epsilon_{12}^2} > \frac{Y_T}{C_{22}} \quad (1.16)$$

$$f_f = \sqrt{\frac{X_T}{X_C}(\epsilon_{11})^2 + \left(X_T - \frac{X_T^2}{X_C}\right) \frac{\epsilon_{11}}{C_{11}}} > \frac{X_T}{C_{11}} \quad (1.17)$$

where the strain components  $\epsilon_{ij}$  correspond to the local material coordinates related to the orientation of the fibres, index 1 refers to the fibre direction, whereas index 2 (in-plane) and index 3 (out-of-plane) refer to the transverse directions.

Linde introduced two different damage parameters  $d_m$  and  $d_f$  to distinguish between fibre failure and matrix failure:

$$d_m = 1 - \frac{Y_T}{f_m} e^{-\left(\frac{C_{22}Y_T(f_m - Y_T)L_C}{G_m}\right)} \quad (1.18)$$

$$d_f = 1 - \frac{X_T}{f_f} e^{-\left(\frac{C_{11}X_T(f_f - X_T)L_C}{G_f}\right)} \quad (1.19)$$

The characteristic element length  $L_C$  is applied to minimize the mesh dependency of the degradation model.  $G_m$  and  $G_f$  denote the matrix and fibre strengths, respectively. The damage parameters  $d_m$  and  $d_f$  are used to calculate the effective elasticity tensor  $C_d$ :

$$\mathbf{C} = \begin{pmatrix} (1-d_f)C_{11} & (1-d_f)(1-d_m)C_{12} & (1-d_f)C_{13} & 0 & 0 & 0 \\ & (1-d_m)C_{22} & (1-d_m)C_{23} & 0 & 0 & 0 \\ & & C_{33} & 0 & 0 & 0 \\ & & & (1-d_f)(1-d_m)C_{44} & 0 & 0 \\ & \text{symmetric} & & & C_{55} & 0 \\ & & & & & C_{66} \end{pmatrix} \quad (1.20)$$

## Summary

Garnich et al. [49] reviewed some existing degradation models distinguishing between sudden and gradual degradation models. Sudden degradation model is based on the assumption that reaching failure criterion means that the material properties should be degraded instantaneously to a small fraction of the undamaged values or zero. Small values are commonly preferred to zero values to avoid numerical instabilities. In contrast, in gradual degradation models the material properties are reduced gradually which allows to reflect the progression of the damage. Following Hühne et al. [67], constant degradation models underestimate the load-carrying capacity delivering more conservative results, therefore gradual degradation models are considered to be more accurate.

In order to determine the initiation of damage and to examine the propagation through the structure by means of the global-local approach, the Linde criterion [86] has been chosen due to several reasons. On the one hand, this criterion already distinguishes between fibre and matrix failure which allows for the adequate reduction of corresponding material properties and for tracing the failure mechanisms responsible for the final collapse. On the other hand, although the Linde criterion does not provide an information considering the failure under compression or tension loading, it incorporates both strength values into the criterion. The main goal of the global-local method is to investigate the influence of the damage propagation at the global level taking into account reduced material properties obtained from the local level. Therefore, this leads to an assumption, that it is not essential to receive an exact type of failure load, as it does not influence the coupling procedure.

It is also important that the implementation of this criterion is relatively straightforward from the computational efficiency point of view, as it requires material properties that are easy to find experimentally and they are usually available in the literature, which means that no artificial assumptions should be done as for the case of the LaRC05 criteria, for instance. Moreover, as the determination of the fracture plane angle is not involved in the Linde criterion, extensive computations required to identify this angle for the 3D stress state case could be avoided. Besides that, the probabilistic analysis of fibre misalignments and following compressive strengths redistribution were not considered in the global-local method, as damage was calculated at both levels in a smeared way without explicit modelling of fibres and matrix.

In regard to the sophisticated IQC criterion by Vogler et al. [139], it has not been chosen for the application to the global-local framework due to the fact, that large material non-linear behaviour such as plasticity, for example, was not considered relevant to a current formulation. Plasticity may play an important role in a case of composites based on thermoplastic resins which are more ductile as compared to thermosets. Thermoplastics also demonstrate softening behaviour while heated at rather low temperatures. Whereas the mechanical behaviour is strongly dominated by fibres when loading in fibre direction, shear loading and transverse loadings are determined by matrix material. In the case of laminated stiffened panels the matrix is typically made of thermoset, also no out-of-plane loadings are expected to take place. Hence, as composite laminates with uni-directional fibres mainly exhibit brittle failure, linear elastic material model has been preferred for both global and local models until first failure occurred, and since that the material degradation was introduced.

Nevertheless, it should be noticed that the developed global-local approach is not restricted to any particular damage criterion or material degradation model. It is worth mentioning that different failure criteria might be used at the global and at the local levels as the aim of the global failure criteria is to identify the probable areas of damage, whereas the local criteria are responsible for the detailed examination of the damage.

### 1.2.1.2 Interlaminar failure

Laminated composite structures experience delamination and, in particular, skin-stringer debonding as one of the prime failure mechanisms in stiffened panels under compression, investigated by many authors to name a few: Wang et al. [141], Consentino and Weaver

[25], Balzani and Wagner [10], Raimondo and Riccio [117, 122], Krueger et al. [82], Dávila and Camanho [28], Yap et al. [146] and Falzon et al. [40].

Accurate modelling of the delamination of the full structure is computationally expensive. That is the reason for the development of the reliable global-local procedure that could be an efficient compromise allowing reduction in a simulation time on the one hand, and considering the damage onset and evolution at both levels, on the other hand.

### Delamination in composite materials

Delamination occurs under various combinations of loads leading to a significant reduction of the load-carrying capacity of the structure. Two approaches are commonly used to numerically model delamination: Virtual Crack Closure Technique (VCCT) and cohesive interface elements.

The VCCT is based on linear fracture mechanics and uses Irwin's assumption to calculate the energy release rate needed for the crack extension by taking it equal to the work required to close this crack back to its original length. Therefore the application of the VCCT is constrained to a linear elastic material with a small plastic zone ahead of the crack tip. In case of large plastic zone the amount of energy dissipation is high and assumption about work could not be used. This work is calculated from multiplication of nodal point forces and corresponding differences in nodal displacements [81]. This approach was further elaborated by Rybicki and Kanninen for application to the finite element analysis [124]. In order to determine whether the crack propagates, the calculated energy release rate has to be compared to the threshold of the critical value. The example of the four-node plane stress or plane strain elements is illustrated in Fig. 1-8 with energy release rates:

$$G_I = -\frac{1}{2\Delta a} F_{zi}(w_l - w_{l*}) \quad (1.21)$$

$$G_{II} = -\frac{1}{2\Delta a} F_{xi}(u_l - u_{l*}) \quad (1.22)$$

where  $\Delta a$  is the element's length at the crack tip and  $F_{xi}$  and  $F_{zi}$  are the corresponding forces at the crack front, superscript  $i$  denotes the nodal point,  $u_{l*}$  and  $w_{l*}$  are nodal displacements at the lower crack face and  $u_l$  and  $w_l$  are corresponding nodal displacements at the upper crack face.

The main drawback of the VCCT is, that it predicts only crack propagation assuming that the crack initiation location is known in advance. Another difficulty is related to the accurate calculation of the nodal variables for the energy release rate. It either implies the requirement of a very fine three-dimensional finite element mesh, or a remeshing technique should be applied during the analysis [134].

Cohesive Zone Modelling (CZM) is based on damage mechanics. CZM assumes existence of the softening region in front of the crack tip, a cohesive damage zone, that is resisted by the tractions. This idea originates from Dugdale [34] and Barenblatt [11]. Dugdale suggested

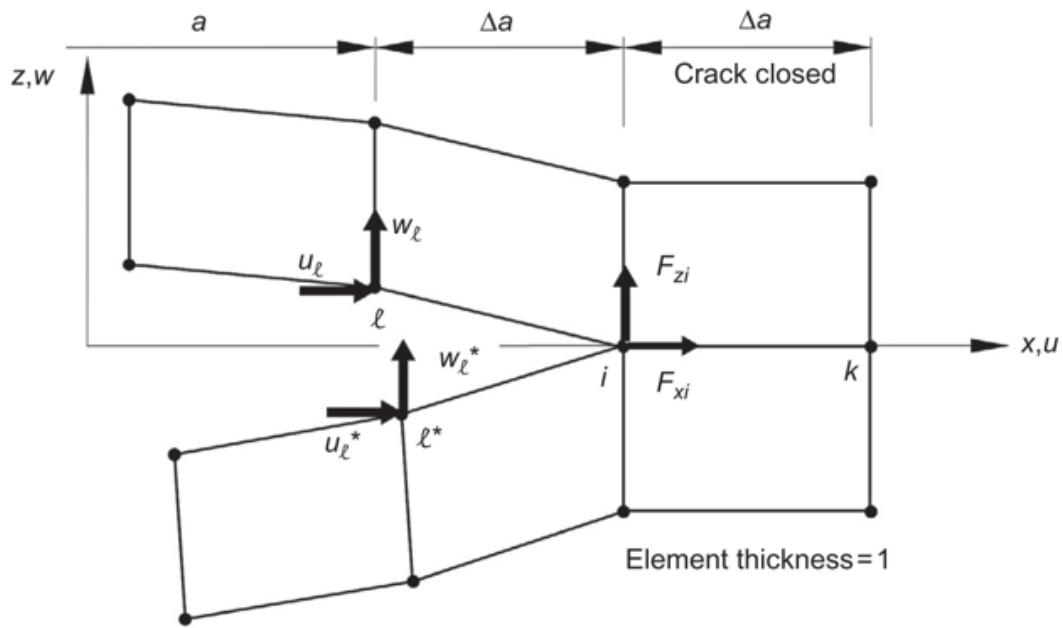


Figure 1-8: VCCT for 2D solid element with four nodes from [81].

that there is a thin plastic area ahead of the crack tip with constant stresses equal to the yield strength. Barenblatt in turn assumed that the stresses vary during the deformation process. Hillerborg [63] proposed a formulation based on this latter suggestion. The method of Hillerborg is based on continuum damage mechanics and it allows the crack to grow and, more importantly, predicts the crack initiation, which takes place when the tensile stress at the crack tip reaches the tensile strength.

Interface elements based on the CZM rely on the traction-separation law that is formulated in terms of the traction versus displacement jumps at the interface of potential crack. Under pure mode I, mode II, or mode III loadings most commonly an initially linear behaviour is assumed until the tensile strength  $\sigma_{max}$  is reached, afterwards it is followed by the softening region until the crack surfaces are completely separated which results in zero traction. Different shapes of the softening curve, such as linear, exponential or trapezoidal, have been proposed in the literature [29], [127]. The bilinear traction-separation law is shown in Fig. 1-9. The fracture toughness  $G_c$  is equal to the area under the traction-separation curve and total crack opening takes place when this toughness is dissipated completely. The penalty or initial stiffness of the interface area has to be chosen as large as possible because physically no degradation of the cohesive elements should take place at this region and perfect adhesion between surfaces is simulated and also quite low to avoid numerical issues [133].

Mixed-mode loading that could include interaction between normal and two shear modes often takes place and requires additional attention. Initiation and growth criteria should be chosen that are able to account for the interaction of complex loadings. Usually stress-based



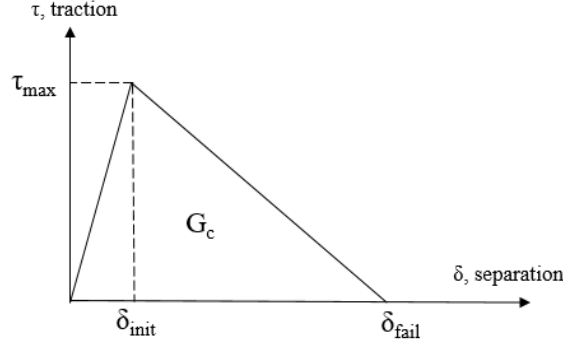


Figure 1-9: Bilinear traction-separation law.

criteria are preferred. One of the commonly used criteria predicting delamination onset is the quadratic stress criterion:

$$\left(\frac{\langle \sigma_n \rangle}{N_{max}}\right)^2 + \left(\frac{\sigma_s}{S_{max}}\right)^2 + \left(\frac{\sigma_t}{T_{max}}\right)^2 = 1 \quad (1.23)$$

Here  $\langle \dots \rangle$  represents McCauley brackets operator applied to remind that compression is generally not involved in interface separation.  $\sigma_n$  is a stress in the pure normal mode,  $\sigma_s$  and  $\sigma_t$  are nominal stresses acting in the first and second shear directions and  $N_{max}$ ,  $S_{max}$ ,  $T_{max}$  are the corresponding strengths.

One of the most commonly applied criteria for the delamination propagation under mixed-mode loading is the Benzeggagh and Kenane criterion [14] extended to three dimensional cases:

$$G_c = G_{IC} + (G_{IIC} - G_{IC}) \left( \frac{G_{II} + G_{III}}{G_I + G_{II} + G_{III}} \right)^\eta \quad (1.24)$$

where  $G_{IC}$  and  $G_{IIC}$  are mode I and II fracture toughness and  $G_I$ ,  $G_{II}$ ,  $G_{III}$  are single mode energy release rates corresponding to fracture modes I, II and III. Their sum is the total energy release rate. The parameter  $\eta$  is determined empirically [134].

A scalar damage variable  $d$  is usually utilized to identify the damage state. This damage variable changes from 0, when no damage is detected, to 1 when the crack is fully opened. Camanho et al. [22] suggested to determine the damage variable for the monotonic loading as following:

$$d = \frac{\delta_{fail}(\delta - \delta_{init})}{\delta(\delta_{fail} - \delta_{init})} \quad (1.25)$$

where  $d$  is a damage variable,  $\delta$  is a current maximum relative displacement,  $\delta_{init}$  corresponds to the displacement of the delamination beginning and  $\delta_{fail}$  is a displacement of the complete failure.

The stiffness of the cohesive element in linear traction-separation law is defined as following [22]:

$$K = \begin{cases} K_0 & \delta \leq \delta_{init} \\ (1-d)K_0 & \delta_{init} < \delta < \delta_{fail} \\ 0 & \delta \geq \delta_{fail} \end{cases} \quad (1.26)$$

where  $K_0$  is an initial penalty stiffness that is degraded after displacement  $\delta$  reaches the value of  $\delta_{init}$  and becomes 0 when the crack opening is equal to  $\delta_{fail}$ .

For the uncoupled behaviour of normal and shear components of stresses Abaqus [1] provides the following stress-strain relation for the elastic behaviour which was suggested by Dávila et al. [29]:

$$\begin{pmatrix} \sigma_n \\ \sigma_s \\ \sigma_t \end{pmatrix} = \begin{pmatrix} K_n & 0 & 0 \\ 0 & K_s & 0 \\ 0 & 0 & K_t \end{pmatrix} \begin{pmatrix} \epsilon_n \\ \epsilon_s \\ \epsilon_t \end{pmatrix} = \mathbf{K} \boldsymbol{\epsilon} \quad (1.27)$$

where  $\sigma_n$  is an out-of-plane stress,  $\sigma_s$  and  $\sigma_t$  are shear stresses and the same holds for the corresponding strains  $\epsilon_n$ ,  $\epsilon_s$  and  $\epsilon_t$ .  $K_n$  is a normal stiffness that is related to the Mode I delamination,  $K_t$  and  $K_s$  are in-plane stiffnesses responsible for the Mode II and III damage behaviour respectively. Although at that time Dávila et al. [29] used the same penalty stiffnesses for all modes, later Turon et al. [136] argued that the penalty stiffness should be mode-dependant to ensure accurate simulation results. Here strains are defined as separation displacements divided by initial thickness  $t$  of the cohesive element:

$$\epsilon_n = \frac{\delta_n}{t}, \epsilon_s = \frac{\delta_s}{t}, \epsilon_t = \frac{\delta_t}{t} \quad (1.28)$$

The Cohesive Zone Model could be implemented by means of the continuum (CCZM) or discrete (DCZM) approaches. To apply CCZM, continuum type interface elements are used to model the cohesive process zone in front of the crack tip. This technique was widely examined and extended by Allix and Ladevèze [9], Turon et al. [133], Camanho et al. [22] among others. One of the drawbacks of CCZM is a high number of cohesive elements required to mitigate mesh sensitivity. DCZM method consists of using point-wise discrete elements instead of continuum elements. This method was applied and developed by Borg et al. [19, 20], Wisnom and Chang [115], Xie and Waas [143], Hallett and Wisnom [59], Jiang et al. [70], Liu et al. [87]. To accurately predict the delamination onset and evolution the DCZM requires an accurate calculation of forces or stresses in nodes of the elements which also involves high computational costs. Therefore, a multi-scale approach could be regarded as a desirable methodology allowing reduction of the computational time with keeping required accuracy of the delamination modelling.

When applying cohesive zone modelling, it is useful to evaluate the admissibly large mesh size for the cohesive elements in order to obtain mesh-independent results. Based on the assumption about the number of cohesive elements lying in the cohesive zone, which is a distance between the crack front to the point where the cohesive traction reaches the maximum, it is possible to find a cohesive element mesh size. Following suggestion of Turon et al. [134] at least three elements in the cohesive zone are required for the delamination investigation in mode I. Moreover, Harper and Hallett [60] concluded that for the accurate numerical analysis at least three cohesive elements are required when various mode ratios are presented. The guidance about the possible determinations of cohesive zone length is summarized by Turon et al. [134], Harper and Hallett [60] and Soto et al. [128]. Following the Hillerborg [63] the cohesive zone length was defined for orthotropic materials by Yang et al. [144, 145] as a material property in an infinite body under the uniform and remote

loading in a general form [134]:

$$l_{czl} = ME \frac{G_c}{\tau_0^2} \quad (1.29)$$

where  $E$  is a Young's modulus,  $G_c$  is a fracture toughness as defined above,  $\tau_0$  is a maximum traction. Parameter  $M$  depends on each cohesive model [134] and was defined differently by the researchers. Turon et al. [134] used the Rice model [123] where the value of  $M$ :

$$M = \frac{9\pi}{32} \quad (1.30)$$

In the case of slender bodies the cohesive zone length is a material and a structural property which also depends on the laminate half-thickness  $t$  and estimated as [144]:

$$l_{czII} = \left( E_I' \frac{G_c}{\tau_{I0}^2} \right)^{1/4} t^{3/4} \quad (1.31)$$

$$l_{czIII} = \sqrt{ E_{II}' \frac{G_{IIc}}{\tau_{II0}^2} t } \quad (1.32)$$

The cohesive element mesh size  $l_e$  could be obtained from the following equation [134] assuming that the number of elements  $N_e$  in the cohesive zone is not less than three:

$$N_e = \frac{l_{czl}}{l_e} \quad (1.33)$$

According to Yang and Cox [144] the cohesive zone length is longer for mode II loading as compared to mode I. Hence, it is accurate enough to identify the required number of cohesive elements based on the formula for the mode I.

In order to overcome the necessity of using large number of cohesive elements with relatively small element size, Turon et al. [134] suggested to consider reduction of the interface strength for mode I, see Eqs. 1.34, 1.35. This approach is based on the observation conducted by Alfano and Crisfield [6] that concluded that reduction of the maximum traction allowed for a coarser mesh to be used.

$$\bar{\tau}_0 = \sqrt{ \frac{9\pi E G_c}{32 N_e l_e} } \quad (1.34)$$

$$T = \min\{\tau_0, \bar{\tau}_0\} \quad (1.35)$$

By reducing the maximum traction, the cohesive zone length is enlarged. The only drawback of this approach is that the stress concentrations near the crack tip are less accurate, but the dissipated energy is calculated properly which allows for capturing the crack evolution.

Later Turon et al. [135] also derived a relation between the interface strength of pure mode I  $\tau_{I0}$  and pure mode II loadings  $\tau_{II0}$ :

$$\tau_{II0} = \tau_{I0} \sqrt{ \frac{G_{IIc}}{G_{Ic}} } \quad (1.36)$$

This framework enables to increase the cohesive element size by using corresponding decreased interface strengths. However, caution must be taken and convergence investigations are required to determine the appropriate mesh size.

For the numerical simulation of delamination by means of the global-local approach, cohesive zone modelling strategy has been selected due to several reasons. In contrast to the VCCT, cohesive elements not only allow to explore crack propagation through the structure, but also to detect the delamination initiation. That is a clear advantage for the stiffened panels under consideration, as the delamination location is typically not known a priori. Another argument in favour of CZM, as compared to VCCT, is an existing engineering solution formulated by Turon et al. [134] that permits to use higher cohesive element sizes leading to decrease in computational efforts.

### 1.2.2 Multi-scale and global-local modelling

Multi-scale methods aim at establishing a bridging relationships between different length scales in materials with various heterogeneities. The complex nature of composite materials has given a rise to a development of multi-scale techniques to link the micro-scale behaviour that could include different nonlinearities with a constitutive response at the macro level. In terms of progressive failure analysis, multi-scale approaches offer an effective tool to capture sufficiently accurate results at the macrostructural level and to investigate the details of the damage behaviour at the microstructural level. It should be mentioned that the main advantage of these methods is that reduced complexity at the macro level and localized size at the micro level result in the considerable reduction of computational costs. An extensive overview of the multi-scale approaches is available in the literature (Ladevèze [84], Kanoute et al. [76], Talreja [130] and Aboudi et al. [2]).

Multi-scale analysis involves consideration of the model at different length scales with a clear scale separation. It should be mentioned that the term “scale” can refer to different levels of space or time. A time separation is usually employed in the cases of nonlinear dynamic analyses. In this work only multi-scale methods in terms of length scales are examined. Thus, in a current context a scale separation means that the characteristic length of the lower level is significantly smaller than the characteristic length of the upper level:

$$L_{lower} \ll L_{upper} \quad (1.37)$$

Hence, the strains and stresses at the lower level can be regarded as constant at the upper level. This condition is required for the application of the so-called classical homogenization techniques that are used to transfer the information from the lower to the upper level. Homogenization by definition means that a heterogeneous material is substituted by a homogeneous effective material and the averaging of the lower scale behaviour is performed through the Representative Volume Element (RVE) concept [62]. In contrast to the multi-scale strategies, global-local approaches do not rely on the assumption of the scale separation between different model levels as the damage evolution usually violates the scale separation.

There are several classifications of the multi-scale and global-local methods that are not

always distinct and may result in overlapping when one method would belong to different categories at the same time. However, both types of methods are referred here as coupling methods, as both scales in case of multi-scale analyses and both levels of fidelity or accuracy in case of the global-local techniques are connected, or “*coupled*”, at least in one-way, which means that the information obtained at the one level is transferred to be used at the other level. Following Katz et al. [77] and Hühne et al. [68] the coupling approaches could be regarded as tight and loose coupling methods. The term “tight coupling” denotes strategies with simultaneous solution of the equations in the global and local systems, whereas under the “loose coupling” technique the global and local systems are solved separately in time and space.

The other important classification encompasses the one-way and two-way coupling methods. During the one-way coupling the information is exchanged in only one direction either from global to local or from local to global levels. The term “two-way” analysis denotes the information transfer between both levels. The tight coupling is automatically a two-way coupling method based on the definition as the mutual interaction between both models leads to concurrent exchange of information in both directions, whereas loose coupling approach might be realized in conjunction with one-way or two-way scenarios.

Pointwise and volumewise categories have been introduced as different coupling procedures in order to distinguish between the methods with and without scale separation. The term pointwise coupling refers to the definition of the global constitutive behaviour at each global integration point through the representative volume element (RVE) defined at the local level. As for the volumewise coupling the finite volume at the global level is described by the local model’s behaviour [24].

Although many different approaches have been formulated based on the tight coupling strategy, only several methods exist nowadays that are based on the loose coupling methodology and even less methods among them enable incorporation of the two-way analysis. These methods are discussed in more detail below.

### 1.2.2.1 Tight coupling approaches

The term “tight coupling” also commonly referred as concurrent coupling [2, 93] is typically employed for the problems where all scales are treated simultaneously with a strong multi-scale coupling and interdependence.

One of the typical implementation of the tight coupling is a combination of two models where the detailed local model is inserted into the coarse global model. It might be also viewed as if a part of the global model is cut and replaced by the local model with a finer mesh. In this case analysis is performed only once and both models are calculated concurrently. There exist various approaches about how to connect these models with usually different mesh sizes and element types. Special interface elements could be used between non-matching meshes or kinematic constraints as multipoint constraints (MPCs), for instance. One of the coupling methodologies based on the multipoint constraints is described in details by Alesi et al. [5]. It is also possible to tie elements with non-matching meshes by pairing the degrees

of freedom on corresponding surfaces.

Skin-stringer debonding was analysed by Krueger et al. [82] in a composite stiffened panel through coupling a coarse shell global model with a 3D refined local model. The two models were connected to each other using multipoint constraints that made the translational and rotational motion equal on the prescribed surfaces of the global and local models.

Borrelli et al. [21] applied coupling methods based on the kinematic constraints to perform tight global-local analysis of initially delaminated stiffened panel. Shell elements were used in the coarse global area, whereas the local area surrounding delamination was modelled with solid elements and a finer mesh. Modified virtual crack closure technique (MVCCT) was applied to model delamination. The results were compared to the reference model with solid elements.

Pietropaoli and Riccio [106] used global-local approach for examination of interlaminar and intralaminar damage onset and growth in composite stiffened panels. Global and local models were tied by interface elements based on coupling equations between the degrees of freedom. Delamination between two layers was modelled by means of multipoint constraints and VCCT was implemented to observe the delamination growth.

Yap et al. [146] performed damage analysis with a focus on a skin-stringer debonding in stiffened composite panels. Meshing discontinuity between the coarse global and refined local model regions was solved by imposing interpolation constraints between nodes of different regions.

Another multi-scale strategy that could be allocated to the group of tight coupling methods implies a definition of the macroscopic constitutive behaviour through the microscopic material modelling including complex mechanisms and various nonlinearities. A representative volume element is assigned to each integration point of the macroscopic model and a numerical homogenization procedure is performed to estimate the macroscopic effective properties from the microlevel calculations, such as effective stresses and effective material tangent, for example. Both models are separated spatially but are solved in parallel with an iteratively coupled scheme to connect both scales. This method could be computationally expensive especially if material nonlinearities and large deformations and rotations are considered. Firstly proposed by Renard et al. [121], this method was further elaborated by Feyel et al. [41], Terada and Kikuchi [132], Ghosh et al. [53], Ghosh et al. [54], Radhavan and Ghosh [116], Miehe et al. [96], Miehe et al. [97] and Miehe and Koch [95] among others. Progressive damage analysis with reduction of the material stiffness was performed by Zohdi et al. [147]. Among these approaches a multi-scale method called  $FE^2$  has been formulated and developed in a general manner by Feyel [41], Feyel and Chaboche [43] and Feyel [42] relying on the coupled numerical homogenization. In this context  $FE^2$  means that both separate scales are treated simultaneously which allows to consider the heterogeneous behaviour of the structure through a multi-scale method. In this case two boundary problems are solved concurrently, and the mechanical behaviour is modelled at the microscale. A localization rule is utilized to find local solutions by applying strains from the macroscopic solution to the RVE of the micro problem. In turn, the homogenization rule is applied to determine the macroscopic stress tensor by averaging of the microscopic stress of each

RVE assigned to the macro integration point. Further extension of this method has been proposed by Geers and al. [50], Kouznetsova et al. [78] and Kouznetsova et al. [79] as so-called second-order homogenization. As compared to the first-order homogenization a full second-order extension gradient is employed at the macrolevel which allows to alleviate the mesh dependency through incorporating the length scale and to account for the presence of moderate localization. More recently Oliver et al. [101] utilized the  $FE^2$  approach to model propagating fracture.

Some hierarchical methods could also belong to the tight coupling methodology. In these methods the scales are linked sequentially, which means that the same domain is solved on different scale levels and only the area of interest is explored at the microscale. Both scales are typically coupled through averaging of the volume microscopic gradients that are imposed at the macroscale and the localization procedure that allows for transferring the macro boundaries to the microscale. In this framework lie several methods. Zohdi et al. [148] and Oden and Zohdi [100] formulated so-called Homogenized Dirichlet Projection Method (HDPM). Belytschko and al. [13] proposed a spectral overlay method for problems with high gradients. Fish [44] introduced the s-version of the finite element method that is based on superimposing meshes of higher-order elements. Multigrid methods for heterogeneous materials were developed by Fish and Belsky [45, 46], Fish and Chen [47], Bayreuther et al. [12] and Miehe and Bayreuther [94]. An adaptive hp-version of the finite-element method was elaborated by Rank [118], and Krause and Rank [80]. Hughes et al. [66] and Garikipati and Hughes [48] worked on variational multi-scale methods. Domain decomposition methods were used by Zohdi and Wriggers [150], Ladevèze [84, 85], Kadowaki and Liu [75], Allix et al. [8], Saavedra et al. [125]. Coupled volume approach was presented by Gitman [55], Gitman et al. [56]. Mesh superposition technique without transition region was proposed by Park et al. [105]. Pineda and Waas [108], and Pineda et al. [107] applied generalized method of cells to perform multi-scale progressive failure analysis.

### 1.2.2.2 Loose coupling approaches

During the loose coupling analysis the global and local models are calculated sequentially and linked through the information exchange in one or two directions. In this case the global and the local models are typically analysed independently and the local models overlap the global model in certain regions of interest to obtain detailed results. The refinement is commonly performed by the submodeling procedure which transfers interpolated displacements as boundary conditions from the global to the local level. While the geometry and the coarse mesh of the global model commonly remain intact during the loose coupling analysis, various averaging techniques exist to enable the update of the global material behaviour.

#### One-way loose coupling

One-way loose coupling approach usually applies the submodeling, or so-called zooming technique in order to investigate the critical area of the coarse global model with a refined independent local model analysis [118]. The information exchange is executed in one direction, typically from the global to the local model. The method relies on St. Venant's

principle, that means that the global boundary conditions introduced instead of actual distribution of stresses and strains would affect the solution only at the boundaries of the local problem [51]. That could be used as a guidance into definition of the correct local model size as the boundaries of the local model should lie away from high stress and strain gradients. This method was successfully applied for one-way global-local transition without clear scale separation by Mote [98], Hirai et al. [65], Noor [99] and Sun and Mao [129], for example. Several methods link results in the opposite direction from the microscale to the macroscale. The effective properties of the heterogeneous material with damage are defined at the microscale to be used in a macroscopic analysis by Zohdi and Wriggers [149], Löhnert [88], plastic deformations have been considered by Reese in meso-macro method [119]. Micro-meso-macro multi-scale procedure including material damage and plasticity in textile composites based on the transition of the homogenized stress-strain curves from the lower to the upper level was formulated by Ernst [37], Ernst et al. [38].

Faggiani and Falzon [39] presented an optimization technique based on a genetic algorithm to improve the damage resistance for the skin-stringer interface in the postbuckling regime of stiffened panels by finding an optimized stacking sequence. The authors made use of a one-way global-local method in their optimization analysis and employed submodeling procedure.

Orifici et al. [104] formulated a one-way global-local approach for detection of the initiation of delamination between the skin and the stiffener in the stiffened panels during postbuckling regime. After completion of the global model analysis with a coarse mesh, several local models were created along the skin-stringer interface in order to find out if the delamination between the skin and the stringer started. For that reason a strength-based criterion was applied at the local level. The initiation of the skin-stringer separation was considered critical for the panel and no further investigations on the delamination propagation were conducted.

Reinoso et al. [120] examined the skin-stringer debonding in a composite panel by means of both one-way loose coupling and also tight coupling approaches. During the one-way coupling procedure, the submodeling technique was employed to assign displacements as boundary conditions from the global to the local level. Cohesive elements at the local level represented the interface layer, whereas solid elements were used for this layer at the global level. The tight coupling was carried out through the so-called shell-to-solid coupling methodology [1] which is in fact a subtracting of the critical region from the global shell model and replacing it by the detailed local region of solid elements. A coupling between two models was enabled through the constraint relations introduced on the boundary surfaces between two models.

A one-way global-local analysis for the Omega-shaped multi-stringer panel loaded in compression was suggested by Vescovini et al. [138]. Both global and local models were composed of shell elements. Cohesive elements were applied between the skin and the stringer in the local models for determination of delamination initiation and growth. Local models that were created by means of submodeling procedure had pre-determined size and local analysis was performed five times moving the local model along the stringer.



### Two-way loose coupling

During a two-way loose coupling analysis both levels are linked through the information passing between the global and local levels in both directions, accounting for interactions of global and local effects. For the time being only several two-way loose global-local methods have been elaborated that can treat global and local models separately. Whitcomb [142] proposed an iterative procedure to enforce equilibrium between global and local solutions. The displacements from the global analysis were used as boundary conditions for the local model. The correction of global displacements was obtained after local model analysis. Similarly, Mao and Sun [92] suggested to improve their original one-way coupling strategy [129]. Along the boundaries of the refined local model the displacements from the coarse global model's computations were introduced, whereas within the local model, the original external forces were prescribed. After completion of the local model analysis, the displacement contribution was calculated for each global element based on the resulting local model displacements. This global-local procedure could be repeated iteratively to obtain further accuracy.

The multi-scale projection method by Löhnert and Belytschko [89] was based on the extended finite element method (XFEM) to model fracture and crack propagation and to examine the macrocracks and microcracks interactions leading to damage. XFEM allows to model an arbitrary number of cracks with not known crack propagation paths without remeshing. As the microcracks in the vicinity of the macrocrack front lead to high stress and displacement field gradients, these areas require modelling of detailed interaction of the cracks, whereas at the macro level only macrocracks can be considered. In this approach both scales were separated and numerical simulations were carried out independently. The meshes were congruent which means that for any element at the upper scale there existed a set of elements at the lower scale in the region of interest. The displacements were transferred as boundary conditions from the coarse to the fine scale, whereas fine scale stresses were returned into the coarse scale equations.

Chrupalla et al. [23] formulated the homogenization-based iterative two-way multi-scale approach (HIMSA) to account for local effects on the global behaviour of composite structures. Similarly to previous methods, displacements from the global model were assigned to the local model's boundaries. The local-to-global coupling was executed through the transfer of the averaged stresses that were calculated for each global integration point and then updated global tangent stiffness operator was determined.

Labeas et al. [83] presented an adaptive progressive damage modelling technique to predict the damage initiation and evolution in composite structures based on the submodeling procedure. The Hashin criterion [61] was applied at the global level to identify the damaged areas, whereas degradation of material stiffness took place at the local level. The degraded material properties for the global model were calculated based on the mean values of the local engineering constants obtained after damage evolution. Then following reduction of the material properties at the global level, the structural equilibrium was established as the stress redistribution can result in new material failures. Thus, the global-local procedure had to be repeated until no new damage evolution was detected. Only afterwards the load was increased and the global-local modelling was performed until the catastrophic failure took place.

The non-intrusive global-local coupling for problems with local plasticity by Gendre et al. [52] connected a global linear elastic model with a nonlinear local model which replaced the global model in the area of interest. The models were linked iteratively in a non-intrusive way implying that both models were never modified or updated during the analysis. After performing global elastic computations each iteration consisted of three steps, see Gendre et al. [51], Allix et al. [7]. First, the submodeling technique was applied to prescribe global displacements or mixed boundary conditions to local model's boundaries. Secondly, the residual load vector was calculated based on the unbalance between the nodal forces of the coarse and the fine models. In case the magnitude of the residual load was small enough, the iterative procedure was terminated. Lastly, the residual load was applied to the global model to introduce the detailed model's influence. Further discussion on the non-intrusive method with a special attention on a coupling between 2D and 3D models was performed by Guguin et al. [57] and a detailed overview of this method was given by Duval et al. [35].

Following non-intrusive coupling methodology and based on previous research on explicit dynamic ([15, 16]) Bettinotti et al. [17] formulated a so-called substitution method for modelling delamination. A numerical analysis was conducted that allows concurrent run of global and local models for a composite panel under high-velocity impact. A refined local model replaced the region of the coarse global model where more accurate solution was required with boundary conditions applied from the global model. The global analysis with linear elasticity was repeated with updated nodal forces from the local solution applied at the interface that connects both models.

El Said et al. [36] proposed a multi-scale modelling approach for the 3D woven composites based on the domain decomposition. An iterative process was performed to ensure compatibility of forces and displacements at the interface of macro and meso models to reduce artificial stress concentrations on the boundaries. A progressive damage model was included that was able to track the stress redistribution after the damage occurred.

The global-local strategy formulated by Orifici et al. [102] could be also regarded as the two-way global-local method. This global-local methodology was dedicated to the detection of the initiation of the delamination between the skin and the stringer in the postbuckling regime of stiffened panels. Both global and local models were treated separately. After the coarse analysis of the global model was conducted, the obtained displacements were used as boundary conditions for the refined local models. Delamination onset was predicted at the local level where 3D stresses were calculated accurately, whereas the subsequent global analysis utilized the VCCT to simulate delamination propagation. Hence, in contrast to the described above two-way global-local techniques, the initiation of the damage was predicted at the local level and further damage evolution was modelled at the global level. In previous approaches the global model was assumed to behave linearly and only the effect of the local nonlinearities was introduced at the global level.

The two-way loose global-local coupling approach proposed by Hühne [68] for the progressive failure analysis differentiates from other techniques by alternative and more accurate homogenization methodology for matrix and fibre failure which ensures that the effect of material intralaminar degradation is accounted for properly at the global level. The method is illustrated in Fig. 1-10 for the case of the stiffened panel where the coupling steps are

repeated until the final collapse of the structure is attained. Hence, the coupling step consists of three major operations that are repeated iteratively at two levels of accuracy:

1. Global analysis with a coarse mesh and linear material behaviour is conducted to evaluate the areas of a probable damage and to define local models' geometry;
2. Local models with refined mesh and nonlinear material behaviour obtain displacements as boundary conditions from the global model solution. After carrying out numerical calculations for local models, degraded engineering constants are extracted;
3. Local part tests are performed and effective material properties for the global model are obtained and transferred to the global model.

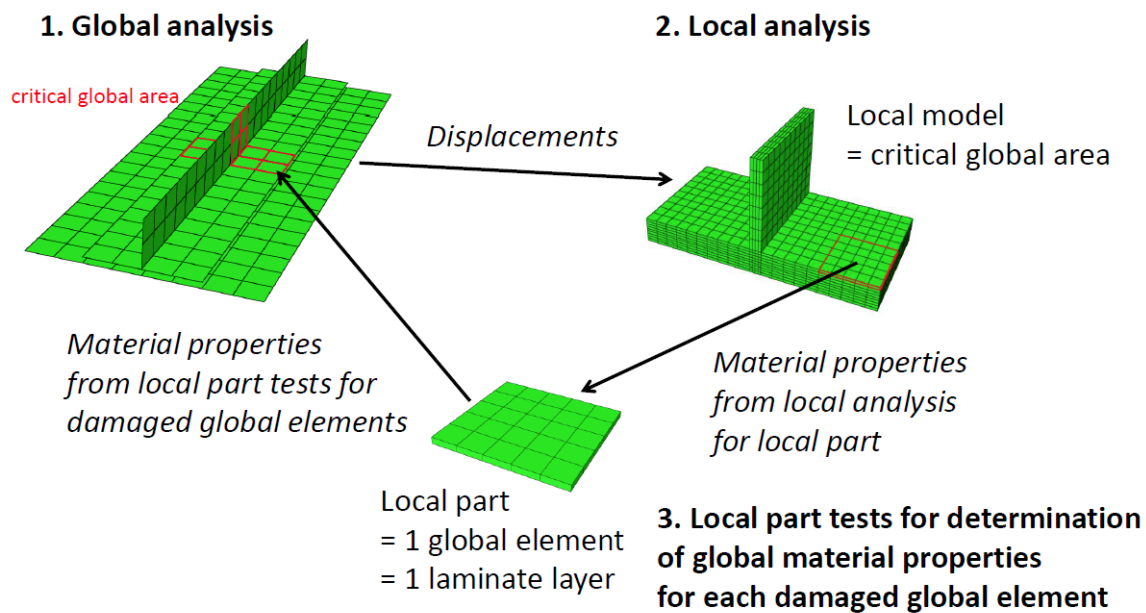


Figure 1-10: Overview of two-way loose coupling procedure with stiffened panel [68].

After the completion of the global-local coupling step, the global model analysis is repeated to check whether the stress redistribution induced by degraded material properties results in the appearance of new critical areas or an extension of existing ones. The global-local procedure is performed until no new intralaminar damage initiation is detected at the prescribed displacement level under consideration. Only then the applied load at the global level is increased and thereby the next “global-local coupling step” is initiated. The procedure is repeated until final failure of the structure is detected.

The skin and the stringer of the panel in the global model are represented by conventional shell elements using one element through the thickness including all laminate layers in order to reduce computational costs. The coarse model with linear elasticity at the global level is used to identify the areas where matrix or fibre failure are expected to take place by applying the Linde criterion [86]. Based on these critical areas at the global level, local models with finer 3D mesh are created through the shell-to-solid submodeling procedure

with displacements from the global solution served as the boundary conditions. These local models include the discussed above material degradation model by Linde [86]. After completion of the local models' numerical analysis the degraded engineering properties are extracted and local part tests are carried out. It is important to notice that direct application of the degraded properties from the local to global level is not possible due to the mesh size difference between two models. That is the reason to apply the homogenization approach formulated by Hühne et al. [68] for this case to obtain the effective global degraded properties. The concept of "local part tests" is introduced following the material homogenization procedure described by Ernst [37], the special displacement boundary conditions could be found in Hund and Ramm [69]. Below the local part tests are presented in detail.

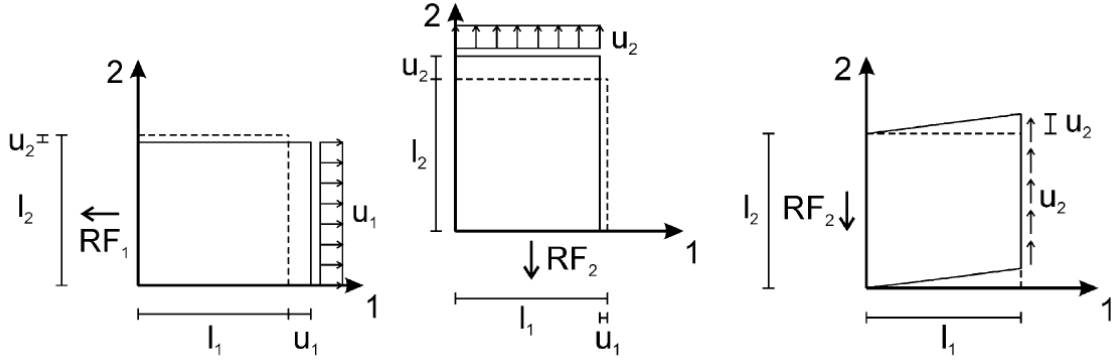


Figure 1-11: Local part tests (Left: Test 1, Middle: Test 2, Right: Test 3) [68].

Each global element ply obtains corresponding new reduced material properties after completion of three linear characterization tests that follow the assumption of a plane stress state at the global level. First, two tension and one shear tests are performed in order to determine the Young's modulus in longitudinal and transverse directions,  $E_{11}$  and  $E_{22}$ , respectively, Poisson's ratio  $\nu_{12}$  and the shear modulus  $G_{12}$  which is demonstrated in Fig. 1-11:

1. Test 1. Tension in global 1-direction:

$$E_{11} = \frac{\sigma_{11}}{\epsilon_{11}} \quad (1.38)$$

$$\nu_{12} = -\frac{\epsilon_{22}}{\epsilon_{11}} \quad (1.39)$$

2. Test 2. Tension in global 2-direction :

$$E_{22} = \frac{\sigma_{22}}{\epsilon_{22}} \quad (1.40)$$

3. Test 3. Shear in global 1-2 plane:

$$G_{12} = \frac{\tau_{12}}{\gamma_{12}} \quad (1.41)$$

Composite laminate usually consists of several lamina with different fibre orientations. Thus,

an additional transformation from the global to the local directions is required for fibre orientations aside from those with  $0^\circ$  orientation as the degraded engineering constants are defined in global direction regardless of the initial orientation. Hühne et al. [68] formulated the following transformation procedure. First, a partly unknown global stiffness matrix  $\mathbf{Q}$  is formed where the values  $Q_{11}$ ,  $Q_{22}$ ,  $Q_{33}$ ,  $Q_{12}$  and  $Q_{21}$  are determined from the results of local part tests:

$$\mathbf{Q} = \begin{pmatrix} Q_{11} & Q_{12} & Q_{13} \\ Q_{21} & Q_{22} & Q_{23} \\ Q_{31} & Q_{32} & Q_{33} \end{pmatrix} \quad (1.42)$$

$$Q_{11} = \frac{E_{11}}{1 - \nu_{12}^2 \frac{E_{22}}{E_{11}}} \quad (1.43)$$

$$Q_{22} = \frac{E_{22}}{1 - \nu_{12}^2 \frac{E_{22}}{E_{11}}} = \frac{E_{22}}{E_{11}} \cdot Q_{11} \quad (1.44)$$

$$Q_{12} = Q_{21} = \nu_{12} \cdot Q_{11} \quad (1.45)$$

$$Q_3 = G_{12} \quad (1.46)$$

and  $Q_{13}$ ,  $Q_{23}$ ,  $Q_{31}$  and  $Q_{32}$  are initially unknown. The values of the local stiffness matrix  $\mathbf{Q}'$  are unknown except for the fact that some entries are zero as the layers are transversely isotropic in local directions:

$$\mathbf{Q}' = \begin{pmatrix} Q'_{11} & Q'_{12} & 0 \\ Q'_{21} & Q'_{22} & 0 \\ 0 & 0 & Q'_{33} \end{pmatrix} \quad (1.47)$$

The transformation matrix  $\mathbf{T}$  that relates these two matrices is defined by:

$$\mathbf{T} = \begin{pmatrix} \cos^2\theta & \sin^2\theta & \sin\theta\cos\theta \\ \sin^2\theta & \cos^2\theta & -\sin\theta\cos\theta \\ -2\sin^2\theta & 2\sin\theta\cos\theta & \cos^2\theta - \sin^2\theta \end{pmatrix} \quad (1.48)$$

where  $\theta$  is a fibre orientation in global coordinates. Thus, the unknown coefficients are found from solving:

$$\mathbf{Q} = \mathbf{T}^T \cdot \mathbf{Q}' \cdot \mathbf{T} \quad (1.49)$$

Finally the system of nine equations and nine unknowns that actually is formed by Eq. 1.49 is solved and the engineering constants in the local direction that correspond to fibre orientation are found. It is important to mention that the system is solved for each lamina ply.

Another procedure for the transformation of engineering constants has been proposed by Akterskaia et al. [3]. It has been motivated by the need to enhance the approach by Hühne et al. [68] for the plies with fibre orientation of  $\pm 45^\circ$ . The previously described technique regarded material with these fibre directions at the global level as isotropic as there is not enough information concerning the transverse isotropy and both Young's modulus in longitudinal and transverse directions are close values after local part tests in global coordinates. Thus, after rotation by  $\pm 45^\circ$  both Young's modulus remain identical. The new process to transform obtained properties from the principal material coordinates to the local

coordinates of the global model is performed following Jones [71]:

$$\frac{1}{E_x} = \frac{1}{E_1} \cos^4 \theta + \left( \frac{1}{G_{12}} - \frac{2\nu_{12}}{E_1} \right) \sin^2 \theta \cos^2 \theta + \frac{1}{E_2} \sin^4 \theta \quad (1.50)$$

$$\nu_{xy} = E_x \left( \frac{\nu_{12}}{E_1} (\sin^4 \theta + \cos^4 \theta) - \left( \frac{1}{E_1} + \frac{1}{E_2} - \frac{1}{G_{12}} \right) \sin^2 \theta \cos^2 \theta \right) \quad (1.51)$$

$$\frac{1}{E_y} = \frac{1}{E_1} \sin^4 \theta + \left( \frac{1}{G_{12}} - \frac{2\nu_{12}}{E_1} \right) \sin^2 \theta \cos^2 \theta + \frac{1}{E_2} \cos^4 \theta \quad (1.52)$$

$$\frac{1}{G_{xy}} = 2 \left( \frac{2}{E_1} + \frac{2}{E_2} + \frac{4\nu_{12}}{E_1} - \frac{1}{G_{12}} \right) \sin^2 \theta \cos^2 \theta + \frac{1}{G_{12}} (\sin^4 \theta + \cos^4 \theta) \quad (1.53)$$

This transformation methodology is faster on the one hand as it does not require the matrix inversion and solving nine equations. On the other hand, these equations allow to determine more accurately engineering constants of arbitrary lamina orientation.

### 1.2.3 Summary

The discussed above methods mainly differ in the approaches used to determine how to degrade material properties and how to transfer the results back from the local to the global level. The submodeling approach is a commonly used practise for the global-to-local exchange of information, but there are only limited amount of works that deal with the data transfer in the opposite direction. In order to investigate the overall structural behaviour until the final collapse it is paramount to perform a full progressive failure analysis which implies reflecting the damage induced behaviour from the local to the global level.

Moreover, it is expected that the initial damage is localized and it is important to account for the growth of the damaged area within the local model. Thus, the two-way loose coupling approaches are preferred as they enable to change the local model's size and geometry in contrast to tight coupling methods where the local model is predefined from the beginning and is tightly connected to the global model which prohibits the simple adaptation of the local model's size during the analysis.

Moreover, among the global-local methods, the two-way coupling approaches are mainly adapted for the intralaminar damage, while there is a gap regarding the two-way coupling methods for the simulation of the interlaminar damage, particularly a skin-stringer debonding as one of the main critical damage mechanisms of stiffened panels.

## 1.3 Research objectives

The aim of the present work is to make a step toward bridging the current and future scenarios described above. That means that an efficient and reliable method for modelling progressive failure analysis suitable for large stiffened panels has to be developed. This method should enable a consideration of the most relevant damage mechanisms that can influence pre-

ture failure of the composite structure in order to simulate a realistic damage scenario. To achieve this goal within a computationally effective framework, a multi-scale approach with a two-way coupling strategy is the most suitable tool. As has been advocated above, a fast computational model with a relatively coarse mesh and elastic material properties is required on the one hand. On the other hand, the detailed local model that includes material damage characteristics should be created. The coupling mechanism between both levels of fidelity is required to enable the global model to include the damage effects. Matrix cracking and fibre breakage as well as skin-stringer debonding are considered as main damage mechanisms.

The developed global-local method establishes a reliable two-way coupling procedure for modelling skin-stringer separation in large stiffened panels and enhances results obtained by Hühne [68] for the intralaminar damage. This approach allows to predict the damage onset and evolution with no preliminary knowledge about the type of failure or expected damage location in a fast and efficient manner. Moreover, introduced formulation of the global-local numerical simulation of the skin-stringer debonding ensures that dissipated energy is preserved to be equal at both global and local levels. This method contributes to the mechanical virtual testing leading to possible decrease in monetary expenses spent on the experimental testing. Thereby, based on the knowledge of the structural performance and the damage behaviour obtained through this global-local coupling strategy the safety region of the operational flight conditions could be shifted leading to less conservative design and cost reductions.

## 1.4 Outline and connection of publications

As a first step, described in Chapter 2 (Paper A), a two-way coupling global-local finite element approach has been modified in order to eliminate undesired stress concentrations leading to more accurate local model analysis results. The updated method has been validated on an example of a large composite panel with intralaminar damage.

In the next step, a two-way coupling global-local finite element approach for modelling skin-stringer separation of stiffened composite panels has been developed, which is presented in Chapter 3 (Paper B). The method also couples discrete and continuum elements on different scale levels and ensures smooth transition of the damage information between both levels. An experimentally tested stiffened panel with an initial debond between the skin and the stringer has been simulated by means of the developed approach.

Following previous results, a combination of intralaminar damage and skin-stringer separation has been modelled through a global-local coupling method which allows for observation of progressive damage evolution similar to that shown in actual structures. These results are introduced in Chapter 4 (Paper C). The numerical calculations of the two-way coupling approach has been validated against existing experimental results demonstrating significant reduction of computational costs as compared to the full reference analysis.

An essential enhancement of the global-local coupling approach was introduced through preserving energy dissipated due to skin-stringer separation between the global and local levels, which is displayed in Chapter 5 (Paper D). Single-mode and mixed-mode loadings

were considered and tested on a double cantilever beam (DCB) and an end notched flexure (ENF) tests, following by mixed-mode bending (MMB) test. Afterwards an updated global-local approach was applied to a case of one-stringer composite panel to investigate the skin-stringer debonding.

To conclude, the last Chapter 6 illustrates a global-local method enriched by the procedure that allows to ensure the preservation of the dissipated energy due to the interlaminar damage between the global and local levels. This updated method is validated on the case of a large curved stiffened panel experiencing intralaminar damage and skin-stringer debonding following by comparison with experimental results.



## **2 Paper A: Efficient progressive failure analysis of multi-stringer stiffened composite panels through a two-way loose coupling global-local approach**

The following paper is published in *Composite Structures*, Volume 183 (2018), pages 137-145 (<https://doi.org/10.1016/j.compstruct.2017.02.011>). The main work was done by the author of this thesis.

The two-way global-local coupling method including intralaminar failure has been extended based on the framework of Hühne et al. [68]. First of all, improved rules for the choice of the size of local models were introduced followed by mesh dependency studies. Then, a two-stringer panel with initial debonding was analysed with an aim to investigate the structure with the localized damage and, thus, to attain the desired advantage in computational costs as compared to the reference solution. A full 3D reference model consisted of solid elements with material degradation modelling. Load-displacement curves of the coupling analysis and the reference analysis were in reasonably good agreement. The maximum load levels predicted by both analyses and the sequence of damage occurrence also proved the validity of the global-local method. Finally, a large five-stringer panel was examined to demonstrate a potential of the developed approach. In this case a reference model with shell elements and material degradation was used for a comparison as usage of solid elements of refined mesh size was prohibitively expensive from the computational point of view. A good agreement between both analyses was obtained. The global-local curves were also compared to the available experimental results. Although a small difference in the prebuckling stiffness was observed, the postbuckling response was in good agreement.

It might be concluded that the global-local approach demonstrated the potential to be effectively applied to large composite panels with a localized damage to explore the intralaminar failure initiation and propagation until final collapse.

Contents lists available at [ScienceDirect](https://www.sciencedirect.com)

# Composite Structures

journal homepage: [www.elsevier.com/locate/compstruct](http://www.elsevier.com/locate/compstruct)

## Efficient progressive failure analysis of multi-stringer stiffened composite panels through a two-way loose coupling global-local approach



Margarita Akterskaia, Eelco Jansen\*, Sina Hühne, Raimund Rolfes

Institute of Structural Analysis, Leibniz Universität Hannover, Appelstr. 9A, 30167 Hannover, Germany

### ARTICLE INFO

#### Article history:

Available online 9 February 2017

#### Keywords:

Composite structures  
Stiffened panels  
Progressive failure analysis  
Multiscale analysis  
Global-local method  
Postbuckling

### ABSTRACT

A two-way coupling global-local finite element approach which has demonstrated its potential on the basis of representative test cases in earlier work, is used for the progressive failure analysis of large stiffened composite panels. In order to realize the capability of the approach to analyze larger panels, the efficiency of the analysis is enhanced and improved rules for the choice of the size of local models are developed.

The potential to carry out a progressive failure analysis for large stiffened panels is illustrated firstly through the analysis of a two-stringer panel with a local defect, in which the adjusted rules to define the local models are applied, and subsequently concretized by applying the approach to a large stiffened composite panel with five stringers. A comparison between the results of the global-local coupling analysis and a reference analysis with shell elements including degradation is presented and the results are discussed. The results of the numerical analyses of the large panel are also compared with experimental results available.

© 2017 Elsevier Ltd. All rights reserved.

## 1. Introduction

Due to their favorable strength-to-weight ratio and stiffness-to-weight ratio, fiber-reinforced composites are often used in aircraft applications. For post-buckled designs, an efficient analysis capability for the nonlinear finite element analysis of panel-type structures is required. For design scenarios in which material degradation can occur before the failure load is reached, a capability of a progressive failure analysis should be available in order to predict the failure load of the structure with sufficient accuracy. Two-way loose coupling methods provide a possibility to simulate the postbuckling progressive failure behavior of a panel-type structure in an efficient way. In the present work a two-way coupling global-local finite element approach which has demonstrated its potential on the basis of representative test cases in earlier work, is used for the progressive failure analysis of large, multi-stringer stiffened composite panels.

### 1.1. Progressive failure of multi-stringer stiffened panels

As stiffened composite panels are widely applied in aircraft design, they are used as typical modeling cases in the present paper. Stiffened panels usually consist of a straight or curved plate, the skin, strengthened by longitudinal stiffeners, also referred to as stringers. Compression load, which is one of the basic loads for this kind of panels, is considered in this paper. However, the loose-coupling method is not limited to this type of load. To describe the structural behavior of the thin stiffened panel under compression, it is useful to remember that usually linear behavior is followed by initial buckling [1], in which the skin is expected to buckle, while the stringers often do not show any significant deformation. The overall stiffness of the panel is reduced, but the structure is still capable of withstanding increased loads. When the compression load is increased, the stringers eventually also start to buckle leading to failure of the panel as a whole. This is associated with a sudden drop of the load-displacement curve.

To date, experiments on postbuckling behavior of curved and flat panels with several stringers have been performed by several authors [2–6]. Structural modifications and imperfections, such as holes and debonding between skin and stringer, were also considered. Degenhardt et al. [2] described the testing of a stiffened

\* Corresponding author.

E-mail addresses: [m.akterskaia@isd.uni-hannover.de](mailto:m.akterskaia@isd.uni-hannover.de) (M. Akterskaia), [e.jansen@isd.uni-hannover.de](mailto:e.jansen@isd.uni-hannover.de) (E. Jansen).

panel and an unstiffened cylinder. In the work of Orifici et al. [3], multi-stringers composite panels were tested experimentally, and analyzed numerically under compressive loading. The panels showed matrix and fiber damage as well as delaminations between skin and stiffener and in the stiffener blade area before the final failure occurred. Lauterbach et al. [4] experimentally tested intact and predamaged five-stringer curved CFRP (carbon fiber reinforced polymer) panels with compressive axial load until final collapse. The numerical analysis took into account delamination, matrix, fiber cracking and matrix-fiber shear failure with a corresponding reduction of material properties, though discrepancies between experimental and numerical results were observed, especially in the stiffness evaluation and total failure load. In another study conducted by Zimmermann et al. [5], experimental data on the buckling and postbuckling behavior of stiffened curved composite panels were obtained. Panels with an even and odd number of stiffeners, different ratios of curvature and different skin thickness were examined. Wagner and Balzani [6] applied shell elements to model a five-stringer laminated panel, by using a brittle material degradation model and comparing it to experimental results. Matrix, fiber and matrix-fiber debonding were considered as damage mechanisms, and the extended Hashin criteria were utilized.

### 1.2. Coupling methods

In the last few decades, coupling methods have attracted attention because of their efficiency meeting the needs of progressive damage analysis. Global-local coupling analyses are based on the following idea. On the one hand, at the global level sufficiently accurate results are obtained at relatively low computational cost. On the other hand, analysis at the local level, with a smaller area of interest, could regard in detail geometrical and material nonlinearities usually ignored during the global analysis.

The submodeling technique or so-called zooming technique was successfully applied in the past for one-way global-local transition in order to obtain accurate results at the local level. Examples can be found in the works of Mote [7], Noor [8], Mao and Sun [9], and Whitcomb [10]. In contrast, during a two-way coupling, the information is exchanged in both directions, accounting for interactions of global and local effects. To cite a few of the recent global-local approaches, the multiscale projection method by Löhnert and Belytshchko [11] and the adaptive progressive damage modeling technique by Labeas et al. [12] are to be mentioned. Two-way loose coupling methods [13–15] provide a promising way to analyze various types of nonlinear structural analysis problems in an efficient way.

The global-local method proposed by Hühne [15] has been applied in the context of postbuckling problems of composite structures with damage and makes use of an efficient homogenization technique for the degraded material properties that are transferred from the local to global levels.

In the approach proposed by Hühne et al. [15], the postbuckling behavior is analyzed through an analysis with a global model discretized with shell elements and the areas in which damage can be expected to occur are identified. In order to obtain these critical damaged areas, a global analysis is performed. The critical regions are examined during the next step – local analysis with solid elements and a finer mesh element discretization. Displacements from the global model are transferred to the selected boundary nodes of the local model by means of the shell-to-solid submodeling available in Abaqus [16]. The material model by Linde et al. [17] is used to define the material degradation. After calculation of the degraded properties, so-called local part tests are carried out layerwise, in order to obtain equivalent properties for each global element and to transfer them back to the global model. With the new global degraded properties, a restart of the global

analysis from the last critical state is carried out. These coupling steps are repeated so long as convergence in reaction forces in the direction of applied load has not been obtained.

### 1.3. Outline

The two-way coupling global-local finite element approach described in [15] has proven its potential on the basis of representative test cases, in particular a one-stringer panel. In the present work, the approach is used for the progressive failure analysis of large stiffened composite panels. In order to realize the capability of the approach to analyze larger panels, the efficiency of the analysis is enhanced and improved rules for the choice of the size of local models are developed. The potential to carry out a progressive failure analysis for large stiffened panels will be shown in a first step through the analysis of a two-stringer panel with a local defect, and furthermore by analyzing a large stiffened composite panel with five stringers.

## 2. Enhancements of the two-way coupling approach for multi-stringer panels

As a necessary prerequisite for the efficient analysis of large panels using the loose coupling global-local approach presented by Hühne [15], the appropriate definition of the local models within this approach is addressed in the following. The objective of this section is to formulate a guideline for the creation of local models for thin stiffened panels, thereby proposing a modification of the approach used in earlier work. A typical one-stringer panel test case is analyzed to check the appropriateness of the new formulation. In addition, a study on the mesh convergence in the local areas is conducted in order to check the influence of the mesh element size refinement on the damage evolution.

### 2.1. Local model definition

The submodeling technique is used to investigate the detailed behavior of a particular region of the structure [18]. In order to define the regions which should be included in the local model, in the following the identification of these areas of interest is addressed, requiring an understanding of the behavior of the structural parts adjacent to the structural element in which damage is detected.

For stiffened panels under compression, after each global analysis, all parts of the panel are checked for damage. This check eliminates the risk of missing the failure initiation in a particular area. Therefore, there is no need to immediately consider all three structural elements – skin, stringer foot and stringer web – together in one local model, if, for example, only the stringer foot is damaged at the global level. This important assumption should decrease the size of the local model and become a new guideline for an appropriate definition of the local model geometry. The local model definition by Hühne [15] represents a damaged area obtained during a global analysis in the following way. If a few elements in the foot of the stiffened panel are damaged, then not only these elements, but also the corresponding adjacent skin and stiffener elements will be included in the local model. Based on a plane stress assumption as well as on the idea that loss of stability of the stiffener will lead to global failure, it can be assumed that there is no need to examine the stiffener until the moment that the failure is predicted through the global analysis. As the whole global-local approach is iterative, there is no risk in missing damage evolution in the adjacent stringer elements. There is further no need to include the adjacent skin elements in the local model until damage has been detected in these skin elements.

Moreover, Fig. 1 demonstrates an issue arising from the incorrect definition of a local model. Damage can be observed in the stringer area of the local model. The absence of damage in the reference solid element model at the same load level indicates that this damage in the local model is artificial and due to edge effects. One should therefore try to avoid stress concentrations due to the boundaries of the local model and pay attention to stress convergence [19]. This issue is addressed in the following. The spurious stress concentrations at the edges of local models can lead to inaccurate results. This might considerably affect the evaluation of the homogenized properties which are transferred back to the global level. A first possibility is to surround the local models by material which in the coupling analysis is assumed not to degrade, adding an additional local layer of elements at each edge where the boundary conditions are applied. Another option is to increase the local model, thereby involving the nearest global elements. The second approach is preferred in view of the submodeling technique. The reason is that in the Abaqus software, boundary conditions from the global model should be interpolated only to the corresponding driven nodes of the local model lying within a certain tolerance [16]. To satisfy the submodeling procedure and to obtain an accurate interpolation of the displacements at the boundaries, the local nodes should lie in the vicinity of the global nodes.

The new local model rules proposed require surrounding the damaged area by at least one neighboring global element. Further, only those parts of the model corresponding to the specific structural element in which damage was identified should be considered, provided that no stress concentrations are expected at the connection of these structural elements. Summarizing, on the one hand, the size of the local model will be increased in-plane by adding elements corresponding to the surrounding global elements. On the other hand, the size of the local model will be decreased in the case of damage in the stringer foot by not considering adjacent skin and stringer web parts until in those parts damage has been detected at the global level. This approach will be used for the stiffened panels in this paper in the cases in which failure initiates in the stringer foot. These rules can be extended to other types of composite structures and load cases. By considering the load distribution and redistribution expected in the structure after initial damage, one can identify the area of finite elements directly influenced by the damaged ones as well as the adjacent areas that are not expected to be influenced in the same local model analysis step.

## 2.2. Analysis of one-stringer composite panel with new local model rules

In order to evaluate their effect on the failure growth prediction, the new local model rules discussed in the previous section were applied in a progressive failure analysis using the global-local coupling approach for a one-stringer panel. Reference models with

shell and solid elements have already been analyzed in the framework of earlier work on an academic one-stringer panel [15]. Geometry as well as material linear properties for the global models are the same as in these previous analyses. In the present case, the new rules to define local models were employed. Prescribed displacements for the progressive analysis and subsequent coupling loops were applied similarly to the analysis in [15] in four steps, in order to ensure consistency when comparing results with the results obtained earlier: prescribed displacements of 0.56 mm, 0.60 mm, 0.63 mm and 0.67 mm, respectively. So-called “overlay” plots combining the global shell model and the local solid models for these four coupling loops in one figure are presented in Fig. 2. The relative error of total failure predicted by global-local analysis with the new local models is 0.65% as compared with the reference solid model, which is satisfactory and comparable with the relative error obtained with the local models used in the earlier analysis (0.53%). Not only the number of global elements examined during the local step has decreased, also the number of local part tests has decreased, as they are performed only for damaged global elements. The properties of non-damaged global edge elements in local models were not homogenized, because this can lead to spurious results.

The damage evolution detected via global-local analysis with the new local model rules is similar to the one in observed in the previous global-local analysis [15]. Matrix cracking in the foot is first detected, see Fig. 3, and progresses with increasing compressive load. Next, fiber damage is found in the foot, followed by the global failure of the panel.

The corresponding load-displacement curve is plotted in Fig. 4, showing that the global-local coupling model results are similar to the load-displacement path of a reference model with solid elements, while initial buckling of the structure occurs slightly earlier. The response curves for the reference model with solid elements and for the coupling analysis after initial buckling also show the same stiffness in the postbuckling region. The first failure in both analyses occurs in the matrix of the stringer foot in the postbuckling regime. Global failure is obtained in the reference solid element model after the occurrence of fiber damage and is satisfactorily captured by the global-local coupling procedure.

## 2.3. Mesh element size dependency study

A mesh element size dependency study was carried out to investigate the influence of the element size of the local models on the global behavior in the postbuckling regime. One possible technique is to carry out a convergence check for one specific local model. Stress differences in the areas or nodes of interest are checked, in order to evaluate if convergence of the local model analysis has been reached, see the work by Kardak [18]. Another option is to refine the mesh for all local models. This latter variant was chosen in the current study. Assuming that one element is used in the thickness direction, the ratio between the element size

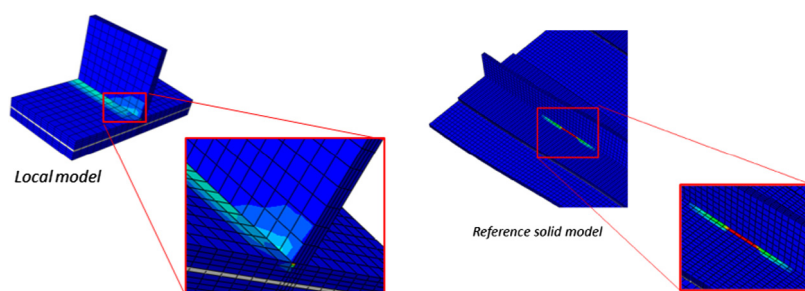


Fig. 1. Matrix damage in the local model (left) and in the solid element reference model (right).

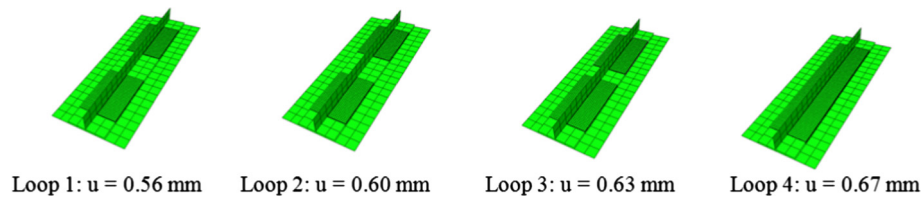


Fig. 2. Overlay plots for global and local models from coupling loops 1–4.

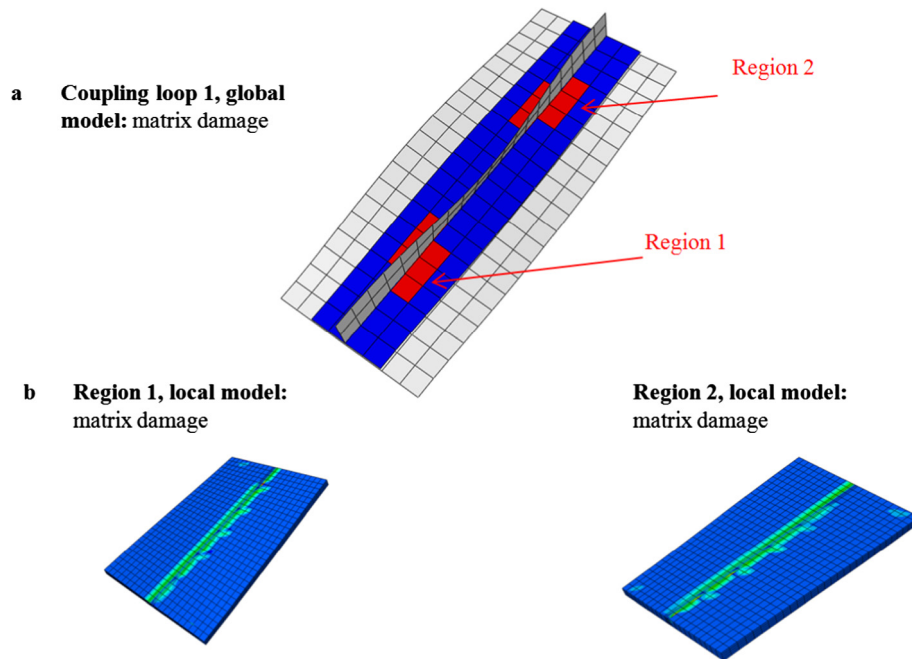


Fig. 3. Coupling loop 1. (a) First critical global areas related to matrix failure, (b) matrix damage initiation for Region 1 and Region 2 on the local level.

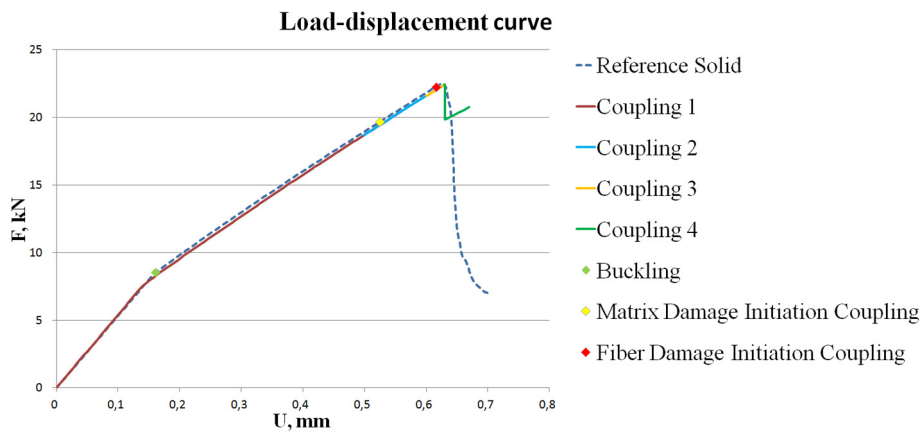


Fig. 4. Load-displacement curves of the coupling and reference analyses.

in z-direction and the in-plane sizes is 1:5 instead of the recommended 1:1 [16]. The appropriateness of the element aspect ratio used is to be demonstrated. A more accurate mesh for all local models could not only lead to more accurate stress and displacement fields, but also to a different damage evolution. This last aspect also needs to be addressed, in order to show the appropriateness of the coupling method used.

A coupling analysis was performed for a test case of a one-stringer panel. The local areas were detected and defined using

the Linde damage criterion and they were modeled with twice as many elements in each in-plane direction than in the analysis, described in the previous section, with the result that the number of elements is quadrupled. The new local model rules from the Section 2.1 were again applied. For consistency, a reference solid element model was created with the same size of elements as used at the refined local level. The difference between the global failure load predicted by the global-local coupling method and the reference solid element analysis is 0.19%, while the difference with

the result obtained with the coarser local models is 0.65%. The relatively small increase in accuracy obtained using the finer discretization demonstrates that the results in this case do not significantly depend on the mesh element size. Load-displacement curves for the reference solid and coupling analyses are presented in Fig. 5.

### 3. Two-stringer composite panel with initial local defect

In this section, as a first step towards the analysis of large panels, a stiffened panel with two stringers is analyzed by means of the two-way coupling method including the enhancements presented in Section 2.

Results obtained by Hühne [15] for one-stringer panels show a reasonably good agreement with the corresponding reference solid element models. Due to the panel configuration and loading conditions, the one-stringer panel showed damage in large areas of the structure. In the present case of a two-stringer panel with an initial local defect, the damage is expected to grow in a localized area. The analysis of a local initial defect, for instance due a flaw in the manufacturing process, also has a practical significance, e.g. [20].

#### 3.1. Model description

The application of the refined method is demonstrated on a flat stiffened panel with two T-stringers shown in Fig. 6, see Table 1 and 2 for geometrical and material characteristics respectively. A debonded area was assumed as an initial localized defect and was incorporated between skin and a flange of the stringer, where  $d = 25$  mm, and the distance between the clamped edge and the debonded area was  $l_d = 15$  mm. The unidirectional layers are of 0.25 mm thickness with a symmetric composite layup of  $[0^\circ, 90^\circ]_s$ .

Progressive damage was examined under the following boundary conditions: The transverse edge and the opposite transverse edge were constrained in all directions (fully clamped) except on one side in the longitudinal direction, where the compressive load was imposed through a prescribed displacement. The longitudinal edges were free. The initial defect, the debonded area, was assumed not to grow under the load applied.

#### 3.2. Coupling results

Four coupling loops with subsequently increased displacements were performed to determine the final damage. At an axial prescribed displacement of  $u = 0.37$  mm, matrix failure was observed in the debonded area, according to the Linde criterion

[17]. Increasing the prescribed displacement to  $u = 0.41$  mm, matrix damage initiation in the skin between two stringers was predicted. Damage spread in the debonded region in the foot part of the panel at a prescribed displacement of  $u = 0.43$  mm. Global failure occurred when fiber failure in the stringer foot and in the skin occurred. The damage evolution is shown in Fig. 7.

Fig. 8 displays load-displacement curves of four iteration loops obtained from the global-local coupling procedure as compared with the reference solid element model analysis results. There is a deviation of approximately 4% between the maximum load predicted by the coupling analysis and that of the solid reference analysis. From the load-displacement curve in Fig. 8, it can be seen that the coupling analysis predicts lower maximum prescribed displacements than the reference solid element model. While the solid element reference models carried a certain amount of additional load after onset of fiber degradation, the panels examined using the coupling procedure collapsed after first fiber failure. The stiffness decrease in the last region of the postbuckling regime is slightly higher than for the reference solid element model.

For this debonded panel with localized damage growth, a reasonably good agreement with the reference solid element model analysis was demonstrated. The new local model rules also played an important role, avoiding unnecessary calculations of undamaged parts and ensuring an appropriate stress and displacement evaluation at the local level. For this case of a two-stringer panel with a local defect, the potential of capturing the localized damage evolution of a larger structure by means of the global-local coupling approach could already be demonstrated.

### 4. Curved five-stringer composite panel

In this section, a realistic, large composite stiffened panel with five stringers is analyzed by means of the two-way coupling method including the enhancements presented in Section 2, concretizing the potential to carry out a progressive failure analysis for large stiffened panels. Larger panels are of particular interest for the global-local techniques, as the localized failure phenomena play an important role in the failure behaviour of the panel as a whole.

#### 4.1. Model description

Characteristics of a realistic five-stringer panel, that was tested experimentally in the COCOMAT project [2] denoted as P29, were used. During the tests, this panel was loaded cyclically until damage was generated. Wagner and Balzani [6] performed a numerical

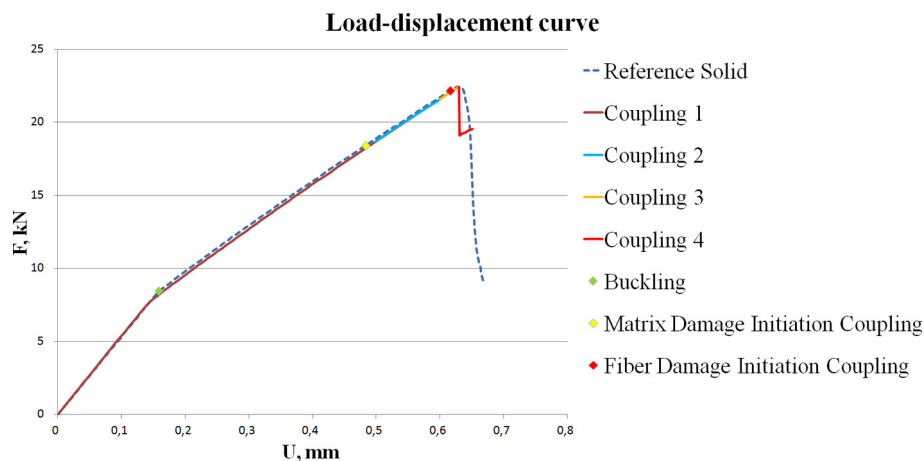


Fig. 5. Load-displacement curves of the coupling and reference analysis in mesh element size dependency study.

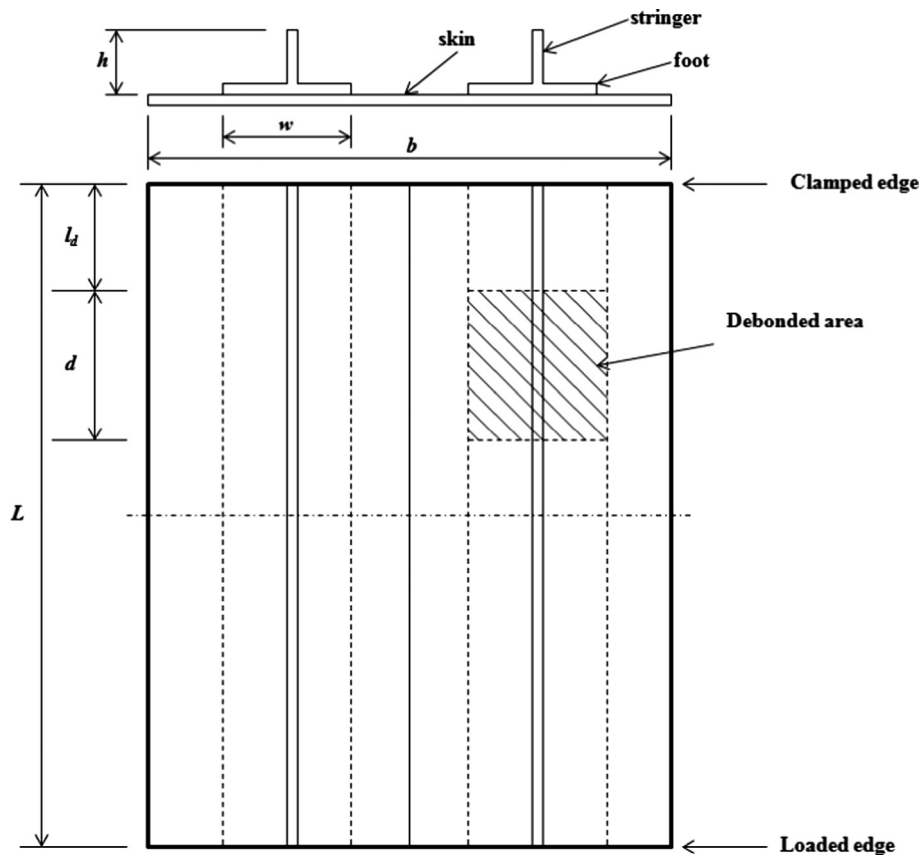


Fig. 6. Geometry of two-stringer composite panel with initial debonding defect.

Table 1  
Geometry of two-stringer composite panel.

Description	Symbol	Value (mm)
Panel length	$l$	100
Panel width	$w$	80
Stringer width	$w_{stringer}$	20
Stringer height	$h$	8
Laminate thickness	$t$	1
Adhesive thickness	$t_{adhesive}$	0.2

analysis for the panel with initial damage. In the present analysis, the panel without predamage is considered.

The panel was composed of a curved skin and five T-shaped stringers, see Fig. 9. An axial displacement was applied in compression to one of the transverse edges, while the opposite edge was fully clamped and both transverse edges were potted. The geometry parameters have been taken from [6] and are summarized in Table 3.

The composite laminate properties for this panel, made of unidirectional CFRC IM7/8552 plies, have been taken from the

aforementioned papers. Material properties correspond to those used for the two-stringer panel, see Table 2. The symmetric composite layups for the skin and for the stringer are  $[90^\circ, +45^\circ, -45^\circ, 0^\circ]_s$  and  $[(+45^\circ, -45^\circ)_3, 0^\circ_6]_s$  respectively [2].

#### 4.2. Coupling results

A global model consisted of 17,940 shell elements, while the local models representing skin and stringer areas consisted of a maximum of 79,380 solid elements with a mesh refinement of 6 times the value used at the global level. Four coupling steps were applied to simulate the progressive failure analysis in the post-buckling regime. Onset of intralaminar damage, matrix damage in the skin, took place between the stringers and was followed by fiber damage at the middle stringer in the next coupling step. Further damaged regions occurred near the edges of the first and the fifth stringer. Final collapse of the panel took place following spreading of fiber damage in the stringers at a prescribed displacement of 3.28 mm.

For reference purposes, the panel with shell elements including a material degradation model based on Linde's approach was used.

Table 2  
Material data for composite and adhesive.

Stiffness properties	Value	Strength and fracture properties	Value
Young's modulus in 1-direction $E_{11}$	146.5 GPa	Tensile strength in 1-direction $X_T$	2.583 GPa
Young's modulus in 2-direction $E_{22}$	9.7 GPa	Compressive strength in 1-direction $X_C$	1.483 GPa
Shear modulus in 12-plane $G_{12}$	5.1 GPa	Tensile strength in 2-direction $Y_T$	0.092 GPa
Poisson's ratio $\nu_{12}$	0.28	Compressive strength in 2-direction $Y_C$	0.270 GPa
Young's modulus of adhesive $E_{adhesive}$	3.0 GPa	Shear strength in 12-plane $S_A$	0.106 GPa
Poisson's ratio of adhesive $\nu_{adhesive}$	0.4	Fracture energy of fibre $G_f$	12.5 N/mm
-	-	Fracture energy of matrix $G_m$	1.0 N/mm

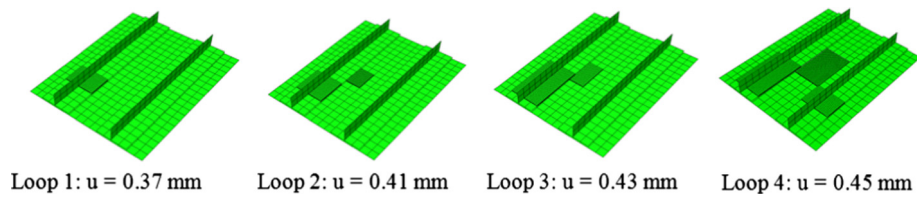


Fig. 7. Overlay plots of global and local models from coupling loops 1–4. Two-stringer panel with initial debonding defect.

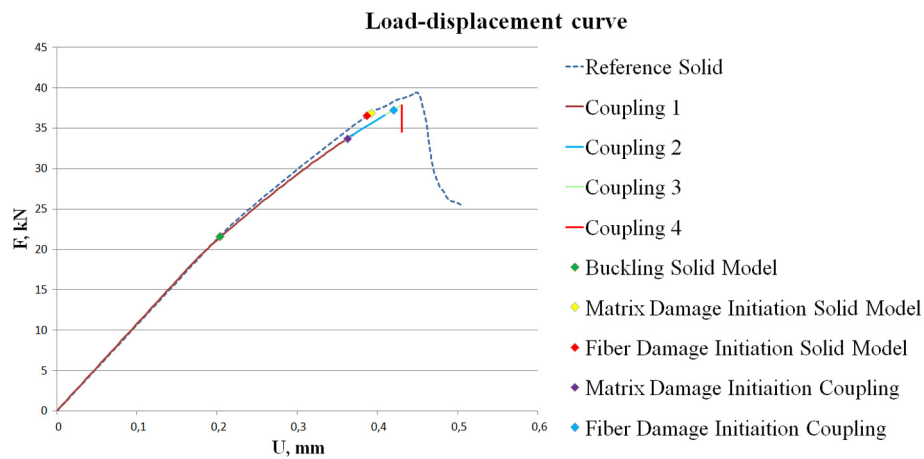


Fig. 8. Load-displacement curves of coupling iterations for two-stringer panel with initial debonding defect in comparison with reference results.

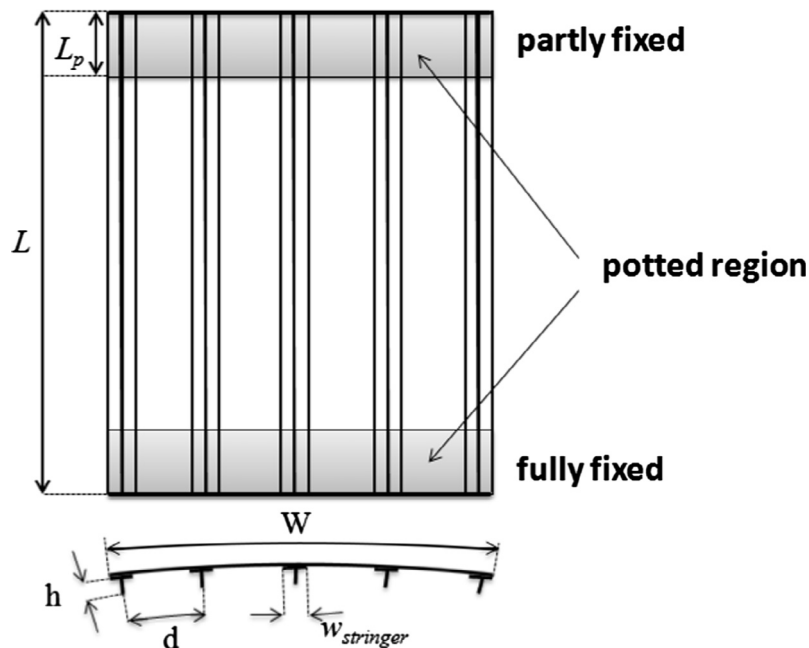


Fig. 9. Curved five-stringer composite panel.

Table 3

Geometry of a five-stringer composite panel.

Description	Symbol	Value (mm)
Panel length	$L$	780.5
Potted length	$L_p$	60.25
Panel width	$W$	560.5
Stringer width	$w_{stringer}$	32
Stringer height	$h$	14.3
Skin thickness	$t_s$	0.98
Stringer thickness	$t_s$	2.9
Panel radius	$R$	848

A numerical calculation of a reference model with solid elements and a mesh discretization corresponding to the local models would require a very high computational time and was not done for the present model.

Load-displacement curves for a reference panel with shell elements, results of the coupling analysis and the experiment results are displayed in Fig. 10. During the experiment, the panel was compressed up to a displacement of 2 mm. The response curves are in reasonable agreement before buckling and also after first buckling has occurred. First buckling (local skin buckling) obtained in the numerical analysis corresponds to a prescribed displacement



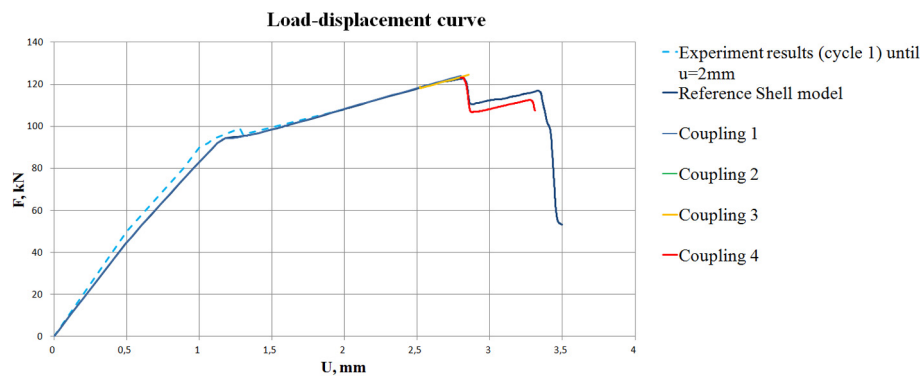


Fig. 10. Load-displacement curves of curved five-stringer panel. Comparison between results of global-local approach, results of reference panel analysis and experimental results.

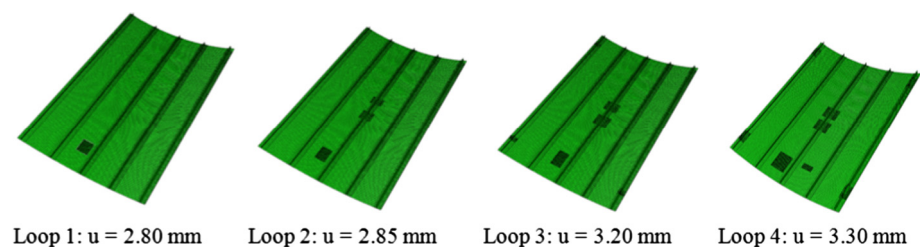


Fig. 11. Overlay plots of global and local models. Curved five-stringer panel.

of  $u = 1.13$  mm. The “overlay” plots showing the damaged areas are presented in Fig. 11. First failure occurred in the matrix of the skin between the second and third stringer at a prescribed displacement of 2.55 mm followed by initial fiber damage in the skin under the middle stringer at the prescribed displacement of 2.68 mm. Subsequently, initial fiber failure was detected in the first and fifth stringer in three areas near the panel edge at a prescribed displacement of 2.69 mm, with further damage growth in the other regions with damage. Final failure of the panel occurred following significant spreading of fiber damage at a prescribed displacement level of 3.28 mm.

It can be seen that the prescribed displacement of the fourth coupling loop is slightly higher than the critical displacement of the final collapse. This was done in order to capture not only the failure onset, but also to ensure the possibility to explore the material damage propagation at the local level and detection of final failure at the global level. The advantage of the current global-local approach is, that the creation of the local models allows an accurate evaluation of the 3D stress and strain states and, since the global analysis is conducted with shell elements, the procedure can also for this large structure be carried out with a reasonable computational time.

## 5. Conclusion

A two-way coupling global-local finite element approach which has shown its potential on the basis of representative test cases in earlier work, was used for the progressive failure analysis of large multi-stringer stiffened composite panels. In order to realize the capability of the approach to analyze larger panels, the efficiency of the analysis was enhanced, and improved rules for the choice of the size of local models were developed.

As a first step towards the analysis of large panels, a case of a two-stringer panel with a local defect was analyzed using the adjusted rules to define the local models. Load-displacement curves of the coupling analysis and the solid element reference

analysis were in reasonably good agreement. This holds for the maximum load levels predicted by both analyses as well as for the sequence of damage occurrence.

The potential to carry out a progressive failure analysis for large stiffened panels was concretized by analyzing a large stiffened composite panel with five stringers. A reference model with shell elements and material degradation was used for a comparison. A reasonable agreement between the results of the coupling analysis and the shell element reference analysis was demonstrated. The numerical results were also compared with experimental results available. The load-displacement response curves observed showed, despite the small difference in the prebuckling stiffness, a reasonable agreement in the postbuckling regime.

## Acknowledgments

The research leading to these results has received funding from European Union’s Horizon 2020 research and innovation program (FULLCOMP/2015–2019) under Marie Skłodowska-Curie actions grant agreement number 642121. The provided financial support is gratefully acknowledged by the authors.

## References

- [1] Stamatelos DG, Labeas GN, Tserpes KI. Analytical calculation of local buckling and post-buckling behavior of isotropic and orthotropic stiffened panels. *Thin Walled Struct* 2011;49(3):422–30. <http://dx.doi.org/10.1016/j.tws.2010.11.008>.
- [2] Degenhardt R, Kling A, Klein H, Hillger W, Goetting HC, Zimmermann R, Rohwer K. Experiments on buckling and postbuckling of thin-walled CFRP structures using advanced measurement systems. *Int J Struct Stabil Dyn* 2007;7(2):337–58.
- [3] Orifici AC, Thomson RS, Degenhardt R, Kling A, Rohwer K, Bayandor J. Degradation investigation in a postbuckling composite stiffened fuselage panel. *Compos Struct* 2008;82:217–24. <http://dx.doi.org/10.1016/j.compstruct.2007.01.012>.
- [4] Lauterbach S, Orifici AC, Wagner W, Balzani C, Abramovich H, Thomson R. Damage sensitivity of axially loaded stringer-stiffened curved CFRP panels. *Compo Sci Technol* 2010;70(2):240–8. <http://dx.doi.org/10.1016/j.compscitech.2009.10.013>.

- [5] Zimmermann R, Klein H, Kling A. Buckling and postbuckling of stringer stiffened fibre composite curved panels tests and computations. *Compos Struct* 2006;73:150–61. <http://dx.doi.org/10.1016/j.compstruct.2005.11.050>.
- [6] Wagner W, Balzani C. Prediction of the postbuckling response of composite airframe panels including ply failure. *Eng Fract Mech* 2010;77(18):3648–57. <http://dx.doi.org/10.1016/j.engfracmech.2010.05.009>.
- [7] Mote CD. Global-local finite element. *Int J Numer Methods Eng* 1971;3:565–74.
- [8] Noor AK. Global-local methodologies and their application to nonlinear analysis. *Finite Elem Anal Des* 1986;2:333–46.
- [9] Mao K, Sun C. A refined global-local finite element analysis method. *Int J Numer Methods Eng* 1991;32:29–43.
- [10] Whitcomb JD. Iterative global/local finite element analysis. *Comput Struct* 1991;40(4):1027–31. [http://dx.doi.org/10.1016/0045-7949\(91\)90334-I](http://dx.doi.org/10.1016/0045-7949(91)90334-I).
- [11] Loehnert S, Belytschko T. A multiscale projection method for macro/microcrack simulations. *Int J Numer Methods Eng* 2007;71:1466–82. <http://dx.doi.org/10.1002/nme>.
- [12] Labeas GN, Belesis SD, Diamantakos I, Tserpes KI. Adaptive progressive damage modeling for large-scale composite structures. *Int J Damage Mech* 2012;21(3):441–62. <http://dx.doi.org/10.1177/1056789511400928>.
- [13] Chrupalla D, Berg S, Kärger L, Doreille M, Ludwig T, Jansen E, Rolfes R, Kling A. A homogenization-based two-way multiscale approach for composite structures. In: Rolfes R, Jansen EL, editors. *Proceedings of the 3rd ECCOMAS thematic conference on the mechanical response of composites*. Germany: Hannover; 2011. p. 263–70.
- [14] Gendre L, Allix O, Gosselet P, Francois C. Non-intrusive and exact global/ local techniques for structural problems with local plasticity. *Comput Mech* 2009;44:233–45. <http://dx.doi.org/10.1007/s00466-009-0372-9>.
- [15] Huehne S, Reinoso J, Jansen E, Rolfes R. A two-way loose coupling procedure for investigating the buckling and damage behaviour of stiffened composite panels. *Compos Struct* 2016;136:513–25. <http://dx.doi.org/10.1016/j.compstruct.2015.09.056>.
- [16] Abaqus, Writing User Subroutines with ABAQUS (V) (2001) 1–172.
- [17] Linde P, Pleitner J, Boer HD, Carmone C. Modelling and Simulation of Fibre Metal Laminates. *ABAQUS Users' Conference*; 2004. p. 421–439.
- [18] Kardak AA. *On an effective submodeling procedure for stresses determined with finite element analysis* PhD Thesis. USA: Louisiana State University and Agricultural and Mechanical College; 2015.
- [19] Bogdanovich AE, Kizhakkethara I. *Three-dimensional finite element analysis of double-lap composite adhesive bonded joint using submodeling approach*. *Compos Part B* 1999;30:537–51.
- [20] C.G. Dávila, P.P. Camanho, Analysis of the effects of residual strains and defects on skin/stiffener debonding using decohesion elements, 44th AIAA/ASME/ASCE/AHS Structures, Structural Dynamics, and Materials Conference, AIAA Paper 2003-1465; 2003.

### **3 Paper B: Analysis of skin-stringer debonding in composite panels through a two-way global-local method**

The following paper is published in *Composite Structures*, Volume 202 (2018), pages 1280-1294 (<https://doi.org/10.1016/j.compstruct.2018.06.064>). The main work was done by the author of this thesis.

Skin-stringer separation during the in service period of stiffened panels is regarded as one of the most critical damage mechanisms that could lead to a significant loss in load-bearing capacities and under certain conditions even bring the panel to a total failure. That is a reason for development of a novel two-way coupling global-local approach to numerically simulate a skin-stringer separation in stiffened composite panels. The method allows to consider skin-stringer debonding through subsequent calculations of global and local models. First of all, global model analysis is performed with a relatively coarse mesh and linear elasticity in order to evaluate the regions of possible damage initiation. Based on this information detailed local models with refined mesh are created that account for the onset of the skin-stringer debonding and the following propagation. While discrete spring-type elements are used at the global level, cohesive elements with continuum damage modelling are applied at the local level. An averaging procedure has been formulated to allow the damage information transfer from the local to global model with not only different mesh sizes, but also not alike mesh types. The developed approach has been firstly applied to a case of a single-stringer panel with a comparison to a 3D reference model. A good agreement was attained in terms of the maximum load predicted and load-displacement curves. During the next step the developed global-local approach has been validated against existing experimental data for a one-stringer panel with initially introduced skin-stringer debonding. Although skin-stringer separation was predicted quite accurately, the final collapse was not attained by the global-local approach. One of the most probable reasons is that no intralaminar damage was accounted for.

The presented global-local method for modelling the skin-stringer debonding overcame a challenge of establishing a link between the local and global models allowing to account for the effect of the skin-stringer separation at the global level until the final collapse. However, the methodology are to be combined with an intralaminar damage in the next studies.



Contents lists available at ScienceDirect

Composite Structures

journal homepage: [www.elsevier.com/locate/compstruct](http://www.elsevier.com/locate/compstruct)

## Analysis of skin-stringer debonding in composite panels through a two-way global-local method



Margarita Akterskaia<sup>a,\*</sup>, Eelco Jansen<sup>a</sup>, Stephen R. Hallett<sup>b</sup>, Paul Weaver<sup>b</sup>, Raimund Rolfes<sup>a</sup>

<sup>a</sup> Institute of Structural Analysis, Leibniz Universität Hannover, Appelstr. 9A, 30167 Hannover, Germany

<sup>b</sup> Advanced Composites Centre for Innovation and Science, (ACCIS), University of Bristol, Bristol BS8 1TR, UK

### ARTICLE INFO

#### Keywords:

Composite structures  
Stiffened panels  
Progressive failure analysis  
Multiscale analysis  
Global-local method  
Postbuckling  
Skin-stringer debonding  
Delamination

### ABSTRACT

According to various experimental results, stiffened panels under compressive loading are prone to debonding between the skin and the flange of the stringer. In this paper, a novel two-way global-local coupling approach is presented that is able to model progressive separation of the skin and stringer in stiffened CFRP panels under compression. The main goal of this methodology is to examine skin-stringer debonding at two levels of accuracy, taking advantage of the fast calculations at the global level and assessing in detail the damage propagation at the local level. First, critical areas are defined in a global model with a standard mesh, and local models with a considerably finer mesh are created by means of a submodeling technique. Secondly, a local model analysis is conducted, in which cohesive elements are applied to simulate debonding. Particularly important is the appropriate information exchange in both directions between the different steps of the coupling analysis. Averaged degraded properties are defined at the local model level and transferred back to the global level. The applied compressive load is increased and induces a progression in skin-stringer separation. The global-local coupling loops are repeated until panel failure occurs. The approach is applied to a case of a representative one-stringer stiffened panel and to a stiffened panel for which test results are available. A good correspondence with reference results and test results demonstrates the effectiveness of the global-local approach presented.

## 1. Introduction

Fiber-reinforced composites and in particular laminated stiffened composite panels are widely used in aircraft design. The reason of the extensive use of composite structures is their remarkable material properties, such as high strength and stiffness to weight ratio. The desire to exploit the advantages of thin, panel-type structures results in post-buckled designs, which make use of the load carrying capability of stiffened panels in the post-buckling regime [1]. For this reason, an efficient and reliable progressive failure analysis method is required in order to examine the damage response, such as damage initiation and evolution, and to determine the final failure load. One of the common failure modes of laminated composite panels is skin-stringer debonding due to relatively low interface strengths. In the current work, the separation between skin and stiffener foot is modelled and investigated by means of a two-way global-local loose coupling approach.

### 1.1. Debonding and delamination modelling

Delamination and skin-stringer separation in particular is one of the

main failure mechanisms of laminated composite structures, together with fibre fracture and matrix cracking. The reason for delamination initiation and propagation is the relatively small interlaminar strength of adjacent plies. Delamination can take place under various combinations of loads and leads to a significant reduction of the load-carrying capacity of the structure. Delamination is commonly modelled numerically by the Virtual Crack Closure Technique (VCCT) or by means of cohesive interface elements.

The VCCT is based on fracture mechanics and the assumption of Irwin that the energy released during the crack extension is equal to the work required to close this crack back to its original length. For the details refer to [2,3]. The main drawback of the VCCT is that the crack initiation zone, which could be difficult to predict in case of large and complex structures, should be known in advance.

Cohesive Zone Modelling (CZM) is another approach based on an assumption for the softening region in front of the crack front, that is kept together by the tractions. This idea goes back to Dugdale [4] and Barenblatt [5]. The method of Hillerborg [6] lies at the origin of cohesive elements, considering both crack growth and predicting the crack initiation, which occurs when the tensile stress at the crack tip

\* Corresponding author.

E-mail address: [m.akterskaia@isd.uni-hannover.de](mailto:m.akterskaia@isd.uni-hannover.de) (M. Akterskaia).

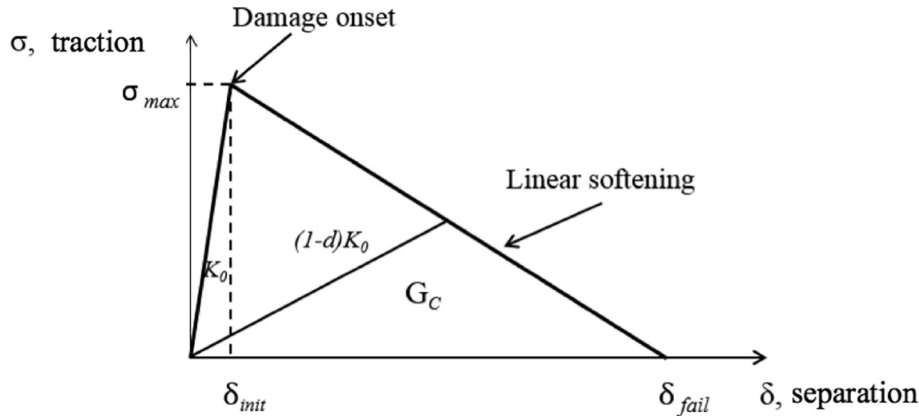


Fig. 1. Bilinear traction-separation law.

reaches the tensile strength.

Interface elements based on the CZM rely on the traction-separation law that is formulated in terms of the traction versus displacement jumps at the interface of potential crack. The most common assumption is that initially linear behaviour until the stress reaches tensile strength for pure mode loading is followed by the softening region until the final separation of the crack surfaces, see Fig. 1. Different shapes of the degradation curve have been proposed in literature – linear, exponential or trapezoidal [7]. In the present studies, the initial stiffness has been chosen equal to  $10^6$  N/mm following recommendation of Davila et al. [7]. However, it should be mentioned that some authors prefer to define stiffness value based on material properties and parameters, see Turon et al. [8], for example.

The Cohesive Zone Model was implemented by many authors most commonly in a continuum form (CCZM) where the process zone ahead of a crack tip is modelled with continuum type interface elements. The continuum approach was examined, discussed and improved by Allix and Ladeveze [9], Jiang et al. [10], Turon et al. [11], Camanho and Davila [12] and others. However, convergence difficulties and mesh sensitivity of cohesive elements based on CCZM reflect in the high number of cohesive elements required and result in high computational time. Alternative approach is to apply point-wise discrete elements or Discrete Cohesive Zone Model (DCZM). Borg et al. [13] formulated a discrete cohesive crack model postulating the existence of maximum load surface of adhesive forces. The method was realized by connecting the coincident nodes at the interface and a force-displacement relation was defined for these node pairs. Adhesive forces were reduced following the calculations of the dissipated work until zero value based on the fracture energy criterion. Good agreement with experimental results for mode I, mode II and mixed mode loading was demonstrated. Wisnom and Chang [14] introduced a nonlinear plastic spring as an interface element to examine delamination between the plies of notched composite test models. Xie and Waas [15] applied the DCZM based on non-linear spring type elements and traction-separation bilinear cohesive law for three fracture tests. On given examples, this technique was shown to be insensitive to mesh density or load increment and no convergence difficulties were encountered. Hallett and Wisnom [16] performed modelling of damage in tension for notched laminates by employing interface elements based on three-degree-of-freedom non-linear springs. Comparison with tests proved the model to be accurate enough until occurrence of fibre failure. Jiang et al. [10] proposed a constitutive law for cohesive interface areas for mixed-mode delamination process. Application was performed on scaled open hole tension tests with a non-linear spring element for the interface modelling. These discussed discrete techniques for the simulation of adhesive behaviour require accurate calculation of forces or stresses which for relatively complex structures could be achieved only with a high

computational cost. Therefore, various multi-scale approaches could be utilized to minimize the number of constitutive equations on the one hand, and to obtain reliable results on the other hand.

### 1.2. Skin-stringer separation in stiffened panels

Skin-stringer separation in composite stiffened panels was considered in many analytical and numerical investigations with the aim of examining their progressive damage, buckling and post-buckling behaviour. In the following, only a few of them will be mentioned. Wang and Bigger [17] studied the stresses between skin and stiffener of composite panels with specific attention on separation between them. Balzani and Wagner [18] examined debonding between skin and stiffener in stiffened panel with cohesive elements. Raimondo and Riccio [19,20] performed skin-stringer debonding analysis on the test case of two single stringer panels by means of improved VCCT. Yap et al. [21] examined skin-stringer debonding of curved T-stringer panels. A stiffened panel was modelled with shell elements and rigid bars were utilized to tie skin and stringer with debonding being modelled based on fracture mechanics. Falzon et al. [22] presented experimental results for three stiffened panels under compression investigating crack propagation through the skin-stiffener interface.

### 1.3. Global-local methods for skin-stringer separation of stiffened panels

Global-local methods are indispensable design tools that gained their recognition for modelling of large and complex structures because of the need to reduce computational effort on the one hand, without losing knowledge about the critical areas prone to damage on the other hand. Skin-stringer separation in laminated panels was observed during numerous experiments [1] and various global-local approaches were suggested and implemented through finite element analyses. Some definitions of coupling global-local methods have been proposed in [23] proposing to distinguish between loose and tight procedures as well as between one-way and two-way approaches. Tight procedure means that global and local models are connected and calculated simultaneously, whereas during the loose coupling analysis both global and local models are treated consecutively. The latter methodology requires the separate creation of local models and could offer great flexibility concerning their size and location which could be adjusted along the analysis. Loose coupling technique can be subdivided in one-way and two-way approaches. The difference between one-way and two-way techniques consists in the direction of the information exchange between the levels. Regarding the one-way coupling method, information is transferred only in one direction. This commonly means, that progressive failure analysis could not be performed because the information regarding the damage state is transferred only once.

However, this could be also helpful when the damage location is known a priori and failure only needs to be investigated at the local level. In more complicated cases when the damage area is not known and might expand when increasing the load, the two-way coupling approach is recommended to overcome aforementioned limitations.

According to the proposed distinction, the term tight coupling could be applied to following works. Krueger et al. [24] analysed a three-stringer panel with embedded debonding under shear loading. The area of probable debonding evolution was accurately modelled with solid elements, whereas the shell elements with a coarser mesh were applied to the whole model. VCCT was implemented to model debonding. Borrelli et al. [25] examined two coupling methods: point-wise kinematic coupling and weighted residual coupling to perform tight global-local analysis of initially delaminated stiffened panel. Shell elements and a coarse mesh were used for the global area, whereas the local area surrounding delamination was modelled with solid elements and a finer mesh. Modified virtual crack closure technique (MVCCT) was used to model delamination. The results were compared to the reference model with solid elements. Alesi et al. [26] presented a global-local method based on coupling with multipoint constraints.

One-way coupling includes mainly methods of the information transfer realized in the global-local direction. Faggiani and Falzon [27] conducted an optimization procedure for a stiffened composite panel through improving damage resistance of the skin-stringer interface by means of a genetic algorithm. The global-local method using a sub-modeling technique was applied. Bertolini et al. [28] presented a global-local one-way coupling approach to model skin-stringer debonding by means of VCCT technique. The method was applied to a one-stringer T-shape panel subjected to seven-point bending. Ultimately, two large stiffened panels with Omega-stringers under compressive and shear loading were examined. Shell and solid elements were utilized to create global and local models respectively. Reinoso et al. [29] applied a one-way global-local procedure to evaluate the computational analysis and experimental results for the stringer runout effect in a composite panel. Two approaches were compared in Abaqus: submodeling technique and shell-to-solid coupling. Vescovini et al. [30] proposed one-way global-local analysis for the Omega-shaped multi-stringer panel loaded in compression. Both global and local models were composed of shell elements. Cohesive elements were applied between skin and stringer in the local models allowing for determination of delamination onset and growth. Local models created by means of submodeling procedure had a pre-determined size and local analysis was performed five times moving the local model along the stringer.

Orifici et al. [31] proposed a global-local methodology that could be regarded as two-way coupling for the detection of the ply damage and skin-stringer separation in the postbuckling regime of stiffened panels. After the coarse analysis of the global model, the obtained displacements were used as boundary conditions for local models with a finer mesh. Delamination onset was predicted at the local level where 3D stresses are calculated accurately. VCCT was applied to simulate debonding propagation at the global level. Bettinotti et al. [32] suggested a substitution method for the multiscale analysis of delamination under high-velocity impact that allows concurrent run of global and local analysis. A comparison was performed with tie constraint between different regions and submodeling approach. The approach was based on the separate code and integration of this algorithm to an Abaqus/Explicit was carried out.

#### 1.4. Objectives

A two-way loose coupling approach was developed earlier to simulate the post-buckling progressive failure behaviour of a panel-type structure with intralaminar damage in an efficient way [23,33]. In these earlier works, the global-local approach has been validated for typical test cases of a panel with one stringer and two stringers. Panels without any initial defects were considered as well as pre-damaged panels.

Satisfactory agreement with numerical and experimental reference results demonstrated the potential of this coupling method. Recently, application of the approach to a larger panel with five stringers was conducted to illustrate the main advantages of this method [33].

The aim of the present work concerns the development of a new global-local coupling approach that enables the numerical simulation of the initiation and propagation of skin-stringer separation. Moreover, a novel procedure is elaborated in order to enable the information transfer from local to global level to overcome the limitations of the aforementioned techniques. This comprises simulation of the damage propagation at the global level by means of accounting for the stiffness degradation from the local level which is not possible within one-way approaches. High flexibility concerning creation, extension and unification of local models during damage evolution is advantageous compared to tight coupling techniques. The developed global-local method can be easily implemented in general-purpose finite element programs.

## 2. Analysis methodology

The two-way loose coupling procedure for modelling skin-stringer separation of a stiffened panel is described below in details. The procedure starts with a global analysis with shell elements and relatively coarse mesh density that is carried out in order to determine critical damage areas. Opposite nodes of skin and stringer are tied in the interface area by spring type connector elements with linear elastic behaviour. The stiffness of particular connector elements along the solution process should be updated and so represent the degradation part of the traction-separation law. Hence, discrete cohesive behaviour is chosen for the global level. Cartesian-type connector elements in Abaqus satisfy these requirements. Initial stiffness of interface elements is specified based on the following relation:

$$K = \frac{EA}{t} \quad (1)$$

where  $E$  is the Young's modulus of an adhesive layer,  $A$  and  $t$  are in-plane nodal area and thickness in the normal direction of the adhesive element respectively.

Estimation of the critical areas prone to delamination is performed through an additional Python script for connector elements based on the quadratic stress criterion the same as for cohesive elements, see Eq. (3). Normal and shear stresses at the nodes of connector elements are calculated accounting for the free edge and internal nodal areas that are tied by connector elements:

$$\sigma_{i3} = \frac{F_i}{A_{el}}, \quad i = \overline{1, 3} \quad (2)$$

where  $F_i$  is a nodal force,  $A_{el}$  determines a nodal area of applied force and here represented as a sum of one quarter of each element area tied to that node. Therefore,  $A_{el}$  either represents the full in-plane area of the shell element  $A_{int}$ , referring to Fig. 2 for interior connectors, or a half of this area denoted as  $A_{ext}$  corresponding to the case when connectors tie the edges. Index  $i$  specifies local Cartesian directions.  $\sigma_{33}$  corresponds to the normal stress that acts through the thickness,  $\sigma_{13}$  and  $\sigma_{23}$  are two in-plane shear stresses. In Eq. (1) the penalty stiffness definition includes non-material parameters such as nodal area  $A$  and thickness  $t$ . The force  $F_i$  from Eq. (2) is proportional to the corresponding stiffness which means that the stresses  $\sigma_{i3}$  are independent from the nodal area and depend only on the thickness of the adhesive layer. Connector elements that tie conventional 2D shell elements of skin and stringer are demonstrated in Fig. 2. Different nodal areas  $A_{ext}$  and  $A_{int}$  described earlier are shown in this figure.

Afterwards, the critical areas are examined during the next step – local analysis where separate local models are created. Solid elements are utilized to model the skin and the stringer and cohesive elements for the interface area between them. Fine mesh discretization is used for

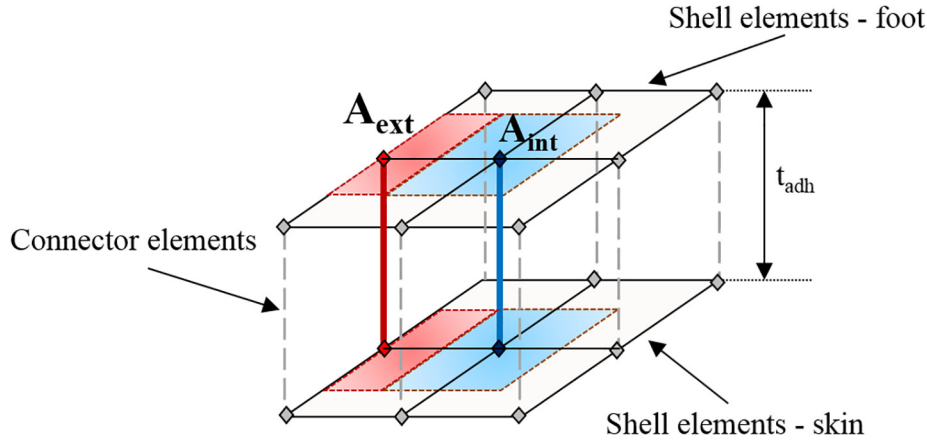


Fig. 2. Discrete interface elements connecting skin and stringer represented by shell elements.

these local models. Nodal displacements from the global model are transferred to the selected boundary nodes of the local model as kinematic constraints by the means of the Abaqus shell-to-solid sub-modeling procedure [34].

The quadratic stress criterion is chosen to predict initiation of debonding in the local model:

$$\left(\frac{\langle \sigma_n \rangle}{N_{max}}\right)^2 + \left(\frac{\sigma_s}{S_{max}}\right)^2 + \left(\frac{\sigma_t}{T_{max}}\right)^2 = 1 \quad (3)$$

Here  $\langle \dots \rangle$  represents McCauley brackets operator used here to recognise that compression is generally not involved in interface separation.  $\sigma_n$  is a stress in the normal through-thickness direction,  $\sigma_s$  and  $\sigma_t$  are nominal stresses acting in the first and second shear directions and  $N_{max}$ ,  $S_{max}$ ,  $T_{max}$  are the corresponding strengths.

Delamination propagation under mixed-mode loading could be traced by means of the Benzeggagh and Kenane criterion [35] extended to three dimensional case:

$$G_c = G_{IC} + (G_{IIC} - G_{IC}) \left( \frac{G_{II} + G_{III}}{G_I + G_{II} + G_{III}} \right)^\eta \quad (4)$$

where  $G_{IC}$  and  $G_{IIC}$  are mode I and II fracture toughness and  $G_I$ ,  $G_{II}$  are single mode energy release rates corresponding to fracture modes I, II and III and their sum is the total energy release rate. The parameter  $\eta$  is determined empirically, assumed to be 2.284 in the current studies [8].

A scalar damage variable  $d$  is utilized to identify the damage state. It varies from 0 when there is no damage to 1 when the interface connection is fully failed. Camanho and Davila [12] suggested the following damage variable for monotonic loading:

$$d = \frac{\delta_{fail}(\delta - \delta_{init})}{\delta(\delta_{fail} - \delta_{init})} \quad (5)$$

where  $d$  is the damage variable,  $\delta$  is the current maximum relative displacement,  $\delta_{init}$  corresponds to the displacement of the delamination beginning and  $\delta_{fail}$  is the displacement of the complete failure.

The stiffness of the cohesive element used in linear traction-separation law is defined following Camanho and Davila [12]:

$$K = \begin{cases} K_0 & \delta < \delta_{init} \\ (1-d)K_0 & \delta_{init} < \delta < \delta_{fail} \\ 0 & \delta > \delta_{fail} \end{cases} \quad (6)$$

where  $K_0$  is the initial penalty stiffness that is degraded after displacement  $\delta$  reaches the value of  $\delta_{init}$  and becomes 0 when the crack opening is equal to  $\delta_{fail}$ .

During the postprocessing phase, that follows the local model analysis, damage variable  $d$  that defines the degradation stage of each particular cohesive element is extracted in order to calculate the

decreased stiffness of an appropriate connector element. According to the global-local approach discussed before, mesh densities at global and local levels do not correspond to each other. In order to overcome this difference and to transfer degraded stiffnesses of each interface element from the local to the global level, a special averaging technique should be applied. First of all, an averaged local stiffness is calculated for each area that corresponds to one connector element:

$$K_{local} = \frac{\sum_{i=1}^N K_{local,i}}{N} = \frac{\sum_{i=1}^N (1-d_i)K_{local,0}}{N} = K_{local,0} \left( 1 - \frac{\sum_{i=1}^N d_i}{N} \right) \quad (7)$$

where  $K_{local,0}$  is the initial stiffness of a cohesive element,  $i$  denotes one of  $N$  local cohesive elements and  $d_i$  is the corresponding damage variable. Hence, to obtain an averaged local stiffness that conforms to one connector element at the global level, initial stiffness should be multiplied by the coefficient that stems from the averaged value of damage variables. This multiplication factor is utilized to obtain degraded stiffness of each particular connector element at the global level and ensure transfer of information of the damaged state from local to global level.

With new reduced global properties for connector elements, the global analysis is performed again applying initial stiffness in the interface area until the increment when the damage was predicted. Starting at that increment new degraded properties are utilized for each connector element. These coupling steps are repeated until convergence in reaction forces in the direction of the applied load is reached. In our case, the reaction force from global analysis is also compared to the reaction force of the reference solid model.

The flowchart of the two-way coupling procedure for the skin-stringer debonding along with information exchange between global and local levels of analyses is presented in Fig. 3.

Hence, the coupling loop consists of three major operations that are repeated iteratively at two levels of accuracy until the final collapse is determined:

1. Global analysis to evaluate the areas of a probable damage and to define local models geometry.
2. Local models obtain displacements as boundary conditions from the global solution. After carrying out numerical calculations for local models, damage variables for each cohesive element are obtained.
3. Global interface stiffness is calculated based on average damage variables and transferred back to the global level.

The main steps of this global-local method are illustrated on a Fig. 4 for an example of a one-stringer panel: global analysis, local analysis,

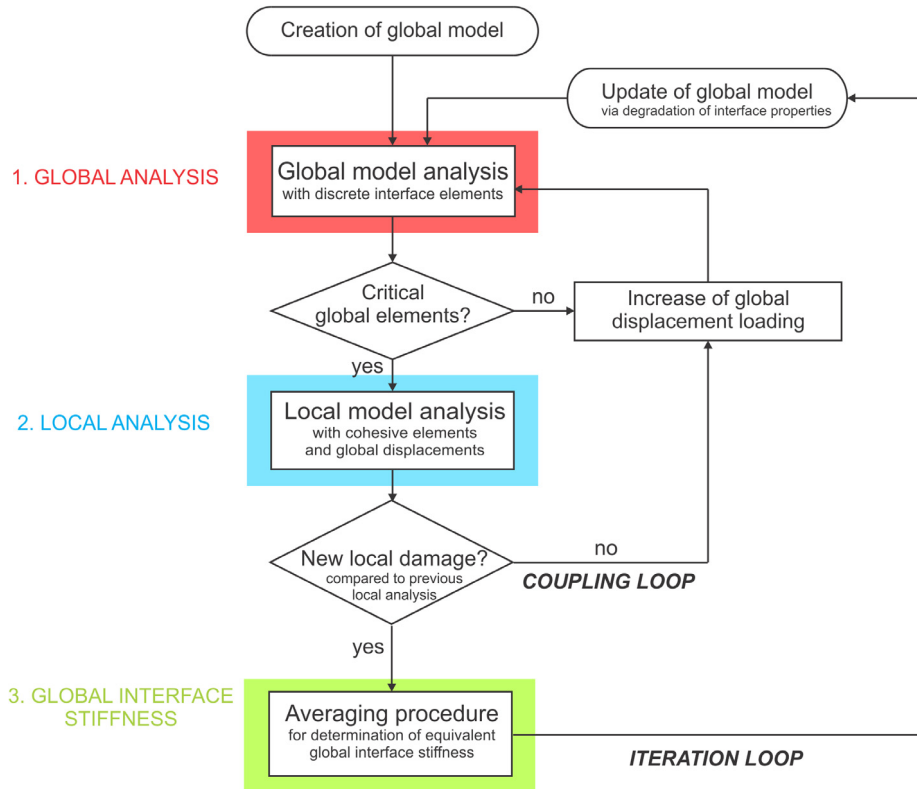


Fig. 3. Flowchart of the two-way loose coupling procedure for the skin-stringer debonding.

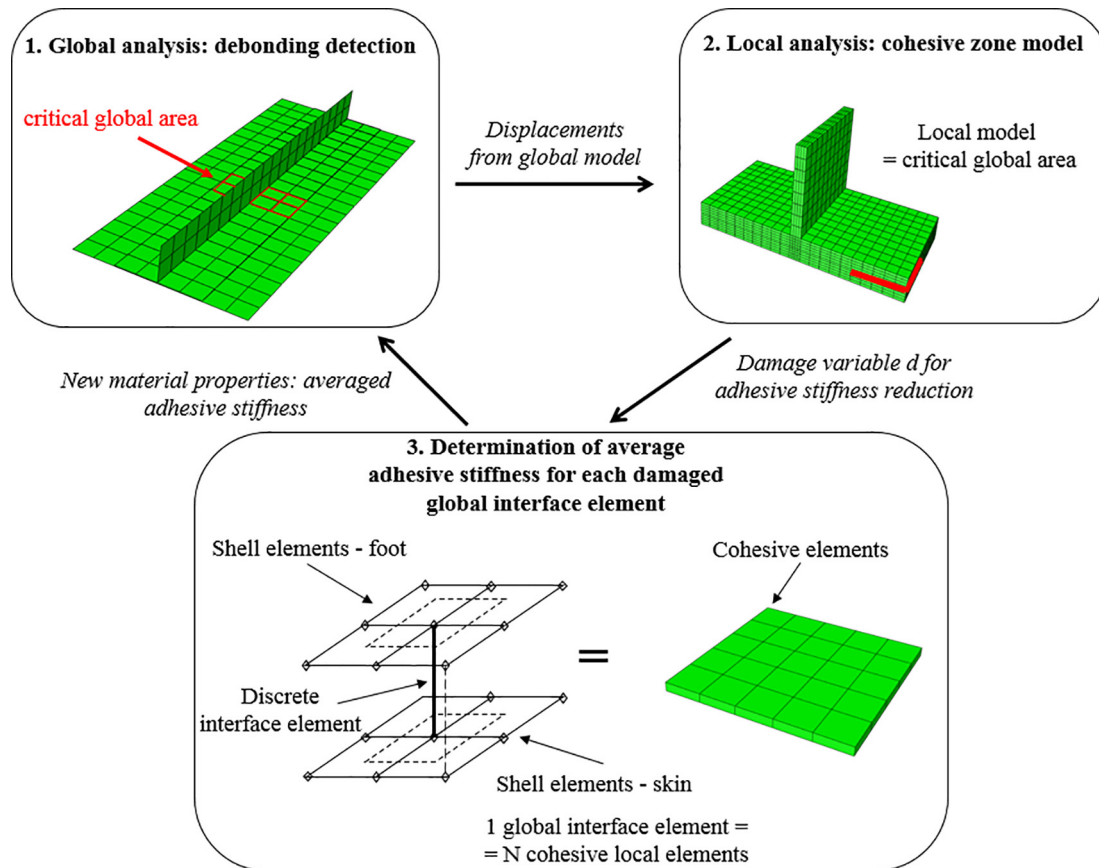


Fig. 4. Two-way loose coupling procedure for the debonding: application to a composite stiffened panel.



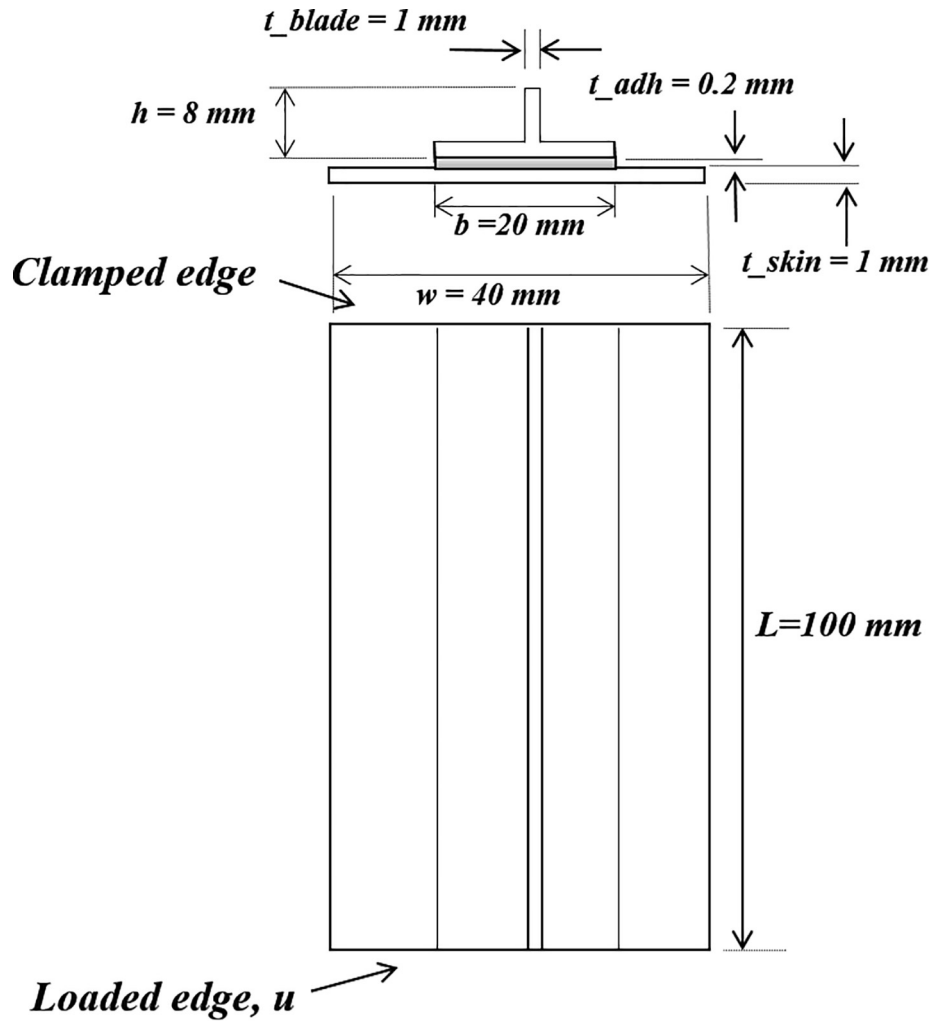


Fig. 5. Geometry of stiffened panel.

and adhesive properties averaging. These three steps are repeated consecutively until the final collapse is detected. The information exchange between global and local level that ensures two-way coupling is performed at each stage.

### 3. One-stringer stiffened panel under compression

In this section, a stiffened composite panel with one T-stringer under compression, see Fig. 5, is analysed in order to capture skin-stringer debonding with the global-local approach. The unidirectional symmetrical layups for the skin and the stringer are chosen as  $[0, 90]_s$ . One of the transverse edges is fully clamped, except for the longitudinal direction, and displacement is applied at the opposite edge. Both longitudinal edges are free to deform. Material and geometrical parameters are listed in Tables 1 and 2 respectively. These values were taken from the academic application suggested by [23].

Table 1  
Geometry of stiffened composite panel.

Description	Value
Panel length, $l$ (mm)	100
Panel width, $w$ (mm)	40
Stringer width, $b$ (mm)	20
Stringer height, $h$ (mm)	8
Laminate thickness, $t_{skin}, t_{blade}$ (mm)	1
Adhesive thickness, $t_{adh}$ (mm)	0.2

Table 2  
Material data for composite and adhesive.

Stiffness properties	Value
Young's modulus in 1-direction, $E_{11}$ (GPa)	146.5
Young's modulus in 2-direction, $E_{22}$ (GPa)	9.7
Shear modulus in 12-plane, $G_{12}$ (GPa)	5.1
Poisson's ratio, $\nu_{12}$	0.28
Young's modulus of adhesive, $E_{glue}$ (GPa)	3.0
Poisson's ratio of adhesive $\nu_{glue}$	0.4

#### 3.1. Global model: linear elasticity

The global model, which is referred to a model with a coarse mesh from first global step consists of 280 conventional 4-node shell elements with reduced integration (S4R in Abaqus) and a side-length of 5 mm, which are used to represent the skin and the stringer. As discussed earlier, the adhesive layer is not modelled with cohesive elements in order to keep the global model analysis fast and consistent. Instead of cohesive elements, 105 connector elements of Cartesian type (CONN3D2 in Abaqus) are applied. The \*Offset parameter is implemented to reference shell surfaces that offsets the nodes of stringer and skin from the middle surfaces towards the lower and upper surfaces respectively. This technique facilitates the implementation of a connection between shell nodes of skin and stringer and also ensures that real lengths and nodal forces are calculated for interface elements. Mesh density is the same for the full structure and corresponding nodes

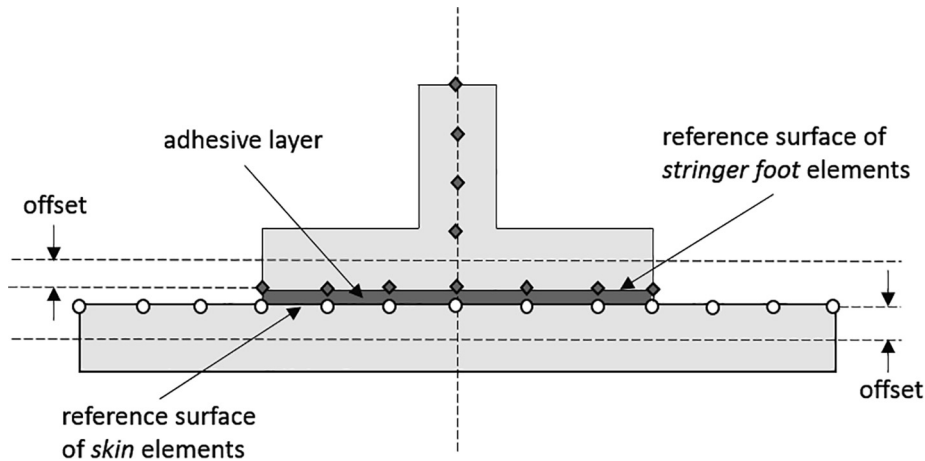


Fig. 6. Geometry of section of stiffened panel.

of skin and stringer are situated in front of each other, as shown in Fig. 6, so that they could be easily tied by connector elements. Critical areas, where the onset of skin-stringer separation is expected, are detected relying on the quadratic stress criterion given in Eq. (3). Buckling is triggered by utilizing an initial geometrical imperfection as the first eigenmode of the preliminary linear buckling simulation of the stiffened panel. However, as skin and stringer are tied by connector elements, the consequent degradation of the interface stiffnesses may lead to the problem concerning layer interpenetration. To avoid this issue, a \*Clearance option available in Abaqus is utilized. An initial clearance of 0.00005 mm is specified to prevent node penetration of two shell surfaces. After completion of the local analysis, degraded stiffnesses of connector elements are calculated based on Eq. (7), multiplying global connector stiffness by the corresponding averaged damage variable from local cohesive elements. Then global analysis is performed from the beginning. Connector elements retain initial properties until the loading displacement is reached when the damage onset was predicted. Afterwards, each connector element obtains degraded or not degraded stiffness based on local analysis information. All the stiffnesses are collected and read from the separate input file.

### 3.2. Local models: nonlinear material model

Locations of local models are identified based on critical areas determined during the global analysis. Local models represent skin and flange of the stringer where the debonding is expected to propagate. The web of the stringer is also included in the local model, as further investigations should be conducted to understand the influence of the stringer on the debonding mechanism. The skin and the stringer are modelled with 8-nodes linear solid elements (C3D8 in Abaqus) and 8-nodes cohesive elements with non-zero thickness (COH3D8 in Abaqus) and bilinear traction-separation law are chosen for the adhesive layer. Interface properties, such as strength and fracture toughness, are summarised in Table 3. The in-plane length of the local element is 1 mm as with preliminary mesh convergence studies it was confirmed to be sufficiently enough for this kind of panel. The out-of-plane length is 0.25 mm which leads to one element per lamina in thickness direction.

Table 3  
Material data for cohesive elements.

Cohesive element properties	Value
Interface element stiffness before the damage onset, $K$ (N/mm <sup>3</sup> )	10 <sup>6</sup>
Interfacial strength, mode I, $\tau_I$ (MPa)	61
Interfacial strength, mode II and III, $\tau_{II}$ , $\tau_{III}$ (MPa)	68
Fracture toughness, mode I, $G_{Ic}$ (N/mm)	0.243
Fracture toughness, mode II and III, $G_{IIc}$ , $G_{IIIc}$ (N/mm)	0.514

Four cohesive elements per length of one local element are utilized, as mesh convergence verification has not determined significant improvements with further increase of the cohesive elements number, see Fig. 7. To connect solid elements of skin and foot of the stringer to the larger number of cohesive elements, \*Tie constraint is utilized. Following the advice in [29], the master surface belongs to solid elements, whereas slave surfaces are defined on the cohesive elements. During the softening behaviour and stiffness degradation that is characteristic for cohesive elements convergence difficulties may occur in Abaqus Standard. That is the reason for using viscous regularization of the constitutive equations to overcome this issue. A relatively high viscous parameter of  $10^{-3}$  has been chosen for the local analysis with cohesive elements. Though each particular case requires a special judgement in order to keep a balance between numerical convergence and experimental results, as higher viscosity parameters might result in higher load peaks.

After local numerical analysis is terminated, the degraded damage variables  $d$ , described in Eq. (5) are extracted for each local cohesive element with the help of an additionally Python written script. The procedure is similar to the extraction of local damaged intralaminar properties conducted in previous studies [23].

### 3.3. Local-global transition

The difference in mesh size between the global and local model requires the implementation of an averaging procedure, see Eq. (7), to determine the equivalent reduced global stiffness of interface elements. Afterwards, a mapping technique is applied to map each global connector element to the area of local cohesive elements and thereby the degraded stiffness of this connector element is determined. This is realized in a Matlab procedure using the coordinates of the elements.

### 3.4. Reference solid model

The reference model is a full 3D model of a stiffened panel. It consists of 30,400 linear solid elements (C3D8 in Abaqus) for skin and stringer of the panel and 38,400 cohesive interface elements (COH3D8 in Abaqus) for the adhesive layer. The preliminary studies also include a test with implementation of 20-node bilinear solid elements for modelling skin and stringer. No significant improvements regarding damage prediction or final failure load were observed. Hence, it has been concluded that linear solid elements exhibit a satisfactory level of accuracy and efficiency. In order to keep consistency, the mesh density chosen for the reference model is the same as for local models. Also a bilinear traction-separation law is utilized for cohesive elements in order to investigate debonding between skin and stringer. An initial geometrical imperfection is represented by the first eigenmode of the

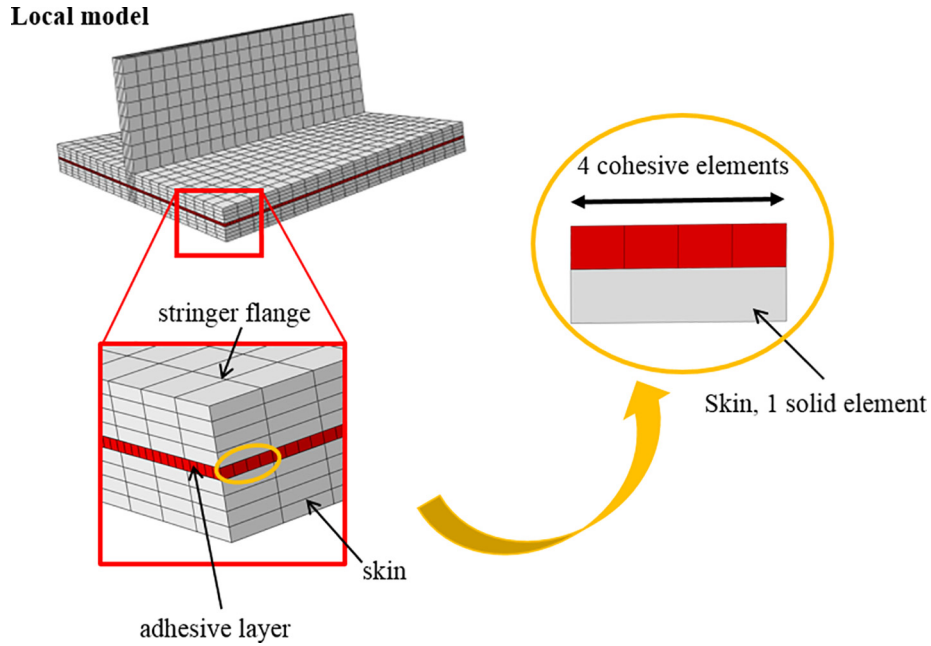


Fig. 7. 3D local model with cohesive elements.

stiffened panel similarly to the global shell model.

### 3.5. Coupling results

The coupling procedure is carried out through six coupling loops, each of them consists of several iterations. During each coupling loop, the prescribed displacement is increased based on the following principle: either critical area should evolve or new critical regions should

appear. This leads to a consequent expansion of the local models. Fig. 8 demonstrates six overlay plots of the separated global shell and the local solid models where increase of the local models could be distinguished from step 1 to step 2 and from step 3 to step 4. It should be mentioned that connector elements demonstrated an evolution of the damage during some coupling loops in the areas of already existing local models. In these cases, local analysis was conducted with the same size of the local model as for the previous coupling loop, as no extension

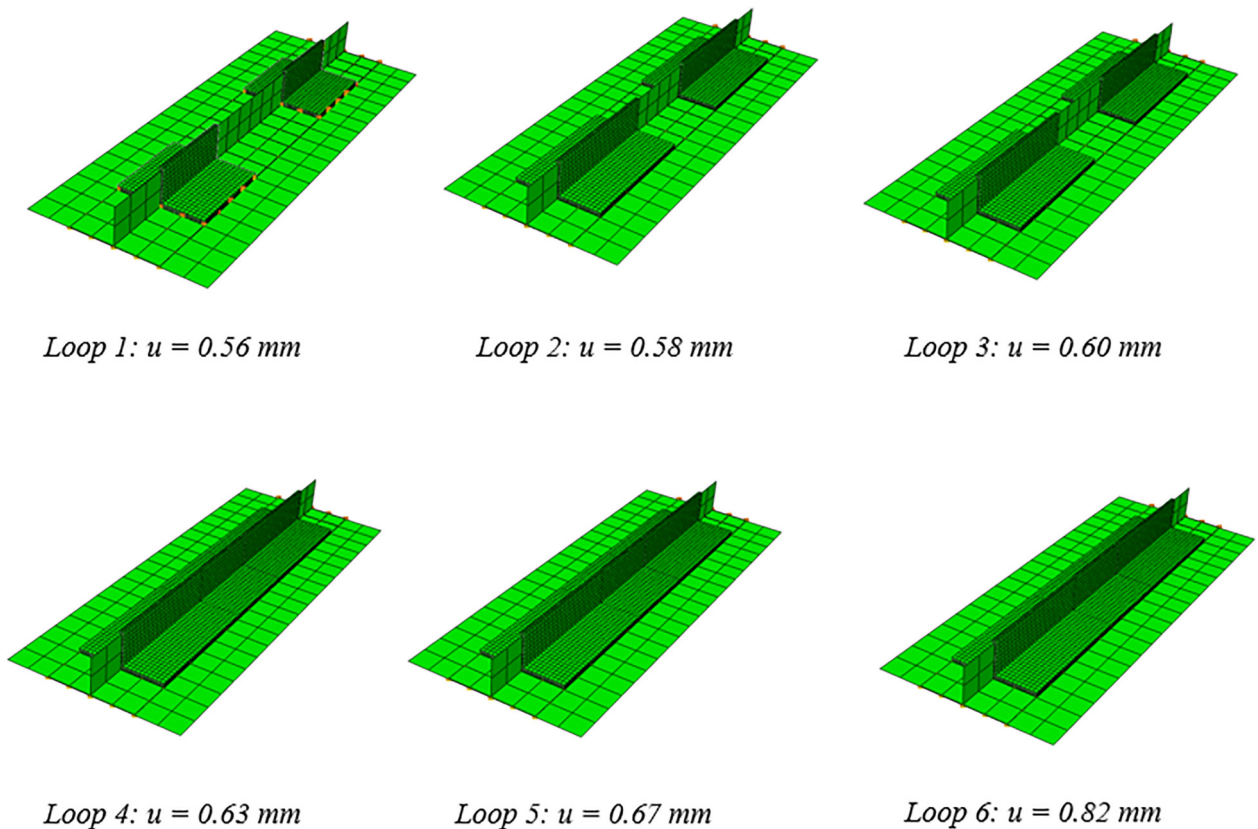


Fig. 8. Overlay plots of stiffened panel of global and local models from coupling loops 1–6.

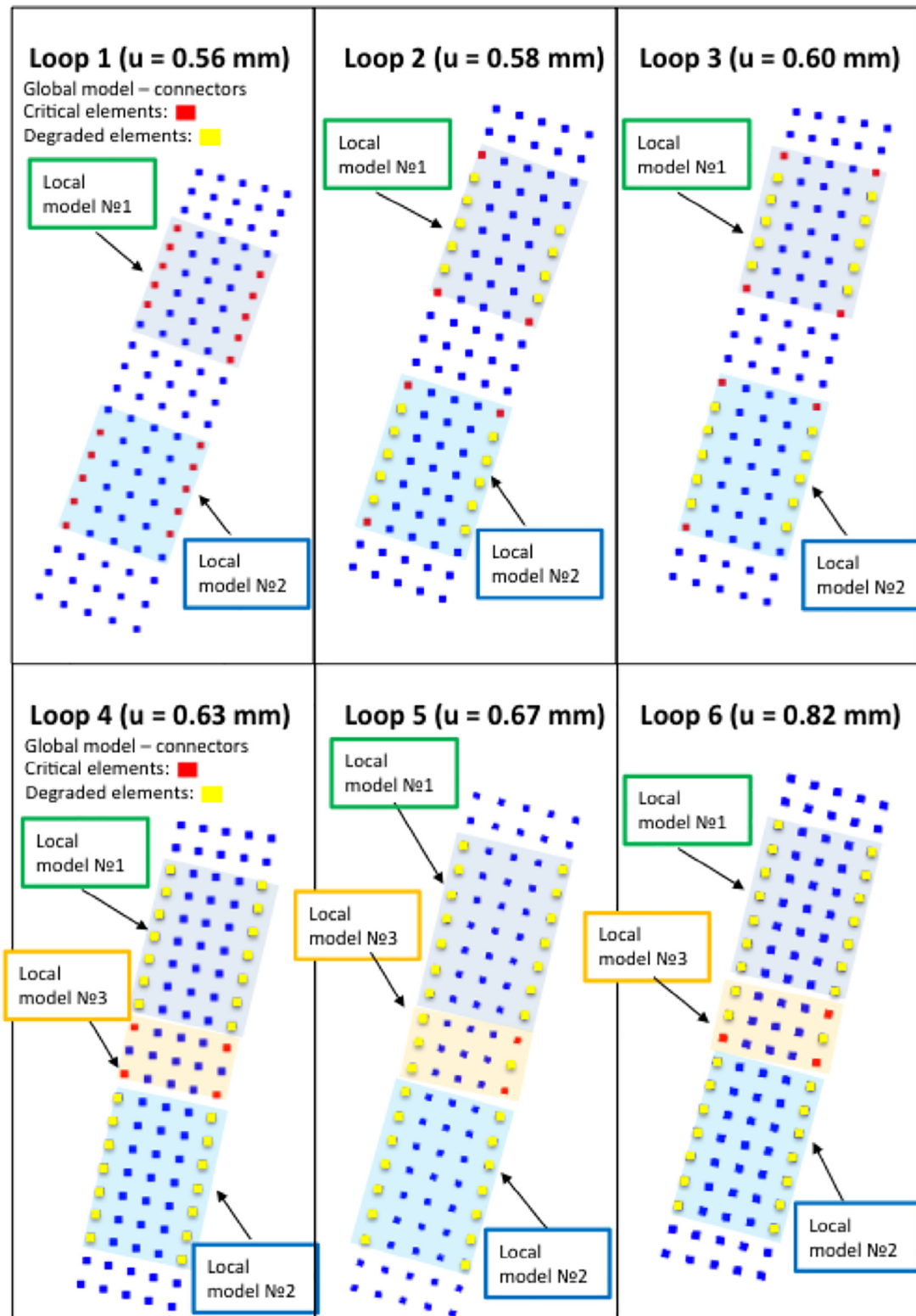


Fig. 9. Coupling loops 1–6. Debonding propagation in the global model.

of the local model would be justified.

The damage evolution in connector elements in the global model for six coupling loops is illustrated in Fig. 9. During the simulation process the first area of probable skin-stringer separation is detected by the quadratic stress criterion, see Eq. (3), at the prescribed displacement of 0.56 mm. At this applied displacement, damage takes place at free edges on both longitudinal sides of the panel, see Fig. 10a. Two local

models are created for these critical regions. The coupling loop is repeated until the convergence at the global level is reached. The skin-stringer debonding onset predicted at the global level is confirmed by the local analysis results, as both local models show cohesive elements degradation at the free edges, see Fig. 10b. Updated reduced stiffnesses for the interface elements are calculated and transferred back to the global model enabling the connection of different model levels.

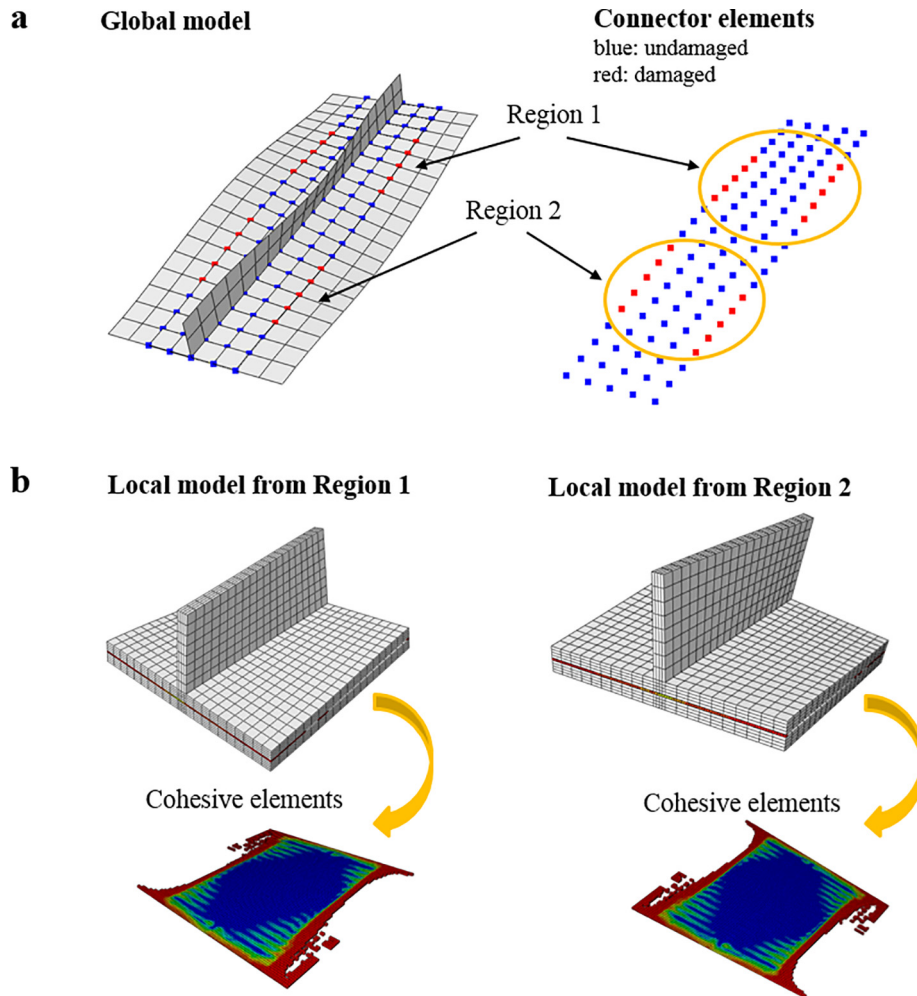


Fig. 10. Coupling loop 1. (a) Critical global regions of interface elements related to skin-stringer separation, (b) local models for the Regions 1 and 2 with corresponding damaged cohesive elements.

Along the second coupling loop with displacement of 0.60 mm damaged areas are enlarged as new connector elements are identified as being critical, see Fig. 9. It is important to mention that due to the previously degraded stiffness of connector elements the load in the interface has been redistributed to the neighbouring elements. The third coupling loop with an increase of applied displacement to 0.58 mm registers no expansion of local models. After the completion of the third coupling loop, an increase of displacement to 0.63 mm during the fourth coupling loop provokes the spread of the skin-stringer debonding along both free edges. The third local model has been created in the middle of the panel, refer to a Fig. 8 where three local models have neighbouring elements. The reason for examining three local models instead of single unified one is that this approach is slightly faster and is assumed to be sufficiently accurate. The fifth coupling loop has prescribed displacement of 0.67 mm and demonstrates damage evolution within the sizes of local models identified previously. Finally, in the sixth coupling loop the prescribed displacement reaches 0.82 mm. This final displacement increase results in a rapid propagation of the damage through the interface, followed by almost full deletion of cohesive elements in the local models and in total stiffness reduction of the whole structure. Consequently, the final failure of the stiffened panel is attained which is regarded as the logical end for the coupling procedure.

Global, local and reference models analyses were carried out under the same computational characteristics. Relative calculation times are 330 s for the last global model step and 40,884 s for the full 3D

reference model, respectively. This difference is due to the high level of discretization and inclusion of material nonlinearity to the reference model. However, in order to determine computational time of the global-local procedure, global model should be solved several times until the detection of the final failure, and this time should be added to the calculation of the local models. In Table 4 numerical characteristics of aforementioned models are represented. In the current studies, local models under consideration demonstrated computational time from 2449 s for the first local model at the first coupling loop to 13,339 s for the second local model at the last coupling loop. Hence, for the selected benchmark panel the global-local approach demonstrates a computational time similar to the one of the reference model. The relatively

**Table 4**  
Computational characteristics of models.

Model	Number of nodes	Number of elements	Degrees of freedom	Relative computational time, s
Reference model	192,136	68,800	463,980	40,884
Global model, 6th coupling loop	756	385	2331	330
Local model, 1st coupling loop	35,636	12,160	86,160	2,449
Local model, 6th coupling loop	51,816	18,240	126,420	13,339

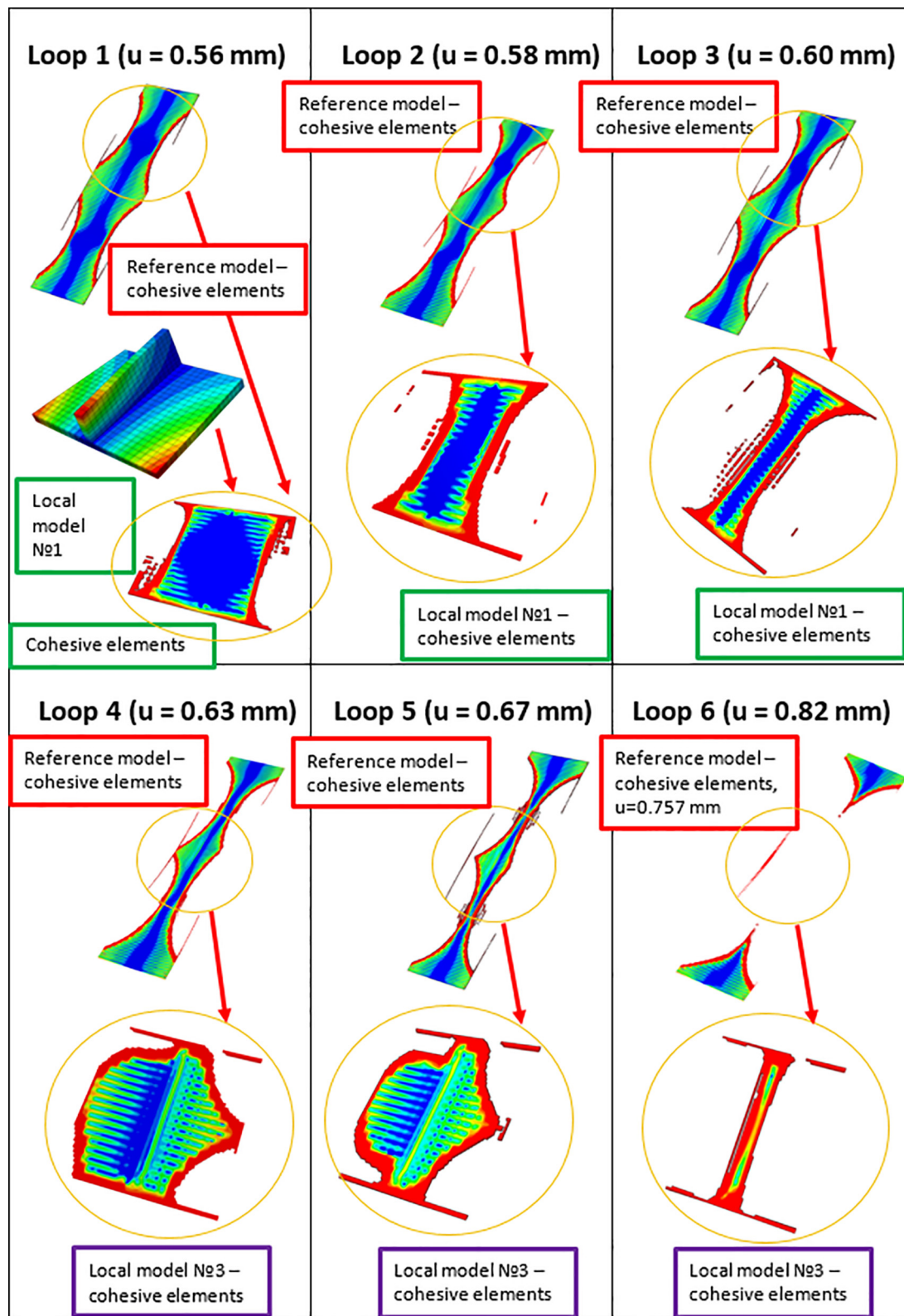


Fig. 11. Comparison of reference model with local models results for cohesive elements.

large computational effort of the global-local results can be attributed to the large size of the local models as compared to the global model, see Fig. 8. It can, however, be noticed that the first local model was solved approximately 16 times faster than the full reference model. It is therefore important to note that in case of the localized and relatively small area of damage the global-local method is not only an accurate

approach, but also advantageous in time-saving.

A comparison between reference model and local models degradation is shown in Fig. 11 for coupling loops 1–6. In Table 5 a comparison between the debonded areas of the local models and the corresponding regions of the reference model is presented for each coupling loop. During the first coupling analysis the local model demonstrates slower

**Table 5**  
Comparison between debonded area of reference and local models.

Model	Loop 1	Loop 2	Loop 3	Loop 4	Loop 5	Loop 6
Reference model, debonded area, mm <sup>2</sup>	199	244	355	151	284	484
Local model, debonded area, mm <sup>2</sup>	118	281	477	154	221	425

deletion of cohesive elements resulting in a difference of 41% in debonded area compared to the reference model, see Table 5. Though already after coupling loop 2, reference and local model results are in a relatively good agreement. During coupling loop 4, damage at free edges in the middle of the panel is detected at the global level. The local model shows degradation in this area, though the damage in the reference model evolves slightly differently. However, in the sixth coupling loop the local model demonstrates the deletion of almost all distorted cohesive elements with a good agreement to the reference model.

Load-displacement curves for both reference solid model and coupling loops are presented in Fig. 12. Distinct drops of the coupling curve correspond to each global-local loop that is characterised by the reduction of interface stiffness. Each coupling loop is enumerated from 1 to 6 on the plot. The reference curve is smoother because the cohesive elements properties have been degraded incrementally. Both curves are in a good agreement, in particular with regard to the structural stiffness before and after first buckling takes place. Buckling in the coupling simulations occurs slightly earlier at a displacement of 0.147 mm and for the reference model at 0.167 mm resulting in a slight difference in curves, though lying in parallel and, thus, having similar stiffnesses. The final failure of the reference model takes place at a displacement of 0.76 mm that corresponds to the load level of 20.54 kN, whereas for the coupling loops the maximum displacement and load are 0.78 mm and 20.68 kN respectively. The relative deviation between maximum supported loads for the stiffened panel in compression is reported to be around 0.7%. The latter conclusion demonstrates the capability of the global-local approach to simulate full 3D behaviour with regard to a reliable prediction of skin-stringer debonding initiation, evolution and final collapse.

**4. Validation with experimental results**

In this section, the applicability of the global-local approach to a real stiffened composite panel with available experimental results is

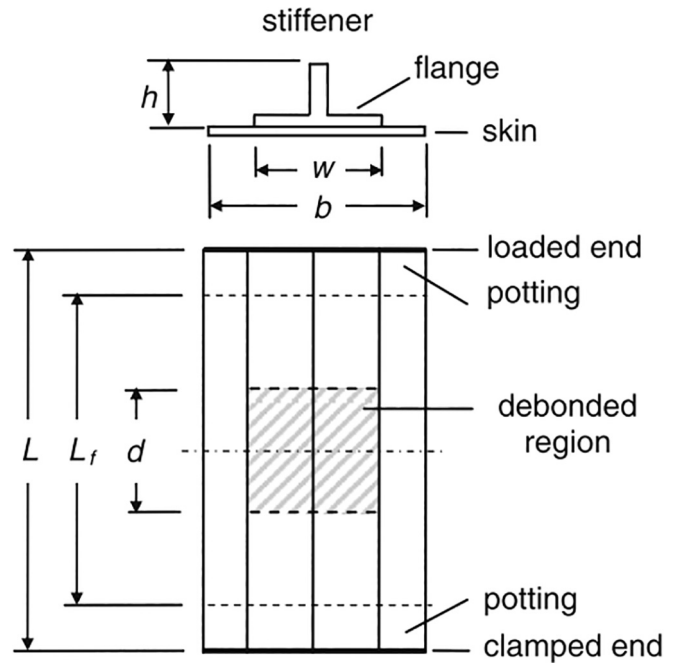


Fig. 13. Geometry of initially debonded stiffened panel design D1 (from [31]).

investigated. The specimen has been tested by Orifici et al. [31] and denoted as initially debonded single-stiffener D1 panel during their studies. This particular choice of a panel with preliminary skin-stringer separation is explained by the goal to examine a specimen with localized debonding that is expected to dominate over the intralaminar damage and demonstrate the full advantage of creating relatively small local models. In Fig. 13 a sketch of geometric configuration for the

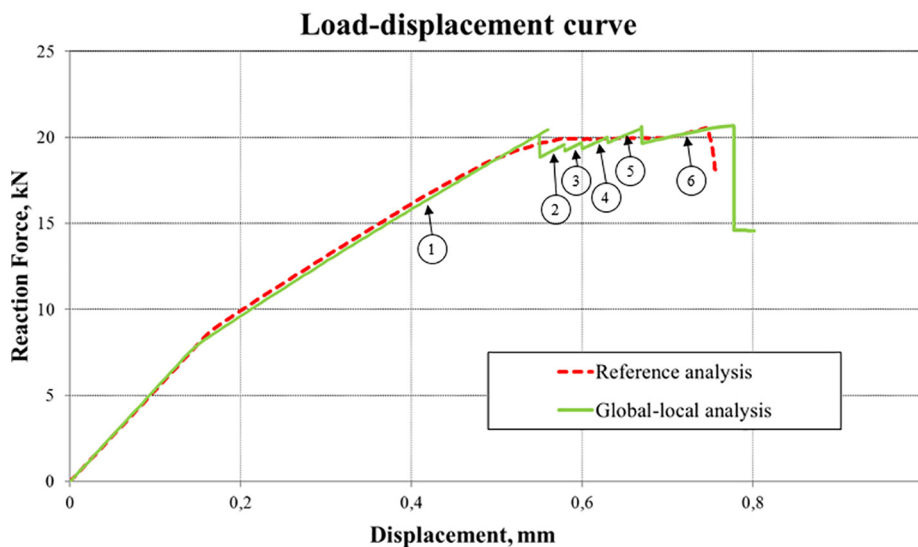


Fig. 12. Load-displacement curve for progressive failure analysis of stiffened panel.

**Table 6**  
Geometry of initially debonded stiffened composite panel D1 (from [31]).

Description	Value
Total length, $L$ (mm)	400
Free length, $L_f$ (mm)	300
Width, $b$ (mm)	64
Skin lay-up	$[90, \pm 45, 0]_s$
Stiffener lay-up	$[(\pm 45)_3, 0_6]_s$
Ply thickness, $t$ (mm)	0.125
Stiffener height, $h$ (mm)	14
Stiffener width, $w$ (mm)	32
Debond length, $d$ (mm)	80

**Table 7**  
Material data for IM7/8552 carbon/epoxy unidirectional tape (from [31]).

Stiffness properties	Value
Young's modulus in 1-direction, $E_{11}$ (GPa)	147
Young's modulus in 2-direction, $E_{22}$ (GPa)	11.8
Shear modulus in 12-plane, $G_{12}$ (GPa)	6
Shear modulus in 31-plane, $G_{31}$ (GPa)	6
Shear modulus in 23-plane, $G_{23}$ (GPa)	4
Poisson's ratio, $\nu_{12}$	0.3

debonded panel is shown, the geometric and material data of the specimen are reported in Tables 6 and 7 respectively with descriptions used by Orifici et al. [31]. The panel was manufactured with IM7/8552 UD material for the skin and stringer, whereas for the adhesive layer FM 300 was utilized. In the previous section the interface properties were taken for this material also from [31], refer to Table 3 for details.

#### 4.1. Global model: linear elasticity

The shell global model is created similarly to the aforementioned benchmark panel. After a preliminary mesh convergence studies, the in-plane size length of 4 mm is determined, which resulted in 2800 conventional shell elements (S4R in Abaqus) and 909 connector elements tying the opposite lying nodes of the skin and stringer surfaces. The first eigenmode is utilized as an initial geometric imperfection to perturb the panel in a postbuckling regime similar to the one described in [31]. The following boundary conditions are applied: (1) one transverse edge is fully restrained denoted as clamped end, (2) the opposite edge is restricted to move in any direction except longitudinal and correspond to a loaded end, (3) two pottings are allowed to move only in the

longitudinal direction, see Fig. 13. Both longitudinal edges remain free to deform.

#### 4.2. Local models: nonlinear material model

The local models have the same structure as the previous model - 8-nodes linear solid elements (C3D8 in Abaqus) with a side-length of 1 mm and 1 element per lamina in thickness direction resulting in a size of 0.125 mm for the skin and the stringer. Cohesive elements with bilinear traction-separation law represent the interface layer in order to track the beginning and development of the skin-stringer debonding. Four cohesive elements are utilized per in-plane side of a solid local element. The selected discretization repeats the previous model - one element per lamina in the thickness direction with 1-mm in-plane size length for structural elements. Four cohesive elements per side of one solid element are chosen.

#### 4.3. Coupling results

Global-local analysis has been conducted through four coupling loops with consequent increase of the prescribed displacement up to the following values: 1.0 mm, 1.4 mm and 1.6 mm and 2.0 mm respectively. According to experimental and numerical results, the skin and the foot of the stiffener have buckled in opposite directions that excludes issues with probable initial interpenetration of the layers during the calculations. The onset of skin-stringer separation is predicted based on the stress quadratic criterion (Eq. (3)) and begins in the areas of the initial debonding at the applied displacement of around 0.8 mm, see Fig. 14. Two local models are created for these regions respectively to examine the debonding evolution in details, see Fig. 15. A determination of global regions that are prone to debonding is proved by both local analyses demonstrating a damage onset and growth in cohesive elements. It is important to mention that the size of local models is selected appropriately, as they both cover not only distorted cohesive elements, but also undamaged ones.

The damage starts from the preliminary debonded areas and propagates further along the pre-debonded edge before growing in the longitudinal directions. The obtained damage evolution path fully corresponds to the experimental results reported in [31]. The full debonded length in global-local analysis increased from 80 mm to 120 mm. As it was reported in [31], the debonding attained the value of 165 mm, though it was also stated that the fibre fracture could interact with debonding in this case and may influence the difference at the final loads.

Load-displacement curves are shown in Fig. 16 for global-local coupling results compared to experimental results. Each of the coupling

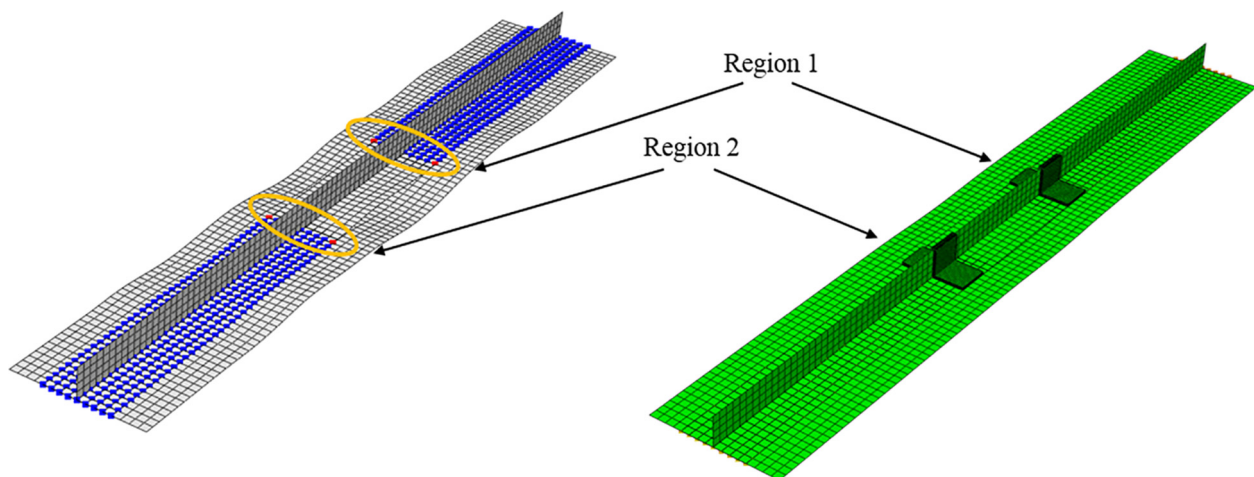


**Fig. 14.** Coupling loop 1. Critical global areas (left) and overlay plot of two corresponding local models (right) for debonded panel D1.



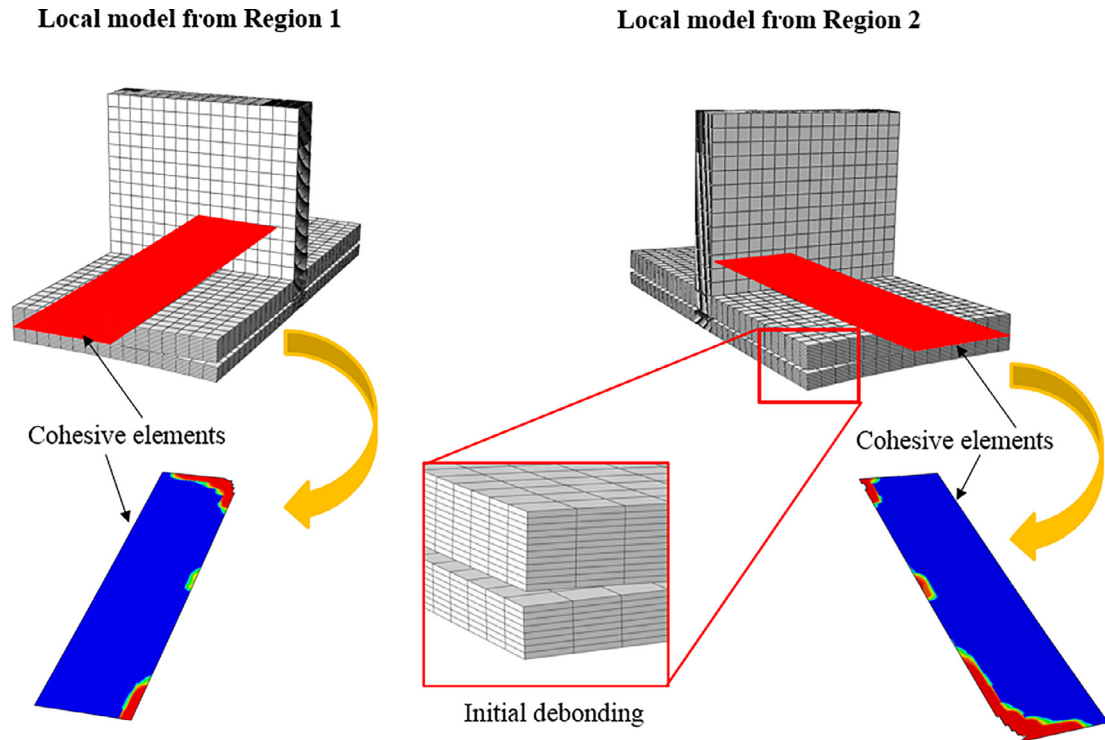


Fig. 15. Coupling loop 1. Local models for Regions 1 and 2 with corresponding cohesive elements.

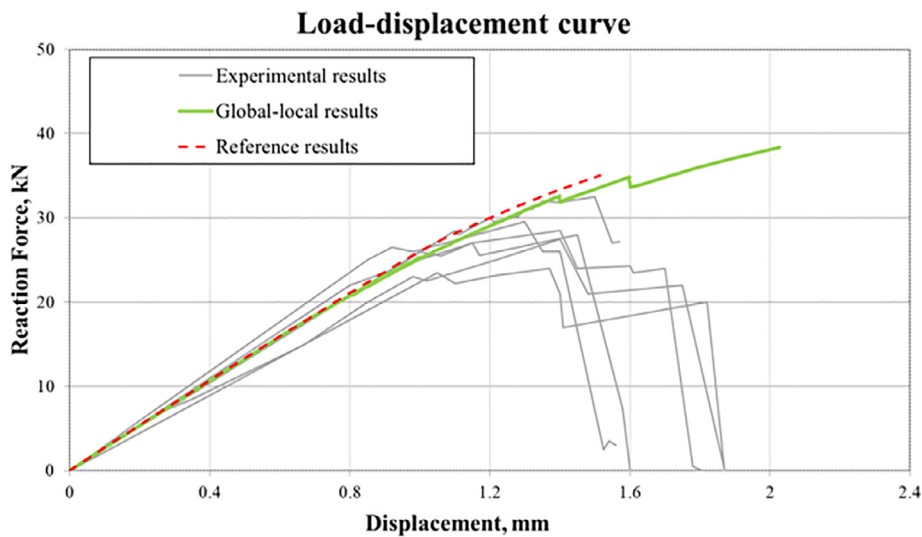


Fig. 16. Load-displacement curves of global-local analysis for debonded panel D1 with comparison to experimental results.

loops has a slight drop-off that corresponds to the reduction of the interface stiffness in the global model after application of new properties from the local models. Comparison to the full solid reference model has been also carried out until a prescribed displacement 1.5 mm, demonstrating a good agreement with the global-local analysis curve. The structural stiffness is regarded as well predicted by global-local analysis, though since no intralaminar damage was considered, the final collapse could not be attained. That is why the procedure was finished after the prescribed load of 2.0 mm. It is important to note that the global-local approach provides an accurate prediction of the structural behaviour during onset and evolution of the debonding in terms of damage location and stiffness reduction.

### 5. Conclusion

A novel two-way coupling global-local finite element approach for skin-stringer separation of stiffened composite panels has been developed. The method is based on different levels of accuracy and separate, subsequent simulations of global and local models that is computationally more efficient than full 3D analysis. A global numerical analysis with a standard mesh is performed to define critical areas prone to debonding. Local models are created based on the locations determined by the global analysis. The key challenge of establishing a link between the two models with different discretization level has been achieved. An accurate information exchange between the global and the local level is ensured by application of discrete and continuum interface elements that follow the same traction-separation law.

Firstly, progressive failure analysis was assessed through the

application to the representative case of a one-stringer panel, which demonstrated the effectiveness of the method. Load-displacement curves of the coupling analysis and the solid element reference analysis were in reasonably good agreement. The predictions of both the maximum load level and the sequence of stiffness reductions in the structure showed similar results.

The applicability of the global-local approach was also validated through a comparison with results of a T-stringer panel with an initial debond, previously tested experimentally in [36]. Reasonably good agreement between coupling analysis and experimental results has been demonstrated until the final collapse. As expected, damage started in the area of the initial debonding and propagated further, leading to an increase of skin-stringer separation. However, the smaller regions of debonding predicted in the numerical simulations might be related to the damage modes considered. Intralaminar damage (matrix and fibre damage) were not accounted for in the analyses presented.

The global-local approach developed shows the possibility to establish an effective and efficient procedure for the modelling of skin-stiffener debonding in stiffened composite panels. This global-local technique can be combined with procedures for interlaminar and intralaminar damage of laminates to model the progressive failure of composite panels considering various failure modes.

### Acknowledgments

The research leading to these results has received funding from European Union's Horizon 2020 research and innovation program (FULLCOMP/2015-2019) under Marie Skłodowska-Curie actions grant agreement number 642121. The provided financial support is gratefully acknowledged by the authors.

### References

- [1] Degenhardt R, Kling A, Klein H, Hillger W, Goetting HC, Zimmermann R, Rohwer K. Experiments on buckling and postbuckling of thin-walled CFRP structures using advanced measurement systems. *Int J Struct Stab Dyn* 2007;7(2):337–58.
- [2] Krueger R. The virtual crack closure technique for modeling interlaminar failure and delamination in advanced composite materials. Elsevier Ltd.; 2015. <http://dx.doi.org/10.1016/B978-0-08-100332-9.00001-3>.
- [3] Rybicki E, Kamminen MF. A finite element calculation of stress intensity factors by modified crack closure integral. *Eng Fract Mech* 1977;9:931–8. [http://dx.doi.org/10.1016/0013-7944\(77\)90013-3](http://dx.doi.org/10.1016/0013-7944(77)90013-3).
- [4] Dugdale DS. Yielding of steel sheets containing slits. *J Mech Phys Solids* 1960;8:100–4.
- [5] Barenblatt GI. The mathematical theory of equilibrium cracks in brittle fracture. *Adv Appl Mech* 1962;7(C):55–129. [http://dx.doi.org/10.1016/S0065-2156\(08\)70121-2](http://dx.doi.org/10.1016/S0065-2156(08)70121-2). arXiv:S0065-2156(08)70121-2.
- [6] Hillerborg A, Modeer M, Petersson P-E. Analysis of crack formation and crack growth in concrete by means of fracture mechanics and finite elements. *Cem Concr Res* 1976;6:773–82.
- [7] Davila C, Camanho P, de Mora M. Mixed-mode decohesion elements for analyses of progressive delamination. *Am Inst Aeronaut Astronaut* 2001. <http://dx.doi.org/10.2514/6.2001-1486>. AIAA-01-1486.
- [8] Turon A, Camanho PP, Costa J. An engineering solution for mesh size effects in the simulation of delamination using cohesive zone models. *Eng Fract Mech* 2007;74:1665–82. <http://dx.doi.org/10.1016/j.engfracmech.2006.08.025>.
- [9] Allix O, Ladevèze P. Interlaminar interface modelling for the prediction of laminate delamination. *Compos Struct* 1992;22:235–42.
- [10] Jiang W-G, Hallett SR, Green BG, Wisnom MR. A concise interface constitutive law for analysis of delamination and splitting in composite materials and its application to scaled notched tensile specimens. *Int J Numer Meth Eng* 2007;69(9):1982–95. <http://dx.doi.org/10.1002/nme.1842>.
- [11] Turon A, Camanho PP. A damage model for the simulation of delamination in advanced composites under variable-mode loading. *Mech Mater* 2006;38:1072–89. <http://dx.doi.org/10.1016/j.mechmat.2005.10.003>.
- [12] Camanho PP, Dávila CG. Mixed-mode decohesion finite elements for the simulation of delamination in composite materials. *NASA/TM-2002-211737*; 2002: 1–37.
- [13] Borg R, Nilsson L, Simonsson K. Simulation of delamination in fiber composites with a discrete cohesive failure model. *Compos Sci Technol* 2001;61(5):667–77. [http://dx.doi.org/10.1016/S0266-3538\(00\)00245-1](http://dx.doi.org/10.1016/S0266-3538(00)00245-1).
- [14] Wisnom MR, Chang FK. Modelling of splitting and delamination in notched cross-ply laminates. *Compos Sci Technol* 2000;60(15):2849–56. [http://dx.doi.org/10.1016/S0266-3538\(00\)00170-6](http://dx.doi.org/10.1016/S0266-3538(00)00170-6).
- [15] Xie D, Waas AM. Discrete cohesive zone model for mixed-mode fracture using finite element analysis. *Eng Fract Mech* 2006;73(13):1783–96. <http://dx.doi.org/10.1016/j.engfracmech.2006.03.006>.
- [16] Hallett SR, Wisnom MR. Numerical investigation of progressive damage and the effect of layup in notched tensile tests. *J Compos Mater* 2006;40(14):1229–45. <http://dx.doi.org/10.1177/0021998305057432>.
- [17] Wang JTS, Bigger SB. Skin-stiffener interface stresses in composite stiffened panels. *NASA Contractor Report* 172261.
- [18] Balzani C, Wagner W. Numerical treatment of damage propagation in axially compressed composite airframe panels. *Int J Struct Stab Dyn* 2010;10(4):683–703. <http://dx.doi.org/10.1142/S0219455410003683>.
- [19] Riccio A, Raimondo A, Scaramuzzino F. A robust numerical approach for the simulation of skin-stringer debonding growth in stiffened composite panels under compression. *Compos Part B* 2015;71:131–42. <http://dx.doi.org/10.1016/j.compositesb.2014.11.007>.
- [20] Raimondo A, Riccio A. Inter-laminar and intra-laminar damage evolution in composite panels with skin-stringer debonding under compression. *Compos Part B* 2016;94:139–51. <http://dx.doi.org/10.1016/j.compositesb.2016.03.058>.
- [21] Yap JWH, Scott ML, Thomson RS, Hachenberg D. The analysis of skin-to-stiffener debonding in composite aerospace structures. *Compos Struct* 2002;57(1–4):425–35. [http://dx.doi.org/10.1016/S0263-8223\(02\)00110-1](http://dx.doi.org/10.1016/S0263-8223(02)00110-1).
- [22] Falzon BG, Davies GAO, Greenhalgh E. Failure of thick-skinned stiffener runout sections loaded in uniaxial compression. *Compos Struct* 2001;53:223–33.
- [23] Hühne S, Reinoso J, Jansen E, Rolfes R. A two-way loose coupling procedure for investigating the buckling and damage behaviour of stiffened composite panels. *Compos Struct* 2016;136:513–25. <http://dx.doi.org/10.1016/j.compstruct.2015.09.056>.
- [24] Krueger R, Ratcliffe JG, Minguet PJ. Panel stiffener debonding analysis using a shell/ 3D modeling technique. *Compos Sci Technol* 2009;69(14):2352–62. <http://dx.doi.org/10.1016/j.compscitech.2008.12.015>.
- [25] Borrelli R, Riccio A, Sellitto A, Caputo F, Ludwig T. On the use of global – local kinematic coupling approaches for delamination growth simulation in stiffened composite panels. *Compos Sci Technol* 2015;115:43–51. <http://dx.doi.org/10.1016/j.compscitech.2015.04.010>.
- [26] Alesi H, Nguyen V, Mileshekin N, Jones R. Global/local postbuckling failure analysis of composite stringer/skin panels. *AIAA J* 1998;36(9):5. <http://dx.doi.org/10.2514/2.575>.
- [27] Faggiani A, Falzon BG. Optimization strategy for minimizing damage in post-buckling stiffened panels. *AIAA J* 2007;45(10):2520–8. <http://dx.doi.org/10.2514/1.26910>.
- [28] Bertolini J, Castanié B, Barrau J-J, Navarro J-P, Petiot C. Multi-level experimental and numerical analysis of composite stiffener debonding. Part 2: Element and panel level. *Compos Struct* 2009;90(4):392–403. <http://dx.doi.org/10.1016/j.compstruct.2009.04.002>.
- [29] Reinoso J, Blázquez A, Estefani A, París F, Cañas J, Arévalo E, Cruz F. Composites: Part B experimental and three-dimensional global-local finite element analysis of a composite component including degradation process at the interfaces. *Compos Part B* 2012;43(4):1929–42. <http://dx.doi.org/10.1016/j.compositesb.2012.02.010>.
- [30] Vescovini R, Dávila CG, Bisagni C. Composites: Part B failure analysis of composite multi-stringer panels using simplified models. *Compos Part B* 2013;45(1):939–51. <http://dx.doi.org/10.1016/j.compositesb.2012.07.030>.
- [31] Orifici AC, de Zarate Alberdi IO, Thomson RS, Bayandor J. Compression and post-buckling damage growth and collapse analysis of flat composite stiffened panels. *Compos Sci Technol* 2008;68(15–16):3150–60. <http://dx.doi.org/10.1016/j.compscitech.2008.07.017>.
- [32] Bettinotti O, Allix O, Perego U, Oancea V, Malherbe B. Simulation of delamination under impact using a global-local method in explicit dynamics. *Finite Elem Anal Des* 2017;125:1–13. <http://dx.doi.org/10.1016/j.finel.2016.11.002>.
- [33] Akterskaia M, Jansen E, Hühne S, Rolfes R. Efficient progressive failure analysis of multi-stringer stiffened composite panels through a two-way loose coupling global-local approach. *Compos Struct* 2018;183:137–45. <http://dx.doi.org/10.1016/j.compstruct.2017.02.011>.
- [34] Abaqus. Abaqus Documentation, Abaqus 6.14 Documentation. Dassault Systemes. 6.14 edn. (V); 2017: 1–172.
- [35] Benzeggagh ML, Kenane M. Measurement of mixed-mode delamination fracture toughness of unidirectional glass/ epoxy composites with mixed-mode bending apparatus. *Compos Sci Technol* 1996;56:439–49.
- [36] Orifici AC, Thomson RS, Degenhardt R, Kling A, Rohwer K, Bayandor J. Degradation investigation in a postbuckling composite stiffened fuselage panel. *Compos Struct* 2008;82:217–24. <http://dx.doi.org/10.1016/j.compstruct.2007.01.012>.

## 4 Paper C: Progressive failure analysis using global-local coupling including intralaminar failure and debonding

The following paper [4] is published in AIAA Journal, Volume 57, Number 7 (2019), pages 3078-3089 (<https://doi.org/10.2514/1.J057677>), and is reprinted by permission of the American Institute of Aeronautics and Astronautics, Inc. The main work was done by the author of this thesis.

A framework for modelling a combination of the intralaminar damage and skin-stringer debonding by means of a two-way global-local approach has been established. The main advantage of the presented strategy is that inclusion of both damage mechanisms in the global-local strategy allows for observation of progressive damage evolution similar to that shown in real composite stiffened panels. Firstly, the method has been applied to a case of a one-stringer panel and compared to a reference solution. The local models included the damage detected at the global level and could be easily adapted to consider only one type of failure or both damage mechanisms through the material degradation and skin-stringer separation with cohesive elements. The information of the damage was transferred to the global model while keeping all reduced material properties due to the previous material degradation. Load-displacement curves of coupling simulation and reference modelling demonstrated a good agreement which holds also for the sequence of the damage events detected in both analyses. Afterwards a global-local approach has been validated on an experimental single-stringer panel with a reduction of about 50% in computational time achieved by the global-local method.

The developed global-local approach combines all principal damages such as a matrix cracking, fibre breakage and skin-stringer debonding and demonstrates a serious potential in computational time savings while keeping acceptably good level of accuracy.



# Progressive Failure Analysis Using Global-Local Coupling Including Intralaminar Failure and Debonding

Margarita Akterskaia\* and Eelco Jansen†  
 Leibniz University Hannover, 30167 Hannover, Germany  
 Stephen R. Hallett‡ and Paul M. Weaver§  
 University of Bristol, Bristol, England BS8 1TR, United Kingdom  
 and  
 Raimund Rolfes¶  
 Leibniz University Hannover, 30167 Hannover, Germany

DOI: 10.2514/1.J057677

Composite laminate stiffened panels are often used in aircraft fuselage design because of their favorable properties. To assess the failure load of these thin-walled structures and to exploit their reserves, a reliable simulation capability for their postbuckling behavior is often necessary. To perform a realistic failure analysis and to accurately detect final collapse, material degradation should be considered. Global-local approaches are computationally efficient techniques to perform a progressive failure analysis and to examine localized damaged areas in detail. In this paper, a two-way coupling global-local approach is presented, including a combination of different damage modes, such as matrix cracking, fiber damage, and skin-stringer debonding. An accurate exchange of information concerning the damage state between global and refined local models is performed. From the global to the local model, the displacements are transferred through a submodeling procedure. Afterward, the degraded material properties obtained from the local model analysis are returned to the global model with a special mapping technique that accounts for the different mesh sizes at the two levels. The two-way coupling procedure is applied to the progressive failure analysis of a one-stringer composite panel loaded in compression. Finally, the numerical results of the procedure are compared with experimental results.

## Nomenclature

$A$	=	area
$C$	=	material stiffness matrix
$d$	=	damage variable for cohesive element
$d_f$	=	damage variable for the fiber degradation by Linde
$d_m$	=	damage variable for the matrix degradation by Linde
$E$	=	Young's modulus
$F$	=	force
$f_f$	=	fiber failure condition for Linde criterion
$f_m$	=	matrix failure condition for Linde criterion
$G$	=	shear stiffness
$G_f$	=	fracture energy of fiber
$G_m$	=	fracture energy of matrix
$G_I, G_{II}, G_{III}$	=	energy release rates in modes I, II and III
$G_{Ic}$	=	total critical energy release rate in mode I
$G_{IIc}$	=	total critical energy release rate in mode II
$K$	=	interface stiffness matrix
$K_0$	=	initial interface stiffness
$L$	=	length
$L_C$	=	characteristic element length
$S_A$	=	axial shear strength

$S_T$	=	transverse shear strength
$t$	=	thickness
$w$	=	width
$X_C$	=	longitudinal compressive strength
$X_T$	=	longitudinal tensile strength
$Y_C$	=	transverse in-plane compressive strength
$Y_T$	=	transverse in-plane tensile strength
$\delta$	=	maximum relative displacement

## I. Introduction

THE extensive use of fiber-reinforced composite laminates in the aircraft application for light-weight structures during the last decades is explained by their excellent material properties, such as high strength and stiffness ratios. However, composite structures demonstrate great advantages, and the numerical assessment and experimental validation involve high costs. A finite element global-local coupling approach is a widely applied methodology in failure analysis of structures that aims at reducing computational efforts on the one hand and at accurately examining critical areas where damage occurs on the other.

### A. Global-Local Coupling Methods

Within the context of coupling approaches, one-way and tight coupling methods prevail. *One-way coupling* is a term used to describe a transfer of information in one direction between separated models, that is, from the global to the local level or vice versa. *Tight coupling* means that global and local models are not separated and systems of equations are solved simultaneously. An overview of these methods can be found in Hühne et al. [1]. Certain two-way methods are available that can treat global and local models separately. The multiscale projection method by Löhnert and Belytschko [2] simulated fracture and crack propagation using XFEM to investigate the effect of macrocracks and microcracks interactions leading to damage. The adaptive progressive damage modeling technique by Labeas et al. [3] was used for the prediction of damage initiation and evolution in composite structures. Their approach combines a progressive damage modeling technique with

Presented as Paper 2018-2794045 at the 2018 AIAA SciTech Forum, Kissimmee, FL, 8–12 January 2018; received 4 July 2018; revision received 14 February 2019; accepted for publication 21 February 2019; published online 17 April 2019. Copyright © 2019 by Margarita Akterskaia. Published by the American Institute of Aeronautics and Astronautics, Inc., with permission. All requests for copying and permission to reprint should be submitted to CCC at [www.copyright.com](http://www.copyright.com); employ the eISSN 1533-385X to initiate your request. See also AIAA Rights and Permissions [www.aiaa.org/randp](http://www.aiaa.org/randp).

\*Research Associate, Institute of Structural Analysis.

†Senior Faculty Member, Institute of Structural Analysis.

‡Professor, Bristol Composites Institute (ACCIS).

§Professor, Bristol Composites Institute (ACCIS); also Bernal Institute, University of Limerick, Castletroy, Ireland.

¶Professor, Institute of Structural Analysis.

the submodeling method. The homogenization-based iterative two-way multiscale approach by Chrupalla et al. [4] accounted for the effects of local damage on the global behavior of composite structures. The main difference between the aforementioned approaches is the way the degraded properties are transferred back from the local to the global level. An efficient local-global transfer technique for composite structures proposed by Hühne et al. [1], which includes matrix and fiber failure, was based on calculation of effective material properties and is extended in the current research. The present technique is different from the ones used in other works. A more accurate homogenization scheme is used than the simplified procedure of averaging the local engineering constants performed by Labeas et al. [3]. Another advantage of the present approach is that it is nonintrusive in the sense that it can be directly combined with standardly available commercial finite element codes.

Skin-stringer debonding in composite panels has been considered by several authors. A loose one-way coupling analysis was performed by Reinoso et al. [5]. In this approach, information was transferred from the global to the local level and cohesive elements were used for the local model. Orifici et al. [6] performed global-local analysis with ply degradation and a method for capturing interlaminar crack growth based on multipoint constraints controlled using the virtual crack closure technique. The creation of the local models was based on monitoring a strength-based criterion in the skin-stiffener interface. An optimization technique employing a genetic algorithm was proposed by Faggiani and Falzon [7], which aimed at minimizing debonding damage in the postbuckling regime of stiffened panels by optimizing the laminate stacking sequence. A global-local method was applied in the analysis of a panel with I-shaped stiffeners in order to make the application of the optimization procedure feasible. The nonintrusive global-local technique by Gendre et al. [8] examined separately a global linear model of the whole structure and a local nonlinear submodel representing the critical area. After each iteration loop, a residual force vector was calculated from the difference between global and local reaction forces at the border of these models. This load vector was applied to the nodes of the global model in order to provoke the deformation of

the global model, transferring the influence of the local non-linearities. Vescovini et al. [9] performed a one-way coupling analysis. Shell elements were used for the global and local models, whereas cohesive elements were applied to model interface layer at the local level. The main limitations of existing coupling approaches are associated with their efficiency in detecting critical areas at the global level and their accuracy in information exchange between global and local levels, in particular their capability to account for mutual interaction. In the current work, a transition of degraded properties from the local to the global level assures that damage propagation is appropriately represented within a progressive failure analysis at the global level.

## B. Developed Global-Local Two-Way Loose Coupling Approach

In the global-local coupling procedure for composite stiffened panels developed by Hühne et al. [1] and enhanced later by Akterskaia et al. [10], intralaminar damage (fiber and matrix damage) was analyzed. Akterskaia et al. subsequently developed a new global-local approach for progressive failure in stiffened panels with skin-stringer separation [11]. In the present paper, the limitation of the previous works where only one type of damage was considered is overcome. The debonding damage between skin and stringer and intralaminar damage are examined together so that various important failure modes are incorporated in the approach. It is important to note that matrix and fiber damage as well as debonding are principal failure modes as observed during experiments conducted for laminated stiffened panels [12]. Skin-stringer separation is recognized as a crucial damage mode that can lead to a final collapse of the structure, or in the case of good bonding between the skin and the stringer, it could trigger other damage mechanisms, such as delaminations in adjacent layers and fiber failure in the stringer [5,13,14]. The main idea of the loose coupling procedure proposed in the current work [10,11] is demonstrated in Fig. 1, where the procedure is shown only for the case of skin-stringer debonding.

The flowchart of the two-way loose coupling procedure [1] is shown in Fig. 2. A global analysis is conducted, followed by local model calculations and local-global transfer of reduced properties.

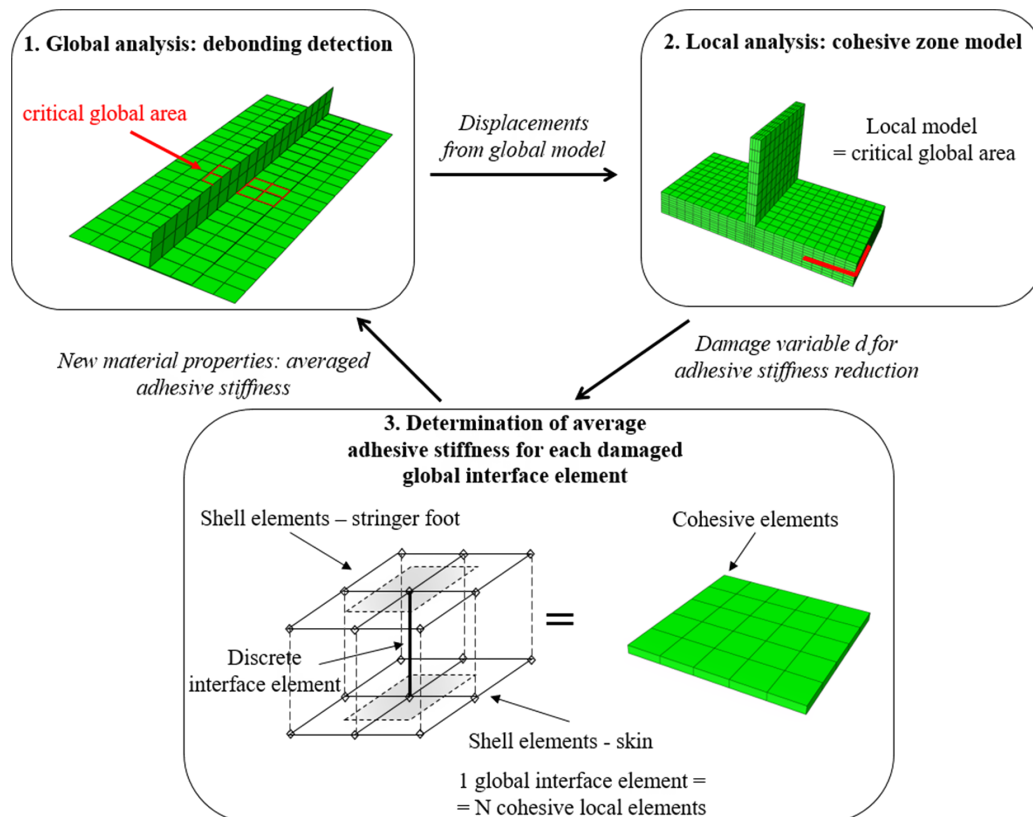


Fig. 1 Two-way loose coupling procedure for skin-stringer debonding: application to a one-stringer stiffened panel. The gray area around connector element corresponds to the nodal area of this connector element.

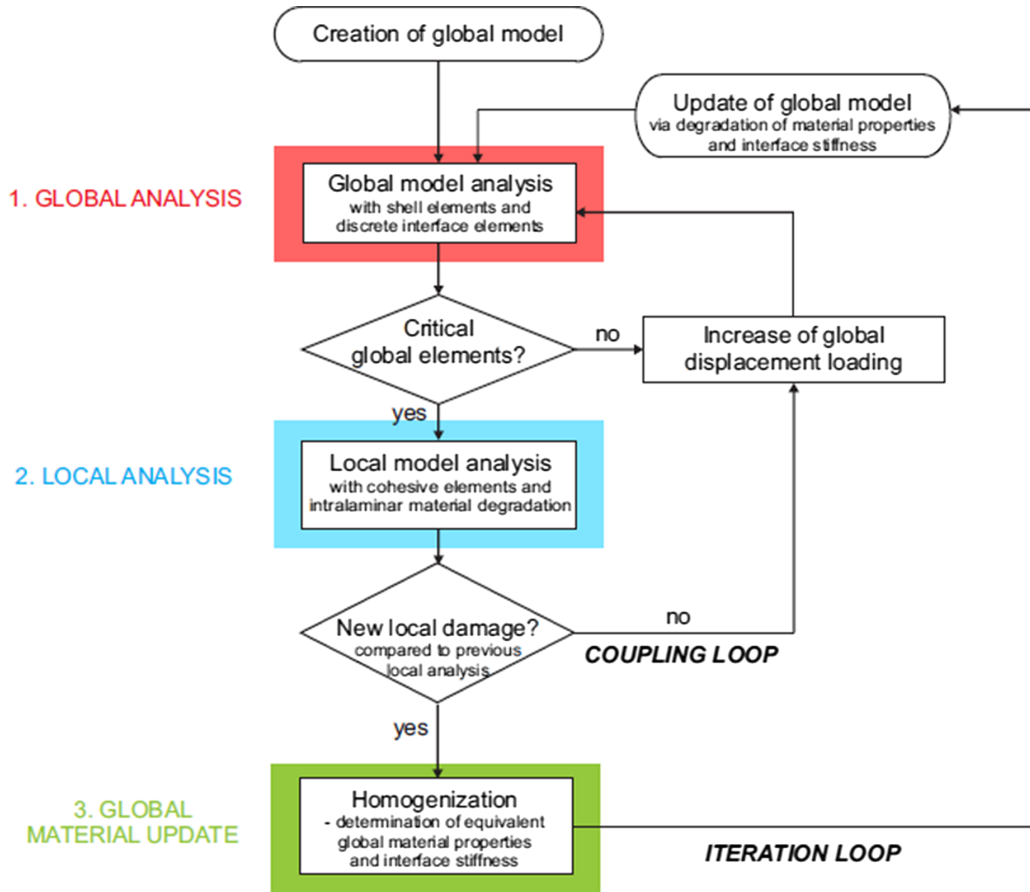


Fig. 2 Flowchart of two-way loose coupling procedure for intralaminar failure and skin-stringer debonding.

Afterward the global analysis is repeated to check whether the stress redistribution induced by degraded material properties results in the appearance of new critical areas or an extension of existing ones that is shown in the flowchart in the diamond called “New local damage.” The global-local procedure is performed until no new intralaminar damage initiation or no new skin-stringer separation onset is detected at the prescribed displacement level under consideration. When this “iteration loop” is completed, the load at the global level is increased and thereby the next “coupling loop” is started. The procedure is performed until final failure of the structure occurs. The proposed global-local method was developed for structures experiencing localized damage. Hence, an assumption has been formulated stating that limited amount of coupling loops is required to reach a state of the final failure. In the present paper, this procedure is applied for the case in which skin-stringer debonding and intralaminar damage occur simultaneously, as happens in realistic experimental tests.

The main advantage of the presented approach is that no preliminary knowledge is required about the location and the size of the intralaminar damage, and the skin-stringer debonding as the damage initiation is monitored at the global level. Another important aspect is the exchange of the damage information from the local to the global level through the reduced material properties, which allows for the performing of the progressive failure analysis until the final collapse.

## II. Detailed Methodology: Two-Way Loose Coupling Approach with Interlaminar and Intralaminar Failure

The progressive failure analysis (using the commercial finite element [FE] software Abaqus) is carried out until global failure of the structure takes place. The skin and the stringer of the panel in the global model are represented by four-node laminated shell elements using reduced integration (S4R elements). The adhesive layer is regarded as a structural connection and was modeled with connector elements of Cartesian type available in Abaqus. These elements were selected because the prediction of debonding initiation in the

adhesive layer requires knowledge of the normal and shear stress, whereas application of 3D solid elements is not recommended because of their inappropriate aspect ratio. The model at the global level is used to identify the areas where matrix or fiber failure is expected to occur by applying the Linde criterion [15], which stems from the Puck criterion and distinguishes between fiber and matrix damage as well as between compressive and tensile stresses. The material damage model performs a gradual degradation of material properties using the fracture energies of fiber and matrix. In the following,  $X_T$  and  $X_C$  denote the longitudinal tensile and compressive strength, respectively, and  $Y_T$  and  $Y_C$  are the transverse in-plane tensile and compressive strength, respectively, whereas  $S_A$  is the axial shear strength and  $C_{ij}$  are the components of the stiffness matrix. Damage initiates in the matrix when the index  $f_m$  exceeds the failure strain perpendicular to the fiber direction in tension and calculated as  $Y_T/C_{22}$  and fiber damage occurs when the index  $f_f$  exceeds  $X_T/C_{11}$ , which is the failure strain in the fiber direction in tension [see Eqs. (1) and (2)]:

$$f_m = \sqrt{\frac{Y_T}{Y_C}(\epsilon_{22})^2 + \left(Y_T - \frac{Y_T^2}{Y_C}\right) \frac{\epsilon_{22}}{C_{22}} + \left(\frac{Y_T}{S_A}\right)^2 \epsilon_{12}^2} > \frac{Y_T}{C_{22}} \quad (1)$$

$$f_f = \sqrt{\frac{X_T}{X_C}(\epsilon_{11})^2 + \left(X_T - \frac{X_T^2}{X_C}\right) \frac{\epsilon_{11}}{C_{11}}} > \frac{X_T}{C_{11}} \quad (2)$$

where the strain components  $\epsilon_{ij}$  correspond to the local material coordinates related to the orientation of the fibers, index 1 refers to the fiber direction, whereas index 2 (in-plane) and index 3 (out-of-plane) refer to the transverse directions. The damage parameters  $d_m$  and  $d_f$  introduced by Linde correspond to the partial matrix and fiber degradation:

$$d_m = 1 - \frac{Y_T}{f_m} e^{-(C_{22} Y_T (f_m - Y_T) L_c / G_m)} \quad (3)$$

$$d_f = 1 - \frac{X_T}{f_f} e^{-(C_{11} X_T (f_f - X_T) L_c / G_f)} \quad (4)$$

The characteristic element length  $L_C$  is used to reduce the mesh dependency of the degradation model. The matrix and fiber strengths are  $G_m$  and  $G_f$ , respectively. The undamaged elasticity tensor is  $C_{ij}$  (where  $i, j = 1, 6$ ). The effective elasticity tensor  $C_d$  used by Linde et al. [15] is defined as:

$$C = \begin{pmatrix} (1-d_f)C_{11} & (1-d_f)(1-d_m)C_{12} & (1-d_f)C_{13} & 0 & 0 & 0 \\ & (1-d_m)C_{22} & (1-d_m)C_{23} & 0 & 0 & 0 \\ & & C_{33} & 0 & 0 & 0 \\ & & & (1-d_f)(1-d_m)C_{44} & 0 & 0 \\ & & & & C_{55} & 0 \\ & & & & & C_{66} \end{pmatrix} \quad (5)$$

symmetric

It is worth mentioning that the presented global-local strategy is not restricted to the particular intralaminar failure criterion used, and other criteria such as LaRC04 by Pinho et al. [16] or developed later by Pinho et al. [17] could be applied. A good overview of existing failure criteria and their comparison have been performed during the effort of three stages of World Wide Failure Exercise (WWFE) (see Hinton et al. [18], Kaddour and Hinton [19], Kaddour et al. [20], and Kaddour et al. [21]). Material degradation models are reviewed in [22] and more recently in [23]. However, the particular choice of the Linde criterion is explained by the aim to obtain reliable results at a relatively low computational costs with an accurate material model, but also with a reasonably simple model that is not excessively demanding in terms of material model parameters required. The Linde criterion is an appropriate criterion for our current purposes. The relative simplicity of the implementation and the possibility of combining it with the material degradation model by Linde are convenient. It is noted that other failure criteria can also be used within the current implementation of the global-local framework. Since the criterion distinguishes between matrix and fiber failure, it retains the possibility of a validation with experimental results.

The regions of the interface layer where the onset of debonding between skin and stringer may take place are determined by means of a quadratic stress criterion, expressed by the following relation:

$$\left(\frac{\langle \sigma_{33} \rangle}{N_{\max}}\right)^2 + \left(\frac{\sigma_{13}}{S_{\max}}\right)^2 + \left(\frac{\sigma_{23}}{T_{\max}}\right)^2 \geq 1 \quad (6)$$

Here  $\langle \dots \rangle$  represents Macauley brackets operator,  $\sigma_{33}$  is a stress in the pure normal mode,  $\sigma_{13}$  and  $\sigma_{23}$  are nominal stresses acting in the first and second shear directions, and  $N_{\max}$ ,  $S_{\max}$ ,  $T_{\max}$  are the maximum corresponding stresses. The normal stress and the two transverse shear stresses,  $\sigma_{33}$  and  $\sigma_{13}$ ,  $\sigma_{23}$  respectively, are calculated based on the total forces:

$$\sigma_{i3} = \frac{F_i}{A_{el}}, \quad i = 1, 2, 3 \quad (7)$$

where  $F_i$  is a force and index  $i$  denotes 1, longitudinal; 2, transverse; and 3, normal axis, respectively;  $A_{el}$  is an area of applied force.  $A_{el}$  is equal to the full in-plane area of the shell element for interior connectors or to half of this area corresponding to the case when connectors tie the edges. There are also connectors applied to the corner nodes of the panel at both edges, respectively. However, these

corners do not represent regions of interest, and hence they are not checked for the damage initiation.

After completion of the global analysis, the required number of local models is created based on the information about the size and the location of critical areas determined by the failure initiation criteria discussed earlier. The detailed model with refined mesh density at the local level allows for considering the influence of the damaged region at the global level. An advantage of interface cohesive elements technique over another common method, the virtual crack closure technique (VCCT), is their ability not only to observe the evolution of the damage through the interface, but also to predict the onset of the layer separation. These elements have already

been successfully applied by other researchers [24,25]. However, preliminary studies are required related to the accuracy of the mesh refinement, because a higher number of cohesive elements compared with the structural elements are needed in order to ensure reliable results [5,26]. In the present study, the evolution of the debonding is assumed to be described through the Benzeggagh and Kenane fracture criterion [27] extended to 3D cases. The mixed-mode critical energy release rate  $G_c$  is supposed to be equal to the area under the curve in the traction-separation diagram (see Fig. 3), and is calculated by:

$$G_c = G_{Ic} + (G_{IIc} - G_{Ic}) \left( \frac{G_{II} + G_{III}}{G_I + G_{II} + G_{III}} \right)^\eta \quad (8)$$

where  $G_{Ic}$  and  $G_{IIc}$  are mode I and II critical energy release rates and  $G_I$ ,  $G_{II}$ , and  $G_{III}$  are single-mode energy release rates corresponding to fracture modes I, II, and III and their sum is the total energy release rate. The parameter  $\eta$  is determined empirically [27] and is assumed to be 2.284 [24].

The initial stiffness of each discrete interface element is defined as follows:

$$K_0 = \frac{EA}{t} \quad (9)$$

where  $E$  is the Young's modulus of the corresponding interface material, and  $A$  and  $t$  are in-plane nodal area and thickness in the normal direction of the interface element, respectively.

The linear degradation of the adhesive element stiffness is described by:

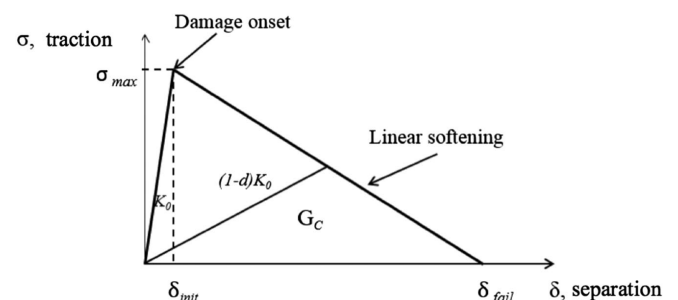


Fig. 3 Bilinear traction-separation law.

$$K_{\text{eff}} = (1 - d)K_0 \quad (10)$$

where the scalar parameter  $d$  varies from 0 for an undamaged element to 1 for a complete crack opening, and  $K_0$  is the initial stiffness. The intralaminar material properties of the skin and the stringer are degraded according to the material degradation model discussed in [1]. Averaged local stiffness was proposed to be calculated [11] for each area that corresponds to one connector element:

$$\begin{aligned} K_{\text{local}} &= \frac{\sum_{i=1}^N K_{\text{local},i}}{N} = \frac{\sum_{i=1}^N (1 - d_i)K_{\text{local},0}}{N} \\ &= K_{\text{local},0} \left( 1 - \frac{\sum_{i=1}^N d_i}{N} \right) \end{aligned} \quad (11)$$

where  $N$  is the number of local continuum interface elements corresponding to one global discrete interface element. Afterward, the multiplication coefficient of the right term that is based on the averaged damage variable parameter  $d$  is used to obtain the degraded global interface stiffness:

$$K_{\text{global},j} = K_{\text{global},0} \left( 1 - \frac{\sum_{i=1}^N d_i}{N} \right), \quad j = 1, \dots, N_{\text{global}} \quad (12)$$

where  $N_{\text{global}}$  is the number of global adhesive elements.

This approach allows an independent calculation of the multiplication coefficient for each global element. It is also important to note that only those global elemental stiffnesses are degraded during the next coupling loop that correspond to the local cohesive elements in the softening regime. Other global adhesive elements keep their initial stiffness.

The required number of coupling loops described in Fig. 2 is carried out until the global panel failure occurs. Comparisons are conducted first with a full reference model with a mesh size that is comparable to the local model, where solid elements are used for the skin and the stringer and cohesive elements are applied for the interface layer. Second, the numerical predictions of the global-local method are compared with the experimental results of a one-stringer panel.

Another interlaminar damage mechanism, such as delamination of the adjacent layers, is not considered within the presented approach. On the one hand, this type of damage was not reported as critical to the structural collapse as the final failure in stiffened panels under compression usually takes place due to the initiation and growth of matrix damage and skin-stringer separation finishing by final fiber failure. On the other hand, within the current framework of the global-local method, it is not directly possible to predict the delamination onset with conventional elements at the global level. However, in cases when it is known in advance at which position a delamination is expected to occur, the initial model could make use of stacked shell elements and our current debonding procedure could be used.

### III. Application of the Two-Way Loose Coupling Procedure to a One-Stringer Composite Panel

First, the method is applied to a stiffened panel with one  $T$ -shaped stringer. This panel is demonstrated in Fig. 4; geometrical and material characteristics are listed in Tables 1 and 2, respectively. The material “1-direction” corresponds to the longitudinal axis of the panel. The unidirectional layers are of 0.25 mm thickness each with a symmetric composite layup  $[0; 90]_s$ . Progressive damage was examined under the following boundary conditions: a fully clamped transverse edge is used and the opposite transverse edge is constrained in all directions except for the longitudinal direction, in which compressive load is imposed as prescribed displacement. Longitudinal edges are free to deform.

#### A. Reference Model

To evaluate the results of the coupling approach, a 3D reference model was created. Linear 8-node solid elements (C3D8) with a nominal element edge length of 1 mm were employed for modeling

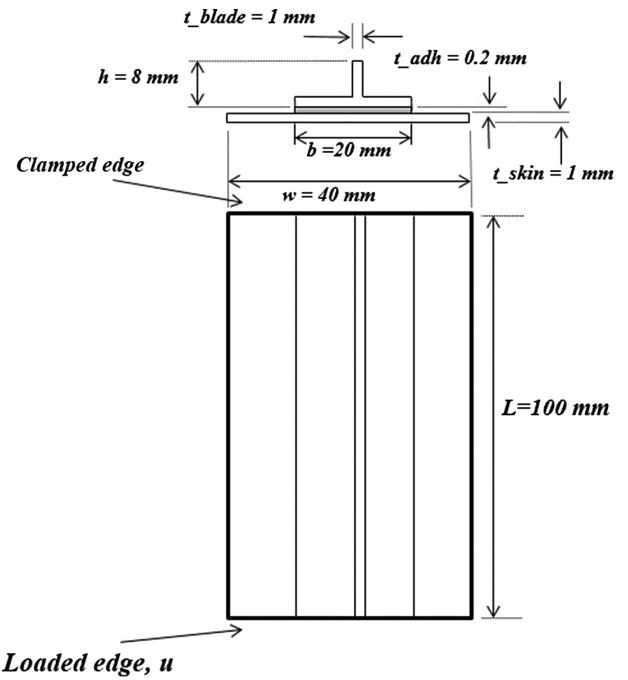


Fig. 4 Geometry of the tested one-stringer stiffened panel.

the skin and the stringer, one element per layer resulting in 4 elements through thickness. Nonzero thickness cohesive elements with bilinear traction-separation law replaced the connector elements in the adhesive area. The adhesive properties are summarized in Table 3. Four cohesive elements per side of one solid element were chosen

Table 1 Geometry of stiffened composite panel

Description	Value
Panel length, $l$ (mm)	100
Panel width, $w$ (mm)	40
Stringer width, $b$ (mm)	20
Stringer height, $h$ (mm)	8
Laminate thickness, $t_{\text{skin}}, t_{\text{blade}}$ (mm)	1
Adhesive thickness, $t_{\text{adh}}$ (mm)	0.2

Table 2 Material data for composite and adhesive

Stiffness properties	Value
Young's modulus in 1-direction, $E_{11}$ (GPa)	146.5
Young's modulus in 2-direction, $E_{22}$ (GPa)	9.7
Shear modulus in 12-plane, $G_{12}$ (GPa)	5.1
Poisson's ratio, $\nu_{12}$	0.28
Tensile failure stress in 1-direction, $X_T$ (MPa)	2583
Compressive failure stress in 1-direction, $X_C$ (MPa)	1483
Tensile failure stress in 2-direction, $Y_T$ (MPa)	92
Compressive failure stress in 2-direction, $Y_C$ (MPa)	270
Shear failure stress in 12-plane, $S_A$ (MPa)	106
Fracture energy of fiber, $G_f$ (N/mm)	12.5
Fracture energy of matrix, $G_m$ (N/mm)	1.0
Young's modulus of adhesive, $E_{\text{adh}}$ (GPa)	3.0
Poisson's ratio of adhesive $\nu_{\text{adh}}$	0.4

Table 3 Material data for cohesive elements, adhesive type FM300 from [6]

Cohesive element properties	Value
Interface element stiffness before the damage onset, $K$ (N/mm <sup>3</sup> )	10 <sup>6</sup>
Interfacial strength, mode I, $\tau_I$ (MPa)	61
Interfacial strength, modes II and III, $\tau_{II}, \tau_{III}$ (MPa)	68
Fracture toughness, mode I, $G_{Ic}$ (N/mm)	0.243
Fracture toughness, modes II and III, $G_{IIc}, G_{IIIc}$ (N/mm)	0.514



after performing convergence studies to estimate the minimum required number of cohesive and solid elements. The total number of elements was defined after the preliminary mesh convergence studies: 68,800 elements in total, from which 38,400 are cohesive elements. To connect different mesh sizes of the skin and the foot of the stringer to the larger number of adhesive elements, the Abaqus \*TIE constraint was used, with special attention to the choice of the master and slave surface [5]. The master surface corresponds to a skin or a stringer surface; slave surfaces correspond to the cohesive elements.

The material degradation model by Linde et al. [15] was implemented through the Abaqus user-defined material subroutine (UMAT) to account for intralaminar damage. Interlaminar damage was examined with cohesive elements with the bilinear traction-separation law. An imperfection with the shape of the first eigenmode obtained from the linear buckling analysis was applied, similar to the global analysis.

### B. Global Model: Linear Elastic Material

The global model consists of 280 four-node shell elements of 5 mm nominal element edge size using reduced integration (Abaqus S4R elements). A user-defined material subroutine (UMAT) was used to define the global material properties obtained from the local-level calculations. An adhesive layer between the skin and the foot of the stringer was modeled with connector elements. The axial compressive displacement was applied to the transverse edge and a static nonlinear analysis in Abaqus Standard was performed. The first eigenmode was chosen to trigger the buckling deformation of the panel. For the postprocessing of the global model results, two Python scripts were used. The first one was developed previously by Hühne et al. [1] to determine the critical global areas through the damage initiation criterion for matrix and fiber by Linde [15] discussed above. The same criterion is also applied to a local model. The second python script was developed with the goal of identification of critical regions due to the debonding onset by the quadratic stress criterion [Eq. (6)] applied to the connector elements.

Four global-local coupling loops were performed with a consequent increase of the applied displacement:  $u = 0.56, 0.60, 0.63, \text{ and } 0.67$  mm until the final failure was detected. An example of damaged areas detected during the global analysis of the first coupling step is demonstrated in Fig. 5. At the applied displacement of 0.56 mm, the postprocessing tool detected the potential areas of matrix damage and debonding initiation between the skin and the stringer. Based on these critical regions, two local models were created: local model 1 and local model 2.

### C. Local Models: Material Nonlinearity and Cohesive Debonding

The local models are created automatically for the critical areas identified during the global simulation by using a MATLAB preprocessor. Input parameters for this script are the location and the respective size of the local model, whereas the obtained output files

contain nodes and elements. The size of the local model is designed such that it should cover one neighboring element in-plane additional to damaged ones in case of the intralaminar damage as suggested in earlier work [10]. The reason is that the paths of the matrix and fiber damage growth are unknown in advance. Although it should be noted that, as the displacements from the global model correspond to the displacement load when the failure criterion was just satisfied, the damage is not expected to evolve outside of these boundaries. As for the interlaminar damage, the local models include only the connector elements detected by the failure criterion as it is expected that the skin-stringer debonding propagates toward the stringer blade, in this buckling shape, transversely to the longitudinal direction. When the damaged regions from the intralaminar and interlaminar damage overlap, one local model is created that covers both areas. Only the damaged parts of the panel are included in the local model in order to decrease the computational costs. Thus, the local models contained the skin and the foot of the stringer until the fourth coupling loop, where the stringer was also damaged and consequently incorporated into the local models. The only required parameter is the position within the global model. Displacements from the global analysis are used as kinematic boundary conditions at the edges of the local model through the submodeling procedure. The same mesh density and material parameters as for the reference model are implemented for the sake of consistency. This means that for the local model the same number (namely, four) of cohesive elements per in-plane side of solid element is employed. Intralaminar damage effects are accounted for through the material degradation model by Linde et al. [15].

The damaged local model created based on the global results of the first coupling loop (Fig. 5) is shown in Fig. 6. Matrix damage developed in the region of the stringer; cohesive elements are degraded according to the global model predictions—near the longitudinal edges of the stringer foot. It might be also noticed that some cohesive elements at the edges are not deleted as they might be physically expected. Cohesive elements in Abaqus [28] are prevented from being deleted under pure compression to prevent interpenetration of the surrounding layers. In this case the degradation parameter of this element is equal to 1, and during the recalculation of the global stiffness it corresponds to the fully damaged element.

### D. Local-Global Transfer of Updated Properties

Different mesh densities at local and global levels are used. The homogenization-based technique for matrix and fiber damage proposed by Hühne et al. [1] was used to determine equivalent properties corresponding to each global element. In the current studies, these effective material properties are calculated for each laminate layer of a global element independently.

Stiffness degradation of the connector elements is performed using Eq. (12) and applied during the next global analysis step making use of the Abaqus \*FIELD option. Hence, the original material properties of the connector elements are used at the global level until the increment at which damage is detected. From that increment,

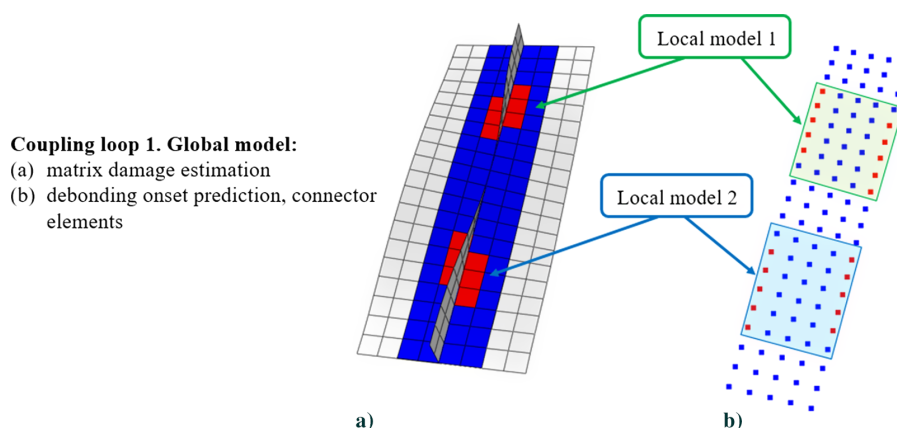
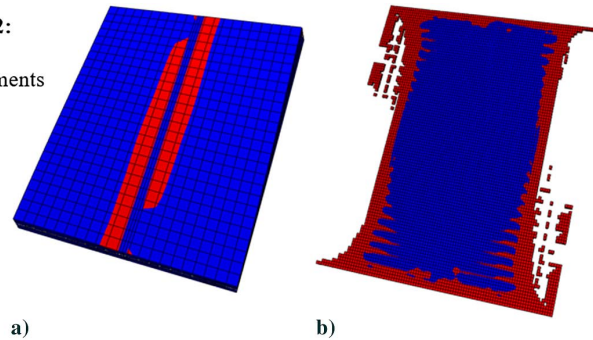


Fig. 5 Coupling loop 1, global level. Elements where damage onset was predicted are displayed in red. a) First critical global areas related to matrix failure; b) first critical connector elements.

**Coupling loop 1. Local model 2:**  
 (a) matrix degradation  
 (b) degradation of cohesive elements



**Fig. 6 Coupling loop 1, local model 2, in red: a) matrix damage; b) cohesive elements degradation.**

degraded material properties (degraded stiffness) are applied. With an increase of the loading, a degradation of material properties at the global level is performed subsequently.

### E. Coupling Results

The load-displacement curves shown in Fig. 7 demonstrate a comparison of the reference model results and of the global-local coupling loops where matrix and fiber damage and debonding between skin and stringer were considered. A good agreement between the reference results and the coupling loops can be observed. After local buckling in both analyses, the coupling curves remain straight until the first failure was predicted. The discrepancy of the first failure prediction between the reference and coupling curves can be explained by the fact that determination of the failure was performed at the global level with a coarse mesh, which again confirms the necessity of a local model with refined mesh to be examined. During the first coupling loop, the global model is loaded with 0.56 mm of compressive displacement. Both matrix cracking at the stringer basement and debonding onset at the free edge were detected. Based on these results, two local models were created and demonstrated both types of damage initiation and evolution (see Figs. 5 and 6). The locations of the intralaminar damage and skin-stringer debonding in the reference model at the corresponding applied displacement of 0.56 mm are shown in Fig. 8 with relatively good agreement to the same prediction in the local model. The updated material properties were transferred back to the global level. Here, the coupling load-displacement curve decreased load due to sudden degradation of the properties and ensuing stress redistribution. However, the reference solid model demonstrates a smoother softening behavior, which is explained by the fact that the material properties of the reference model are degraded gradually during the numerical analysis. For the coupling simulations, a sudden drop of the load-displacement curve is provoked by the sudden degradation of the material stiffness parameters. The subsequent

increase of the compressive displacement up to 0.60 mm demonstrated the evolution of the matrix damage and debonding at both critical areas identified at the first step. The compression was further increased until a displacement of 0.63 mm, where due to the debonding growth two local models join into one. Finally, the displacement increase up to 0.67 mm provoked the spreading of fiber and matrix damage across the structure. The panel was severely damaged at that stage, corresponding to a large drop in the load-carrying capacity (see Fig. 7), and the final failure occurred.

Global, local, and reference models analyses were carried out under the same computational characteristics. The total calculation times are 168 s for the first and 265 s for the last global model steps, respectively, and 191,084 s for the full 3D reference model. Material nonlinearity is included in both global and reference models. However, the reference model numerical analysis described previously allows for the incremental degradation of the stiffness parameters, whereas the stiffness update in the global model is performed only four times according to the number of steps. It is important to note that the total computational time required for the global-local procedure is the sum of the analysis time of global and local model analysis. It includes four coupling analyses for the global model, with relatively low computational effort (see Table 4, where only global time for the first and last coupling loops are presented to demonstrate the value range). The computational time for local models varies from 23,601 s for the local model of the first coupling step to 42,594 s for the second coupling step. During the third and fourth coupling steps, cohesive damage was recognized as not being significant at the local level and was not accounted for. Hence, the computational time was reduced for local models during the fourth step to 5445 s for the first local model, for example. It can be concluded that for this test case the computational time of the global-local analysis is comparable with the computational time of the reference model due to relatively large areas of damage. In Table 4, numerical parameters of these models are represented to give an overview of the order of difference between the

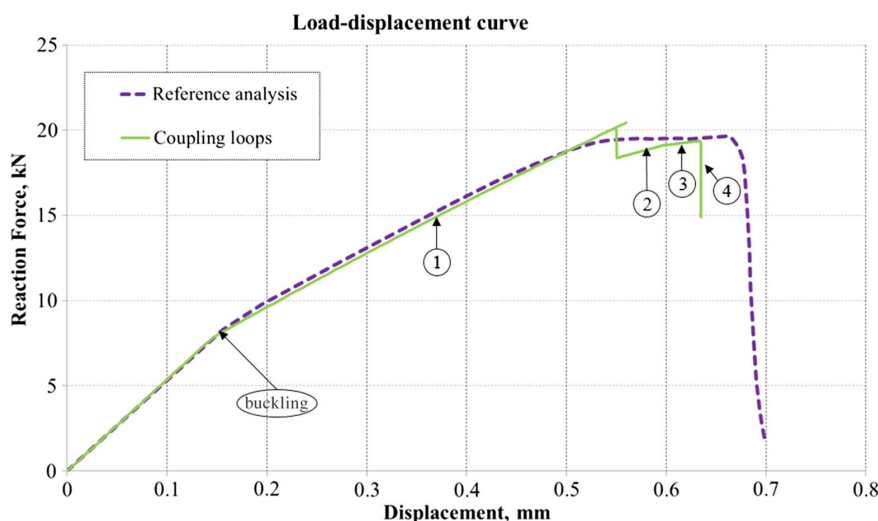


**Fig. 7 Load-displacement curve of the coupling and references analyses.**

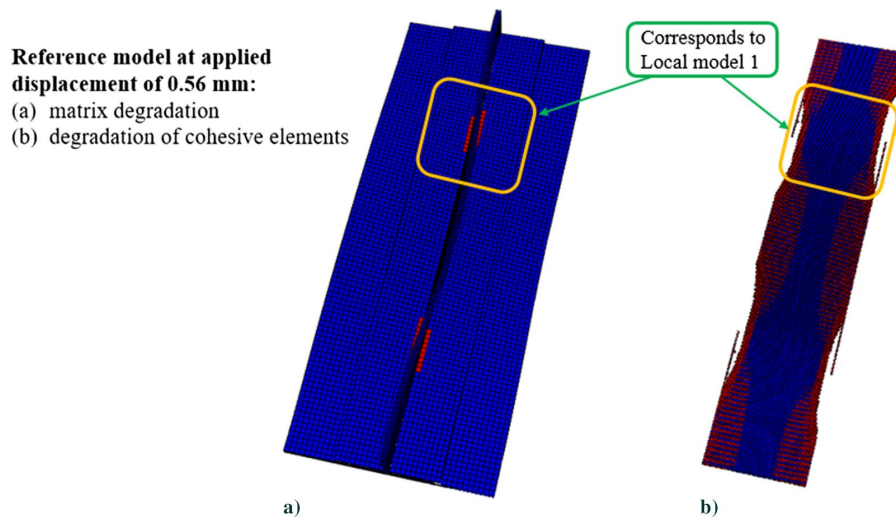


Fig. 8 Reference model, displacement  $u = 0.56$  mm, in red: a) matrix damage; b) cohesive elements degradation.

reference, local, and global-local analyses. In this table the computational time of the first local model is shown for each coupling loop. Both local models could be calculated independently and in parallel. Hence, only the largest computational time of the two models during the same coupling loop is important.

#### IV. Comparison with Experimental Results

Finally, a comparison of the numerical calculations of the extended global-local approach with existing experimental results is carried out. The chosen specimen was examined within the COCOMAT project in [6] and was denoted as D1 in these studies (see Fig. 9). The global-local method was previously validated for this case considering only matrix and fiber damage modes [1] with some differences in behavior when reaching the failure load. Following the observations during the experimental procedure, a separation between skin and stringer also took place. For this reason, it is interesting to compare the experimental results with the coupling calculations including the combination of skin-stringer debonding and intralaminar failure.

Geometric data and the stacking sequence corresponding to skin and stringer and their resulting total thickness are summarized in Table 5. The unidirectional CFRC material IM7/8552 UD was used for manufacturing the skin and the stringer of the panel and FM 300 for the adhesive (see Table 6 for the material properties). The mechanical properties of the adhesive layer were used as for the previous analysis (see Table 2); they correspond to the FM 300 material.

##### A. Reference Model

A reference model is created with linear solid elements (C3D8 of Abaqus) used for skin and stringer of the composite panel, and the nonlinear material degradation model is included in the analysis. The cohesive elements discussed earlier with bilinear traction-separation law are applied to model skin-stringer separation with four cohesive elements per side of one solid element. Mesh convergence studies were performed in order to choose an in-plane solid element length of 1 mm. One element through the thickness represents one composite layer. Finally, the mesh of the reference model consists of 678,800 brick and 198,400 cohesive elements. The first eigenmode is used as

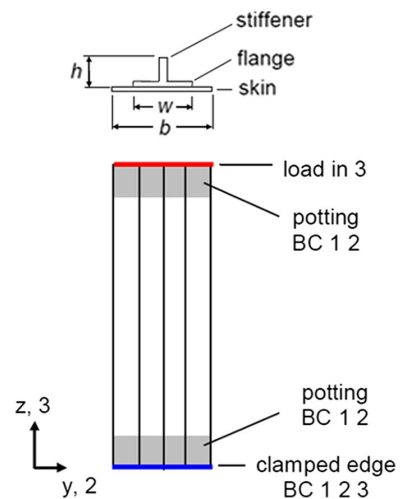


Fig. 9 Geometry of D1 stiffened panel (from [6]).

an initial imperfection to trigger the postbuckling shape. The geometry and boundary conditions of the composite panel are created with reference to the experimental data presented in Fig. 9. One of the transverse edges is fully clamped at the end, an opposite edge is constrained in all degrees of freedom except the longitudinal direction where the displacement was applied in compression.

##### B. Global Model: Linear Elastic Material

The global model consists of 2800 linear shell elements (S4R) with an in-plane element size equal to 4 mm, which means 100 elements in longitudinal direction and 909 connector elements for the adhesive layer. The boundary conditions are similar to the reference solid model. The stiffness of the connector elements is degraded consequently during the coupling procedure with regard to the degradation at the local level. The linear elastic material model is defined by means of a user-defined subroutine (UMAT) and the material properties are decreased.

Table 4 Computational characteristics of models

Model	Number of nodes	Number of elements	Degrees of freedom	Total computational time, s
Reference model	192,136	68,800	463,980	191,084
Global model, 1st coupling loop	756	385	2,331	168
Global model, 4th coupling loop	756	385	2,331	265
Local model 1, 1st coupling loop	40,510	21,608	99,906	23,601
Local model 1, 2nd coupling loop	40,510	21,608	99,906	42,594
Local model 1, 3rd coupling loop	7,750	6,480	23,250	21,816
Local model 1, 4th coupling loop	10,440	8,680	31,320	5,445

**Table 5** Geometry data of a D1 stiffened panel (from [6])

Description	Value
Total length, $L$ (mm)	400
Free length, $L_f$ (mm)	300
Width, $b$ (mm)	64
Stiffener width, $w$ (mm)	32
Stiffener height, $h$ (mm)	14
Ply thickness, $t$ (mm)	0.125
Skin lay-up	$[90, \pm 45, 0]_s$
Stiffener lay-up	$[(\pm 45)_3, 0_6]_s$
Ply thickness, $t_{skin}$ (mm)	1.5
Stringer flange thickness, $t_{flange}$ (mm)	1.5
Stringer web thickness, $t_{skin}$ (mm)	1.0

**Table 6** Material data for composite layer of D1 stiffened panel (from [6])

Stiffness properties	Value
Young's modulus in 1-direction, $E_{11}$ (MPa)	147,000
Young's modulus in 2-direction, $E_{22}$ (MPa)	11,800
Shear modulus in 12-plane, $G_{12}$ (MPa)	6,000
Shear modulus in 31-plane, $G_{31}$ (MPa)	6,000
Shear modulus in 23-plane, $G_{23}$ (MPa)	4,000
Poisson's ratio, $\nu_{12}$	0.3
Tensile failure stress in 1-direction, $X_T$ (MPa)	2,583
Compressive failure stress in 1-direction, $X_C$ (MPa)	1,483
Tensile failure stress in 2-direction, $Y_T$ (MPa)	92
Compressive failure stress in 2-direction, $Y_C$ (MPa)	270
Shear failure stress in 12-plane, $S_A$ (MPa)	106
Fracture energy of fiber, $G_f$ (N/mm)	12.5
Fracture energy of matrix, $G_m$ (N/mm)	1.0

### C. Local Models: Material Nonlinearity and Cohesive Debonding

The local models are created with the same mesh density and the same type of solid element (C3D8 of Abaqus) as the reference solid model. The size and position of the local models are defined based on the critical areas observed at the global level.

### D. Coupling Results

During the experimental tests, the D1 specimen demonstrated all types of damage instantaneously, such as skin-stringer separation, fiber fracture in the stringer, and matrix cracking around the skin-stringer interface [6], not allowing for a proper definition of the damage sequence. The final failure happened due to intralaminar damage near the loaded or clamped edges. In accordance with the experimental results, the numerical analysis of the global-local coupling loops and the reference solid model both demonstrated sudden initiation and evolution of the damage in the blade of the stiffener, and separation between skin and stringer together with extensive matrix damage at the foot of the stringer.

One coupling loop at the displacement load level of 1.9 mm was performed and it was observed that the damage had already started at a slightly lower level. After three iterations of coupling loops, the simulation of the damage propagation in the global model resulted in a final collapse of the panel. At the displacement level of around 1.89 mm, the fiber damage started symmetrically at the stringer blade in the regions close to the potting system. Two local models were created that account for the material damage evolution in the stringer, corresponding to regions 1 and 2 in Fig. 10. Approximately at the same load level, the debonding between skin and stringer was detected (see Fig. 11). The evolution of the damage in blades of the stringer after the second iteration required an increase of the local models' sizes, which is illustrated in Fig. 12. The intralaminar damage in the reference

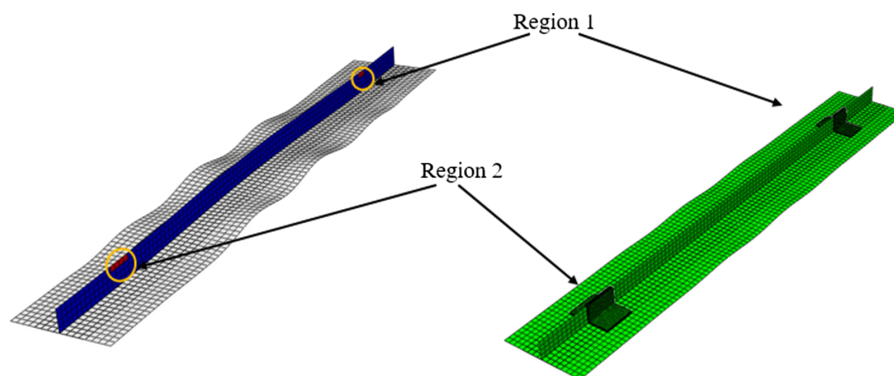


**Fig. 10** Iteration 1. Critical global areas for the fiber damage in the blade of the stiffener (left) and overlay plot of two corresponding local models (right) for the intact panel D1.

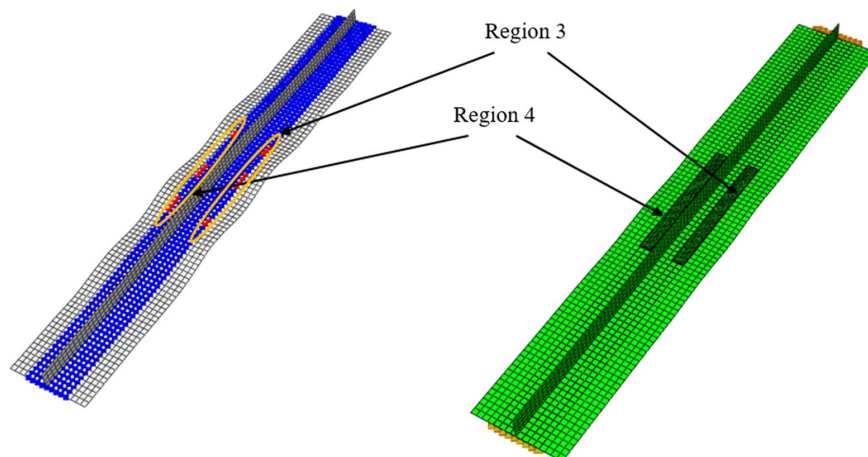


**Fig. 11** Iteration 1. Critical global areas for the skin-stringer debonding (left) and overlay plot of two corresponding local models (right) for the intact panel D1.

**Coupling loop 1. Local model 1:**

- (a) matrix degradation  
(b) fiber degradation fiber

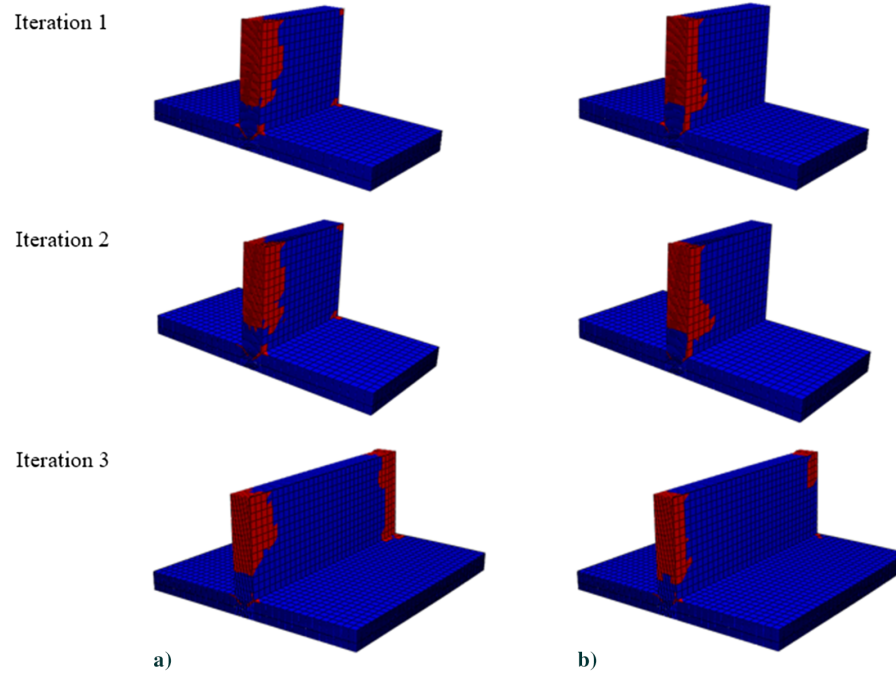


**Fig. 12** Matrix and fiber damage of local model 1 for the intact panel D1 (iterations 1–3). In red: new local damage.

**Reference model,  $u=1.98$  mm:**

- (a) matrix degradation  
(b) fiber degradation fiber

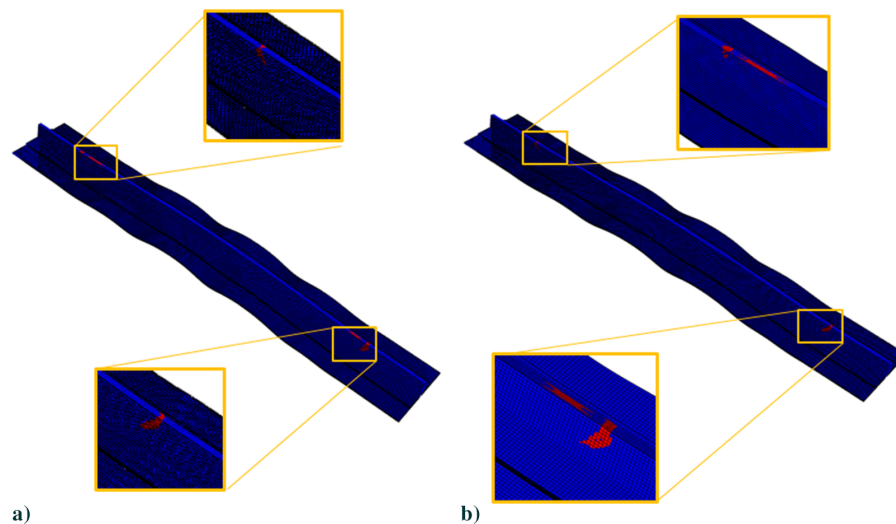


**Fig. 13** Matrix and fiber damage of reference model for the intact panel D1 at the displacement of 1.9 mm.

model shown in Fig. 13 also occurred in two areas similarly to the global model predictions, but it should be noted that the damage in the blade of the reference model developed differently than in the local models. This difference might be explained by the submodeling procedure that only transfers displacements without satisfying the equilibrium requirements. As the damage started at both sides of the stringer, two types of local models creation approaches were compared: one full local model covering both sides and two separate local models. The aim was to choose the computationally most effective approach without important loss in accuracy of the degradation prediction. Finally, it was concluded that two separate local models, located as shown in Fig. 11 symmetrically to the stringer and covering the damaged regions 3 and 4, are sufficiently accurate. The damage in cohesive elements from these local models is demonstrated in Fig. 14

and agrees sufficiently well with the damage in the reference model at the displacement of 1.9 mm. The load-displacement curves for three experimental results [14] and numerical simulations obtained from the coupling procedure and reference solid model are shown in Fig. 15. The initial structural stiffness of the numerical simulations correlates well with one of the experimental measurements, whereas the slight discrepancy with the other two experimental results could be explained by the applied material properties that were suggested by Orifici et al. [14]. The developed global-local strategy accords to experimental solution in terms of the location and sequence of detected damage events as well as in the final collapse.

Similarly to the previous case, numerical parameters of the global, local, and reference models are presented in Table 7. The computation time is shown for the first local model that was created to

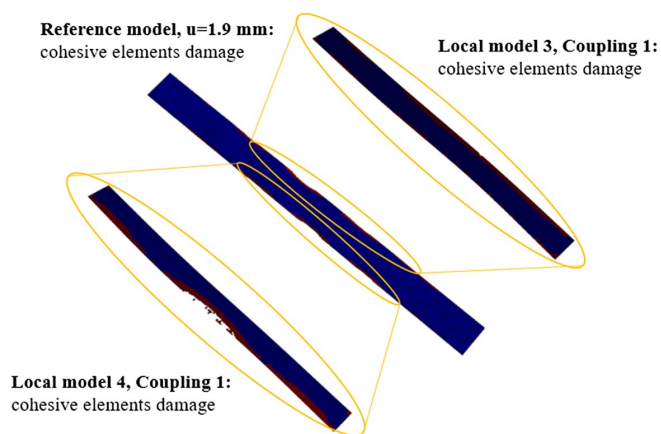


**Fig. 14** Cohesive element damage of reference model and local models 3 and 4 for the intact panel D1 at the displacement of 1.9 mm.

account for the damage in the blade of the stringer (see Fig. 10) as the maximum computational time during the iteration loops for local models. Thus, the total computational time to complete the global-local coupling analysis was 964,806 s, whereas for the full reference model this time was 1,932,780 s. The decrease of the computational time by around 50% obtained by the global-local simulation compared with the full 3D modeling is a significant achievement of the developed method.

The comparison of the coupling method results with experimental observations and the reference solid model analysis revealed that the coupling method was able to predict realistic damage modes and to account for their growth. The occurrence of fiber damage in the blade of the stringer was predicted as in the earlier global-local analysis in [1] including intralaminar damage only, but unlike the results in [1], in the current simulations the fiber damage propagated over a considerably larger region during the global-local analysis. This increase of the damaged area can be attributed to the consideration of the skin-stringer debonding in the current analysis and the corresponding stress redistribution over the structure. The results of the global-local coupling analysis compare reasonably well with the

experimental results; there is a deviation of less than 10% in the prediction of the final failure load.

## V. Conclusions

In this paper, a two-way loose coupling approach for progressive failure analysis was presented for the combination of intralaminar and debonding damage modes. Inclusion of both damage mechanisms in the global-local strategy allows for observation of progressive damage evolution similar to that shown in actual structures. The creation of separate global and local models allows the evolution of damage in the local models to be considered, while the material linearity and standard mesh with shell elements of the global model ensures a fast computational time. One of the advantages of using separate models is the fact that the position of the local model can be easily adjusted based on the increase of the critical area at the global level. The studies performed in particular assess the effect of skin-stringer debonding growth on the global panel failure while including intralaminar damage (matrix and fiber damage). The local models obtain interpolated displacements as boundary conditions from the global model through a submodeling procedure. In turn, the global model uses the decreased material properties transferred from the local model to simulate the degradation of the material at the global level and can thus carry out a progressive failure analysis.

The method was illustrated for one-stringer composite panels. First, a numerical simulation of the coupling procedure was compared with the results of a reference model with 3D elements. For another test case, the numerical calculations of the two-way coupling approach were compared with existing experimental results. A reasonable agreement for load-displacement curves between reference model and global-local coupling analysis in the first case, and between experimental data and the coupling approach in the second case was obtained. A reduction of about 50% in computational time achieved by the global-local method demonstrates a significant potential for this approach. The global-local analysis for debonding damage can be further enhanced by also considering the mixed-mode damage evolution in the debonding analysis.

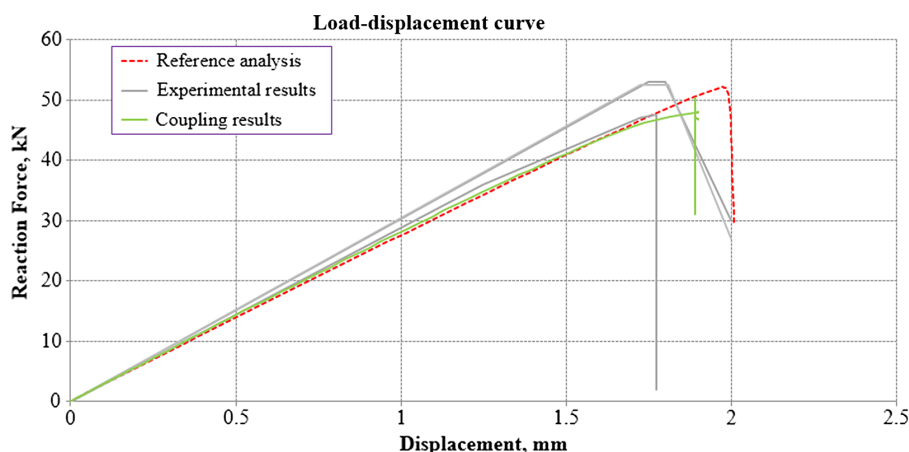


**Fig. 15** Load-displacement curve of the D1 stiffened panel.

**Table 7** Computational characteristics of models for the intact panel D1

Model	Number of nodes	Number of elements	Degrees of freedom	Total computational time, s
Reference model	1,166,160	857,600	4,272,111	1,932,780
Global model, 1st iteration	3,030	3,709	22,878	323
Global model, 2nd iteration	3,030	3,709	22,878	742
Global model, 3rd iteration	3,030	3,709	22,878	709
Global model, 4th iteration	3,030	3,709	22,878	2,089
Local model 1, 1st iteration	82,198	54,144	241,419	271,937
Local model 1, 2nd iteration	82,198	54,144	241,419	268,128
Local model 1, 3rd iteration	108,918	72,192	396,039	420,878

### Acknowledgments

The research leading to these results has received funding from European Union's Horizon 2020 research and innovation program (FULLCOMP/2015-2019) under Marie Skłodowska-Curie actions grant agreement number 642121. The provided financial support is gratefully acknowledged by the authors. Paul M. Weaver would like to thank Science Foundation Ireland for funding VARICOMP (15/RP/2773) under its Research Professor scheme.

### References

- [1] Hühne, S., Reinoso, J., Jansen, E., and Rolfes, R., "A Two-Way Loose Coupling Procedure for Investigating the Buckling and Damage Behaviour of Stiffened Composite Panels," *Composite Structures*, Vol. 136, Feb. 2016, pp. 513–525. doi:10.1016/j.compstruct.2015.09.056
- [2] Loehnert, S., and Belytschko, T., "A Multiscale Projection Method for Macro/Microcrack Simulations," *International Journal for Numerical Methods in Engineering*, Vol. 71, Feb. 2007, pp. 1466–1482. doi:10.1002/nme.2001
- [3] Labeas, G. N., Belesis, S. D., Diamantakos, I., and Tserpes, K. I., "Adaptative Progressive Damage Modeling for Large-Scale Composite Structures," *International Journal of Damage Mechanics*, Vol. 21, No. 3, 2012, pp. 441–62. doi:10.1177/1056789511400928
- [4] Chrupalla, D., Kreikemeier, J., Berg, S., Kärger, L., Doreille, M., Ludwig, T., Jansen, E., Rolfes, R., and Kling, A., "A Loose Coupling Multiscale Approach for the Detailed Analysis of the Influence of Critical Areas on the Global Behaviour of Composite Structures," *Computers, Materials and Continua*, Vol. 32, No. 3, 2012, pp. 159–176. doi:10.3970/cm.2012.032.159
- [5] Reinoso, J., Blázquez, A., Estefani, A., París, F., Cañas, J., Arévalo, E., and Cruz, F., "Experimental and Three-Dimensional Global-Local Finite Element Analysis of a Composite Component Including Degradation Process at the Interfaces," *Composites Part B: Engineering*, Vol. 43, No. 4, 2012, pp. 1929–1942. doi:10.1016/j.compositesb.2012.02.010
- [6] Orifici, A. C., Ortiz, I., Alberdi, D. Z., Thomson, R. S., and Bayandor, J., "Compression and Post-Buckling Damage Growth and Collapse Analysis of Flat Composite Stiffened Panels," *Composites Science and Technology*, Vol. 68, Nos. 15–16, 2008, pp. 3150–3160. doi:10.1016/j.compstruct.2008.07.017
- [7] Faggiani, A., and Falzon, B. G., "Optimization Strategy for Minimizing Damage in Postbuckling Stiffened Panels," *AIAA Journal*, Vol. 45, No. 10, 2007, pp. 2520–2528. doi:10.2514/1.26910
- [8] Gendre, L., Allix, O., Gosselet, P., and Francois, C., "Non-Intrusive and Exact Global/Local Techniques for Structural Problems with Local Plasticity," *Computational Mechanics*, Vol. 44, No. 2, July 2009, pp. 233–245. doi:10.1007/s00466-009-0372-9
- [9] Vescovini, R., Dávila, C. G., and Bisagni, C., "Failure Analysis of Composite Multi-Stringer Panels Using Simplified Models," *Composites Part B: Engineering*, Vol. 45, No. 1, 2013, pp. 939–951. doi:10.1016/j.compositesb.2012.07.030
- [10] Akterskaia, M., Jansen, E., Hühne, S., and Rolfes, R., "Efficient Progressive Failure Analysis of Multi-Stringer Stiffened Composite Panels Through a Two-Way Loose Coupling Global-Local Approach," *Composite Structures*, Vol. 183, Jan. 2018, pp. 137–145. doi:10.1016/j.compstruct.2017.02.011
- [11] Akterskaia, M., Jansen, E., Hallett, S., Weaver, P., and Rolfes, R., "Analysis of Skin-Stringer Debonding in Composite Panels Through a Two-Way Global-Local Method," *Composite Structures*, Vol. 202, Oct. 2018, pp. 1280–1294. doi:10.1016/j.compstruct.2018.06.064
- [12] Degenhardt, R., Kling, A., Klein, H., Hillger, W., Goetting, H. C., Zimmermann, R., and Rohwer, K., "Experiments on Buckling and Postbuckling of Thin-Walled CFRP Structures Using Advanced Measurement Systems," *International Journal of Structural Stability and Dynamics*, Vol. 7, No. 2, 2007, pp. 337–358. doi:10.1142/S0219455407002253
- [13] Zimmermann, R., Klein, H., and Kling, A., "Buckling and Postbuckling of Stringer Stiffened Fibre Composite Curved Panels—Tests and Computations," *Composite Structures*, Vol. 73, No. 2, May 2006, pp. 150–161. doi:10.1016/j.compstruct.2005.11.050
- [14] Orifici, A. C., Thomson, R. S., Degenhardt, R., Kling, A., Rohwer, K., and Bayandor, J., "Degradation Investigation in a Postbuckling Composite Stiffened Fuselage Panel," *Composite Structures*, Vol. 82, No. 2, Jan. 2008, pp. 217–224. doi:10.1016/j.compstruct.2007.01.012
- [15] Linde, P., and Boer, H. D., "Modelling of Inter-Rivet Buckling of Hybrid Composites," *Composite Structures*, Vol. 73, No. 2, May 2006, pp. 221–228. doi:10.1016/j.compstruct.2005.11.062
- [16] Pinho, S. T., Dávila, C. G., Camanho, P. P., Iannucci, L., and Robinson, P., "Failure Models and Criteria for FRP Under in-Plane or Three-Dimensional Stress States Including Shear Non-linearity," NASA TM-2005-213530, 2005, pp. 68.
- [17] Pinho, S. T., Vyas, G. M., and Robinson, P., "Response and Damage Propagation of Polymer-Matrix Fibre-Reinforced Composites: Predictions for WWFE-III Part A," *Journal of Composite Materials*, Vol. 47, Nos. 20–21, 2013, pp. 2595–2612. doi:10.1177/0021998313476972
- [18] Hinton, M. J., Kaddour, A. S., and Soden, P. D., "A Comparison of the Predictive Capabilities of Current Failure Theories for Composite Laminates, Judged Against Experimental Evidence," *Composites Science and Technology*, Vol. 62, Nos. 12–13, Sept.–Oct. 2002, pp. 1725–1797. doi:10.1016/S0266-3538(02)00125-2
- [19] Kaddour, A. S., and Hinton, M. J., "Maturity of 3D Failure Criteria for Fibre-Reinforced Composites: Comparison Between Theories and Experiments: Part B of WWFE-II," *Journal of Composite Materials*, Vol. 47, Nos. 6–7, March 2013, pp. 925–966. doi:10.1177/0021998313478710
- [20] Kaddour, A. S., Hinton, M. J., and Soden, P. D., "A Comparison of the Predictive Capabilities of Current Failure Theories for Composite Laminates: Additional Contributions," *Composites Science and Technology*, Vol. 64, Nos. 3–4, March 2004, pp. 449–476. doi:10.1016/S0266-3538(03)00226-4
- [21] Kaddour, A. S., Hinton, M. J., Smith, P. A., and Li, S., "Mechanical Properties and Details of Composite Laminates for the Test Cases Used in the Third World-Wide Failure Exercise," *Journal of Composite Materials*, Vol. 47, Nos. 20–21, 2013, pp. 2427–2442. doi:10.1177/0021998313499477
- [22] Garnich, M. R., and Akula, V. M. K., "Review of Degradation Models for Progressive Failure Analysis of Fiber Reinforced Polymer Composites," *Applied Mechanics Reviews*, Vol. 62, No. 1, 2009, pp. 1–33. doi:10.1115/1.3013822
- [23] Forghani, A., Shahbazi, M., Zobeiry, N., Poursartip, A., and Vaziri, R., "An Overview of Continuum Damage Models Used to Simulate Intralaminar Failure Mechanisms in Advanced Composite Materials," *Numerical Modelling of Failure in Advanced Composite Materials*, Woodhead Publishing Series in Composites Science and Engineering, Elsevier, The Officers' Mess Business Centre, Duxford, United Kingdom, 2015, pp. 151–173. doi:10.1016/B978-0-08-100332-9.00006-2
- [24] Turon, A., Camanho, P. P., and Costa, J., "An Engineering Solution for Mesh Size Effects in the Simulation of Delamination Using Cohesive Zone Models," *Engineering Fracture Mechanics*, Vol. 74, No. 10, July 2007, pp. 1665–1682. doi:10.1016/j.engfracmech.2006.08.025
- [25] Wagner, W., and Balzani, C., "Simulation of Delamination in Stringer Stiffened Fiber-Reinforced Composite Shells," *Computers and Structures*, Vol. 86, No. 9, May 2008, pp. 930–939. doi:10.1016/j.compstruc.2007.04.018
- [26] Harper, P. W., and Hallett, S. R., "Cohesive Zone Length in Numerical Simulations of Composite Delamination," *Engineering Fracture Mechanics*, Vol. 75, No. 16, Nov. 2008, pp. 4774–4792. doi:10.1016/j.engfracmech.2008.06.004
- [27] Benzeggagh, M. L., and Kenane, M., "Measurement of Mixed-Mode Delamination Fracture Toughness of Unidirectional Glass/Epoxy Composites with Mixed-Mode Bending Apparatus," *Composites Science and Technology*, Vol. 56, No. 4, 1996, pp. 439–449. doi:10.1016/0266-3538(96)00005-X
- [28] Abaqus, "Abaqus Documentation, Abaqus 6.14 Documentation. Dassault Systemes. 6.14 edn," No. V, 2017, pp. 1–172.

C. Bisagni  
Associate Editor





## **5 Paper D: Progressive delamination analysis through two-way global-local coupling approach preserving energy dissipation for single-mode and mixed-mode loading**

The following paper is published in *Composite Structures*, Volume 223 (2019), pages 110892 (<https://doi.org/10.1016/j.compstruct.2019.110892>). The main work was done by the author of this thesis.

A two-way coupling global-local finite element approach based on the equality in dissipated energies due to delamination between the global and local models has been introduced. This approach ensures that the energy dissipated in the global model due delamination under single or mixed-mode loading is the same as in the local model. First, global analysis is conducted with a relatively coarse mesh and spring-type discrete elements with an aim to detect the critical areas where the delamination might happen. Then detailed local models are created with cohesive elements that allow to model the initiation and evolution of the delamination. To couple the local and global models a next step is required that performs an automatic calculation of the reduced global interface stiffness for each element based on the energy dissipated at the local level. Hence, the degradation of the interface properties at the global model is performed based on the energy dissipated in the refined local model.

The proposed technique has been applied to a single and mixed-mode loading tests, for instance, the double cantilever beam (DCB) test, the end notched flexure (ENF) test and the mixed-mode loading (MMB) test. A relatively good agreement with analytical results has been attained for all test cases in terms of load-displacement curves. Afterwards, the global-local approach has been verified on a test case of a single-stringer composite panel with a following comparison to a reference solution. An excellent agreement has been obtained in load-displacement curves between the global-local solution and reference results for modelling skin-stringer debonding.

The discussed above global-local numerical method is proved to be an accurate tool to model delamination under a mixed-mode loading at different levels of refinement being computationally efficient on the one hand, and physically robust on the other hand.



Contents lists available at ScienceDirect

Composite Structures

journal homepage: [www.elsevier.com/locate/compstruct](http://www.elsevier.com/locate/compstruct)

# Progressive delamination analysis through two-way global-local coupling approach preserving energy dissipation for single-mode and mixed-mode loading



Margarita Akterskaia<sup>a,\*</sup>, Pedro P. Camanho<sup>b,c</sup>, Eelco Jansen<sup>a</sup>, Albertino Arteiro<sup>b</sup>, Raimund Rolfes<sup>a</sup>

<sup>a</sup> Institute of Structural Analysis, Leibniz Universität Hannover, Appelstr. 9A, 30167 Hannover, Germany

<sup>b</sup> DEMec, Faculdade de Engenharia, Universidade do Porto, Rua Dr. Roberto Frias, 4200-465 Porto, Portugal

<sup>c</sup> INEGI, Rua Dr. Roberto Frias, 4200-465 Porto, Portugal

## ARTICLE INFO

### Keywords:

Composite structures  
DCB tests  
ENF tests  
MMB tests  
Progressive failure analysis  
Multiscale analysis  
Global-local method  
Skin-stringer debonding  
Delamination

## ABSTRACT

Together with fiber breakage and matrix cracking, delamination is one of the common damage mechanisms occurring in laminated fiber-reinforced composite structures. Delamination initiates due to the relatively low interlaminar strength of adjacent plies. Delamination onset and propagation can be induced by various combinations of loads and usually leads to a significant reduction of the load-carrying capacity of the structure. For this reason, an efficient and reliable progressive failure analysis capability is required. In this work, the delamination process is simulated by means of a two-way global-local coupling approach. In particular, within this novel global-local approach a method is introduced that ensures the preservation of the dissipated energy when switching between the global and local level. This approach is tested and illustrated under single-mode I and II, and mixed-mode loading in the double cantilever beam (DCB), the end-notched flexure (ENF) and the mixed-mode bending (MMB) benchmark tests, respectively, and the results are compared to available analytical solutions. Finally, the developed method has been applied to a one-stringer stiffened panel and a good agreement was attained compared to the solid model reference solution.

## 1. Introduction

Composite laminated stiffened panels are widely used in aircraft design as components of fuselages because of their excellent material properties, such as high strength and stiffness to weight ratio. To increase the failure load of these structures and to exploit possible reserves, reliable simulations of postbuckling behavior of thin-walled structures are required [1]. For this reason, an accurate prediction of the failure behavior of composite structures is of great importance. One of the most common methods is to employ a material degradation model to perform a realistic failure analysis and to accurately detect the final collapse. Due to high computational costs associated with numerical simulation of the full composite structure, global-local approaches have been developed as a reliable and efficient tool to study localized nonlinearities, such as onset and evolution of damage, for example. A two-way global-local coupling method to simulate the post-buckling progressive failure behavior of composite stiffened panels with intralaminar damage and skin-stringer separation was developed in earlier work [2,3]. In this method, first, critical areas are defined at the

global level and local models with a considerably finer mesh are created by means of a submodeling technique. Secondly, a local model analysis is conducted. Cohesive elements are applied to model delamination with special attention to the exchange of information between the global and local models. The global-local coupling loops are repeated until final global collapse occurs. In the earlier work [4], the averaged damage scalar parameter obtained from the cohesive elements of the local model was utilized to determine the degraded stiffness of the adhesive layer in the global model.

In the approach proposed in [4], preservation of the energy dissipation between the local and global models was not guaranteed. However, anticipating the need to extend the global-local approach to more complex scenarios (e.g. impact loading), ensuring the energy balance between the local and global models is considered highly relevant [5,6]. Thus, the goal of the present work is to develop a global-local coupling method that ensures the correct and consistent preservation of energy dissipation between local and global models.

In the current study, a global-local method is formulated ensuring the preservation of dissipated energy between the global and local

\* Corresponding author.

E-mail address: [m.akterskaia@isd.uni-hannover.de](mailto:m.akterskaia@isd.uni-hannover.de) (M. Akterskaia).

<https://doi.org/10.1016/j.compstruct.2019.110892>

Received 27 September 2018; Received in revised form 18 April 2019; Accepted 22 April 2019

Available online 23 April 2019

0263-8223/ © 2019 Elsevier Ltd. All rights reserved.

analysis for single-mode and mixed-mode loadings by a novel strategy of information transfer from the local to the global level. To achieve this, the degraded stiffness of the adhesive layer in the global model is calculated based on the energy dissipated due to delamination in the local model. The dissipated energy in the local model is obtained for each area of cohesive elements that corresponds to each discrete element representing the adhesive layer in the global model. Subsequently, the degraded stiffness of each global adhesive element is calculated ensuring that the same amount of energy will be dissipated as in the cohesive elements of the local model. Its application to the double cantilever beam (DCB), the end-notched flexure (ENF) and the mixed-mode bending (MMB) benchmark test, respectively, is demonstrated with a comparison to analytical solutions based on Fracture Mechanics. The skin-stringer debonding is investigated in a one-stringer stiffened panel with the developed global-local methodology and compared to the full 3D reference solution.

### 1.1. Continuum and discrete elements for delamination

Delamination takes place in interface layers of composite laminates and can lead to drastic consequences, such as the reduction in load-bearing capacities of the structure. Delamination onset and propagation occurs due to the relatively low interlaminar strength of adjacent plies and under various combinations of loads. There are two main modeling techniques to simulate delamination: the Virtual Crack Closure Technique (VCCT) [7,8], and cohesive interface elements [9–11]. The VCCT, which is based on Fracture Mechanics, requires information about the place where the crack initiates. This is a disadvantage of this method when applying it to large and complex structures where delamination onset is usually not known *a priori*. Cohesive Zone Modeling (CZM) [12–14] is based on the hypothesis that tractions keep together the softening region in front of the crack tip. In this work, a common bilinear traction-separation law is used which assumes that an initially linear behavior is followed by a softening region when the strength is attained. The fracture toughness  $G_c$  is equal to the area under the traction-separation curve, refer to Fig. 1, and total crack opening takes place when this toughness is completely dissipated.

On the one hand, the Cohesive Zone Model could be applied in continuum form with interface elements, and on the other hand, it could be implemented by using point-wise discrete elements in the crack zone. The concept of interface elements was extensively developed by many authors, e.g., Allix and Ladevèze [15], Camanho and Dávila [11] and Turon et al. [16]. The discrete cohesive zone approach was formulated in the works of Borg et al. [17], Wisnom and Chang [18], Xie and Waas [19], Hallett and Wisnom [20] and Jiang et al. [21]. Liu et al. [22] implemented discrete two-dimensional spring-like elements with a softening behavior to simulate delamination and fiber debonding and matrix cracking. This work was extended by Jimenez et al. [23] for the mixed-mode delamination fatigue analysis. Later studies were also conducted by Cabello et al. [24] in the application to a DCB bonded joint in an analytical solution. Both continuum and discrete modeling approaches require a relatively high number of elements to accurately estimate tractions in interface elements. For this reason,

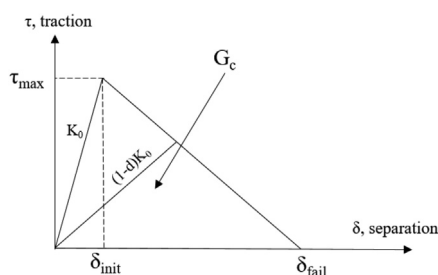


Fig. 1. Bilinear traction-separation law.

global-local methods are used to reduce computational time and to provide an accurate solution in damaged areas.

### 1.2. Global-local methods for delamination modeling

Global-local methods are paramount for simulating progressive damage in large and complex structures due to their effectiveness in reducing computational efforts without compromising the accuracy of damage analysis, which would happen if using a coarse analysis. Delamination is one of the critical failure modes that can significantly reduce the load-carrying capacity of a structure and lead to the final collapse. The current research aims at investigating delamination between adjacent layers of laminated composites. An overview of existing global-local approaches for delamination analysis was given in [4]. These approaches were applied to skin-stringer debonding in stiffened panels with different stringer shapes. It is useful to distinguish between one-way and two-way global-local coupling methods. The one-way coupling technique is based on the information transfer in one direction, either from the global to the local model, or less commonly, from the local to the global model. Contrarily, two-way coupling incorporates information exchange between global and local models in both directions. Orifici et al. [25] calculated global and local models separately. Delamination onset was predicted at the local level, while at the global level, delamination evolution was modeled using VCCT. Reinoso et al. [26] applied the one-way coupling method, comparing the submodeling procedure and the shell-to-solid coupling technique for the local model. Delamination was simulated using cohesive elements at the local level. Vescovini et al. [27] conducted one-way coupling using global and local models composed of shell elements. Cohesive elements were used at the local level. Borrelli et al. [28] examined delamination growth with global and local models calculated simultaneously, as the local model represented a refined part of the global model around the delaminated area. The global model consisted of shell elements, whereas solid elements were used for the local model. Delamination was modeled with the modified virtual crack closure technique (MVCCT). Bettinotti et al. [29] conducted a numerical analysis for a composite panel under high-velocity impact. A local model was incorporated into the global model. Continuum shell elements were used for both models and cohesive elements were applied to the local model. Saavedra et al. [30] utilized the Domain Decomposition Method (DDM) to perform a multiscale analysis where delamination was modeled with cohesive interfaces. The influence of boundary conditions and the geometry of the model on the convergence rate was demonstrated.

### 1.3. Objectives

A global-local two-way coupling method for modeling the initiation and further propagation of skin-stringer separation in stiffened panels has been developed earlier [4,31]. The method was validated by a comparison to experimental results of a one-stringer panel with and without initial skin-stringer debonding. The global model was represented by conventional shell elements with a relatively coarse mesh. Discrete elements were used to represent the interface layer. The local models were created based on the areas where the debonding was predicted at the global level. Solid elements were utilized in local models for the skin and the stringer with finer mesh. The interface layer of the local model was modeled with cohesive elements. Information exchange from the local to the global level was performed via transfer of the degraded interface stiffness of each particular global interface element. The global stiffness was degraded following the averaging of scalar damage variables obtained from the local model. Although this approach has demonstrated good results, it did not ensure the preservation of energy dissipation across both levels.

The objective of this work is to develop a new global-local coupling methodology that will allow a shell type model with a coarse mesh in

combination with local models with a fine solid mesh and cohesive elements to simulate the delamination behavior of a solid element reference model ensuring the energy balance across levels. Therefore, local-global information transfer is based on the energy dissipation at both global and local levels. Single-mode and mixed-mode loadings are considered. The approach is tested and verified under single-mode loading test cases, such as the double cantilever beam (DCB) test and the end notched flexure (ENF) test for the modes I and II respectively. Mixed-mode loading was verified with the mixed-mode bending (MMB) test [32]. These tests are standardized by ASTM. All global-local coupling results have been compared to reference solutions obtained with fine discretization and to available analytical solutions. Finally, the proposed approach has been applied to a single-stiffened panel and the results obtained were compared to a reference full 3D solution.

## 2. Analysis methodology

To the authors' knowledge, previous studies addressing global-local delamination analysis have not been applied to standard test cases for validation on simpler, single- and mixed-mode loading cases. In this section, global-local analysis of single-mode and mixed-mode delamination was performed to assess the formulation and validate the global-local method proposed herein (see also Section 3). Further validation at a more complex level will be presented in Section 4.

### 2.1. Global-local approach

The global-local method consists of several coupling loops repeated consecutively. First, the global model is created using a coarse mesh. Shell elements are utilized due to their advantage in terms of low computational time and their ability to accurately predict structural behavior of slender structures.

Discrete elements of the connector type in Abaqus tie the corresponding nodes of shell elements as shown in Fig. 2. These elements enable the definition of stiffness in three directions. Following the stiffness definition of connector elements, the normal and shear stiffness are calculated as:

$$K_n = \frac{EA}{t} \quad (1)$$

$$K_s = \frac{GA}{t} \quad (2)$$

where  $E$  and  $G$  are the Young's modulus and shear modulus of the adhesive zone, respectively,  $A$  is the area associated with a node and  $t$  is the interface thickness. The critical areas where debonding might take place are determined by the quadratic stress criterion commonly used for cohesive elements:

$$\left(\frac{\langle \sigma_n \rangle}{\tau_I}\right)^2 + \left(\frac{\sigma_s}{\tau_{II}}\right)^2 + \left(\frac{\sigma_t}{\tau_{III}}\right)^2 = 1 \quad (3)$$

Here  $\langle \dots \rangle$  is used for the Macauley brackets operator in order to exclude compression from interface separation.  $\sigma_n$  is the stress acting in the

normal through-thickness direction,  $\sigma_s$  and  $\sigma_t$  are shear stresses, and  $\tau_I$ ,  $\tau_{II}$ ,  $\tau_{III}$  are the corresponding strengths.

Normal and shear stresses at the nodes of connector elements are calculated from forces in connector elements distinguishing between free edge and internal nodal areas that are tied by connector elements:

$$\sigma_{i3} = \frac{F_i}{A_{el}}, \quad i = 1, 2, 3 \quad (4)$$

where  $F_i$  is a nodal force, and  $A_{el}$  determines a nodal area of applied force and taken as the sum of one quarter of each element area tied to that node. Therefore,  $A_{el}$  either represents the full in-plane area of the shell element  $A_{int}$ , referring to Fig. 2 for interior connectors, or half of this area denoted as  $A_{ext}$  corresponding to the case when connectors tie the edges, or a quarter if connectors tie corner elements. Index  $i$  specifies local Cartesian directions.  $\sigma_{33}$  corresponds to the normal stress that acts through the thickness,  $\sigma_{13}$  and  $\sigma_{23}$  are two in-plane shear stresses. In Eq. (1), the penalty stiffness definition includes non-material parameters, such as nodal area  $A$  and thickness  $t$ . The force  $F_i$  from Eq. (4) is proportional to the corresponding stiffness which means that the stresses  $\sigma_{i3}$  are independent from the nodal area and depend only on the thickness of the adhesive layer. Connector elements that tie four-node 2D shell elements are shown in Fig. 2, indicating the nodal areas  $A_{ext}$  and  $A_{int}$ .

Based on the areas detected as probable damaged regions, the local models are created with a finer mesh and solid elements to capture full 3D stress states. The interface layer is modeled with cohesive elements with a bilinear traction-separation law shown in Fig. 1 to simulate delamination. Displacements as kinematic boundary conditions are transferred to the boundaries from the global to the local model through a submodeling procedure. Moreover, the stress-based criterion, see Eq. (3), is used to predict the initiation of delamination, whereas the Benzeggagh and Kenane criterion [33] is applied for modeling the delamination propagation. This criterion was developed for mixed-mode loading and is used later for this case, see Eq. (15), but it is also applicable to single-mode loading. A scalar damage variable  $d$  varies from 0, when the crack is not yet opened and no energy is dissipated, until 1, when the crack is fully opened and energy is completely dissipated. The cohesive element stiffness is represented as follows [11]:

$$K = \begin{cases} K_0 & \delta < \delta_{init} \\ (1-d)K_0 & \delta_{init} < \delta < \delta_{fail} \\ 0 & \delta > \delta_{fail} \end{cases} \quad (5)$$

where  $K_0$  is the initial penalty stiffness, the displacement  $\delta$  is changed from 0 to  $\delta_{init}$ , which corresponds to crack initiation, to  $\delta_{fail}$ , which is the full crack opening displacement. The initial stiffness of the cohesive element is defined similarly to the global model interface stiffness:

$$K_{local_n} = \frac{E}{t} \quad (6)$$

$$K_{local_s} = \frac{G}{t} \quad (7)$$

where  $K_{local_n}$  and  $K_{local_s}$  are cohesive normal and shear stiffnesses, respectively.

A straightforward global-local approach, developed for progressive failure analysis in application to stiffened panels, employed an averaged scalar variable  $d$  to transfer damage information from the local to the global level [4]. This method, based on the averaging  $d$ -parameter, demonstrated good results. However, in order to preserve energy dissipated at the local level due to delamination evolution and to degrade global interface stiffness accordingly, the following procedure is used. First, similarly to the previous approach, a mapping procedure is necessary to allocate corresponding cohesive elements to one global connector element. Energy dissipated by these cohesive elements should be equal to the energy dissipated due to stiffness degradation by one connector element.

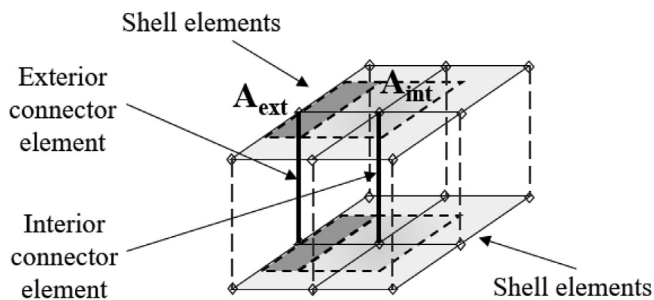


Fig. 2. Shell elements connected by connector elements.

$$E_{diss.local} = \sum_{i=1}^N E_{diss.local,i} = E_{diss.global} \quad (8)$$

where  $E_{diss.local,i}$  is the dissipated energy of a cohesive element,  $i$  denotes one of  $N$  local cohesive elements from the region corresponding to one connector element, and  $E_{diss.global}$  is the dissipated energy of one connector element due to delamination. A developed method allowing the calculation of energies dissipated at the global level based on the information from the local level is discussed in detail in the following sections for single-mode and mixed-mode loadings.

When the global degraded stiffness is recalculated for each particular connector element, the global analysis is performed again to check if no critical areas appeared due to stress redistribution. Initial global interface stiffness is used until the increment when the damage was detected first. From that increment, global interface stiffness is updated to degraded. It is important to notice that as a result of the mapping procedure relating each global interface element to the region of local elements that usually consists of more than one element due to mesh refinement, all global interface elements might have different degraded stiffnesses. The applied load is increased until the moment when new damaged areas are found in the global model and the global-local coupling procedure is repeated until the final collapse occurs.

Hence, the coupling global-local loop includes three internal stages:

1. Global analysis to detect probable areas of delamination initiation and to determine the position and geometry of the local models.
2. Local analysis with cohesive elements to accurately detect the onset of delamination and to observe the delamination evolution. Energy dissipated from the later process is obtained.
3. The global interface stiffness is calculated based on the dissipated energy of cohesive elements and transferred back to the global level.

These coupling loops are repeated within one coupling step with the same load level until convergence in reaction forces is reached. The new coupling step and, hence, the increase of the displacement load applied at the global level is defined by one of the following conditions. Either new local damage is detected or the previous damaged area is extended with the increase of the load. Therefore, the location and extension of the local models is not defined *a priori* and the method can be applied to generic cases. That means that local models can be created and updated based on the knowledge of the damage sizes at the regions identified after the global model analysis in a partially automated process. Using a Python script, the criterion for interlaminar damage is applied in all increments of the global model and interface elements in order to determine the increment when the new elements are damaged. Based on this information the displacement, when the new elements satisfy the failure criterion, becomes a displacement of the coupling step and the global-local procedure is started.

## 2.2. Single-mode loading

In order to obtain a degraded stiffness of each connector element for the single-mode loading, the equations derived in the following should be solved for a given dissipated energy. The cohesive traction-separation curve and discrete force-separation curve for a mode I loading are shown in Fig. 3.

First, the displacement of the final separation in the cohesive element is defined:

$$\delta_{max} = \frac{2G_I}{\tau} \quad (9)$$

Then for the force-separation curve of the connector element in the softening region with force  $F^*$  and opening  $\delta$ :

$$F^* = (A - \frac{E_{diss}}{G_I})\tau \quad (10)$$

The global dissipated energy can be obtained as follows:

$$E_{diss} = \frac{1}{2}(\delta - \delta^*)\tau A \quad (11)$$

From the same plot in Fig. 3 (right),  $\delta^*$  is defined:

$$\delta^* = \frac{F^*}{K_{gl}} \quad (12)$$

Using Eq. (10)–(12):

$$\delta = \frac{2E_{diss}}{\tau A} + (A - \frac{E_{diss}}{G_I})\frac{\tau}{K_{gl}} \quad (13)$$

Knowing  $F^*$  and  $\delta$ , a new degraded global stiffness of a particular connector element could be defined as:

$$K_{gl}^* = \frac{F^*}{\delta} \quad (14)$$

Both normal and shear stiffness of the connector elements are updated based on previous equations and applied within the next step to the global model.

## 2.3. Mixed-mode loading

The mixed-mode fracture toughness is calculated using the Benzeggagh and Kenane criterion [33] extended to the 3D case:

$$G_c = G_{Ic} + (G_{IIc} - G_{Ic}) \left( \frac{G_{II} + G_{III}}{G_I + G_{II} + G_{III}} \right)^\eta \quad (15)$$

where  $G_{Ic}$  and  $G_{IIc}$  are the mode I and II fracture toughness and  $G_I$ ,  $G_{II}$ ,  $G_{III}$  are the single-mode energy release rates corresponding to the fracture modes I, II and III and their sum is the total energy release rate.

The value in brackets can be obtained directly in the damage evolution procedure available in Abaqus and, hence, the mixed-mode energy release rate is assumed to be known. The maximum traction is defined as follows:

$$\tau = \sqrt{\tau_I^2 + \tau_{II}^2 + \tau_{III}^2} \quad (16)$$

Following these assumptions, the degraded mixed-mode stiffness of the connector element can be calculated for the mixed-mode loading as:

$$K_{mixed} = K_I + (K_{II} - K_I) \left( \frac{G_{II} + G_{III}}{G_I + G_{II} + G_{III}} \right)^\eta \quad (17)$$

which is also derived similarly by Turon et al. [34].

## 3. Validation and verification examples

In this section, the global-local approach based on preservation of dissipated energies between global and local levels is applied to DCB, ENF and MMB test cases and compared to analytical solutions [35].

### 3.1. Double cantilever beam (DCB) specimen

The selected DCB specimen shown in Fig. 4 is a CFRP laminate with uni-directional fibers in longitudinal direction, which is 150 mm long, 20.0 mm wide, with arms of 1.55 mm thickness and an initial crack of 35 mm. The geometry and material properties for this specimen are listed in Tables 1 and 2, respectively. The interface properties used for cohesive elements in the local model are listed in Table 3.

#### 3.1.1. Reference model

The reference model was created with solid elements to model the arms and cohesive elements of 0.01 mm thickness, which is small enough compared to the maximum values [36]. The influence of the viscosity parameter, the number of cohesive elements per solid element,

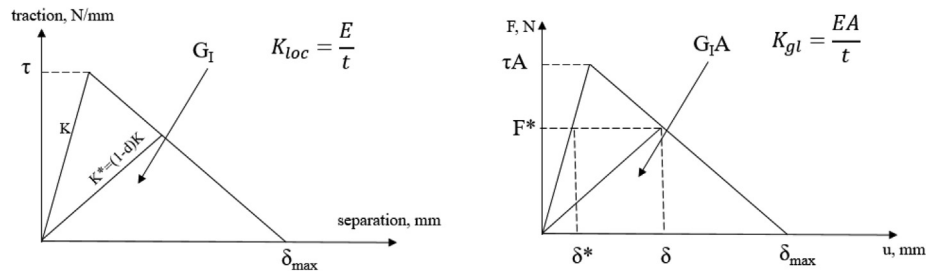


Fig. 3. Traction-separation law for cohesive elements (left) and for connector elements (right).

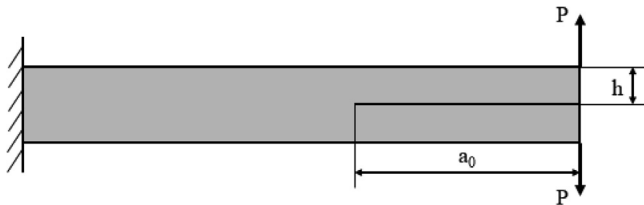


Fig. 4. Double cantilever beam specimen.

Table 1  
Geometry of the DCB specimen.

Description	Value
Length, $L$ (mm)	150
Width, $b$ (mm)	20
Half of the specimen thickness, $h$ (mm)	1.55
Initial crack length, $a_0$ (mm)	35

Table 2  
Material data for composite and adhesive.

Stiffness properties	Value
Young's modulus in 1-direction, $E_{11}$ (GPa)	171.4
Young's modulus in 2-direction, $E_{22}$ (GPa)	9.08
Shear modulus in 12-plane, $G_{12}$ (GPa)	5.29
Shear modulus in 23-plane, $G_{23}$ (GPa)	3.24
Young's modulus for adhesive, $E_{adh}$ (GPa)	3.00
Poisson's ratio, $\nu_{12}$	0.32
Poisson's ratio, $\nu_{23}$	0.4
Poisson's ratio for adhesive, $\nu_{adh}$	0.4

Table 3  
Material data for interface.

Cohesive element properties	Value
Interfacial strength, mode I, $\tau_I$ (MPa)	30.0
Interfacial strength, mode II and III, $\tau_{II}$ , $\tau_{III}$ (MPa)	50.6
Fracture toughness, mode I, $G_{Ic}$ (N/mm)	0.277
Fracture toughness, mode II and III, $G_{IIc}$ , $G_{IIIc}$ (N/mm)	0.788
$\eta$	1.634

the mesh size and the number of solid elements was investigated to select the suitable parameters for the local models assuming that their influence and importance are the same for the reference and local models.

**3.1.1.1. Effect of viscosity parameter.** Three analyses were conducted for the full reference model created with solid elements of 1 mm in-plane size, one cohesive element per solid element and 4 solid elements through the thickness of each arm, see Fig. 6. No viscosity,  $10^{-5}$  and  $10^{-7}$  viscosity parameters were chosen. Load-displacement curves for all three solutions are presented in Fig. 5 with comparison to the analytical solution. With no viscosity, the analysis failed to converge in reasonable

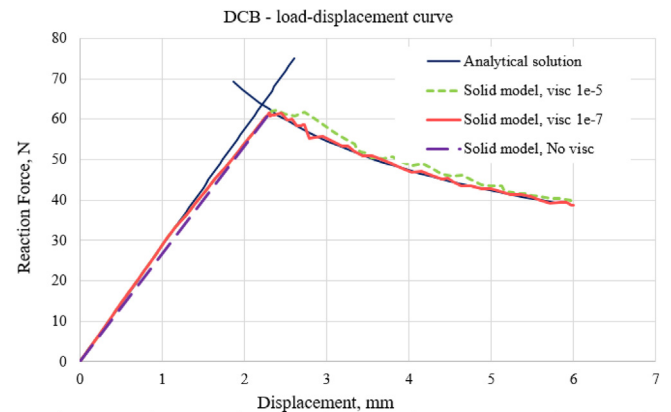


Fig. 5. Load-displacement curve for the studies of viscosity parameter in the solid model compared to the analytical solution.

time. The load-displacement curve of the analysis with a viscosity parameter of  $10^{-5}$  demonstrates relatively high oscillations in the softening region compared to the analytical solution. An artificial viscosity parameter of  $10^{-7}$  showed good agreement with the analytical curve and has been chosen as a good compromise.

**3.1.1.2. Effect of number of elements through the thickness.** The influence of the number of solid elements through the thickness was examined with one, two and four elements, see Fig. 6. The results of the load-displacement curves are presented in Fig. 7. It has been concluded that four elements through the thickness demonstrate results that are

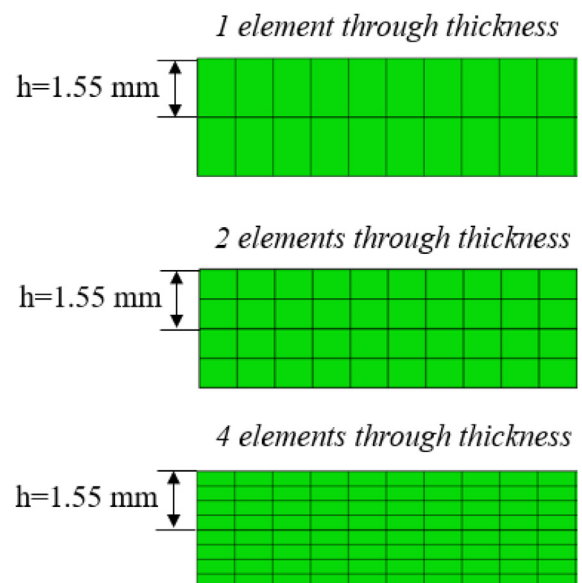


Fig. 6. Through-thickness mesh densities with 1, 2 or 4 elements per arm.

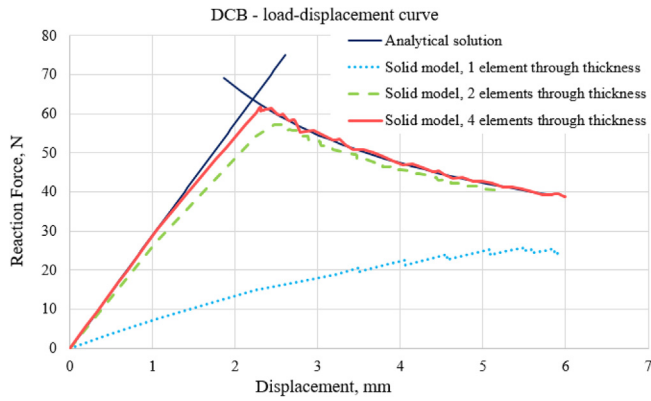


Fig. 7. Load-displacement curve for the convergence studies of the number of solid elements through thickness compared to the analytical solution.

reasonably close to the analytical solution.

**3.1.1.3. Effect of number of cohesive elements per solid element.** Further analyses were conducted with one and four cohesive elements per side of each solid element in the crack plane resulting in 1 and 16 cohesive elements connected to each solid element, respectively. Corresponding numerical meshes are demonstrated in Fig. 8. To overcome the difficulties related to non-corresponding nodes of solid and cohesive elements, it has been proposed to define element based surfaces and use a \*TIE constraint to connect the surfaces. This approach has also been recommended by [26], though the author used second-order solid elements. The slave surface corresponded to the cohesive elements and the master surface to the solid elements. The results obtained for the DCB test case are presented in Fig. 9 compared to one cohesive element per solid element. The behavior of the model with four cohesive elements per solid element in the softening region can be explained by the problems related to the surface definition for the application of \*TIE constraints when cohesive elements are deleted. Hence, it was concluded that for this type of structure and load, one cohesive element per solid element provides better results and should be chosen as a benchmark.

Finally, the following parameters have been selected for the reference and local model: a viscosity of  $10^{-7}$ , four solid elements through the thickness and one cohesive element per solid element. Good agreement with analytical solution was attained for this reference model using the in-plane element size of 1 mm. Reducing the element size would increase the computational cost without major gains in terms of accuracy, and increasing the element size is not desired,

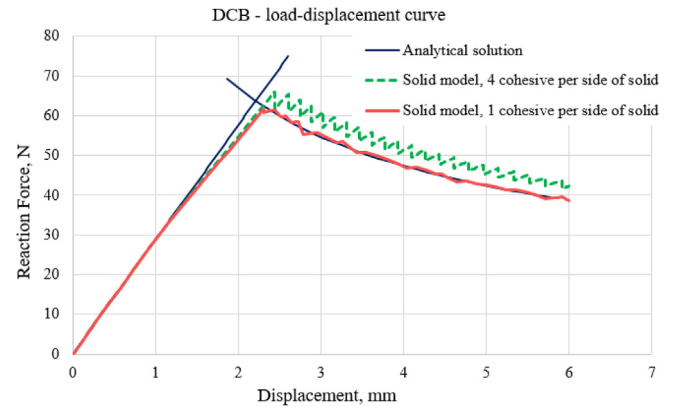


Fig. 9. Load-displacement curve for the selection of the number of cohesive elements per one solid element in the crack plane compared to the analytical solution.

because solid elements are recommended to keep the aspect ratio close to one.

**3.1.2. Global model**

The global model was created with shell elements of 5 mm mesh size. Surface elements have been connected to the shell top and bottom surfaces using \*TIE constraints connecting element-based surfaces, instead of using the offset parameter for shell elements. It allows a more accurate transfer of displacements to the local models. The connector elements were used to tie the corresponding nodes of the upper and lower surfaces representing two arms of the DCB specimen. It allows the definition of actual forces and elongations in the connector elements. Using Eqs. (1) and (2), the normal and shear stiffnesses of cohesive elements were obtained as  $7.5 \times 10^6$  N/mm and  $2.7 \times 10^6$  N/mm, respectively. The prediction of the delamination initiation at the global level utilizes the nodal area to calculate the stresses and the quadratic stress criterion from Eq. (3).

**3.1.3. Local model**

The local model consisted of solid elements of 1 mm in-plane size and 4 elements through the thickness with one cohesive element per solid element corresponding to the reference solid model. A length of 40 mm for the local model with a pre-crack area of 15 mm has been chosen as short as possible and as long as required to allow the crack propagation, see Fig. 10.

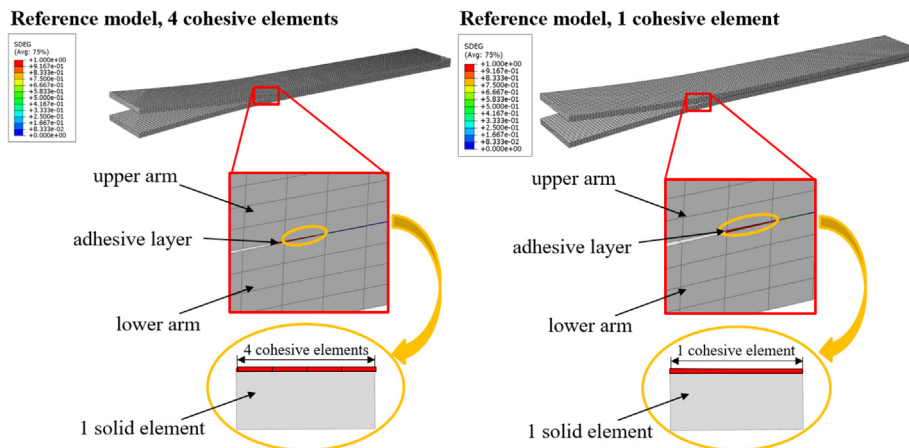


Fig. 8. 3D reference models with four cohesive elements per one solid element in the crack plane (left) and one cohesive element per one solid element in the crack plane (right).

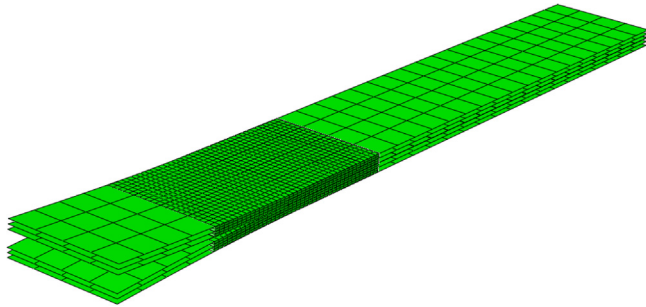


Fig. 10. Overlay plot of global and local models for the DCB test.

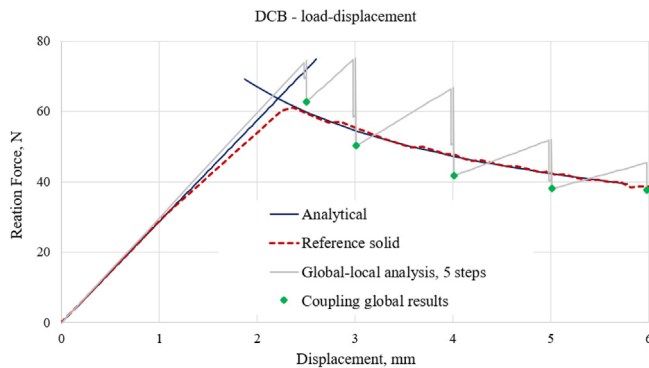


Fig. 11. Load-displacement curve for the DCB test with 5 global-local coupling steps compared to the reference and analytical solutions.

### 3.1.4. Results

Five coupling steps have been performed with a consequent increase of applied displacement at the global level:  $u = 2.5$  mm, 3.0 mm, 4.0 mm, 5.0 mm and 6.0 mm. That means that each arm was loaded with half of the displacement to reach the desired loading. The load-displacement curves of the analytical solution and coupling results are presented in Fig. 11. Several iterations were needed to finish each coupling global-local step, which means that the applied load was increased only after a convergence in the resulting loads between global current and previous iteration was achieved. Each drop of the curve of the coupling results corresponds to the next global analysis where the degraded interface stiffness was used from the local analysis. Afterwards, as there is no other information, the global model continues to be linear, but it is updated again through the next coupling step results. This is why only the results that follow the drops in the global-local coupling step are assumed to be representative and comparable to the reference solution. Each local minimum value of each global coupling drop shows the force-displacement relation obtained with the global-local approach and a good agreement with analytical and reference solutions is obtained.

In order to demonstrate convergence of the global-local approach to the analytical solution with an increasing number of coupling steps, a global-local analysis with eight coupling steps was performed. The arms of the DCB specimen were successively loaded with the applied displacement of  $u = 2.5$  mm, 2.7 mm, 2.9 mm, 3.1 mm, 3.3 mm, 3.5 mm, 3.7 mm and 3.9 mm. The results are shown in Fig. 12 and a good agreement between the global-local strategy and the analytical results is obtained in both linear and softening curves. The load drops of the global curve are explained by the sudden decrease of the material stiffness of some interface elements, which become smaller with increasing step number, as expected. It should be noted here that an increase of the applied displacement from one coupling step to another at the global level is judged based on the damage evolution. However, it should be recognized that the definition of the damage extension required to start a new global-local coupling step will depend on the

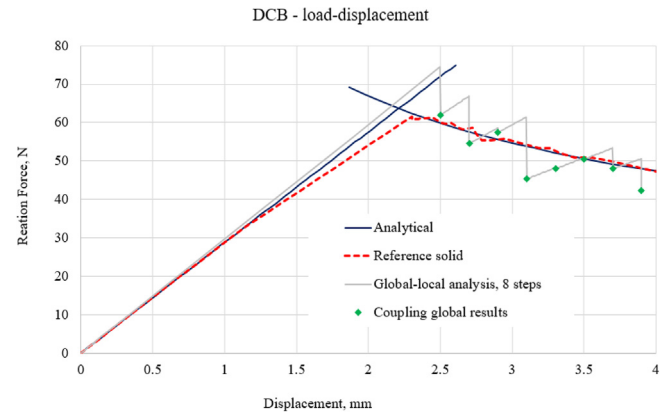


Fig. 12. Load-displacement curve for the DCB test with 8 global-local coupling steps compared to the reference and analytical solutions.

problem and cannot be known *a priori*. In the present case, a finite number of coupling steps was defined upon damage initiation (5 in Fig. 11 and 8 in Fig. 12). In the first case (Fig. 11), damage growth was predicted at all displacement increments, prompting coupling steps that led to the load drops in Fig. 11. In the second case (Fig. 12), some displacement increments led to negligible damage growth, as can be observed by the small load drops at 3.3 mm and 3.5 mm applied displacement. Hence, in general, the following recommendation applies: one should find a balance between an increase in the number of global-local coupling steps that leads to a better accuracy together with an undesired increase in computational time.

The energy dissipated during the cohesive elements damage was compared between the local and reference models for the case of the five coupling steps and is shown in Table 4. Both results correlate with each other. However, the highest difference in the initial global-local coupling step 1 is attributed to the fact that the displacements transferred from the global to the local models were higher than in the reference model at the same displacement level. The reason behind is that in the reference model the cohesive elements were damaged and deleted gradually within each load increment leading to the stress redistribution in the model, whereas in the global model the properties were not reduced until the first coupling step. It is also important to notice that the global model predicts the damage initiation slightly later as compared to the reference solution which is a consequence of a coarser mesh. That is a reason for the initial overestimation of the load and it is corrected through the global-local coupling step.

Numerical analyses for global, local and reference models were performed under the same computational characteristics. Relative calculation times for these models for the analysis with five coupling steps are shown in Table 5. In order to obtain the numerical solution through the global-local method, global and local analyses should be carried out for each coupling step and each iteration that is required to achieve convergence in forces. Hence, the total global-local computational time is a sum of all these analyses times. It should be mentioned here that local models were recalculated from the previous step using the restart

Table 4

Energy dissipated in the local and reference models of the DCB specimen for 5 coupling steps.

Coupling step	Dissipated energy, N*mm	
	Local model	Reference model
Coupling step 1, $u = 1.35$ mm	33.7	21.2
Coupling step 2, $u = 1.50$ mm	42.6	34.9
Coupling step 3, $u = 2.00$ mm	90.9	77.2
Coupling step 4, $u = 2.50$ mm	117.0	105.7
Coupling step 5, $u = 3.00$ mm	121.1	134.3



**Table 5**  
Computational characteristics of the models for the DCB test.

Model	Number of nodes	Number of elements	Degrees of freedom	Relative computational time, s
Reference model	101,014	58,516	206,394	3,659
Global models	1410	840	4,440	1,250
Local models	28,374	16,236	57,114	11,457

procedure in Abaqus which allowed for the considerable reduction of the computational effort. The relative calculation time for the global model changes from 10 s to 126 s for the first and last steps, respectively, whereas the full 3D reference model with cohesive elements required 3659 s. The calculations of the local models lasted a maximum of 2473 s for the first local model and were lower for the local model restart procedure. However, the total computational time for the local models is 11457 s which is higher than for the reference model. This is due to the fact that, in this case, the local model is relatively large (40 mm length as compared to the reference model of 150 mm length). Both models have the same mesh densities, which implies comparable calculation costs, especially taking into account that following the global-local methodology, the local model should be numerically analysed several times. Nonetheless it is important to note that the DCB test case has been chosen for the purpose of validating the approach developed for single-mode loading. In the case of localized damage with a relatively small local model, the global-local method based on the preservation of dissipated energies should be preferred due to the computational efficiency.

### 3.2. End notched flexure (ENF) specimen

The next test was conducted for mode II driven delamination for an end notched flexure (ENF) specimen, see Fig. 13, followed by comparison with the analytical solution. The material and cohesive element characteristics are the same as for the DCB test, see Tables 2 and 3, respectively. Geometry parameters are listed in Table 6.

The numerical parameters for the reference and local models were chosen as for the DCB specimen except for the viscosity parameter, since a value of  $10^{-5}$  already gives a satisfactory agreement with the analytical load-displacement curve.

The global-local analysis was carried out following the methodology suggested for the single-mode delamination. The size of the local model was the same as for the DCB test. A comparison of the load-displacement curves for the reference analysis, the analytical solution and the coupling procedure is demonstrated in Fig. 14. The global-local coupling analysis includes four consecutive steps based on prescribed displacements: 2.2 mm, 2.5 mm, 2.8 mm and 3.4 mm. Good agreement between the analytical curve and the global-local simulation is achieved for the linear part and the second part of the softening curve. The difference in the first part of the nonlinear solution is related to the fact that it is hard to predict the onset of the delamination with a coarse mesh at the global level. However, the application of the local analysis allowed to mitigate this with subsequent load increase.

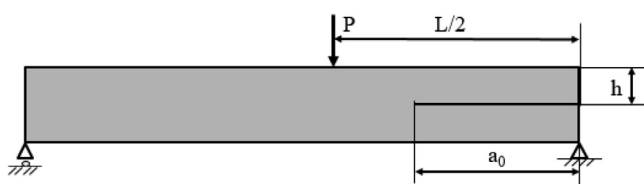


Fig. 13. End notched flexure specimen.

**Table 6**  
Geometry of the ENF specimen.

Description	Value
Length, $L$ (mm)	100
Distance of applied load, $L/2$ (mm)	50
Width, $b$ (mm)	20
Half of the specimen thickness, $h$ (mm)	1.55
Initial crack length, $a_0$ (mm)	35

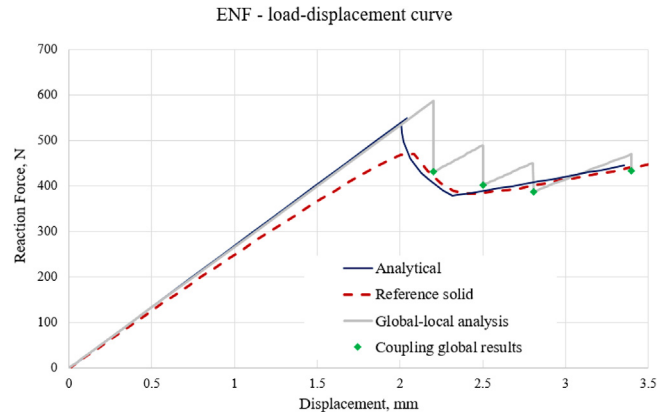


Fig. 14. Load-displacement curve for the ENF specimen test with 4 global-local coupling steps compared to the reference and analytical solutions.

### 3.3. Mixed-mode bending (MMB) specimen

A mixed-mode bending (MMB) specimen with 50% mode ratio has been selected to verify the global-local approach. The material properties are the same as for the DCB test, see Tables 2 and 3, and the geometry of the specimen is shown in Fig. 15 with the parameters given in Table 7.

The applied load was modeled by means of dummy nodes and their relation to the structure was ensured by specifying equations. The reference and local model parameters were chosen as previously with the viscosity parameter of  $10^{-5}$ . The load-displacement curves are presented in Fig. 16. Four coupling steps were used in the global-local analysis: increase of prescribed displacement to 6.0 mm, 6.5 mm, 7.0 mm and 7.5 mm. Each global analysis was followed by local analysis simulations. The degraded global interface stiffnesses were calculated for each global connector element and transferred back to the global model. Each load-displacement drop corresponds to the global analysis recalculated with updated properties. The softening behavior of the load-displacement curve obtained with the global-local approach demonstrated good agreement with the analytical solution, whereas onset of delamination was predicted later than in the full 3D reference model and analytical results. The coupling results for the single-mode loadings are slightly more accurate than for the mixed-mode loading. However, after the first coupling step, the solution of the global-local model tended to the reference model curve resulting in less than 7% relative difference in the delamination initiation load (143.8 kN for the

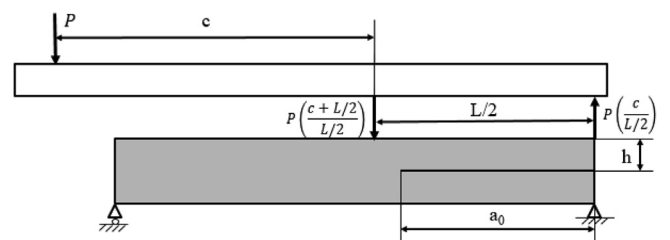
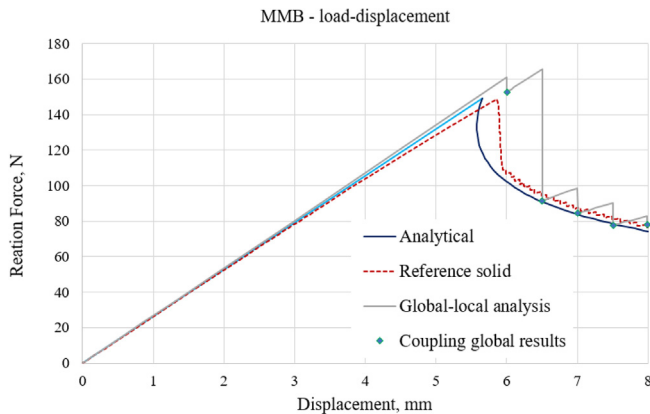


Fig. 15. Mixed-mode bending specimen.

**Table 7**  
Geometry of the MMB specimen.

Description	Value
Length, $L$ (mm)	150
Distance of applied load, $c$ (mm)	63.18
Width, $b$ (mm)	20
Half of the specimen thickness, $h$ (mm)	1.55
Initial crack length, $a_0$ (mm)	35



**Fig. 16.** Load-displacement curve for the MMB specimen test with 4 global-local coupling steps compared to the reference and analytical solutions.

**Table 8**  
Comparison between debonded area of reference and local models.

Model	Step 1	Step 2	Step 3	Step 4	Step 5
Reference model, debonded area, mm <sup>2</sup>	300	420	520	620	700
Local model, debonded area, mm <sup>2</sup>	0	380	500	560	600

reference model and 153.5 kN for the global-local model). In Table 8 a comparison between the debonded areas of the local model and the corresponding region of the reference areas of the reference model is presented for each global-local coupling step. During the first coupling analysis, the cohesive elements in the local model were not completely damaged and, hence, were not deleted. However, due to the partial damage the energy was dissipated, which in turn led to the reduction of the global interlaminar stiffness and consequently a load drop. Nevertheless, after the second coupling step, the results of the reference and local model demonstrated a good agreement.

### 3.4. Discussion

The results of the pure and mixed-mode delamination cases presented herein show that the proposed global-local coupling approach can predict interlaminar damage in composite structures. Discrepancies between the coupling and reference analyses were observed, but these can be attributed to the coarse mesh employed in the global model, leading to the discrete load drops obtained by the coupling approach. For instance, during the first coupling step, the global model indicates damage initiation slightly later due to the coarse mesh discretization. However, it also leads to a sudden reduction of the stiffness, which in turn results in sudden load drops.

On the other hand, the reference model employs a fine mesh of solid and cohesive elements. To achieve convergence after delamination initiation, Abaqus' implicit solver automatically reduces the increments within the step, leading to a relatively smooth load-displacement curve corresponding to the progressive delamination propagation. It is important to emphasize that the updated degraded stiffness is applied in

the global model after the local analysis only at the displacement level where the damage was predicted by the global model. This inevitably leads to the load drops in the global response prediction. Nevertheless, after the first coupling step, the results tend to the reference solution. In addition, the effects of mesh and incrementation are expected to be reduced when applying the coupling approach to more complex models. This becomes clear in the analysis of the one-stringer stiffened panel (Section 4).

It should be noted that the main goal of the approach is to capture a nonlinear interlaminar material behaviour with a linear global model only "correcting" the global interlaminar stiffnesses after each global-local coupling step. Hence, the coupling steps are coarse by nature. If the global response was not corrected through the global-local procedure, the global solution would deviate more and more from the nonlinear reference solution with an increase of the applied displacement in the nonlinear regime of the load-displacement curve. Thus, the global response should be always interpreted as a coarse representation – stepwise damage propagation through a finite number of coupling steps – of the actual response of the structure. With the current approach the progressive damage extension modelled by means of the global-local technique gives a robust prediction of damage propagation at a reduced computational cost.

## 4. One-stringer stiffened panel under compression

In order to investigate skin-stringer debonding the developed approach has been implemented to a stiffened composite panel with one T-stringer loaded under compression, see Fig. 17. This panel has been already examined through the global-local approach with the averaging procedure of degraded parameters, see [31]. The new method that ensures transition of dissipated energy from local to the global level, and thus accounting for local effects in the global model, has been used for the current analysis. The skin and the stringer of the panel is composed of unidirectional symmetrical layups [0, 90]<sub>s</sub>. The axial compressive load is applied to the transverse edges, whereas the other edge is clamped on all directions, except for the longitudinal. Material and geometry parameters are summarized in Tables 9 and 10 respectively.

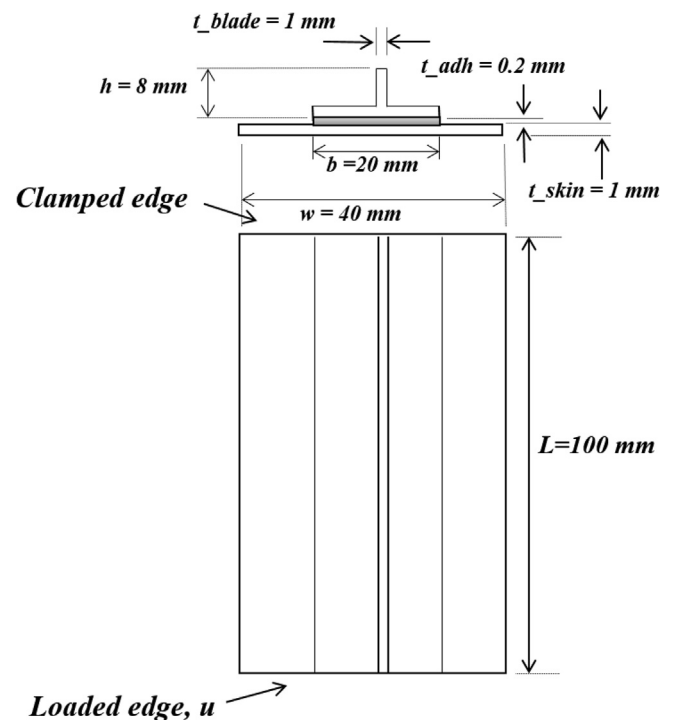


**Fig. 17.** Geometry of stiffened panel.

**Table 9**  
 Geometry of the stiffened composite panel.

Description	Value
Panel length, $l$ (mm)	100
Panel width, $w$ (mm)	40
Stringer width, $b$ (mm)	20
Stringer height, $h$ (mm)	8
Laminate thickness, $t_{skin}, t_{blade}$ (mm)	1
Adhesive thickness, $t_{adh}$ (mm)	0.2

**Table 10**  
 Material data for composite and adhesive for a one-stringer stiffened panel.

Stiffness properties	Value
Young's modulus in 1-direction, $E_{11}$ (GPa)	146.5
Young's modulus in 2-direction, $E_{22}$ (GPa)	9.7
Shear modulus in 12-plane, $G_{12}$ (GPa)	5.1
Poisson's ratio, $\nu_{12}$	0.28
Young's modulus of adhesive, $E_{glue}$ (GPa)	3.0
Poisson's ratio of adhesive $\nu_{glue}$	0.4

#### 4.1. Global model: linear elasticity

The global model was created with conventional 4-node shell elements with reduced integration (S4R in Abaqus) and 5 mm size. Buckling was triggered by an imperfection with the shape of the first eigenmode of the linear analysis. The \*Offset parameter was applied to move the reference shell surfaces of the stringer and the skin from the middle surfaces towards the lower and upper surfaces respectively, so that connector elements will have real lengths of the interface thickness, see Fig. 18. The quadratic stress criterion from Eq. (3) is used to detect the critical areas of the skin-stringer debonding initiation. During the consecutive coupling loops, the global stiffnesses of the connector elements were degraded following the procedure described in detail for the mixed-mode loading case.

#### 4.2. Local models: nonlinear material model

Local models were built with linear solid elements (C3D8 in Abaqus) of 1 mm length used to model the skin and the stringer and non-zero thickness cohesive elements (COH3D8 in Abaqus) used for the interface layer to examine skin-stringer debonding onset and growth. It is worth mentioning that application of higher order solid elements did not result in improvements in damage prediction. One solid element per lamina in the thickness direction was used. Following the suggestion in

**Table 11**  
 Material data for cohesive elements.

Cohesive element properties	Value
Interfacial strength, mode I, $\tau_I$ (MPa)	61
Interfacial strength, mode II and III, $\tau_{II}, \tau_{III}$ (MPa)	68
Fracture toughness, mode I, $G_{Ic}$ (N/mm)	0.243
Fracture toughness, mode II and III, $G_{IIc}, G_{IIIc}$ (N/mm)	0.514

[4], relatively high viscosity of  $10^{-3}$  and four cohesive elements per solid element were selected, resulting in 0.25 mm in-plane size. Their strength and fracture toughness are listed in Table 11.

It is important to mention that the local models are generated based on the size and location of the damage identified during the global analysis by using a MATLAB preprocessor. The output parameters of the script are the nodes and elements for the local models. Thus, when the delamination propagates the local models are increased to include the expansion of the damaged area.

After completion of the local analysis calculations, the degraded stiffness of each global connector element was updated based on the approach described in Section 2 for the mixed-mode loading case.

#### 4.3. Reference solid model

The reference solid model consisted of linear solid elements and cohesive elements with the same mesh density chosen for the local model. An initial geometrical imperfection to trigger buckling was included using the first eigenmode as for the global model.

#### 4.4. Coupling results

Six global-local coupling steps were performed similarly to the work in [4] with the following increase of the applied displacement: 0.56 mm, 0.58 mm, 0.60 mm, 0.63 mm, 0.67 mm, and 0.82 mm. The convergence in reaction forces has been attained after several iterations for each coupling step, followed by an increase of the prescribed displacement. Local models based on the critical regions and determined at the global level have been created. Overlay plots for the first, third and fourth coupling steps are demonstrated in Fig. 19 as the most representative ones for the current examination. Two local models corresponded to the first two coupling steps. They were placed symmetrically each covering an area of  $400 \text{ mm}^2$  of the adhesive surface during the first and the second coupling steps. The size and the location of these models were unchanged for these first two steps, as the increased area of damaged connector elements was fully covered by these models. Expansion of the skin-stringer debonding initiation detected at

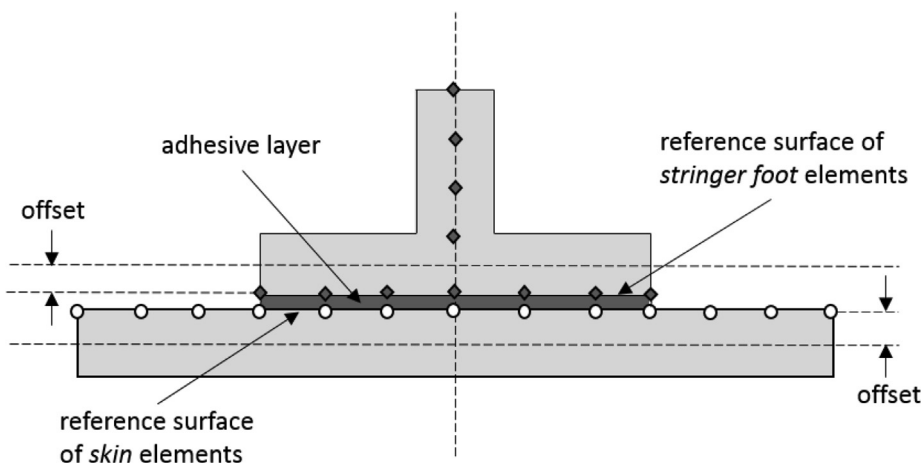


Fig. 18. Geometry of a section of the stiffened panel.

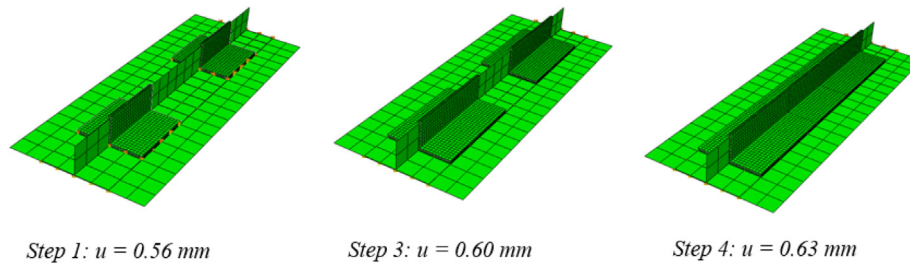


Fig. 19. Overlay plots of the global and local models of the stiffened panel for coupling steps 1, 3 and 4.

the global level provoked an enlargement of the local models to  $600 \text{ mm}^2$  of adhesive surface covered during the third coupling step. It is important to mention that the onset of the debonding started at the free edge surfaces between the skin and the stringer and propagated in the direction of the web of the stringer. During the fourth coupling step the third local model was generated according to a new set of critical connector elements. It should be noted that although three local models could be joined in one large local model, this approach was regarded as undesirable. Separate local models allowed for the parallel computation and proved to be more computationally effective without much loss in accuracy. During the fifth and sixth coupling steps the same local models were employed as they fully covered the damaged areas.

Fig. 20 shows the load-displacement curves for the global-local coupling analyses based on dissipated energies and based on averaging of damage variables [31] and full 3D reference solution. The difference in the first buckling displacement between global-local approaches (0.147 mm) and the reference solution (0.167 mm) leads to the slight difference in the curves, although the structural stiffness was predicted very well. In the postbuckling regime the global-local curves also match well with the reference curve by virtue of the slight drops of the global-local curves that adjust the overall global behavior after each global-local coupling step. The final collapse of the structure is defined by a large drop in the load-displacement curve which implies dramatic reduction in the load-carrying capacity. The final collapse in the global-local simulation based on dissipated energies occurs at a load level of 22.35 kN which corresponds to the displacement of around 0.75 mm. The final collapse predicted by the global-local model based on the assumption of the averaged damage variables occurred at a load level of 20.68 kN and a displacement of 0.78 mm. The maximum carried load by the reference model is 20.54 kN at the displacement of 0.76 mm. At around 0.77 mm of applied displacement the global buckling shape changed and the stringer kinked leading to the drop in the load-displacement curve of the global-local analysis. The comparison with the reference model demonstrated that due to incremental damage the final

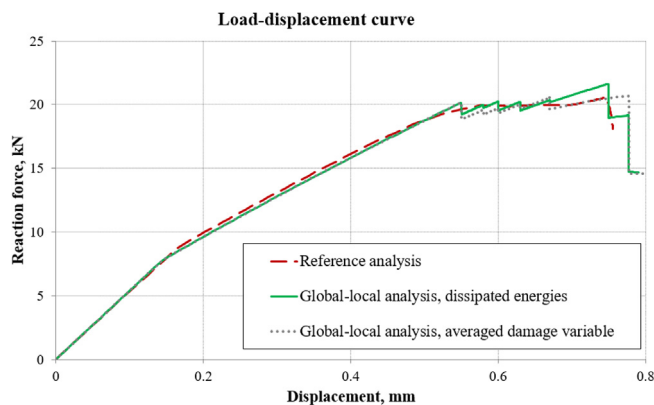


Fig. 20. Load-displacement curves for progressive failure analysis of the stiffened panel. Two approaches: global-local method based on dissipated energies and global-local method based on averaging of damage parameter compared to the reference solution.

failure of the reference model took place slightly earlier – at 0.76 mm, which did not allow to capture the same effect. However, it should be noted that the displacement of the final collapse, corresponding to a sudden drop of the load-displacement curve, of the reference analysis was predicted very closely by the global-local method based on the dissipated energies, whereas the maximum supported load was slightly overestimated resulting in 9% of relative difference. It should be noted that only delamination growth is considered in all models.

A comparison between the two global-local approaches has been conducted in terms of the dissipated energies. The results are demonstrated in Table 12. The local model selected, denoted "Local model 1", corresponds to the initial damaged area located symmetrically with respect to the stringer and grows with increasing damage. The dissipated energy in the reference model was calculated for the region corresponding to the region of the local model. Although both results for the local models show discrepancies with respect to the reference model, it is noted that a difference in the prediction of the damage initiation will take place due to the difference in mesh refinement. In the reference model, the criterion that identifies the damage initiation, is checked iteratively. In the global model the same happens but during the post-processing procedure, hence, with lower accuracy, as the global model has a coarser mesh that consists of shell elements. Nevertheless, the dissipated energy in the local model of the "averaging" global-local approach presented in [4] clearly shows a considerably larger difference as compared with the reference model results. In the averaging procedure in the method presented in [4] (also resulting in reasonable results for the global-local progressive failure analysis) the equivalence between the dissipated energies of the global and local models was not enforced.

A comparison of the mixed-mode ratios at damage initiation in the cohesive elements has been performed for the reference model, for the local model based on the averaging procedure and for the local model obtained following the preservation of dissipated energies, illustrated in Fig. 21. This demonstrates that, although both local models of different approaches give similar results to the reference solution, the way the damage propagates in terms of the correct damage mode is predicted closer by the method that preserves the dissipated energy across the levels. Table 13 shows that the percentage of cohesive elements in the local model 1 obtained by means of the dissipated energy preservation technique is higher as compared to the same local model from the averaging procedure. For instance, 75.4% of the cohesive elements from the energy-based method lie within 10% relative difference to the reference model cohesive elements when the mixed-mode ratios of damage initiation are compared, whereas for the averaging approach this value is 68.8%. Hence, on one hand, an application of the new method to a one-stringer panel confirmed that the method attains good agreement with the reference calculations. On the other hand, it also showed that for the chosen example the final collapse as well as skin-stringer separation are predicted well by both approaches with a difference that is explained in the following. The global-local coupling method which is based on the preservation of the dissipated energy between the local and global levels, leads to a closer prediction of the mixed-mode damage initiation in comparison to the reference solution.

**Table 12**

Energy dissipated in the local and reference models of the stiffened panel due to the skin-stringer separation for 6 coupling steps.

Coupling step	Dissipated energy, $Nmm$		
	Local model 1 <i>Averaging</i>	Local model 1 <i>Diss. Energies</i>	Reference model
Coupling step 1, $u = 0.56$ mm	60.9	60.9	32.2
Coupling step 2, $u = 0.58$ mm	167.4	80.2	50.2
Coupling step 3, $u = 0.60$ mm	235.0	185.6	80.6
Coupling step 4, $u = 0.63$ mm	388.0	228.8	122.2
Coupling step 5, $u = 0.67$ mm	435.5	263.0	182.6
Coupling step 6, $u = 0.82$ mm	604.9	303.8	330.9

However, it does not have large influence on the load-displacement curve as well as on the locations of the damaged areas. As the debonding started at the free edges due to the excessive buckling in this case, it was not so important how exactly the adhesive properties were reduced as it did not affect the path of the damage extension. But it is important to emphasize that for larger models with multiple delaminations this accuracy in predicting the damage modes could have an impact on the damage redistribution. It can be concluded that the global-local approach based on the preservation of the energy dissipation demonstrated its effectiveness and accuracy in application to a complex structure.

**5. Conclusion**

A novel two-way coupling global-local finite element approach for delamination preserving dissipated energy at both global and local levels has been formulated. This method establishes a procedure of dissipated energy calculation for the global model due to delamination based on the dissipated energy in the local model. This new global-local method also permits a reliable and efficient simulation of the delamination propagation by virtue of information exchange between separated global and local models. Single-mode and mixed-mode loading cases were examined for the first time as benchmark applications of the

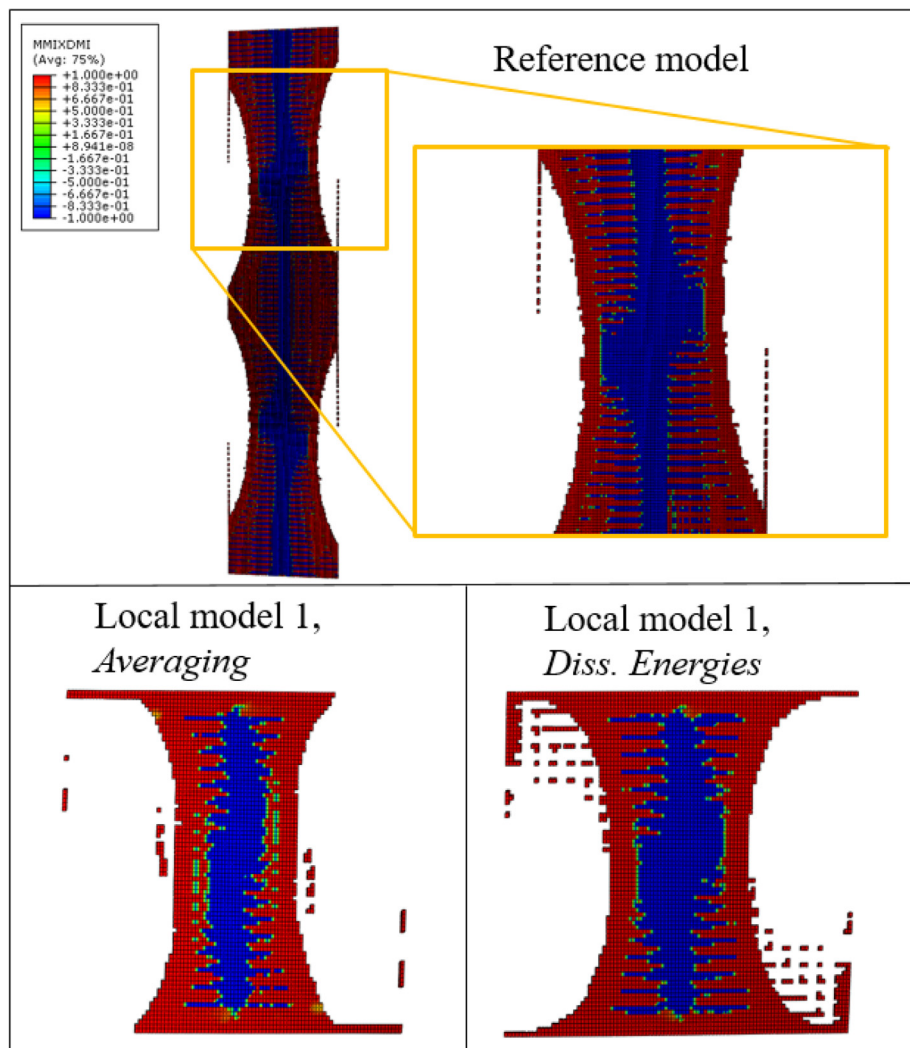


**Fig. 21.** Mixed-mode ratio of the damage initiation for cohesive elements of the reference model at the displacement of 0.58 mm and local models 1 obtained from the averaging procedure and for the preservation of the energies dissipated after the Coupling step 2 (corresponding to a displacement of 0.58 mm at the global level).

**Table 13**

Comparison of relative difference of mixed-mode ratio of damage initiation in reference model at the displacement of 0.58 mm and local models 1 obtained from the averaging procedure and for the preservation of the energy dissipated after the Coupling step 2 (corresponding to a displacement of 0.58 mm at the global level).

Relative difference with Ref. model	Percentage of cohesive elements, %	
	Local model 1 <i>Averaging</i>	Local model 1 <i>Diss. Energies</i>
≤10%	68.8	75.4
≤ 15%	73.2	79.4
≤ 20%	74.4	80.5

proposed methodology, showing that the approach captures the physics of delamination propagation correctly. In particular, the double cantilever beam (DCB) test, the end notched flexure (ENF) test and the mixed-mode loading (MMB) test were considered. In regard to the DCB benchmark, the results obtained for the global-local coupling approach correlate with a good agreement to the analytical and reference numerical results. In the case of the ENF test, the global-local approach also showed the ability to predict the delamination response closely to the analytical solution. With respect to the MMB test, the global-local numerical solution was able to capture the softening part of the load-displacement curve, but delamination initiation was predicted later than in the analytical solution and, thus, the overall structural strength was overestimated. This is due to the coarse nature of the mesh in the global model, whereas the global models provide an estimation of critical areas and local models with finer mesh are utilized for detailed analysis. The skin-stringer debonding onset and propagation leading to final collapse was examined with this global-local approach as a further validation, resulting in a very good agreement with a full 3D reference numerical simulation proving the capability of the method. The developed global-local numerical method is an effective tool for modeling delamination propagation at separated global and local levels, ensuring that the energy dissipated due to delamination evolution at the local level will be captured at the global level, triggering the reduction of load-bearing capacity at the global level up to the final collapse. In the future, the proposed strategy could be applied to more complex scenarios (e.g. impact loading of stiffened panels) structures to exploit the potential of the global-local method.

### Acknowledgments

The research leading to these results has received funding from European Union's Horizon 2020 research and innovation program (FULLCOMP/2015-2019) under Marie Skłodowska-Curie actions grant agreement number 642121. The provided financial support is gratefully acknowledged by the authors.

### References

- [1] Degenhardt R, Kling A, Klein H, Hillger W, Goetting HC, Zimmermann R, Rohwer K. Experiments on buckling and postbuckling of thin-walled cfrp structures using advanced measurement systems. *Int J Struct Stability Dyn* 2007;7(2):337–58.
- [2] Hühne S, Reinoso J, Jansen E, Rolfes R. A two-way loose coupling procedure for investigating the buckling and damage behaviour of stiffened composite panels. *Compos Struct* 2016(136):513–25. <https://doi.org/10.1016/j.compstruct.2015.09.056>.
- [3] Akterskaia M, Jansen E, Hühne S, Rolfes R. Efficient progressive failure analysis of multi-stringer stiffened composite panels through a two-way loose coupling global-local approach. *Compos Struct* 2018;183:137–45. <https://doi.org/10.1016/j.compstruct.2017.02.011>.
- [4] Akterskaia M, Jansen E, Hallett S, Weaver P, Rolfes R. Analysis of skin-stringer debonding in composite panels through a two-way global-local method. *Compos Struct* 2018. <https://doi.org/10.1016/j.compstruct.2018.06.064>.
- [5] Pineda EJ, Bednarczyk BA, Arnold SM, Waas AM. On multiscale modeling: Preserving energy dissipation across the scales with consistent handshaking methods. In: 54th AIAA/ASME/ASCE/AHS/ASC Structures, Structural Dynamics,

- and Materials Conference 35(2) (2013) 1–23. doi:10.2514/6.2013-1474.
- [6] Cater C, Xiao X. Energy based multiscale modeling with non-periodic boundary conditions, Proceedings of the American Society for Composites 28th Technical Conference.
- [7] Krueger R. The virtual crack closure technique for modeling interlaminar failure and delamination in advanced composite materials. Elsevier Ltd.; 2015. <https://doi.org/10.1016/B978-0-08-100332-9.00001-3>.
- [8] Rybicki E, Kanninen MF. A finite element calculation of stress intensity factors by modified crack closure integral. *Eng Fracture Mech* 1977;9:931–8. [https://doi.org/10.1016/0013-7944\(77\)90013-3](https://doi.org/10.1016/0013-7944(77)90013-3).
- [9] Crisfield M. Progressive delamination using interface elements; 1998.
- [10] Alfano G, Crisfield MA. Finite element interface models for the delamination analysis of laminated composites: \mbox{mechanical and computational issues. *Int J Numer Meth Eng* 2001;50(March 2000):1701–36. (March 2000).
- [11] Camanho P, Davila C. Mixed-mode decohesion finite elements in for the simulation composite of delamination materials, Nasa TM-2002-21 (June) (2002) 1–37. doi:10.1177/002199803034505.
- [12] Dugdale DS. Yielding of steel sheets containing slits. *J Mech Phys Solids* 1960;8:100–4.
- [13] Barenblatt GI. The mathematical theory of equilibrium cracks in brittle fracture. *Adv Appl Mech* 1962;7(C):55–129. [https://doi.org/10.1016/S0065-2156\(08\)70121-2](https://doi.org/10.1016/S0065-2156(08)70121-2).
- [14] Hillerborg A, Modeer M, Petersson P-E. Analysis of crack formation and crack growth in concrete by means of fracture mechanics and finite elements. *Cem Concr Res* 1976;6:773–82.
- [15] Allix O, Ladevèze P. Interlaminar interface modelling for the prediction of laminated delamination. *Compos Struct* 1992;22:235–42.
- [16] Turon A, Camanho PP. A damage model for the simulation of delamination in advanced composites under variable-mode loading. *Mech Mater* 2006;38:1072–89. <https://doi.org/10.1016/j.mechmat.2005.10.003>.
- [17] Borg R, Nilsson L, Simonsson K. Simulation of delamination in fiber composites with a discrete cohesive failure model. *Compos Sci Technol* 2001;61(5):667–77. [https://doi.org/10.1016/S0266-3538\(00\)00245-1](https://doi.org/10.1016/S0266-3538(00)00245-1).
- [18] Wisnom MR, Chang FK. Modelling of splitting and delamination in notched cross-ply laminates. *Compos Sci Technol* 2000;60(15):2849–56. [https://doi.org/10.1016/S0266-3538\(00\)00170-6](https://doi.org/10.1016/S0266-3538(00)00170-6).
- [19] Xie D, Waas AM. Discrete cohesive zone model for mixed-mode fracture using finite element analysis. *Eng Fracture Mech* 2006;73(13):1783–96. <https://doi.org/10.1016/j.engfractmech.2006.03.006>.
- [20] Hallett SR, Wisnom MR. Numerical investigation of progressive damage and the effect of layup in notched tensile tests. *J Compos Mater* 2006;40(14):1229–45. <https://doi.org/10.1177/0021998305057432>.
- [21] Jiang W-G, Hallett SR, Green BG, Wisnom MR. A concise interface constitutive law for analysis of delamination and splitting in composite materials and its application to scaled notched tensile specimens. *Int J Numer Methods Eng* 2007;69(9):1982–95. <https://doi.org/10.1002/nme.1842>.
- [22] Liu X, Duddu R, Waisman H. Discrete damage zone model for fracture initiation and propagation. *Eng Fracture Mech* 2012;92:1–18. <https://doi.org/10.1016/j.engfractmech.2012.04.019>.
- [23] Jimenez S, Liu X, Duddu R, Waisman H. A discrete damage zone model for mixed-mode delamination of composites under high-cycle fatigue. *Int J Fracture* 2014;190:53–74. <https://doi.org/10.1007/s10704-014-9974-0>.
- [24] Cabello M, Turon A, Zurbitu J, Renart J, Sarrado C, Martínez F. Progressive failure analysis of dcB bonded joints using a new elastic foundation coupled with a cohesive damage model. *Eur J Mech, A/Solids* 2017;63:22–35. <https://doi.org/10.1016/j.euromechsol.2016.12.004>.
- [25] Orifici AC, de Zarate Alberdi IO, Thomson RS, Bayandor J. Compression and post-buckling damage growth and collapse analysis of flat composite stiffened panels. *Compos Sci Technol* 2008;68(15–16):3150–60. <https://doi.org/10.1016/j.compstruct.2008.07.017>.
- [26] Reinoso J, Blázquez A, Estefani A, París F, Cañas J, Arévalo E, Cruz F. Experimental and three-dimensional global-local finite element analysis of a composite component including degradation process at the interfaces. *Compos Part B* 2012;43(4):1929–42. <https://doi.org/10.1016/j.compositesb.2012.02.010>.
- [27] Vescovini R, Dávila CG, Bisagni C. Failure analysis of composite multi-stringer panels using simplified models. *Compos Part B* 2013;45(1):939–51. <https://doi.org/10.1016/j.compositesb.2012.07.030>.
- [28] Borrelli R, Riccio A, Sellitto A, Caputo F, Ludwig T. On the use of global – local kinematic coupling approaches for delamination growth simulation in stiffened composite panels. *Compos Sci Technol* 2015;115:43–51. <https://doi.org/10.1016/j.compstruct.2015.04.010>.
- [29] Bettinotti O, Allix O, Perego U, Oancea V, Malherbe B. Simulation of delamination under impact using a global-local method in explicit dynamics. *Finite Elements Anal Des* 2017;125(June 2016):1–13. <https://doi.org/10.1016/j.finel.2016.11.002>.
- [30] Saavedra K, Allix O, Gosselet P, Hinojosa J, Viard A. An enhanced nonlinear multiscale strategy for the simulation of buckling and delamination on 3d composite plates. *Comput Methods Appl Mech Eng* 2017;317:952–69. <https://doi.org/10.1016/j.cma.2017.01.015>.
- [31] Akterskaia M, Jansen E, Hallett S, Weaver P, Rolfes R. Progressive failure analysis using global-local coupling including intralaminar failure and debonding. *AIAA J* 2019. <https://doi.org/10.2514/1.J057677> [accessed 21 April 2019].
- [32] Reeder JR, Crews JH. Mixed-mode bending method for delamination testing. *AIAA J* 1990;28(7):1270–6. <https://doi.org/10.2514/3.25204>.
- [33] Benzeggagh ML, Kenane M. Measurement of mixed-mode delamination fracture toughness of unidirectional glass/epoxy composites with mixed-mode bending apparatus. *Compos Sci Technol* 1996;56:439–49.

- [34] Turon A, González EV, Sarrado C, Guillaumet G, Maimí P. Accurate simulation of delamination under mixed-mode loading using a cohesive model with a mode-dependent penalty stiffness. *Compos Struct* 2018;184:506–11. <https://doi.org/10.1016/j.compstruct.2017.10.017>. (September 2017).
- [35] Turon A, Camanho PP, Costa J, Renart J. Accurate simulation of delamination growth under mixed-mode loading using cohesive elements: Definition of interlaminar strengths and elastic stiffness. *Compos Struct* 2010;92(8):1857–64. <https://doi.org/10.1016/j.compstruct.2010.01.012>.
- [36] Gonzalez EV, Maimi P, Turon A, Camanho PP, Renart J. Simulation of delamination by means of cohesive elements using an explicit finite element code. *Cmc-Comput Mater Continua* 2009;9(1):51–92. <https://doi.org/10.3970/cmc.2009.009.051>.





## 6 Validation of the global-local method on a five-stringer composite panel

In this chapter the developed global-local approach is applied to a large stiffened panel with initial skin-stringer separation. This curved five-stringer panel has been experimentally analysed during the COCOMAT project [32] and the damage patterns as well as load-displacement curve were obtained.

### 6.1 Model description

During experiments, the panel was loaded cyclically under compression until the damage was generated. The panel was loaded with 2000 cycles under 1,08 mm of compressive displacement and with 1700 cycles up to 1.93 mm. Afterwards, as the initial damage was detected, the panel was statically loaded until the final collapse. Orifici et al. [103] reported the locations and sizes of the damage introduced between the skin and the stringer after the cyclic loading, see Fig. 6-1, which allows to create a realistic simulation model. In order to avoid confusion, it is clarified here, that in all Figures presented the load was applied at the bottom of the panel, whereas the top of the panel was fixed. The panel was denoted pre-damaged panel D1 in their work. The load-displacement curve obtained after experimental testings and out-of-plane displacements are shown in Fig. 6-2. At around 0.75 mm of the axial compressive displacement local buckling occurred in the panel resulting in 13 to 15 longitudinal half waves per stiffener bay with a global buckling at around 1 mm of the axial loading. After 3700 cycles of loading the debonded area reached  $2016 \text{ mm}^2$  and  $1920 \text{ mm}^2$  under the second and the central (third) stringer if looking from the skin side, see Fig. 6-1. During the subsequent static loading the debonded areas started to grow rapidly at around 2.5 mm with next evolution at around 2.81 mm leading to the drop in load-carrying capacity and causing the fibre and matrix damage around debonded regions. Final collapse of the panel took place at the axial compressive displacement of 3.31 mm with a significant fibre fracture through the central stringer.

The panel was composed of a curved skin and five T-shaped stringers, see Fig. 6-3. An axial displacement was applied in compression to one of the transverse edges, while the opposite edge was fully clamped and both transverse edges were potted. The measured geometry parameters differed from the nominal which is explained by the residual stresses after the curing process. However, the residual stresses were neglected as they tend to be smaller than the stresses occurring due to external loads [140]. The nominal and measured geometry properties are summarized in Table 6-1 [32]. The areas of the introduced debonding were measured and consequently approximated by Orifici et al. [103]. These values, see Fig. 6-4, were used in a current simulation modelling at the global and local levels with implementation of intralaminar damage mechanism and skin-stringer debonding described

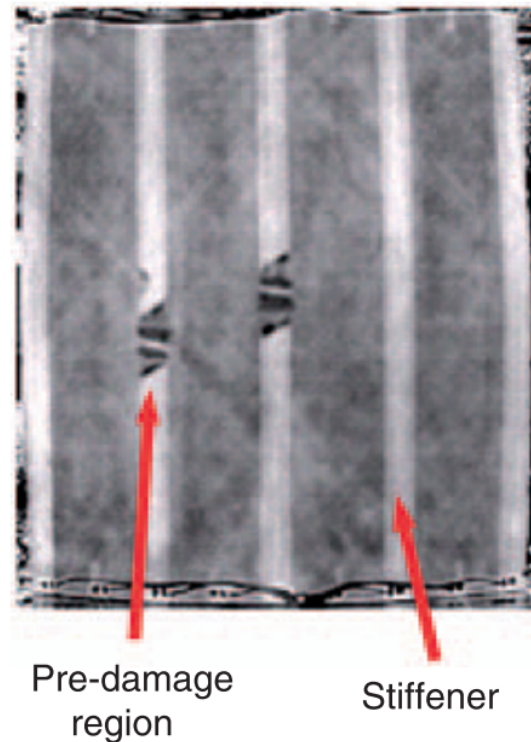


Figure 6-1: Thermography scan after 3700 cycles from the skin side for the pre-damaged D1 panel [103]. Both dark areas in the second and the central stringers correspond to pre-damaged regions.

in previous chapters.

The panel was made from the unidirectional CFRP prepreg material IM7/8552. Material properties were also measured for this case. However, the reported parameters resulted in a prediction of the incorrect lower initial structural stiffness by Orifici et al. [103] and Wagner and Balzani [140]. That is a reason for the choice of the higher Young's modulus in the longitudinal direction that corresponds to one of the measured mean values in [32], which allowed to reach better agreement between the experimental initial stiffness and initial stiffness obtained numerically. The material properties are summarized in Table 6-2, where the strength values were taken from [140]. The symmetric composite layups for the skin and for the stringer are  $[90^\circ, +45^\circ, -45^\circ, 0^\circ]_s$  and  $[(+45^\circ, -45^\circ)_3, 0^\circ_6]_s$  respectively, from [32].

## 6.2 Reference model for the pre-damaged D1 panel

The large size of the investigated panel motivated for using conventional shell elements with composite layup resulting in one element through the thickness instead of solid elements with many elements through the thickness which even for the reference model would be prohibitively expensive from the computational point of view. Application of continuum shell elements was not considered as the associated increase of computational effort would

Table 6-1: Geometry of a pre-damaged D1 five-stringer composite panel.

Description	Symbol	Nominal Value (mm)	Measured Value (mm)
Panel length	L	780	780.5
Potted length	$L_p$	60	60.25
Panel width	W	560	560.5
Stringer width	$w_{stringer}$	32	32
Stringer height	h	14	14.3
Skin thickness	$t_s$	1	0.98
Stringer thickness	$t_s$	3	2.9
Panel radius	R	1000	848

Table 6-2: Material data of the unidirectional CFRP material IM7/8552 UD.

Stiffness properties		Value	Strength and fracture properties		Value
Young's modulus in 1-direction	$E_{11}$	164.1.3 GPa	Tensile strength in 1-direction	$X_T$	2.379 GPa
Young's modulus in 2-direction	$E_{22}$	10.1 GPa	Compressive strength in 1-direction	$X_C$	1.365 GPa
Shear modulus in 12-plane	$G_{12}$	5.3 GPa	Tensile strength in 2-direction	$Y_T$	0.039 GPa
Shear modulus in 23-plane	$G_{23}$	4.0 GPa	Compressive strength in 2-direction	$Y_C$	0.170 GPa
Poisson's ratio	$\nu_{12}$	0.3	Shear strength in 12-plane	$S_A$	0.102 GPa
Young's modulus of adhesive	$E_{glue}$	3.0 GPa	Fracture energy of fibre	$G_f$	12.5 N/mm
-	-	-	Fracture energy of matrix	$G_m$	1.0 N/mm

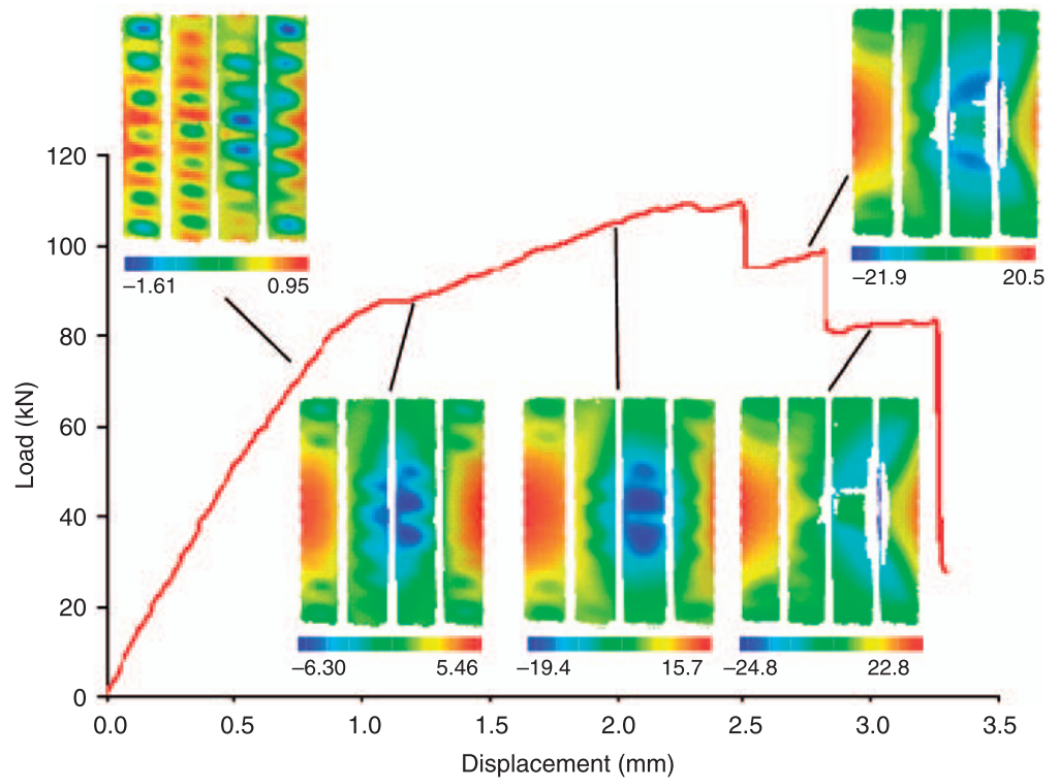


Figure 6-2: Experimental load-displacement curve with radial displacement contours (mm) (stiffener side) for the pre-damaged D1 panel [103].

not be compensated by the results if only one continuum element would be used through the thickness. In case of stacked continuum shell elements that would represent the individual layers, the reason of not using them is similar to the solid elements problem and is related to unacceptable demand of computational resources. Resulting reference shell model consisted of 17,940 conventional shell elements with in-plane size of 6 mm. That fact also demonstrates an advantage of the global-local approach where it is possible to inspect a critical region in detail with refined 3D local model and obtain accurate 3D stress state to access the damage consequences.

One of the transverse edges was fully clamped at the end, in all degrees of freedom which corresponds to the upper edge in Fig. 6-3. The opposite edge was also clamped except the longitudinal direction, and displacement was applied in this direction in compression. Potted regions at both transverse edges of the panel were used to ensure an even application of the loading and to prevent lateral movements during experiment. They were also fixed in all directions except longitudinal.

Material degradation model based on Linde [86] definitions was included into the reference model's analysis to detect the initiation and propagation of the intralaminar damage. Skin-stringer debonding was modelled by means of cohesive elements introduced between the skin and the stringer. To account for the relatively large size of cohesive elements, the strength

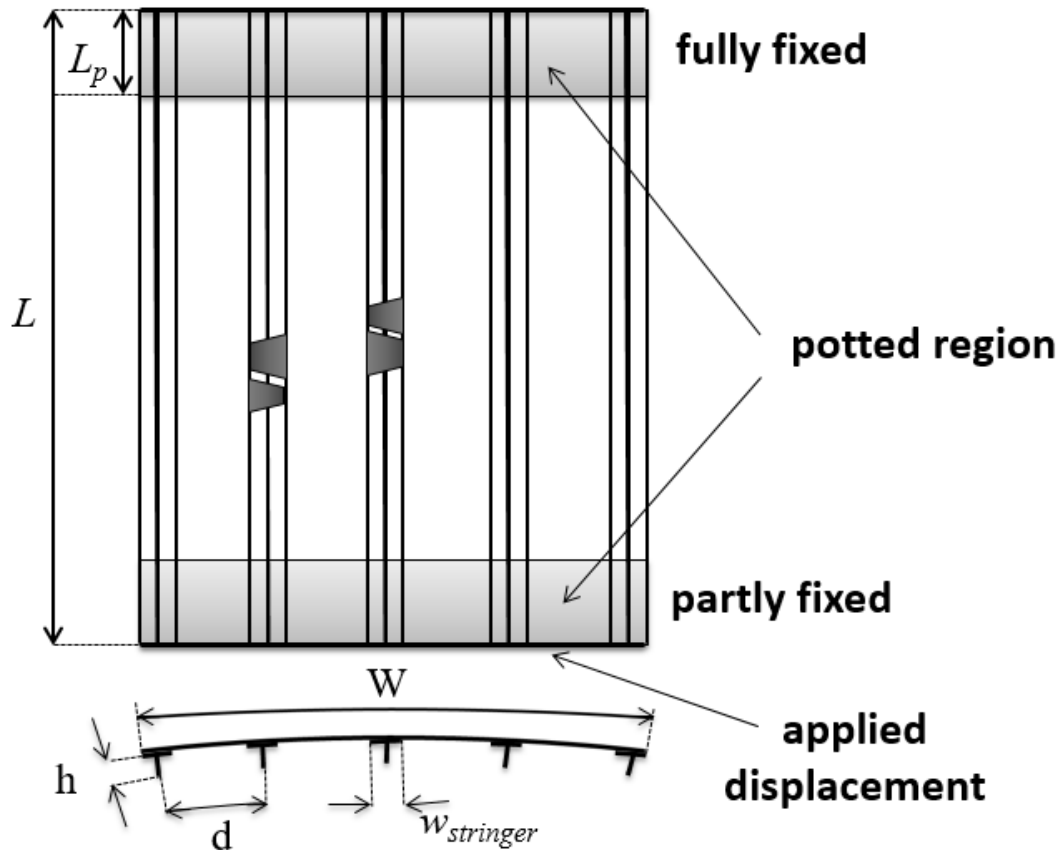


Figure 6-3: Curved five-stringer composite panel from the skin side.

values of cohesive elements were reduced following an engineering procedure by Turon et al. [134] that is described in detail in Chapter 1, see Eqs. 1.34, 1.35 and 1.36.

Contour plots of the numerically obtained radial displacements of the buckling shapes are presented in Fig. 6-6 with a comparison to the experimental radial displacements provided in [140] that are shown in Fig. 6-5. They demonstrate that the buckling modes are in a good agreement. The load-displacement curves for the reference shell model and experimental results are illustrated in Fig. 6-7. Although the recommended material parameters were adjusted, it can be seen that there is a slight difference between the initial stiffness of the two models. That might be explained by the fact that correction of the Young's modulus was performed under constraint of the highest measured mean Young's modulus in tension, but it was stated that the material was manufactured by different partners [32] and it might lead to even higher resulting material properties. Under loading, a local skin buckling pattern was detected for the experimental panel at around 0.5 mm of axial displacement followed by a global symmetric buckling pattern at around 1 mm loading that started to move and at the loading of about 1.54 mm was already located in between the debonded stringers. This behaviour correlated very well with numerical solution where the global buckling shifted in the area between the damaged inner stringers at displacement level of about 1.64 mm.

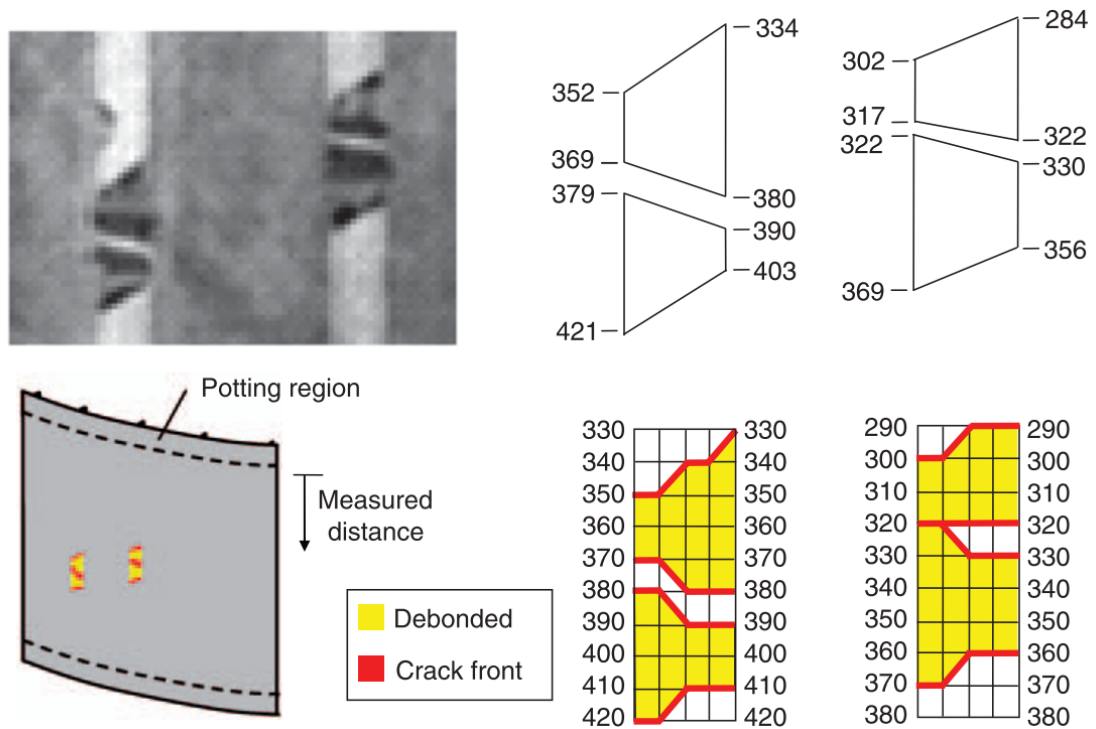


Figure 6-4: Thermographic image and approximated geometry of the debonded areas [103].

The final collapse also occurred very closely in both panels, at around 2.5 mm of axial compression for the experimental panel and at about 2.6 mm of axial shortening for the reference panel. Although Orifici et al. [103] suggested to consider the final failure to be provoked by the second large drop of the load-displacement curve, it is regarded as not conservative enough. The numerical model was not able to capture two large load drops that preceded the final collapse predicted by experimental measurements. That is probably due to the fact of introducing initial imperfection in the form of a first buckling mode with a goal to capture right buckling shape in the reference solution. That had to be done in an absence of exact geometric measurements from the experimental panel and might lead to this discrepancy.

In both cases the extensive debonding growth was detected under the initially debonded stringers which is shown in Fig. 6-8. Matrix cracking and fibre breakage also contributed to the final collapse. Intralaminar failure in the skin predicted by the numerical simulation is demonstrated in Fig. 6-9 with a good correspondence to the experimental data where the matrix damage also took place at the outer plies of the skin mainly in the centre and edges of the debonded regions and fibre fracture in the central stringer.

### 6.3 Coupling results

A global model was made of 17,940 shell elements similarly to the reference model, but in order to reduce computational time cohesive elements were replaced by connector elements

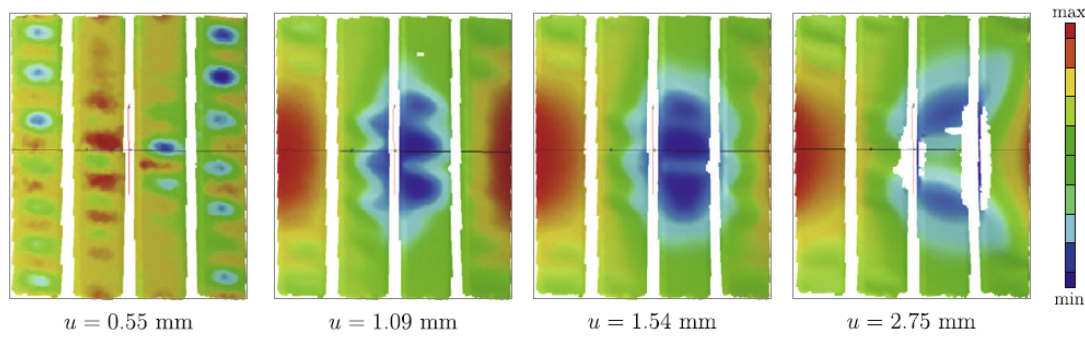


Figure 6-5: Experimental results of the buckling shapes from the stringers side [140].

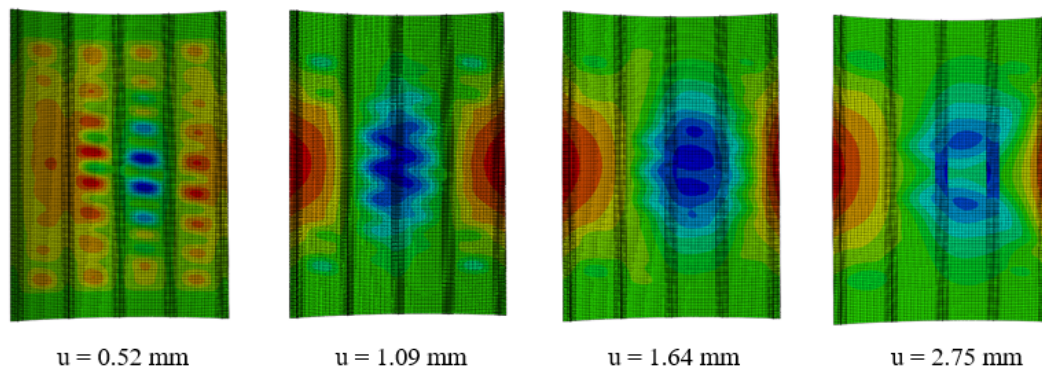


Figure 6-6: Reference shell results of the buckling shapes from the stringers side.

of a spring-type with no damage modelling between the skin and the stringer elements. Both interface area and the structural elements of the skin and the stringer were linearly elastic in the global model. The local models in contrast, incorporated the material modelling used for the reference solution such as material degradation modelling and cohesive elements. However, in contrast to the reference model, 8-node linear solid elements were employed for local models with a finer mesh size of 1 mm in-plane and one solid element per layer of the laminate.

Four coupling steps were used to simulate damage progression of this large stiffened panel through the global-local approach. Fig. 6-10 illustrates evolution of the fibre failure identified by means of the global-local analysis in the stringer which took place mainly in the region of the skin-stringer debonding. Another representative damage occurred in the skin of the panel and it was a matrix damage that propagated through significant part of the structure, see Fig. 6-11. During the first step of the axial compression of 1.40 mm an onset of the intralaminar failure was detected at a matrix of the skin located between the inner stringers and especially in the region of the debonded stringers as well as in a potted area, refer to Fig. 6-11. It was followed by a fibre damage at the middle and inner stringers at the debonded area, see Fig. 6-10. While there was no fibre damage detected in the reference model at this load level, the matrix damage locations correspond well to the results of the global-local coupling step, see Fig. 6-9. Also debonding initiation was predicted in the global model in

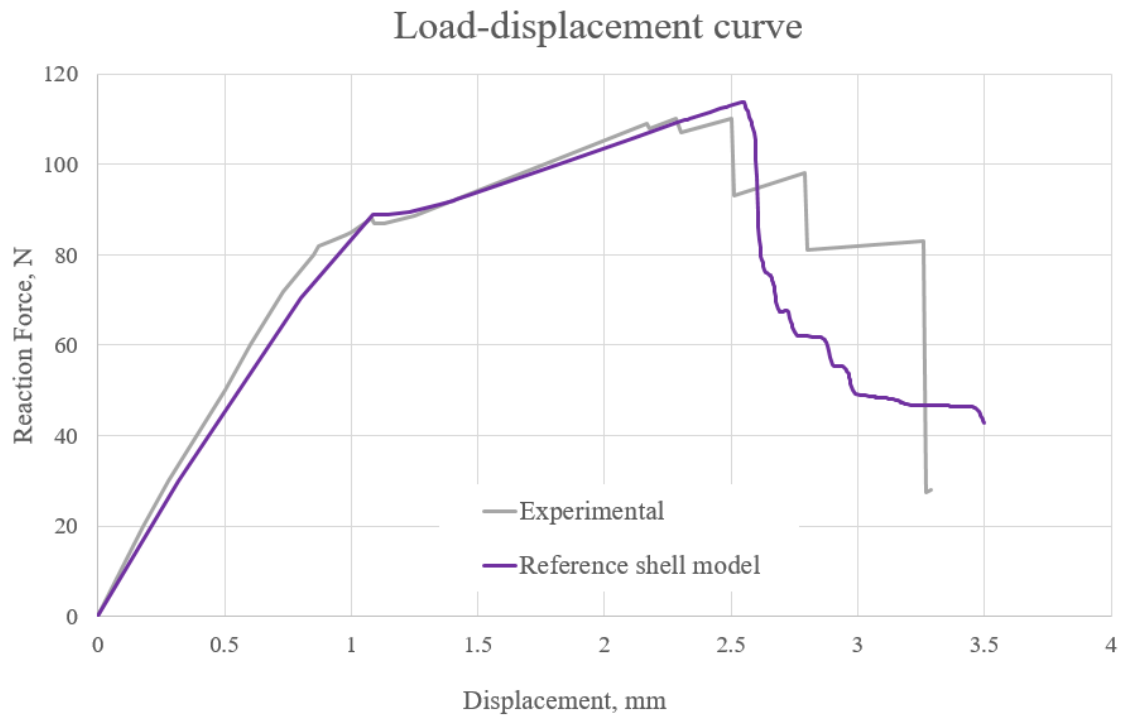


Figure 6-7: Load-displacement curves of the experimental panel [103] and reference shell numerical solution.

the regions where the panel was pre-damaged, which was similar to the reference model and experimental data reported. Six local models were created to inspect the damaged regions in detail, see Fig. 6-12. It is important to mention that the initial debonding was also taken into account during creation of the local models by allocating cohesive elements only in between undebonded regions. Meanwhile, during the second global-local coupling step with axial compression of 2.52 mm, debonding between the skin and the stringer was growing in the initially debonded regions, followed by the debonding at free edges, as was reported in the experimental results [103] and determined by the reference analysis. Next coupling step of 2.82 mm determined an increase of the overall damage. Final collapse of the panel occurred at the load level of 3.33 mm due to the loss of the stability of the panel that was a result of the extensive debonding growth and sequential reduction of the material properties due to the intralaminar damage. It should be mentioned that, though with consecutive increase of the axial compressive displacement the damage initiation was detected in the overall structure, only the region of the initial debonding was investigated with detailed local models. This decision was based on several assumptions. On the one hand, the damage was localized near the debonded stringers where all types of damage were found to occur such as matrix cracking, fibre breakage and growth of the skin-stringer separation. Hence, it was essential to examine these areas with the refined models. On the other hand, the damage that was spreading all over the structure was not recognized as critical as no fibre breakage was left without attention, whereas matrix cracking and skin-stringer debonding happening separately are not usually the cause of the catastrophic collapse.



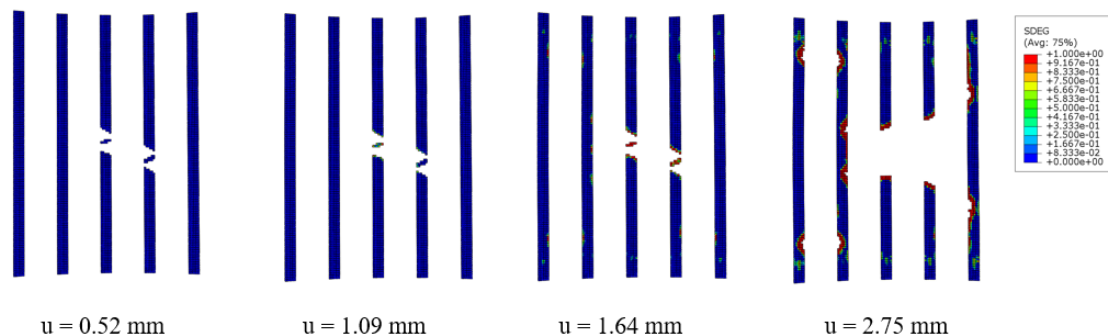


Figure 6-8: Degraded cohesive elements of the reference shell model. View from the stringers side.

Numerical analyses for global, local and reference models were performed under the same computational characteristics. Relative calculation times for these models for the analysis with four coupling steps are shown in Table 6-3. In order to obtain numerical solution through the global-local method, global and local analyses should be carried out for each coupling step and each iteration that is required to achieve convergence in forces. Hence, the total global-local computational time is a sum of all these analyses times. Moreover, it should be emphasized that, as all local models' analyses have been conducted in parallel, only the maximum computational time is important for the total computational time. It might be seen that the global-local analysis is several times faster as compared to rather coarse reference model. It is explained by several reasons. First, the main damage in the stiffened panel under investigation was localized in the pre-damaged region which led to a creation of relatively small local models. Secondly, the material degradation model with iterative procedure was incorporated only at the local level, which allowed global models to keep their advantage of relatively fast solutions. And lastly, local models were calculated in parallel, and no interaction between them was included at the local level which also saved the computational resources. The influence of the different damage propagation mechanisms was accounted for in the global model, based on the results obtained from local models.

Load-displacement curves for a reference panel with shell elements, coupling global-local results and experimental results are displayed in Fig. 6-13. The initial buckling occurred under slightly higher compressive displacement in the global model leading to a very close prediction in post-buckling stiffness and with a load drop at around 2.5 mm which is confirmed by the experimental data. However, the global model continued to withstand further loading most probably because not all damage introduced under the cyclic loading was incorporated into the model. In contrast, the final failure of the reference model took place earlier. This might be attributed to the fact that the chosen mesh size was too coarse to be able to capture real material behaviour. That is why very accurate representation of the initial geometry and material imperfections are required. In the case of this five-stringer panel not all the data was available to account for such exact geometrical shape and locations of the damage that might be also introduced apart from the skin-stringer debonding. The other difficulty that was encountered is that with increase of the load the damage ceased to

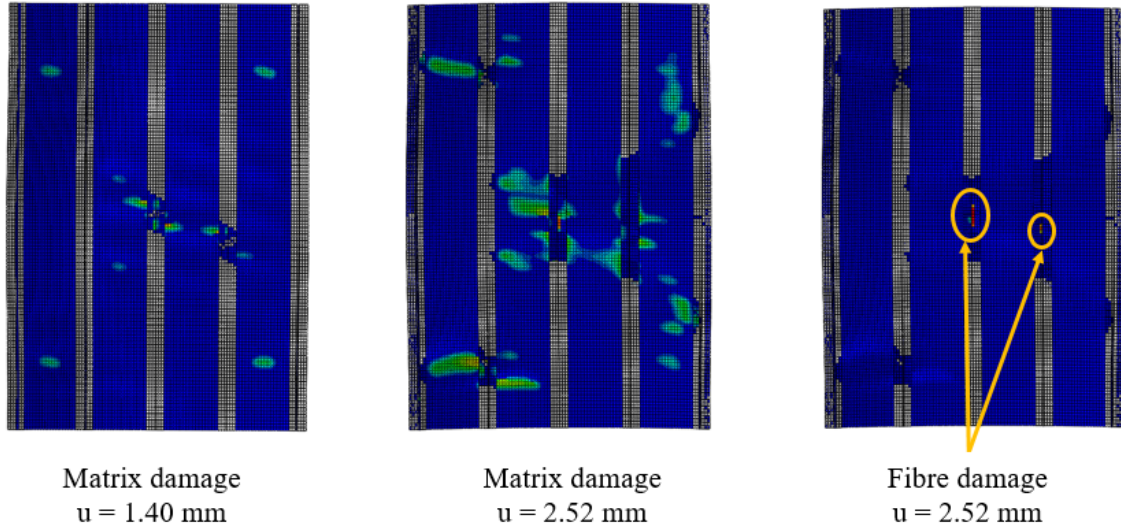


Figure 6-9: Reference model. Left: matrix damage at applied displacement of 1.40 mm. Middle: matrix damage at applied displacement of 2.52 mm (final failure). Right: fibre damage at applied displacement of 2.52 mm (final failure). View from the stringers side.

be localized which might result in a fact, that more local models are needed to be created. However, the application of the global-local method allowed to capture the skin-stringer debonding and intralaminar damage initiation and explore these damages evolution in the local models.

Table 6-3: Computational characteristics of models.

Model	Number of nodes	Number of elements	Degrees of freedom	Relative computational time, s
Reference model	18,864	21,727	113,184	1,456,330
Global model, 1 <sup>st</sup> coupling step	45,786	26,963	140,253	4008
Global model, 4 <sup>th</sup> coupling step	45,786	26,963	140,253	65,335
Local model 1, 1 <sup>st</sup> coupling step	98,101	66,936	221,691	12,713
Local model 1, 4 <sup>th</sup> coupling step	131,857	91,296	301,935	113,705
Total global-local coupling	-	-	-	221,541

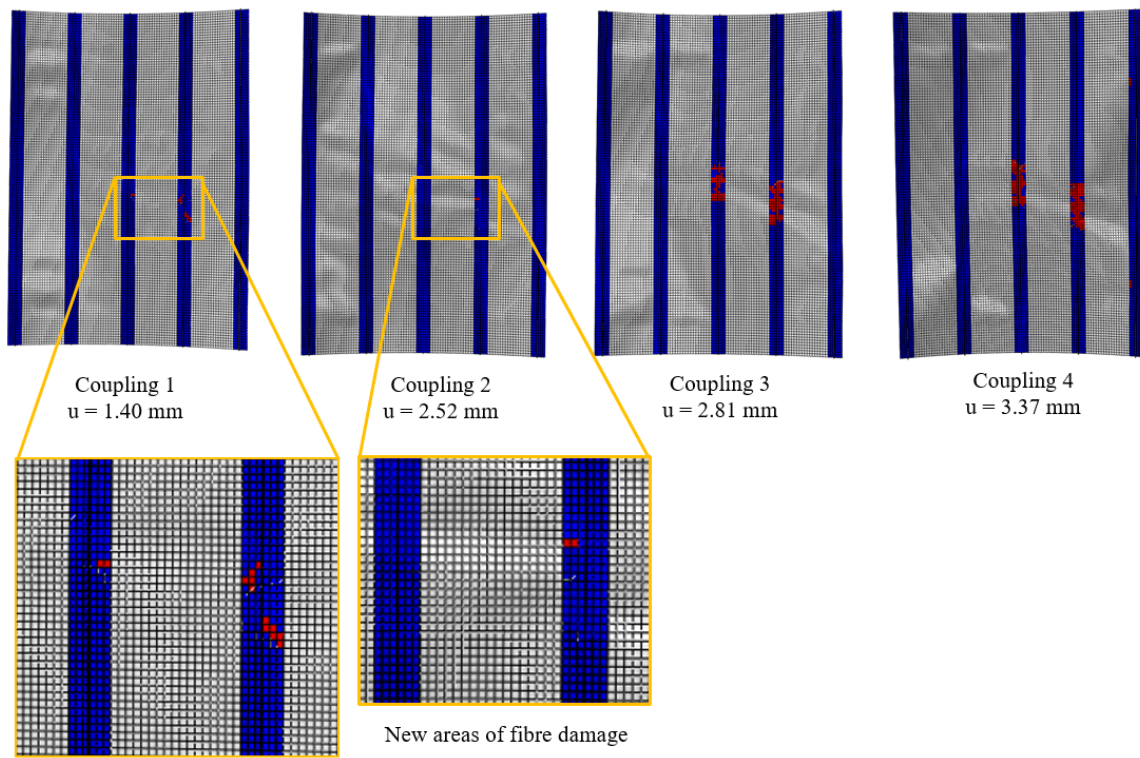


Figure 6-10: New areas of the fibre damage in the global model detected at each step of the global-local coupling procedure in the stringer. View from the stringers side.

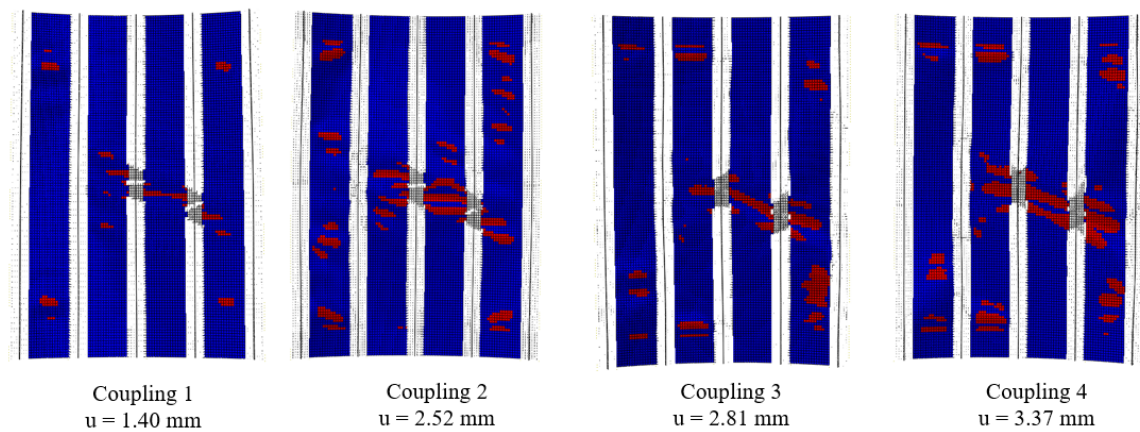


Figure 6-11: New areas of the matrix damage in the global model detected at each step of the global-local coupling procedure in the skin. View from the stringers side.

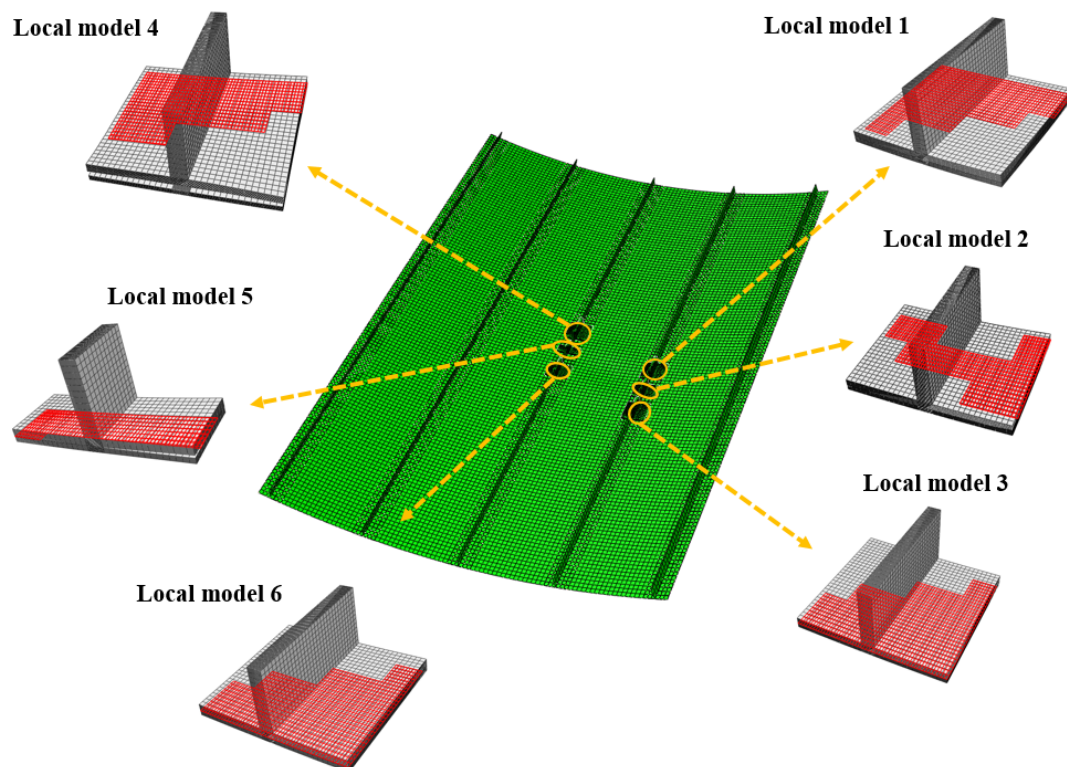


Figure 6-12: Global model and six local models created in the regions of the initial debonding. Cohesive elements in red in local models to account for the initial debonding.

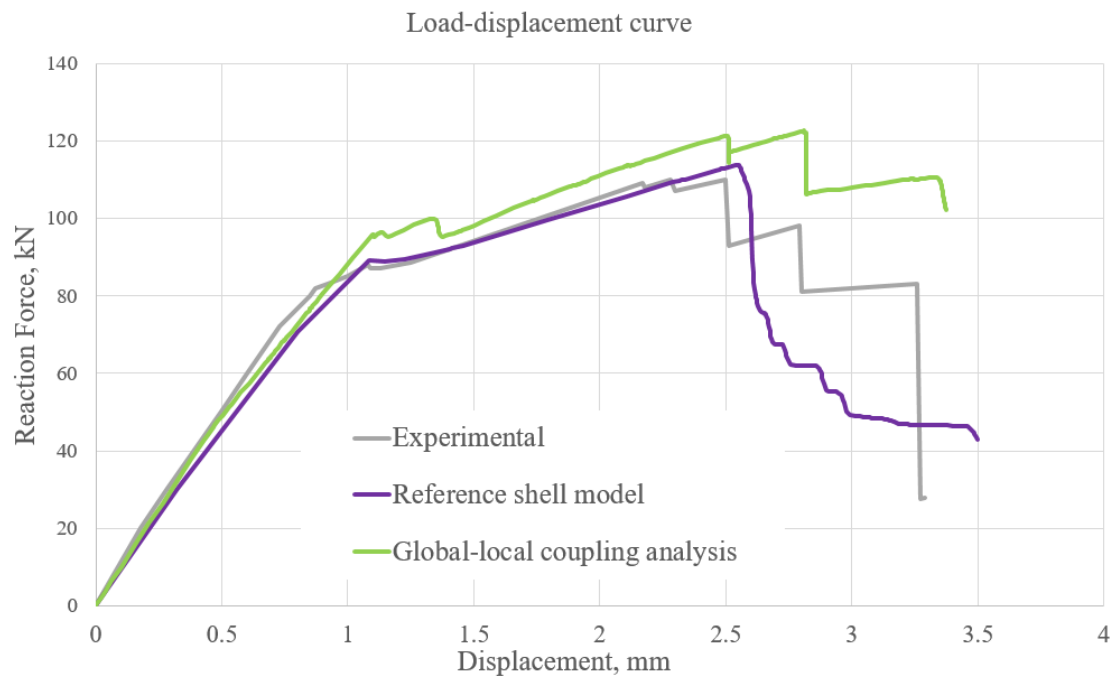


Figure 6-13: Load-displacement curves of the experimental panel [103], reference shell numerical solution and global-local coupling results.



# 7 Summary and outlook

## 7.1 Summary

The overall goal of this work was to establish a computationally effective methodology that would be able to accurately capture the progressive failure behaviour of large composite panels in the postbuckling regime. The more global objectives were to contribute to the replacement of expensive experimental tests by efficient mechanical virtual testings and to make a step toward increasing the design load to the damage onset instead of the buckling load. While the reduction of the number of experimental tests leads to decrease in certification costs, the extension of the design load enables an exploitation of possible reserves in the load carrying capacities of stiffened panels. A detailed review of the current state of the art was presented.

A two-way loose coupling strategy has been chosen with the purpose of answering both requirements: fast computational tool on the one hand that allows to conduct the detailed analysis of the critical areas on the other hand. This choice over a tight coupling is explained by the fact that a loose coupling technique implies flexibility in defining the local model's size and location that could be easily adjusted during analysis without intrusively changing the global model. The main challenge of the coupling methods is an information exchange between two different models. On the one hand, the submodeling technique is commonly used to drive the local analysis through applying interpolated global displacements on the boundary nodes of the local model. On the other hand, it is indispensable to include the effect of damage from the local results to the global model to ensure that correct stress redistribution due to the damage occurrence is accounted for. Only through the iterative exchange of the information between the local and the global models it is possible to conduct a full progressive failure analysis until final collapse. Moreover, the global-local method is computationally more efficient than the full 3D solution including material non-linearities, such as damage initiation and evolution, for instance, and accurate enough as the global model includes the response from the localized damage. For the case of large complex structures, full 3D simulation could be not only prohibitively expensive, but also impossible to perform due to the current computational limitations. That is the main reason of the evolution of global-local techniques as quick simulation tools of the structural behaviour which include material damage degradation obtained at the refined level.

The existing two-way coupling approach with intralaminar damage model was modified through including possibility to consider layups with 45 degrees, the local models were investigated with attention paid on the alleviation of spurious stress concentrations. Finally, the method was validated on the example of a large stiffened panel and compared to the experimental results.

During the next step a novel two-way coupling approach was developed incorporating a

skin-stringer debonding which is a typical damage mechanism during compressive loading of stiffened panels. The main advantage of the method is information exchange between local and global models performed through gradual material degradation of the interface stiffness. In this framework a discrete and cohesive continuum damaged elements were coupled together which allowed to exploit their particular advantages at corresponding levels of accuracy. The validation of the developed two-way coupling method for the case of the one-stringer panel with initial debonding demonstrated a good agreement with experimental results. Although the final collapse was not predicted by the method as the intralaminar failure was not taken into account.

A two-way global-local approach for the combination of both intralaminar failure and skin-stringer separation has been formulated in order to incorporate both critical failure modes into the coupling method. Following the assumption that material degradations occur in parallel, the local models incorporated both damages through continuum material degradation for the matrix and fibre failure and cohesive elements to track the skin-stringer debonding but only in case if both damages were detected at the global level. In case only one type of damage met respective failure criterion, the local material degradation model was restricted to this type of damage. Good comparison to the experimental results and achieved reduction of about 50% in computational time demonstrated significant potential of the method.

A global-local coupling methodology was further enhanced through preserving energy dissipated due to skin-stringer separation between the global and local levels. The method was applied first to two cases of a single-mode loading, such as a double cantilever beam (DCB) and an end notched flexure (ENF) tests, and then to a mixed-mode loading on example of a mixed-mode bending (MMB) test. Finally, the developed method has been verified on a test case of a single-stringer panel under compression where the interface layer experiences mixed-mode loading.

Finally, the method was implemented to a large stiffened panel in order to obtain the advantages of the computational time savings during the localized damage and to validate the method with experimental data. To increase the accuracy, a global-local approach has been enhanced by preserving dissipated energies from the skin-stringer debonding between the global and the local levels.

In conclusion, the formulated objectives are successfully achieved and a two-way global-local coupling method has been developed for the investigation of the failure behaviour of large stiffened panels. The approach combines an advantage of a fast computational tool for the relatively accurate estimation of the structural behaviour in a postbuckling regime and a possibility to efficiently account for the intralaminar damage and skin-stringer debonding.

## 7.2 Outlook

The developed two-way coupling approach has been dedicated to deal with quasi-static loads which is regarded as a first step toward the full assessment of this approach with a future



potential to be implemented in numerical tests of real aircraft and aerospace structures. Although quasi-static loads are usually considered when the damage is investigated and the damage tolerance is accessed at the beginning, there are other important mechanisms that should be taken into account to simulate real in-service events and loads. Composite components of aircrafts experience long-time repeated loadings that could cause a fatigue damage. Therefore, it is important to ensure that not only the cracks initiations are predicted accurately, but also that the cracks lengths will stay below the critical lengths between the planned inspections. Experimental studies of the fatigue damage are very costly processes. That is why the development of a robust global-local approach incorporating the fatigue damage could significantly reduce the design and even maintenance costs. Correct numerical estimation of the fatigue damage will also lead to an increase of the limit load and will allow to exploit possible reserves of the stiffened panels. Hence, fatigue damage consideration is a very important aspect of the possible future work.

Another common source of damage and succeeding decrease in strength and load carrying capabilities is an impact damage that could be introduced during the production, maintenance or lifetime service. This type of damage is often hard or even impossible to detect through visual inspection. For this reason, physical testing might be expensive to perform and it also requires to establish a framework of tools to capture the impact damage. A reliable and efficient computational solution for the impact damage prediction and consideration of the following complex damage propagation are to be created to partially replace the experimental testings. The developed global-local method could be extended by including the impact damage into consideration due to the commonly localized nature of this type of damage.

The presented global-local method for modelling progressive failure in the stiffened panels examined compression as one of the most typical loads for these panels as they were designed to withstand primarily the loads aligned with stringer directions. Although during the service time the panels may undergo a combination of loads that include shear loading, for instance. That is an incentive to examine different loads under the global-local methodology and validate results against experimental data. The other improvement that could be envisaged is inclusion of more complex material behaviour such as comprising the uncertainties at the local level. However, it should be recognized that it might be difficult to validate such enhancement. The current global-local method aimed at encompassing the most relevant damage mechanisms such as matrix cracking, fibre breakage and skin-stringer debonding. Delamination at the free edge of the stringer foot or stringer blade is another common damage that occurs under compressive loading of the stiffened panel. Although delamination is not recognized to be critical for the overall structural collapse, it might represent an area of the future development as delamination may interact with other damage mechanisms such as matrix cracking, for example. It is important to notice that the introduced global-local approach will require significant elaboration to incorporate the effect of delamination at the global level as currently to reduce computational costs only one element through the thickness represents the full layup of the stringer. Hence, in the current configuration it is hard to predict delamination initiation at the global level and for this purpose the global model should be modified.

An important direction identified for the future progression is an application of the measured geometrical imperfections for each validated structure. It becomes essential to introduce

---

accurately all imperfections as it leads to correctly captured buckling shapes of the stiffened panels. When considering stiffened panels under compressive loads the final collapse may take place under the loads much higher than the first buckling load. With an objective to exploit the postbuckling regime of these stiffened panels it is imperative that the buckling shapes simulated numerically are identical to real buckling patterns which could be attained only through introducing initial imperfections into numerical model.

The two-way global-local approach has been developed and implemented to model progressive failure in stiffened panels which constitute parts of the aircraft design. The future work could be dedicated to extension of the method into application to even larger structures such as full fuselages and wing boxes in order to establish a robust and efficient mechanical virtual tool suitable to unprecedentedly large structures.

# Bibliography

- [1] ABAQUS. Abaqus 6.14 Documentation. Dassault systemes. 6.14 edn. 1–172.
- [2] ABOUDI, J., ARNOLD, S. M., AND BEDNARCYK, B. A. Multiscale modeling of composites. In *Micromechanics of composite materials*. Springer, Dordrecht, 2013, pp. 447–540.
- [3] AKTERSKAIA, M., JANSEN, E., HALLETT, S., WEAVER, P., AND ROLFES, R. Post-buckling progressive failure analysis of composite panels using a two-way global-local coupling approach including intralaminar failure and debonding. In *Advances in Predictive Models and Methodologies for Numerically Efficient Linear and Nonlinear Analysis of Composites*. Springer International Publishing, 2019, pp. 83–102.
- [4] AKTERSKAIA, M., JANSEN, E., HALLETT, S., WEAVER, P., AND ROLFES, R. Progressive failure analysis using global-local coupling including intralaminar failure and debonding. *AIAA Journal* 57, 7 (2019), 3078–3089.
- [5] ALESI, H., NGUYEN, V., MILESHKIN, N., AND JONES, R. Global/local postbuckling failure analysis of composite stringer/skin panels. *AIAA Journal* 36, 9 (1998), 1699–1705.
- [6] ALFANO, G., AND CRISFIELD, M. A. Finite element interface models for the delamination analysis of laminated composites: mechanical and computational issues. *Int. J. Numer. Meth. Eng.* 50 (2001), 1701–1736.
- [7] ALLIX, O., GENDRE, L., GOSSELET, P., AND GUGUIN, G. Non-intrusive coupling: an attempt to merge industrial and research software capabilities. In *Recent Developments and Innovative Applications in Computational Mechanics*. Springer, Berlin, Heidelberg, 2011.
- [8] ALLIX, O., GOSSELET, P., KERFRIDEN, P., AND SAAVEDRA, K. Virtual delamination testing through non-linear multi-scale computational methods: some recent progress. *CMC* 32, 2 (2012), 107–132.
- [9] ALLIX, O., AND LADEVÈZE, P. Interlaminar interface modelling for the prediction of laminate delamination. *Composite Structures* 22 (1992), 235–242.
- [10] BALZANI, C., AND WAGNER, W. Numerical treatment of damage propagation in axially compressed composite airframe panels. *International Journal of Structural Stability and Dynamics* 10, 4 (2010), 683–703.
- [11] BARENBLATT, G. I. The mathematical theory of equilibrium cracks in brittle fracture. *Advances in Applied Mechanics* 7, C (1962), 55–129.
- [12] BAYREUTHER, C. G., MIEHE, C., AND SCHRÖDER, J. Aspects of homogenization techniques and multigrid solving. In *Multifield Problems: State of the Art*. Springer Berlin Heidelberg, 2000, pp. 88–95.
- [13] BELYTSCHKO, T., FISH, J., AND BAYLISS, A. The spectral overlay on finite elements for problems with high gradients. *Comput. Methods Appl. Mech. Engrg.* 81 (1990),

- 71–89.
- [14] BENZEGGAGH, M. L., AND KENANE, M. Measurement of mixed-mode delamination fracture toughness of unidirectional glass/epoxy composites with mixed-mode bending apparatus. *Composites Science and Technology* 56 (1996), 439–449.
  - [15] BETTINOTTI, O., ALLIX, O., AND MALHERBE, B. A coupling strategy for adaptive local refinement in space and time with a fixed global model in explicit dynamics. *Comput Mech (2014)* 53 (2014), 561–574.
  - [16] BETTINOTTI, O., ALLIX, O., PEREGO, U., AND OANCEA, V. A fast weakly intrusive multiscale method in explicit dynamics. *Int. J. Numer. Meth. Engng* 100 (2014), 577–595.
  - [17] BETTINOTTI, O., ALLIX, O., PEREGO, U., OANCEA, V., AND MALHERBE, B. Simulation of delamination under impact using a global-local method in explicit dynamics. *Finite Elements in Analysis and Design* 125 (2017), 1–13.
  - [18] BISHARA, M., ROLFES, R., AND ALLIX, O. Revealing complex aspects of compressive failure of polymer composites. part i: Fiber kinking at microscale. *Composite Structures* 169 (2017), 105–115.
  - [19] BORG, R., NILSSON, L., AND SIMONSSON, K. Simulation of delamination in fiber composites with a discrete cohesive failure model. *Composites Science and Technology* 61, 5 (2001), 667–677.
  - [20] BORG, R., NILSSON, L., AND SIMONSSON, K. Modeling of delamination using a discretized cohesive zone and damage formulation. *Composites Science and Technology* 62 (2002), 1299–1314.
  - [21] BORRELLI, R., RICCIO, A., SELITTO, A., CAPUTO, F., AND LUDWIG, T. On the use of global-local kinematic coupling approaches for delamination growth simulation in stiffened composite panels. *Composites Science and Technology* 115 (2015), 43–51.
  - [22] CAMANHO, P., DÁVILA, C., AND DE MOURA, M. M. Numerical simulation of mixed-mode progressive delamination in composite materials. *Journal of Composite Materials* 37 (2003), 1415–1438.
  - [23] CHRUPALLA, D., BERG, S., KÄRGER, L., DOREILLE, M., LUDWIG, T., JANSEN, E., ROLFES, R., AND KLING, A. A homogenization-based two-way multiscale approach for composite structures. In: *Rolfes R, Jansen EL, editors. Proceedings of the 3rd ECCOMAS thematic conference on the mechanical response of composites. Germany: Hannover; (2011), p. 263–70.*
  - [24] CHRUPALLA, D., KREIKEMEIER, J., BERG, S., KÄRGER, L., DOREILLE, M., LUDWIG, T., JANSEN, E., ROLFES, R., AND KLING, A. A loose coupling multiscale approach for the detailed analysis of the influence of critical areas on the global behaviour of composite structures. *Computers, Materials and Continua* 32, 3 (2012), 159–176.
  - [25] COSENTINO, E., AND WEAVER, P. Approximate nonlinear analysis method for debonding of skin/stringer composite assemblies. *AIAA Journal* 46, 5 (2008).
  - [26] COX, B., AND YANG, Q. In quest of virtual tests for structural composites. *Science* 314 (2006), 1102–1107.
  - [27] DAVIES, G. A. O., AND ANKERSEN, J. Virtual testing of realistic aerospace composite structures. *Mater Sci*, 43 (2008), 6586–6592.

- [28] DÁVILA, C. G., AND CAMANHO, P. P. Analysis of the effects of residual strains and defects on skin/stiffener debonding using decohesion elements. *44th AIAA/ASME/ASCE/AHS Structures, Structural Dynamics, and Materials Conference* (2003).
- [29] DÁVILA, C. G., CAMANHO, P. P., AND DE MOURA, M. F. Mixed-mode decohesion elements for analyses of progressive delamination. *42nd AIAA/ASME/ASCE/AHS/ASC Structures, Structural Dynamics and Materials Conference* (2001), AIAA-01-1486.
- [30] DÁVILA, C. G., CAMANHO, P. P., AND ROSE, C. A. Failure criteria for frp laminates in plane stress. *Journal of Composite Materials* 39 (2005), 323–345.
- [31] DÁVILA, C. G., JAUNKY, N., AND GOSWAMI, S. Failure Criteria for FRP Laminates in Plane Stress. *Tech. Rep. NASA TM-2003-212663. USA: National Aeronautics and Space Administration* (2003).
- [32] DEGENHARDT, R., KLING, A., KLEIN, H., HILLGER, W., GOETTING, H. C., ZIMMERMANN, R., AND ROHWER, K. Experiments on buckling and postbuckling of thin-walled cfrp structures using advanced measurement systems. *International Journal of Structural Stability and Dynamics* 7, 2 (2007), 337–358.
- [33] DEGENHARDT, R., ROLFES, R., ZIMMERMANN, R., AND ROHWER, K. COCOMAT - improved material exploitation of composite airframe structures by accurate simulation of postbuckling and collapse. *Composite Structures* 73 (2006), 175–178.
- [34] DUGDALE, D. S. Yielding of steel sheets containing slits. *J. Mech. Phys. Solids* 8 (1960), 100–104.
- [35] DUVAL, M., PASSIEUX, J.-C., SALAÜN, M., AND GUINARD, S. Non-intrusive coupling: recent advances and scalable nonlinear domain decomposition. *Arch Computat Methods Eng* 23 (2016), 17–38.
- [36] EL SAID, B., DAGHIA, F., IVANOV, D., AND HALLETT, S. R. An iterative multiscale modelling approach for nonlinear analysis of 3D composites. *International Journal of Solids and Structures* 132-133 (2018), 42–58.
- [37] ERNST, G. *Multiscale analysis of textile composites - stiffness and strength*. PhD thesis, Institut für Statik und Dynamik, Leibniz Universität Hannover, Hannover, Germany, 2009.
- [38] ERNST, G., VOGLER, M., HÜHNE, C., AND ROLFES, R. Multiscale progressive failure analysis of textile composites. *Composites Science and Technology* 70 (2010), 61–72.
- [39] FAGGIANI, A., AND FALZON, B. G. Optimization strategy for minimizing damage in postbuckling stiffened panels. *AIAA Journal* 45, 10 (2007), 2520–2528.
- [40] FALZON, B. G., DAVIES, G. A. O., AND GREENHALGH, E. Failure of thick-skinned stiffener runout sections loaded in uniaxial compression. *Composite Structures* 53 (2001), 223–233.
- [41] FEYEL, F. Multiscale FE2 elastoviscoplastic analysis of composite structures. *Computational Materials Science* 16 (1999), 344–354.
- [42] FEYEL, F. A multilevel finite element method (fe2) to describe the response of highly non-linear structures using generalized continua. *Comput. Methods Appl. Mech. Engrg.* 192 192 (2003), 3233–3244.

- [43] FEYEL, F., AND CHABOCHE, J.-L. Fe2 multiscale approach for modelling the elastoviscoplastic behaviour of long fibre sic/ti composite materials. *Computer Methods in Applied Mechanics and Engineering* 183, 3-4 (2000), 309–330.
- [44] FISH, J. The s-version of the finite element method. *Computers & Structures* 43, 3 (1992), 539–547.
- [45] FISH, J., AND BELSKY, V. Multigrid method for periodic heterogeneous media Part 1: Convergence studies for one-dimensional case. *Comput. Methods Appl. Mech. Engrg.* 126 (1995), 1–16.
- [46] FISH, J., AND BELSKY, V. Multigrid method for periodic heterogeneous media Part 2: Multiscale modeling and quality control in multidimensional case. *Comput. Methods Appl. Mech. Engrg.* 126 (1995), 17–36.
- [47] FISH, J., AND CHEN, W. Discrete-to-continuum bridging based on multigrid principles. *Comput. Methods Appl. Mech. Engrg.* 193 (2004), 1693–1711.
- [48] GARIKIPATI, K., AND HUGHES, T. J. R. A variational multiscale approach to strain localization formulation for multidimensional problems. *Comput. Methods Appl. Mech. Engrg.* 188 (2000), 39–60.
- [49] GARNICH, M. R., AND AKULA, V. M. Review of degradation models for progressive failure analysis of fiber reinforced polymer. *Applied Mechanics Reviews* 62 (2018).
- [50] GEERS, M., KOUZNETSOVA, V., AND BREKELMANS, W. Gradient-enhanced computational homogenization for the micro-macro scale transition. *J. Phys. IV France* 11 (2001), 145–152.
- [51] GENDRE, L., ALLIX, O., AND GOSSELET, P. A two-scale approximation of the Schur complement and its use for non-intrusive coupling. *Int. J. Numer. Meth. Engrg.* 87 (2011), 889–905.
- [52] GENDRE, L., ALLIX, O., GOSSELET, P., AND COMTE, F. Non-intrusive and exact global/local techniques for structural problems with local plasticity. *Comput Mech* 44 (2009), 233–245.
- [53] GHOSH, S., LEE, K., AND MOORTHY, S. Multiple scale analysis of heterogeneous elastic structures using homogenization theory and voronoi cell finite element method. *Int. J. Solids Structures Vol. 32*, 1 (1995), 27–62.
- [54] GHOSH, S., LEE, K., AND RAGHAVAN, P. A multi-level computational model for multi-scale damage analysis in composite and porous materials. *International Journal of Solids and Structures* 38, 14 (2001), 2335–2385.
- [55] GITMAN, I. *Representative volumes and multi-scale modelling of quasi-brittle materials*. PhD thesis, TU Delft, Delft University of Technology, Delft, The Netherlands, 2006.
- [56] GITMAN, I. M., ASKES, H., AND SLUYS, L. J. Coupled-volume multi-scale modelling of quasi-brittle material. *European Journal of Mechanics A/Solids* 27 (2008), 302–327.
- [57] GUGUIN, G., ALLIX, O., GOSSELET, P., AND GUINARD, S. Nonintrusive coupling of 3D and 2D laminated composite models based on finite element 3D recovery. *Int. J. Numer. Meth. Engrng* 98 (2014), 324–343.
- [58] HALLETT, S. R., JIANG, W.-G., KHAN, B., AND WISNOM, M. R. Modelling the interaction between matrix cracks and delamination damage in scaled quasi-isotropic specimens. *Composites Science and Technology* 68 (2008), 80–89.

- [59] HALLETT, S. R., AND WISNOM, M. R. Numerical investigation of progressive damage and the effect of layup in notched tensile tests. *Journal of Composite Materials* 40, 14 (2006), 1229–1245.
- [60] HARPER, P. W., AND HALLETT, S. R. Cohesive zone length in numerical simulations of composite delamination. *Engineering Fracture Mechanics* 75 (2008), 4774–4792.
- [61] HASHIN, Z. Failure criteria for unidirectional fiber composites. *Journal of Applied Mechanics* 47 (1980), 329–334.
- [62] HILL, R. Elastic properties of reinforced solids: some theoretical principles. *J. Mech. Phys. Solids* 11 (1963), 357–372.
- [63] HILLERBORG, A., MODEER, M., AND PETERSSON, P.-E. Analysis of crack formation and crack growth in concrete by means of fracture mechanics and finite elements. *Cement and concrete research* 6 (1976), 773–782.
- [64] HINTON, M. J., KADDOUR, A. S., AND SODEN, P. D. A comparison of the predictive capabilities of current failure theories for composite laminates, judged against experimental evidence. *Composites Science and Technology* 62 (2002), 1725–1797.
- [65] HIRAI, I., UCHIYAMA, Y., MIZUTA, Y., AND PILKEY, W. An exact zooming method. *Finite Elements in Analysis and Design* 1 (1985), 61–69.
- [66] HUGHES, T. J. R., FEIJOO, G. R., MAZZEI, L., AND QUAINCY, J.-B. The variational multiscale method—a mechanics paradigm for computational mechanics. *Comput. Methods Appl. Mech. Engrg.* 166 (1998), 3–24.
- [67] HÜHNE, C., ZERBST, A., KUHLMANN, G., STEENBOCK, C., AND ROLFES, R. Progressive damage analysis of composite bolted joints with liquid shim layers using constant and continuous degradation models. *Composite Structures* 92 (2010), 189–200.
- [68] HÜHNE, S., REINOSO, J., JANSEN, E., AND ROLFES, R. A two-way loose coupling procedure for investigating the buckling and damage behaviour of stiffened composite panels. *Composite Structures*, 136 (2016), 513–525.
- [69] HUND, A., AND RAMM, E. Locality constraints within multiscale model for non-linear material behaviour. *Int. J. Numer. Meth. Engrng* 70 (2007), 1613–1632.
- [70] JIANG, W.-G., HALLETT, S. R., GREEN, B. G., AND WISNOM, M. R. A concise interface constitutive law for analysis of delamination and splitting in composite materials and its application to scaled notched tensile specimens. *International Journal for Numerical Methods in Engineering* 69, 9 (2007), 1982–1995.
- [71] JONES, R. M. *Mechanics of composite materials*. CRC Press, 1998.
- [72] KADDOUR, A. S., AND HINTON, M. J. Maturity of 3d failure criteria for fibre-reinforced composites: Comparison between theories and experiments: Part b of wwfe-ii. *Journal of Composite Materials* 47 (2013), 925–966.
- [73] KADDOUR, A. S., HINTON, M. J., SMITH, P. A., AND LI, S. Mechanical properties and details of composite laminates for the test cases used in the third world-wide failure exercise. *Journal of Composite Materials* 47, 20-21 (2013), 2427–2442.
- [74] KADDOUR, A. S., HINTON, M. J., AND SODEN, P. D. A comparison of the predictive capabilities of current failure theories for composite laminates: additional contributions. *Composites Science and Technology* 64 (2004), 449–476.

- [75] KADOWAKI, H., AND LIU, W. K. Bridging multi-scale method for localization problems. *Computer Methods in Applied Mechanics and Engineering* 193 (2004), 3267–3302.
- [76] KANOUTÉ, P., BOSO, D., CHABOCHE, J., AND SCHREFLER, B. Multiscale methods for composites: a review. *Arch Comput Methods Eng* 16 (2009), 31–75.
- [77] KATZ, D. S., RIPEANU, M., AND WILDE, M. Many-task computing tools for multiscale modeling. *arXiv:1110.0404 [cs.DC]* (2011).
- [78] KOUZNETSOVA, V., GEERS, M. G. D., AND BREKELMANS, W. A. M. Multi-scale constitutive modelling of heterogeneous materials with a gradient-enhanced computational homogenization scheme. *Int. J. Numer. Meth. Engng* 52 (2002), 1235–1260.
- [79] KOUZNETSOVA, V. G., GEERS, M. G. D., AND BREKELMANS, W. A. M. Multi-scale second-order computational homogenization of multi-phase materials: A nested finite element solution strategy. *Computer Methods in Applied Mechanics and Engineering* 193, 48-51 (2004), 5525–5550.
- [80] KRAUSE, R., AND RANK, E. Multiscale computations with a combination of the h- and p-versions of the finite-element method. *Comput. Methods Appl. Mech. Engrg.* 192 (2003), 3959–3983.
- [81] KRUEGER, R. The virtual crack closure technique for modeling interlaminar failure and delamination in advanced composite materials. In *Numerical Modelling of Failure in Advanced Composite Materials*. Elsevier Ltd., 2015, pp. 3–53.
- [82] KRUEGER, R., RATCLIFFE, J. G., AND MINGUET, P. J. Panel stiffener debonding analysis using a shell/3d modeling technique. *Composites Science and Technology* 69 (2009), 2352–2362.
- [83] LABEAS, G. N., BELESIS, S. D., DIAMANTAKOS, I., AND TSERPES, K. I. Adaptative Progressive Damage Modeling for Large-scale Composite Structures. *International Journal of Damage Mechanics* 21(3) (2012), 441–62.
- [84] LADEVÈZE, P. Multiscale modelling and computational strategies for composites. *Int. J. Numer. Meth. Engng* 60 (2004), 233–253.
- [85] LADEVÈZE, P., LOISEAU, O., AND DUREISSEIX, D. A micro-macro and parallel computational strategy for highly heterogeneous structures. *Int. J. Numer. Meth. Engng.* 52 (2001), 121–138.
- [86] LINDE, P., PLEITNER, J., BOER, H. D., AND CARMONE, C. Modelling and Simulation of Fibre Metal Laminates. *ABAQUS Users' Conference* (2004), 421–439.
- [87] LIU, X., DUDDU, R., AND WAISMAN, H. Discrete damage zone model for fracture initiation and propagation. *Engineering Fracture Mechanics* 92 (2012), 1–18.
- [88] LÖHNERT, S. *Computational homogenization of microheterogeneous materials at finite strains including damage*. PhD thesis, Universität Hannover, Institut für Baumechanik und Numerische Mechanik, Hannover, Germany, 2005.
- [89] LÖHNERT, S., AND BELYTSCHKO, T. A multiscale projection method for macro / microcrack simulations. *International Journal for Numerical Methods in Engineering*, 71 (2007), 1466–1482.
- [90] MAIMÍ, P., CAMANHO, P. P., MAYUGO, J. A., AND TURON, A. Matrix cracking



- and delamination in laminated composites. Part I: Ply constitutive law, first ply failure and onset of delamination. *Mechanics of Materials* 43 (2011), 169–185.
- [91] MAIMÍ, P., CAMANHO, P. P., MAYUGO, J. A., AND TURON, A. Matrix cracking and delamination in laminated composites. Part II: Evolution of crack density and delamination. *Mechanics of Materials* 43 (2011), 194–211.
- [92] MAO, K., AND SUN, C. A refined global-local finite element analysis method. *International Journal for Numerical Methods in Engineering* 32 (1991), 29–43.
- [93] MATOUŠ, K., GEERS, M. G., KOUZNETSOVA, V. G., AND GILLMAN, A. A review of predictive nonlinear theories for multiscale modeling of heterogeneous materials. *Journal of Computational Physics* 330 (2017), 192–220.
- [94] MIEHE, C., AND BAYREUTHER, C. G. On multiscale FE analyses of heterogeneous structures: from homogenization to multigrid solvers. *Int. J. Numer. Meth. Engng.* 71 (2007), 1135–1180.
- [95] MIEHE, C., AND KOCH, A. Computational micro-to-macro transitions of discretized microstructures undergoing small strains. *Archive of Applied Mechanics* 72 (2002), 300–317.
- [96] MIEHE, C., AND SCHOTTE, J. Computational micro-macro transitions and overall moduli in the analysis of polycrystals at large strains. *Computational Materials Science* 16 (1999), 372–382.
- [97] MIEHE, C., SCHOTTE, J., AND LAMBRECHT, M. Homogenization of inelastic solid materials at finite strains based on incremental minimization principles. application to the texture analysis of polycrystals. *Journal of the Mechanics and Physics of Solids* 50 (2002), 2123–2167.
- [98] MOTE, C. D. Global-local finite element. *International Journal for Numerical Methods in Engineering* 3 (1971), 565–574.
- [99] NOOR, A. K. Global-local methodologies and their application to nonlinear analysis. *Finite Elements in Analysis and Design* 2 (1986), 333–346.
- [100] ODEN, J. T., AND ZOHDI, T. I. Analysis and adaptive modeling of highly heterogeneous elastic structures. *Comput. Methods Appl. Mech. Engrg.* 148 (1997), 367–391.
- [101] OLIVER, J., CAICEDO, M., ROUBIN, E., HUESPE, A., AND HERNANDEZ, J. Continuum approach to computational multiscale modeling of propagating fracture. *Comput. Methods Appl. Mech. Engrg.* 294 (2015), 384–427.
- [102] ORIFICI, A. C., DE ZARATE ALBERDI, I. O., THOMSON, R. S., AND BAYANDOR, J. Compression and post-buckling damage growth and collapse analysis of flat composite stiffened panels. *Composites Science and Technology* 68 (2008), 3150–3160.
- [103] ORIFICI, A. C., THOMSON, R. S., DEGENHARDT, R., BISAGNI, C., AND BAYANDOR, J. A finite element methodology for analysing degradation and collapse in postbuckling composite aerospace structures. *Journal of Composite Materials* 43 (2009), 32–39.
- [104] ORIFICI, A. C., THOMSON, R. S., HERSZBERG, I., WELLER, T., DEGENHARDT, R., AND BAYANDOR, J. An analysis methodology for failure in postbuckling skin-stiffener interfaces. *Composite Structures* 86 (2008), 186–193.
- [105] PARK, J. W., HWANG, J. W., AND KIM, Y. H. Efficient finite element analysis using

- mesh superposition technique. *Finite Elements in Analysis and Design* 39 (2003), 619–638.
- [106] PIETROPAOLI, E., AND RICCIO, A. A global/local finite element approach for predicting interlaminar and intralaminar damage evolution in composite stiffened panels under compressive load. *Appl Compos Mater* (2011), 113–125.
- [107] PINEDA, E. J., BEDNARCYK, B. A., WAAS, A. M., AND ARNOLD, S. M. Progressive failure of a unidirectional fiber-reinforced composite using the method of cells : Discretization objective computational results. *International Journal of Solids and Structures* 50 (2013), 1203–1216.
- [108] PINEDA, E. J., WAAS, A. M., BEDNARCYK, B. A., COLLIER, C. S., AND YARRINGTON, P. W. A novel multiscale physics based progressive failure methodology for laminated composite structures. In *Forty-ninth AIAA/ASME/ASCE/AHS/ASC structures, structural dynamics, and materials conference* (2008), no. 1929.
- [109] PINHO, S. T., DÁVILA, C. G., CAMANHO, P. P., IANNUCCI, L., AND ROBINSON, P. Failure models and criteria for frp under in-plane or three-dimensional stress states including shear non-linearity. *Nasa/Tm-2005-213530*, NASA/TM-2005-213530 (2005), 68.
- [110] PINHO, S. T., IANNUCCI, L., AND ROBINSON, P. Physically based failure models and criteria for laminated fibre-reinforced composites with emphasis on fibre kinking. Part II: FE implementation. *Composites Part A: Applied Science and Manufacturing* 37, 5 (2006), 766–777.
- [111] PINHO, S. T., VYAS, G. M., AND ROBINSON, P. Material and structural response of polymer-matrix fibre-reinforced composites. *Journal of Composite Materials* 47, 6-7 (2013), 679–696.
- [112] PUCK, A. Festigkeitsanalyse von faser-matrix-laminaten: Modelle für die praxis, 1996.
- [113] PUCK, A., KOPP, J., AND KNOPS, M. Guidelines for the determination of the parameters in puck’s action plane strength criterion. *Composites Science and Technology* 62 (2002), 371–378.
- [114] PUCK, A., AND SCHÜRMAN, H. Failure analysis of frp laminates by means of physically based phenomenological models. *Composites Science and Technology* 62 (2002), 1633–1662.
- [115] R. WISNOM, M., AND CHANG, F. K. Modelling of splitting and delamination in notched cross-ply laminates. *Composites Science and Technology* 60, 15 (2000), 2849–2856.
- [116] RAGHAVAN, P., AND GHOSH, S. Concurrent multi-scale analysis of elastic composites by a multi-level computational model. *Comput. Methods Appl. Mech. Engrg.* 193 (2004), 497–538.
- [117] RAIMONDO, A., AND RICCIO, A. Inter-laminar and intra-laminar damage evolution in composite panels with skin-stringer debonding under compression. *Composites Part B* 94 (2016), 139–151.
- [118] RANK, E. A zooming technique using a hierarchical hp-version of the finite element method. In *The Mathematics of Finite Elements and Applications - Highlights*, U. Elsevier, Ed. J. Whiteman (Ed.), 1993.

- [119] REESE, S. Meso-macro modelling of fibre-reinforced rubber-like composites exhibiting large elastoplastic deformation. *International Journal of Solids and Structures* 40 40 (2003), 951–980.
- [120] REINOSO, J., BLÁZQUEZ, A., ESTEFANI, A., PARÍS, F., CAÑAS, J., ARÉVALO, E., AND CRUZ, F. Experimental and three-dimensional global-local finite element analysis of a composite component including degradation process at the interfaces. *Composites Part B* 43 (2012), 1929–1942.
- [121] RENARD, J., AND MARMONIER, M. Etude de l’initiation de l’endommagement dans la matrice d’un matériau composite par une méthode d’homogénéisation. *Aerospace Science and Technology* 6 (1987), 37–51.
- [122] RICCIO, A., RAIMONDO, A., AND SCARAMUZZINO, F. A robust numerical approach for the simulation of skin-stringer debonding growth in stiffened composite panels under compression. *Composites Part B* 71 (2015), 131–142.
- [123] RICE, J. The mechanics of earthquake rupture. In *Physics of the Earth’s Interior (Proc. International School of Physics “Enrico Fermi”, Course 78, 1979; ed. A.M. Dziewonski and E. Boschi)*. Italian Physical Society and North-Holland Publ. Co., 1980, pp. 555–649.
- [124] RYBICKI, E., AND M.F. KANNINEN. A finite element calculation of stress intensity factors by modified crack closure integral. *Engineering Fracture Mechanics* 9 (1977), 931–938.
- [125] SAAVEDRA, K., ALLIX, O., GOSSELET, P., HINOJOSA, J., AND VIARD, A. An enhanced nonlinear multi-scale strategy for the simulation of buckling and delamination on 3d composite plates. *Computer Methods in Applied Mechanics and Engineering* 317 (2017), 952–969.
- [126] SERRA, J., PIERRÉ, J., PASSIEUX, J., PÉRIÉ, J., BOUVET, C., AND CASTANIÉ, B. Validation and modeling of aeronautical composite structures subjected to combined loadings: The vertex project. part 1: Experimental setup, fe-dic instrumentation and procedures. *Composite Structures* 179 (2017), 224–244.
- [127] SHET, C., AND CHANDRA, N. Effect of the shape of  $t$ - $\delta$  cohesive zone curves on the fracture response. *Mechanics of Advanced Materials and Structures* 11 (2010), 249–275.
- [128] SOTO, A., GONZÁLEZ, E. V., MAIMÍ, P., TURON, A., SAINZ DE AJA, J. R., AND DE LA ESCALERA, F. M. Cohesive zone length of orthotropic materials undergoing delamination. *Engineering Fracture Mechanics* 159 (2016), 174–188.
- [129] SUN, C., AND K.M., M. A global-local finite element method suitable for parallel computations. *Computers & Structures* 29, 2 (1988), 309–315.
- [130] TALREJA, R. On multi-scale approaches to composites and heterogeneous solids with damage. *Philosophical Magazine* 90, 31-32 (2010), 4333–4348.
- [131] TALREJA, R. Assessment of the fundamentals of failure theories for composite materials. *Composites Science and Technology* 105 (2014), 190–201.
- [132] TERADA, K., AND KIKUCHI, N. A class of general algorithms for multi-scale analyses of heterogeneous media. *Comput. Methods Appl. Mech. Engrg.* 190 (2001), 5427–5464.
- [133] TURON, A., CAMANHO, P., COSTA, J., AND DÁVILA, C. A damage model for

- the simulation of delamination in advanced composites under variable-mode loading. *Mechanics of Materials* 38 (2006), 1072–1089.
- [134] TURON, A., CAMANHO, P. P., AND COSTA, J. An engineering solution for mesh size effects in the simulation of delamination using cohesive zone models. *Engineering Fracture Mechanics* 74 (2007), 1665–1682.
- [135] TURON, A., CAMANHO, P. P., COSTA, J., AND RENART, J. Accurate simulation of delamination growth under mixed-mode loading using cohesive elements: Definition of interlaminar strengths and elastic stiffness. *Composite Structures* 92, 8 (2010), 1857–1864.
- [136] TURON, A., GONZÁLEZ, E. V., SARRADO, C., GUILLAMET, G., AND MAIMÍ, P. Accurate simulation of delamination under mixed-mode loading using a cohesive model with a mode-dependent penalty stiffness. *Composite Structures* 184 (2018), 506–511.
- [137] VAN DER MEER, F. P., AND SLUYS, L. J. Mesh-independent modeling of both distributed and discrete matrix cracking in interaction with delamination in composites. *Engineering Fracture Mechanics* 77, 4 (2010), 719–735.
- [138] VESCOVINI, R., DÁVILA, C. G., AND BISAGNI, C. Failure analysis of composite multi-stringer panels using simplified models. *Composites Part B* 45 (2013), 939–951.
- [139] VOGLER, M., ERNST, G., AND ROLFES, R. Invariant Based Transversely-Isotropic Material and Failure Model for Fiber-Reinforced Polymers. *CMC* 16, 1 (2010), 25–49.
- [140] WAGNER, W., AND BALZANI, C. Prediction of the postbuckling response of composite airframe panels including ply failure. *Engineering Fracture Mechanics* 77 (2010), 3648–3657.
- [141] WANG, J. T. S., AND BIGGER, S. B. Skin-stiffener interface stresses in composite stiffened panels. *NASA Contractor Report 172261* (1984).
- [142] WHITCOMB, J. D. Iterative global/local finite element analysis. *Computers and Structures* 40, 4 (1991), 1027–1031.
- [143] XIE, D., AND WAAS, A. M. Discrete cohesive zone model for mixed-mode fracture using finite element analysis. *Engineering Fracture Mechanics* 73, 13 (2006), 1783–1796.
- [144] YANG, Q., AND COX, B. Cohesive models for damage evolution in laminated composites. *International Journal of Fracture* 133 (2005), 107–137.
- [145] YANG, Q. D., COX, B. N., NALLA, R. K., AND RITCHIE, R. O. Fracture length scales in human cortical bone : The necessity of nonlinear fracture models. *Biomaterials* 27 (2006), 2095–2113.
- [146] YAP, J. W. H., SCOTT, M. L., THOMSON, R. S., AND HACHENBERG, D. The analysis of skin-to-stiffener debonding in composite aerospace structures. *Composite Structures* 57 (2002), 425–435.
- [147] ZOHDI, T., FEUCHT, M., GROSS, D., AND WRIGGERS, P. A description of macroscopic damage through microstructural relaxation. *Int. J. Numer. Meth. Engng* 43 (1998), 493–506.
- [148] ZOHDI, T. I., ODEN, J. T., AND RODIN, G. J. Hierarchical modeling of heterogeneous bodies. *Comput. Methods Appl. Mech. Engng* 138 (1996), 273–298.
- [149] ZOHDI, T. I., AND WRIGGERS, P. Computational micro-macro material testing. *Archives of Computational Methods in Engineering* 8, 2 (2001), 131–228.

- 
- [150] ZOHDI, T. W. P. A domain decomposition method for bodies with heterogeneous microstructure based on material regularization. *International Journal of Solids and Structures* 36 (1999), 2507–2525.
- [151] ZUBILLAGA, L., TURON, A., MAIMÍ, P., COSTA, J., MAHDI, S., AND LINDE, P. An energy based failure criterion for matrix crack induced delamination in laminated composite structures. *Composite Structures* 112 (2014), 339–344.
- [152] ZUBILLAGA, L., TURON, A., RENART, J., COSTA, J., AND LINDE, P. An experimental study on matrix crack induced delamination in composite laminates. *Composite Structures* 127 (2015), 10–17.



# Curriculum vitae

## Personal details

Name: Margarita Akterskaia  
Date of birth: 11.02.1989  
Place of birth: Saint-Petersburg, Russia  
Nationality: Russian

## Education

1996-2002: School education (Saint-Petersburg, Russia)  
2002-2006: Lyceum “Physical-Technical High School” (PTHS) (Saint-Petersburg, Russia)  
2006-2010: Bachelor degree programme in Computational Mechanics, Bachelor Thesis on “Homogenization and heterogenization of unidirectional fiber composite materials” (Peter the Great St.Petersburg Polytechnic University, Russia)  
(GPA 5.0/5.0)  
2010-2012: Master degree programme in Computational Mechanics, Master Thesis on “Injection molding simulation of a frontal BMW bumper with application of Moldex3D” (Peter the Great St.Petersburg Polytechnic University, Russia)  
(GPA 4.95/5.0)

## Scientific career

2017: Research stay at the University of Bristol, UK  
2018: Research stay at the University of Porto, Portugal  
since 2016: Research associate at the Institute of Structural Analysis, Leibniz Universität Hannover, Germany

## Awards

- 
- 2015: Marie-Curie Fellowship Grant within the FULLCOMP project  
2006-2012: Scholarship for the best students and for winners of mathematical competitions (Peter the Great St.Petersburg Polytechnic University, Russia)
- 2008: Saint-Petersburg State Olympiad on Strength of materials  
2002-2005: Awards in Physics and Mathematics Olympiads, St. Petersburg, Russia
- 2002: Alferov's foundation scholarship (Lyceum "Physical-Technical High School" (PTHS), Saint-Petersburg, Russia)